UiO : Faculty of Medicine
University of Oslo

Karine Flem Karlsen

Investigating therapeutic candidates and the use of preclinical models to predict treatment response in melanoma

Thesis for the degree of Philosophiae Doctor

Department of Pathology, the Norwegian Radium Hospital, Oslo University Hospital

Faculty of Medicine, University of Oslo

HELSE SØR-ØST

RADIUM HOSPITALETS LEGATER

Oslo University Hospital
Norwegian Radium Hospital

Series of dissertations submitted to the
Faculty of Medicine, University of Oslo

ISBN 978-82-8377-614-0

Cover: Hanne Baadsgaard Utigard.
Print production: Reprosentralen, University of Oslo.

Table of contents

Acknowledgements

First, I gratefully acknowledge the financial support provided by the South-Eastern Norway Regional Health Authority and Radiumhospitalets Legater.

I would like to express my gratitude to my main supervisor, Professor Vivi Flørenes. Especially, I am thankful for your trust in my ideas and suggestions. You have always encouraged my thoughts and critical thinking, and I hope I now can be considered quite the independent researcher because of it. Additionally, I thank you for your thorough feedback. I am also thankful for the essential feedback and ideas I have received from my co-supervisor Professor Gunhild Mælandsmo. I am particularly grateful to both of you for the time you have dedicated to me during the past years.

My first meeting with research was through my co-supervisor Dr. Caroline Nunes-Xavier, who took me on as a master student in 2014. Thank you for launching my scientific career, for everything you have taught me, and all the valuable comments and suggestions I have received over the years. I admire your dedication and creativity.

The contribution of all my co-authors is greatly appreciated and I thank you for the collaboration. I am especially grateful for the fruitful discussions with Dr. Marta Nyakas and for sharing your vast knowledge on melanoma treatment and resistance from a clinician's point-of-view. Further, big thanks to Geir Øy, for invaluable help in the animal facility. I would also like to thank Professor emeritus Øystein Fodstad for continuous support and encouragement.

While writing this section, I have reflected on the number of people who have contributed to this work and the number of great colleagues I have encountered. I am thankful for all chats, advice, corrections and help I have received during the past years. Particularly, I am deeply grateful for my lab 'mothers' Erin and Elisabeth. Thank you for your great support.

Last, but not least, my dear family, friends and Tormod. Thank you for your interest and endless support. I am so lucky to have you in my life.

Abbreviations

Abbreviation	Full name
ADAM	A disintegrin and metalloproteinase domain-containing
AKT	Protein kinase B
AP-1	Activator protein 1
APC	Antigen-presenting cell
ATF2	Cyclic AMP-dependent transcription factor ATF-2
ATM	Ataxia-telangiectasia mutated
ATP	Adenosine triphosphate
ATR	ATM- and Rad3-related
AXL	Tyrosine-protein kinase receptor UFO
B7-1	T-lymphocyte activation antigen CD86
B7-2	T-lymphocyte activation antigen CD80
B7-H3	B7 homolog 3
BAD	Bcl-2-associated death promoter
BAX	Bcl-2-associated X protein
c-Abl	Tyrosine-protein kinase ABL1
CAR	Chimeric antigen receptor
CD28	T-cell-specific surface glycoprotein CD28
CD4	T-cell surface glycoprotein CD4
CD8	T-cell surface glycoprotein CD8
CDC25C	M-phase inducer phosphatase 3
CDK	Cyclin-dependent kinase
CHK	Serine/threonine-protein kinase CHK
CKI	Cyclin-dependent kinase inhibitor
CT	Computerized tomography
CTLA-4	Cytotoxic T-lymphocyte protein 4
DDR	DNA damage response
DKK	Dickkopf-related protein
DMSO	Dimethyl sulfoxide
DNA	Deoxyribonucleic acid
DTIC	Dacarbazine
DUSP10	Dual specificity protein phosphatase 10
EGFR	Epidermal growth factor receptor
ELISA	Enzyme-linked immunosorbent assay
EMT	Epithelial-to-mesenchymal transition
ERK1/2	Extracellular signal-regulated kinase 1 and 2
FDA	Food and Drug Administration
FLT3	Fibromyalgia-like tyrosine kinase 3
GAS6	Growth arrest-specific protein 6
GDP	Guanosine diphosphate

GRB2	Growth factor receptor bound protein 2
GSK3	Glycogen synthase kinase 3
GTP	Guanosine triphosphate
H2AX	H2A histone family member X
HER2	Receptor tyrosine-protein kinase erbB-2
HER3	Receptor tyrosine-protein kinase erbB-3
HIF-1	Hypoxia-induced factor 1
IFN	Interferon
Ig	Immunoglobulin
IgC	Immunoglobulin constant
IGF1R	Insulin-growth factor 1 receptor
IgV	Immunoglobulin variable
IL	Interleukin
JAK	Tyrosine-protein kinase JAK
JNK	C-Jun N-terminal kinase
LAG-3	Lymphocyte-activation gene 3
LDH	Lactate dehydrogenase
MAPK	Mitogen-ativated protein kinase
MAPKK	Mitogen-ativated protein kinase kinase
MAPKKK	Mitogen-ativated protein kinase kinase kinase
MDM2	Mouse double minute 2 homolog
MEK1/2	Dual specificity mitogen-activated protein kinase kinase 1/2
MELAN-A	Melanoma antigen recognized by T-cells 1
MER	Tyrosine-protein kinase Mer
MET	Mesenchymal-to-epitelial transition
MHC	Major histocompatibility complex
MITF	Microphthalmia-associated transcription factor
MMP	Matrix metalloproteinase
mRNA	Messenger RNA
mTOR	Mammalian target of rapamycin
NK	Natural killer
NSCLC	Non-small cell lung cancer
NSG	NOD scid gamma
OS	Overall survival
$p21^{WAF1/CIP1}$	Cyclin-dependent kinase inhibitor 1
p53	Cellular tumor antigen p53
p73	Tumor protein p73
PARP	Poly [ADP-ribose] polymerase
pAXL	Phosphorylated AXL
PCR	Polymerase chain reaction
PD-1	Programmed cell death protein 1
PDGFRβ	Platelet-derived growth factor receptor β
PD-L1	Programmed cell death 1 ligand 1

PD-L2	Programmed cell death 1 ligand 2
PDX	Patient-derived xenograft
PFS	Progression-free survival
PI3K	Phosphoinositide 3-kinase
PIP2	PtdIns(4,5)P2
PIP3	PtdIns(3,4,5)P2
PtdIns	Phosphateidylinositol
PtdSer	Posphateidylserine
PTEN	Phosphatase and tensin homolog
qPCR	Quantitative PCR
RAF	RAF proto-oncogene serine/threonine kinase
RAS	C-Rat Viral Oncogene Homolog
RBD	Ras-binding domain
RNA	Ribonucleotide
RTK	Receptor tyrosine kinase
sAXL	Soluble AXL
sB7-H3	Soluble B7-H3
SH	SRC homology
siRNA	Small interfering RNA
SLUG	Zinc finger protein SNAI2
SMAD1	Mothers against decapentaplegic homolog 1
SNAIL	Zinc finger protein SNAI1
SOS	Son of sevenless
SOX-10	Transcription factor SOX-10
STAT3	Signal transducer and activator of transcription 3
TIM3	T cell immunoglobulin and mucin domain-containing molecule 3
TIMP	TIMP metalloproteinase inhibitor
TNF	Tumor necrosis factor
TWIST	Twist-related protein
TYRO3	Tyrosine-protein kinase receptor TYRO3
VEGF	Vascular endothelial growth factor
VISTA	V-domain Ig suppressor of T cell activation
WEE1	WEE1-like protein kinase
ZEB2	Zinc finger E-box-binding homeobox 2

List of publications

This thesis is based on the following original articles that will be referred to in the text by their roman numerals I-IV.

I. **A three-dimensional *ex vivo* viability assay reveals a strong correlation between response to targeted inhibitors and mutation status in melanoma lymph node metastases.**
Flørenes VA, Flem-Karlsen K, McFadden E, Bergheim IR, Nygaard V, Nygård V, Farstad IN, Øy GF, Emilsen E, Giller-Fleten K, Ree AH, Flatmark K, Gullestad HP, Hermann R, Ryder T, Wernhoff P, Mælandsmo GM.
Translational Oncology. 2019 Jul;12(7):951-958.

II. **Targeting AXL and the DNA damage response pathway as a novel therapeutic strategy in melanoma.**
Flem-Karlsen K, McFadden E, Omar N, Haugen MH, Øy GF, Ryder T, Gullestad HP, Hermann R, Mælandsmo GM, Flørenes VA.
Manuscript in second revision, Molecular Cancer Therapeutics

III. **Soluble AXL as a marker of disease progression and survival in melanoma.**
Flem-Karlsen K, Nyakas M, McFadden E, Wernhoff P, Farstad IN, Flørenes VA, Mælandsmo GM.
Manuscript in second revision, PLOS ONE.

IV. **p38 MAPK activation through B7-H3-mediated DUSP10 repression promotes chemoresistance.**
Flem-Karlsen K, Tekle C, Øyjord T, Flørenes VA, Mælandsmo GM, Fodstad Ø, Nunes-Xavier CE.
Scientific Reports. 2019 April;9(1):5839.

1 Introduction

Melanoma incidences are on the rise both worldwide and in Norway. Although prognosis is good for early-stage melanoma, once the cancer spreads survival drops dramatically. Currently, treatment of late-stage melanomas consists of immunotherapy and targeted treatment of the mitogen-activated protein kinase (MAPK) pathway. However, many patients do not respond, develop resistance, or are not eligible for current therapy. It is therefore important to identify approaches to determine response and examine new targets or strategies to enhance therapeutic regimens. This thesis has investigated the potential of employing an *ex vivo* drug efficacy assay using lymph node metastases harvested from melanoma patients and patient-derived xenografts (PDX) as preclinical models to measure response to targeted treatments. Additionally, the therapeutic potential of two proteins, tyrosine protein kinase receptor UFO (AXL) and immune checkpoint protein B7 homolog 3 (B7-H3), both upregulated in melanoma and associated with aggressive cancer characteristics and lower survival, was investigated. Inhibition or reduced expression of these proteins was examined either alone or in combination with inhibitors of the deoxyribonucleic acid (DNA) damage response (DDR) pathway or chemotherapy.

To present the themes related to the articles, the following introduction consists of subjects such as a general introduction to cancer and metastasis, cell signaling mechanisms, the DDR pathway and immune regulation in cancer, before melanoma specific epidemiology, mutations and treatments are described.

1.1 Cancer

Cancer is a group of diseases that arises due to genomic or epigenetic alterations, leading to abnormal proliferation or failure to undergo apoptosis which ultimately may result in the formation of mass(es) of tissue, called tumors. Tumors can be classified as benign or malignant. Tumors of the former classification are not capable of invading surrounding tissue or other parts of the body. Malignant tumors, however, acquire the ability to grow into or invade nearby tissues and travel via the blood and lymph system to extravasate at distant sites, in a process termed metastasis. Metastasis is accountable for nearly all cancer-related mortalities (1).

Cancer will affect one in three people during their lifetime. In Norway, 33 352 people were diagnosed with cancer in 2018, where the most common sites were prostate, breast, lung and

colon (2). For most cancers, incidence increases with age, contributing to constantly heightened number of cancers cases each year due to overall longer life span of the population. In addition, the prevalence of people living with cancer is increasing due to improved treatment options and earlier diagnosis. Nevertheless, 11 016 cancer-related deaths were reported in Norway in 2017 (2), making cancer the second most common cause of death, after cardiovascular diseases (3).

Cells turn cancerous due to a series of aberrations in the DNA, arising in an evolutionary manner. DNA alterations can be introduced by inherited genes or throughout a person's lifetime, either spontaneously or caused by exposure to specific environmental factors such as cigarette smoke, ultraviolet radiation and dietary habits. Although the DNA alterations are individual to each patient, certain mutations are frequently observed and are found to be drivers of cancer progression, known as oncogenes. Oncogenes are gain-of-function mutations, which result in a gene product with increased function. Oppositely, loss-of–function mutations resulting in decreased or complete lack of function in genes coding for tumor-suppressor proteins that prevent uncontrolled proliferation or repair DNA damage, are also common in cancers. Recently, the Cancer Genome Atlas published an overview of common mutations in cancers and verified that there were prevalent mutations in genes of the MAPK and phosphoinositide 3-kinase (PI3K) pathways (4). Furthermore, they reported frequent mutations in genes coding for tumor-suppressor proteins associated with DDR, DNA repair and the cell cycle, such as *TP53* and *CDKN2A* (encoding cell cycle regulators INK4 family members $p16^{INK4A}$ and $p14^{ARF}$) (4).

Furthermore, cancer cells acquire survival advantages through co-operation with surrounding cells. The extended hallmarks of cancer, described by Hanahan and Weinberg in 2011 (5), highlight characteristics that are common denominators for cancer cells to thrive. The hallmarks comprise of the following capabilities: sustaining proliferative signaling, evading growth suppressors, activating invasion and metastasis, enabling replicative immortality, inducing angiogenesis and resisting cell death. In addition, two emerging hallmarks, avoiding immune destruction and tumor-promoting inflammation, and two enabling characteristics, genome instability and mutation and deregulating cellular energetics, have been proposed. Importantly, the hallmarks were never intended to portray all the characteristics a cancer cell must have at any given time. Rather, the hallmarks of cancer describe features cancer cells must possess over the course of becoming oncogenic. Additional characteristics have been suggested as hallmarks of cancer, with the ability to de-differentiate as perhaps the most prominent suggestion (6).

Unlike many of the current hallmarks describing sustained and immortal growth, de-differentiation is not usually shared between benign and metastatic tumors. Additionally, de-differentiation may be important in cancer survival in response to cellular stress, for instance in melanoma (7). Hallmarks relevant for this thesis, such as activating invasion and metastasis, sustaining proliferative signaling, resisting cell death, and avoiding immune destruction, will be discussed in the following paragraphs.

1.2 Metastasis

Metastasis is a sequential process where cancer cells escape their primary site and travel to distant sites in the body, as illustrated in Figure 1. To colonize other organs, the metastatic cells have to undergo several changes and adaptions. Namely, they have to able to infiltrate adjacent tissue, migrate into nearby vessels (intravasation), survive in the circulatory system and migrate out of the vessel (extravasation), before proliferating in a new environment at a distant site. The vast majority of cells fail to complete this process, and it is estimated that less than 0.02% of disseminated tumor cells metastasize (8).

Already in 1889, Stephen Paget proposed a "seed and soil" theory which states that the pattern of metastasis is not random and that tumor cells (the seeds) exhibit an inclination towards metastasizing to certain organs (the soil) (9). In line with this, studies have determined that tumor cells release factors that promote the formation of microenvironments in distant organs that contribute to the survival of cancer cells upon their arrival at these sites (termed pre-metastatic niches) (10). The released factors are comprised of growth factors, hormones, and cytokines that may travel freely or be transported in extracellular vesicles and may influence non-cancerous cells, such as fibroblasts and immune cells, to facilitate in the progression of the pre-metastatic niche (11).

Two models for how cells spread to distant organs have been proposed. In the linear progression model, cells metastasize only when they have acquired several mutations to be able to thrive in the new environment. This leads to minimal genetic distinction between the primary and the metastatic tumor (12). Oppositely is the parallel-progression model, where metastatic cells disseminate at an early stage of tumor progression and develops in parallel to the primary tumor, leading to high genetic diversity between a patient's tumors (12).

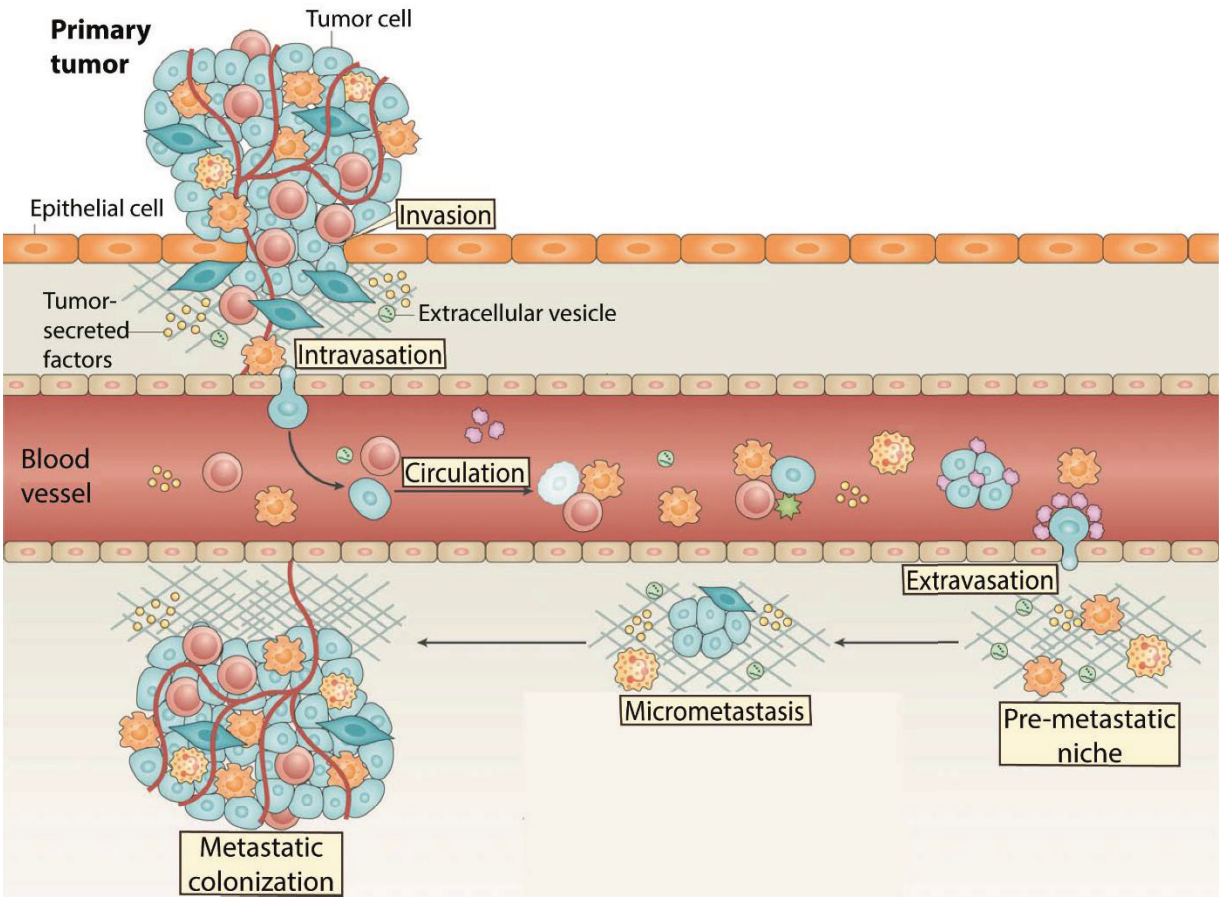

Figure 1. Overview of the metastatic process. The figure illustrates the steps of the metastatic cascade and include cells and vesicles that aid the tumor cells in the process. The figure is modified from Anderson R.L. *et al*, Nat Rev Clin Oncol, 2019 (13) and is licensed under a Creative Commons Attribution 4.0 International License (https://creativecommons.org/licenses/by/4.0/).

The metastatic process has been linked to the epithelial-to-mesenchymal transition (EMT) in epithelial cells. During EMT, cells lose the polarity and cell-cell junctions associated with an epithelial phenotype and display characteristics representing an invasive and motile mesenchymal phenotype (14). EMT occurs in the initiation of metastasis, before the reverse process, mesenchymal-to-epithelial transition (MET), occurs upon colonization of the distant organ. Not only does EMT allow cells to metastasize, the process is also associated with resistance to therapy (14).

1.3 Cell signaling

Cells respond and adapt to signals from the external environment and thus alter internal signaling to process the information they receive. Membrane receptors receive signals and transmit these into the cells. Some of these receptors are also capable to act as enzymes, of which one subclass are the receptor tyrosine kinases (RTK), consisting of twenty subfamilies (15). The RTKs are single-pass transmembrane proteins. Once activated by growth factors, RTKs dimerizes with other RTK proteins and autophosphorylates to induce downstream signaling resulting in various outcomes such as proliferation, differentiation, migration and cell death (15). For instance, RTK proteins are responsible for activating main signaling pathways involved in cancer proliferation and survival, such as the MAPK cascades and the PI3K pathway. Dysregulation of the MAPK cascades and the PI3K pathway are central in many cancers and consist of several clinically employed or potential therapeutic targets, and will thus be introduced below.

MAPK cascades

The MAPK cascades are comprised of several serine-threonine kinases that are named after the principal MAPK component, such as extracellular signal-regulated kinase 1 and 2 (ERK1/2, ERK/MAPK), p38 (p38/MAPK) and c-Jun N-terminal kinase (JNK, JNK/MAPK) (Figure 2). The MAPK components are activated in succession through phosphorylation of their upstream MAPK kinase kinases (MAPKKK) and MAPK kinases (MAPKK). The MAPK may be regulated by dual-specificity phosphatases (DUSP) that dephosphorylates and inactivates the MAPK (16). Only some of the abundant MAPKKK, MAPKK and MAPKs are presented in Figure 2.

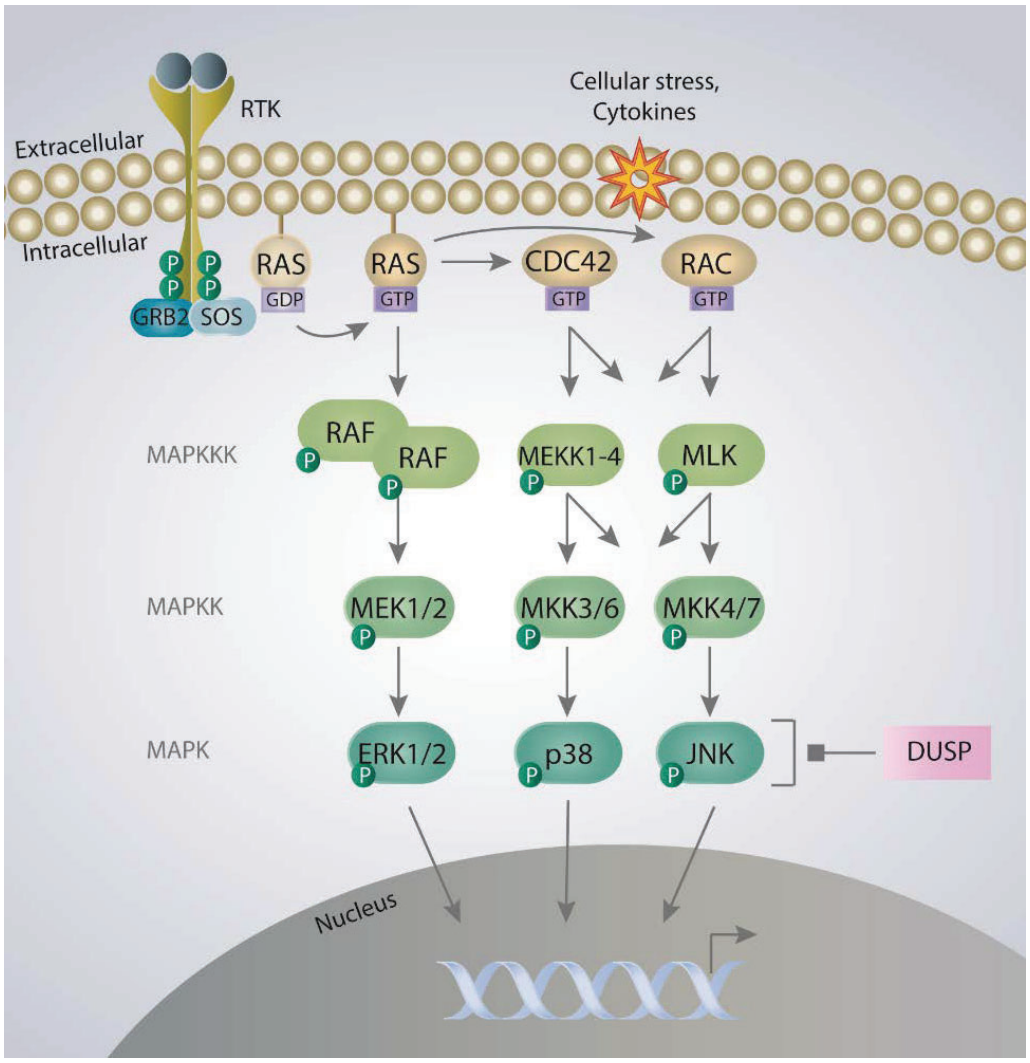

Figure 2. The MAPK cascades. The figure illustrates the MAPK cascades which, when activated, may lead to signaling pathways that results in the transcription of genes involved in proliferation, differentiation or survival. Green circles with P depict phosphorylation events and square arrowheads illustrate inhibition. RTK – Receptor tyrosine kinase, GDP – guanosine diphosphate, GTP – guanosine triphosphate.

The ERK/MAPK pathway is activated by stimuli such as growth factors binding to RTKs (17). Once activated, RTKs recruit adaptor proteins, for example growth factor receptor bound protein 2 (GRB2). The SRC homology (SH) 2 and SH3 domains of GRB2 binds son of sevenless (SOS), a protein responsible for exchanging guanosine diphosphate (GDP) for guanosine triphosphate (GTP) to c-rat viral oncogene homolog (RAS), thus converting RAS to its active conformation (18). The GTPase RAS consists of three related family members, which are found mutated in a third of all cancers and may lead to constitutive active downstream signaling (19) (Figure 3B). However, targeting RAS by small-molecular inhibitors has proven difficult as the proteins lack an active site for the inhibitors to bind. Efforts to target the binding

of RAS to farnesyl, which sequesters RAS to the plasma membrane, proved fruitless as the mechanism was compensated by alternative prenylation by geranyl-geranyl in the most commonly RAS mutated members, KRAS and NRAS (20). Downstream of RAS is the MAPKKK RAF proto-oncogene serine/threonine kinase (RAF), which is recruited to the plasma membrane and phosphorylated by GTP-bound RAS through a RAS-binding domain (RBD) on RAF. The serine/threonine protein kinase RAF consists of three members, ARAF, BRAF and CRAF (21). The RAF proteins dimerize, resulting in a catalytically active kinase conformation that phosphorylates and activates its downstream target (Figure 3A), the MAPKK MEK1/2. BRAF is commonly mutated in cancers, which may result in constitutive active kinase signaling independent of RAS (Figure 3C and 3D). Activation of MEK1/2 in turn phosphorylates and activates ERK1/2, which ultimately results in the transcription of genes involved in proliferation. Mutations in the ERK/MAPK pathway in melanoma are described in Section 1.6.

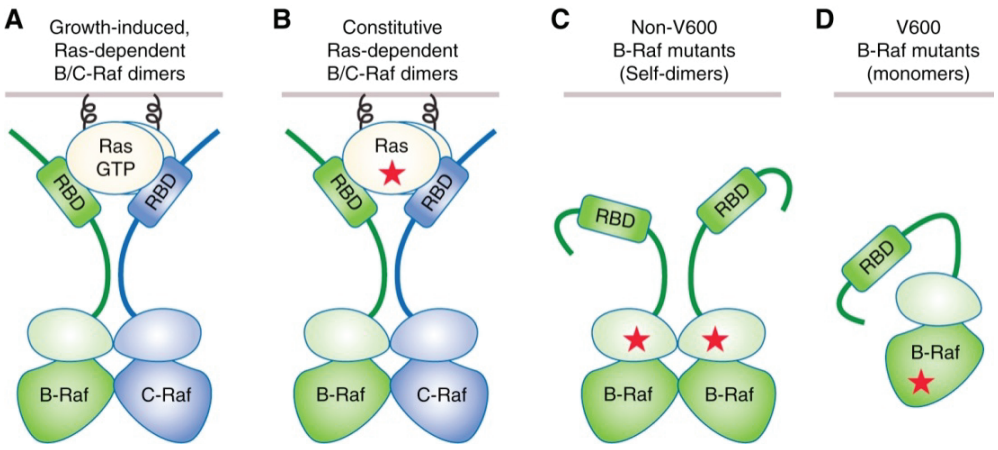

Figure 3. RAF dimerization in normal and BRAF mutated events. In non-malignant cells (A) and in RAS mutated cells (B), RAS-dependent dimerization of (predominantly) BRAF and CRAF is required for downstream signaling. In oncogenic signaling driven by BRAF non-V600 mutations (C), BRAF proteins may dimerize independently of RAS, while BRAF V600 mutants (D) may attribute to downstream signaling as a monomer. Red stars depict mutations. The figure is from Durrant D. and Morrison D.K., Br J Cancer, 2018 (19) and is licensed under a Creative Commons Attribution 4.0 International License (https://creativecommons.org/licenses/by/4.0/). RBD – RAS-binding domain.

The p38/MAPK and JNK/MAPK pathways are mainly activated in response to inflammatory cytokines and cellular stresses, for instance DNA damage, oxidative stress and radiation (22). These external stimuli will activate GTPases, such as RAC and CDC42, to initiate a MAPK cascade that phosphorylates p38 or JNK. p38 is comprised of four isoforms, p38α, p38β, p38δ

and p38γ, that share a great degree of homology and downstream effectors, but are expressed at various sites in the body (22). p38/MAPK downstream signaling is mediated through transcription factors, such as cyclic AMP-dependent transcription factor (ATF2), heat shock proteins and regulatory molecules that are involved in inflammation, chemotactic cell migration and cell differentiation (23). Although p38/MAPK has been implicated in reduced tumor growth, it may also play a pro-oncogenic role in cancer cells (24). This is also the case for JNK signaling. One of the main outcomes of JNK/MAPK is apoptosis through activation or transcription of pro-apoptotic proteins such as cellular tumor antigen p53 (p53), Bcl-2-associated death promoter (BAD) or Bcl-2-associated X protein (BAX) (24). On the other hand, JNK signaling may also result in cell survival through the activator protein 1 (AP-1) (25).

PI3K pathway

The PI3K pathway (Figure 4) is important in many aspects of proliferation and survival and is often mutated and activated in cancers (4). PI3K consists of three classes that have distinct function and regulation (26). Upon RTK activation and autophosphorylation, the p85 (regulatory) and p110 (catalytic) subunits of class IA PI3K will be recruited to the cell membrane to produce phosphateidylinositol-3,4,5-biphosphate (PtdIns(3,4,5)P_2, PIP3) by phosphorylation of PtdIns(4,5)P_2, PIP2). PIP3 phosphorylates and activates protein kinase B (AKT).

The tumor-suppressor protein phosphatase and tensin homolog (PTEN) is responsible for dephosphorylating PIP3 to abolish downstream signaling. Additionally, PI3K subunit p110 may be activated by RAS to drive downstream signaling (26). Through phosphorylation, activated AKT in turn enhances or inhibits activation of several proteins involved in cell survival and cell cycle progression, such as cyclin-dependent kinase inhibitor 1 ($p21^{WAF1/CIP1}$), glycogen synthase kinase 3 (GSK3), mouse double minute 2 homolog (MDM2) and BAD (27), resulting in cell survival. Furthermore, AKT phosphorylates mammalian target of rapamycin (mTOR), leading to enhanced protein synthesis and proliferation through the S6 kinase (27).

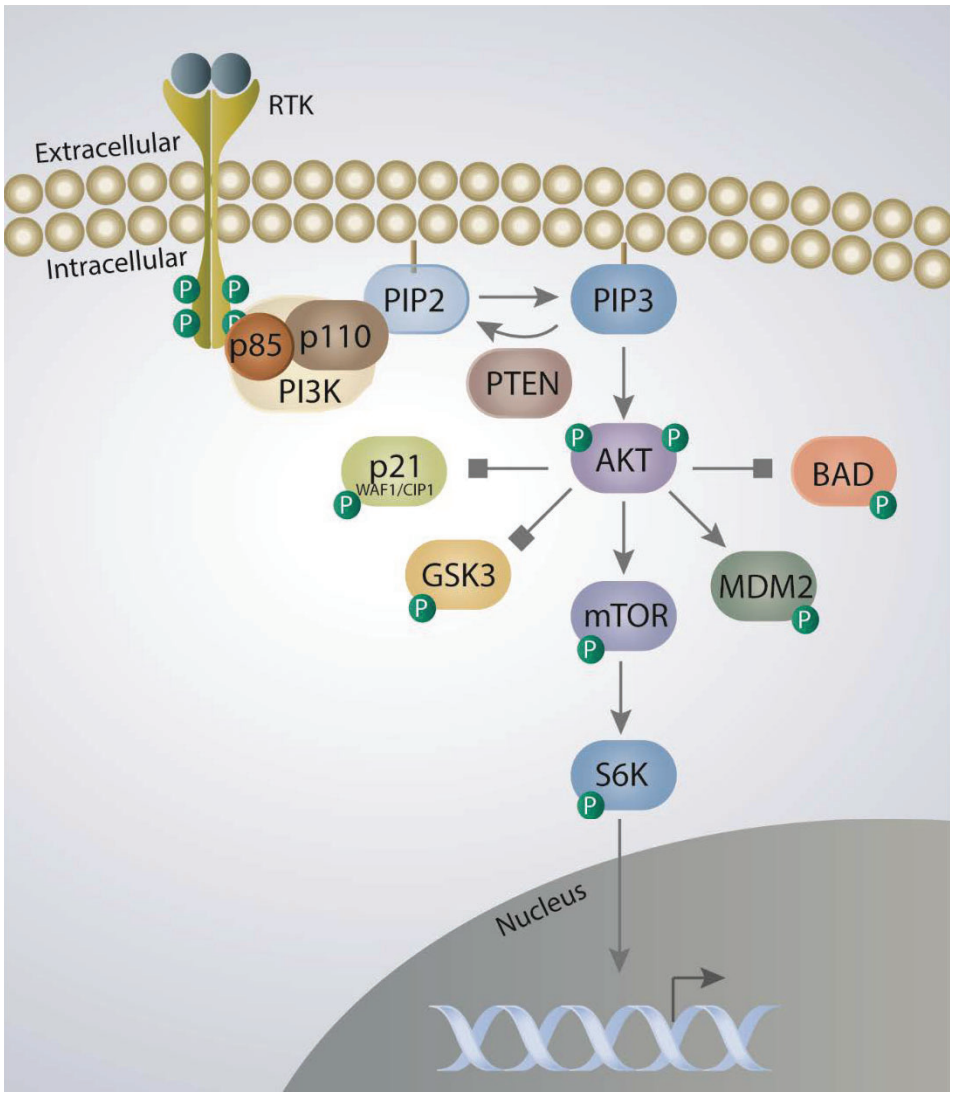

Figure 4. The PI3K pathway. The figure illustrates the PI3K pathway that results in the phosphorylation of AKT, which regulates other proteins resulting in enhanced cell survival and cell cycle progression. Green circles with P depict phosphorylation events and square arrowheads illustrate inhibition. RTK – receptor tyrosine kinase.

There is a substantial amount of crosstalk between the PI3K and ERK/MAPK pathways through various mechanisms, such as negative feedback loops, cross-activation or inhibition or pathway convergence (28). For example, AKT may regulate BRAF, which can promote melanocyte transformation (29). Interactions between PI3K and ERK/MAPK are also prominent in melanoma treatment resistance, which is described in Section 1.6.

Receptor tyrosine kinase AXL

Deriving its name from the Greek word “anexelekto”, meaning uncontrolled, RTK AXL was first characterized in 1991 as a transforming gene in chronic myelogenous leukemia (30). Together with tyrosine-protein kinase receptor TYRO3 (TYRO3) and tyrosine-protein kinase MER (MER), AXL forms the TAM-family. The TAM-family members are structurally alike, with an N-terminal extracellular domain, a transmembrane domain and an intracellular tail (31). The extracellular region is comprised of two fibronectin type III domains and two immunoglobulin (Ig)-like domains (Figure 5A) (31). For AXL, the tyrosine kinase domain includes an adenosine triphosphate (ATP) binding site that docks the tyrosine binding and SH2 domains on intracellular signaling proteins. Additionally, the cytoplasmic tail of AXL contains several tyrosine residues that may be phosphorylated, which represents activation of the protein (32). Three of these, Y698, Y702 and Y703, are conserved among the TAM-family members and are phosphorylated in response to ligand binding (32).

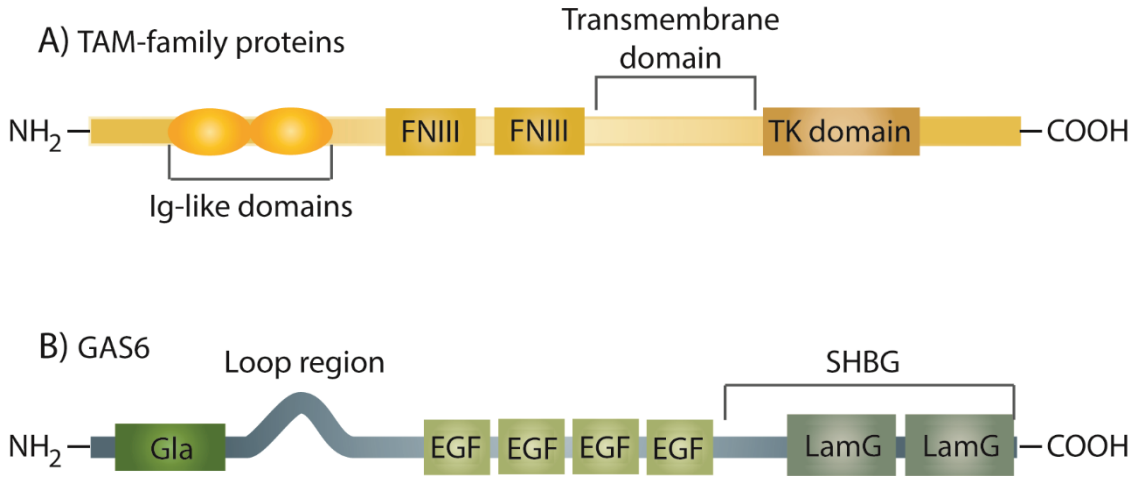

Figure 5. The domains of TAM-family proteins and GAS6. The figure illustrates the domains of A) TAM-family member proteins and B) the ligand GAS6. Ig – immunoglobulin, FNIII – fibronectin type III, TK – tyrosine kinase, Gla –γ-glutamic acid-rich domain, EGF – epidermal growth factor repeat, LamG – laminin G-like, SHBG – sex binding hormone globulin. The figure is inspired by Wu, G., et al, Cell Death Dis., 2017 (33).

The TAM-family shares the ligand growth arrest-specific protein 6 (GAS6) with AXL having the highest affinity (34). GAS6 contains a γ-glutamic acid-rich domain (Gla) (Figure 5B), which is γ-carboxylated in a vitamin K-dependent process (Figure 6). Subsequently, GAS6 may bind phosphatidylserines (PtdSer), which are commonly found on the inner part of the plasma membrane but are flipped to the on the outer leaflet under certain conditions, such as apoptosis (35). There are ambiguous reports of the importance of the γ-carboxylation process and PtdSer-

binding of GAS6 to activate the TAM-family proteins. However, it seems that these mechanisms are important for increasing binding affinity to the TAM-family proteins and thus, yields a higher activation (36-38).

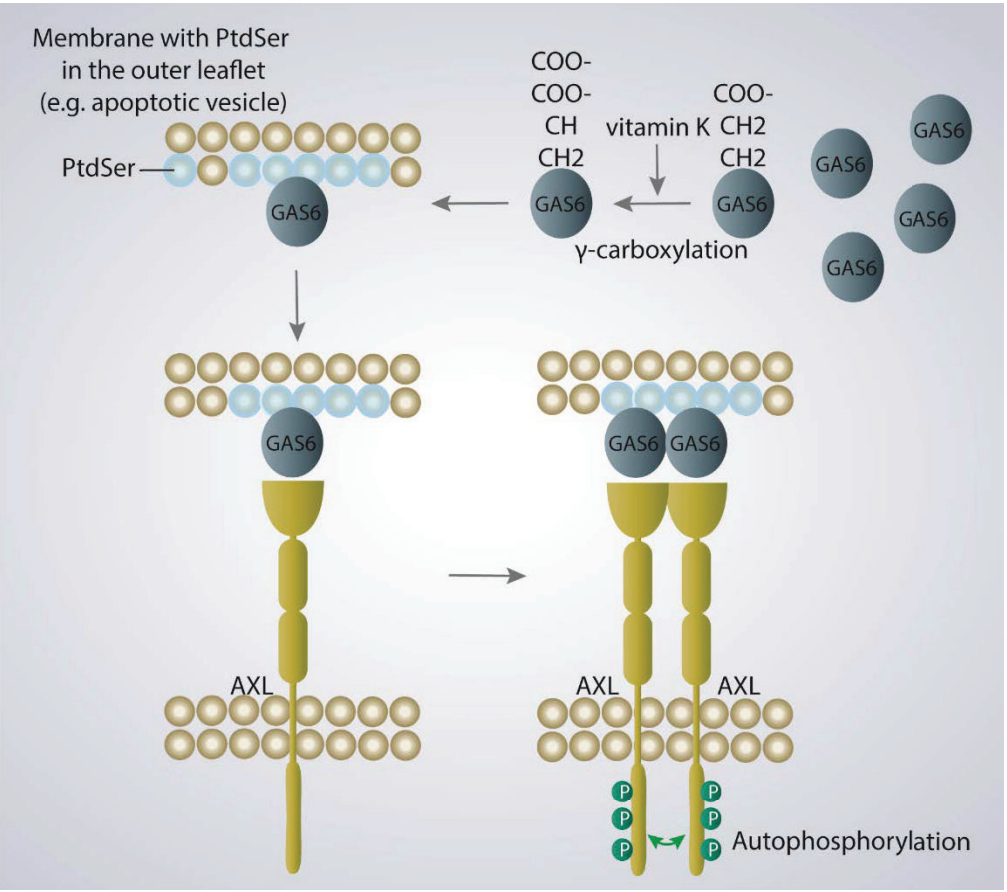

Figure 6. GAS6 and AXL activation. The figure shows the activation of GAS6 by vitamin K-dependent γ-carboxylation and binding to phosphatidylserines (PtdSer). These processes optimize binding of GAS6 to AXL, which leads to AXL dimerization with other GAS6:AXL complexes and activation through autophosphorylation. Green circles depict phosphorylation events.

When GAS6 binds, GAS6:AXL complexes will dimerize, leading to autophosphorylation and activation of AXL. Additionally, other TAM-receptors or RTKs (e.g. fibromyalgia-like tyrosine kinase 3 (FLT3)) may dimerize with AXL to activate the proteins (39) (Figure 7A). Additionally, ligand-independent activation by dimerization with other transmembrane receptors (e.g. epidermal growth factor receptor (EGFR)) or extracellular binding of AXL proteins present on neighboring cells may occur (40) (Figure 7B). Ligand-independent activation of AXL may be more pronounced when AXL is overexpressed and could thus be a more prominent activation process in conditions where AXL is highly expressed, such as cancer (41).

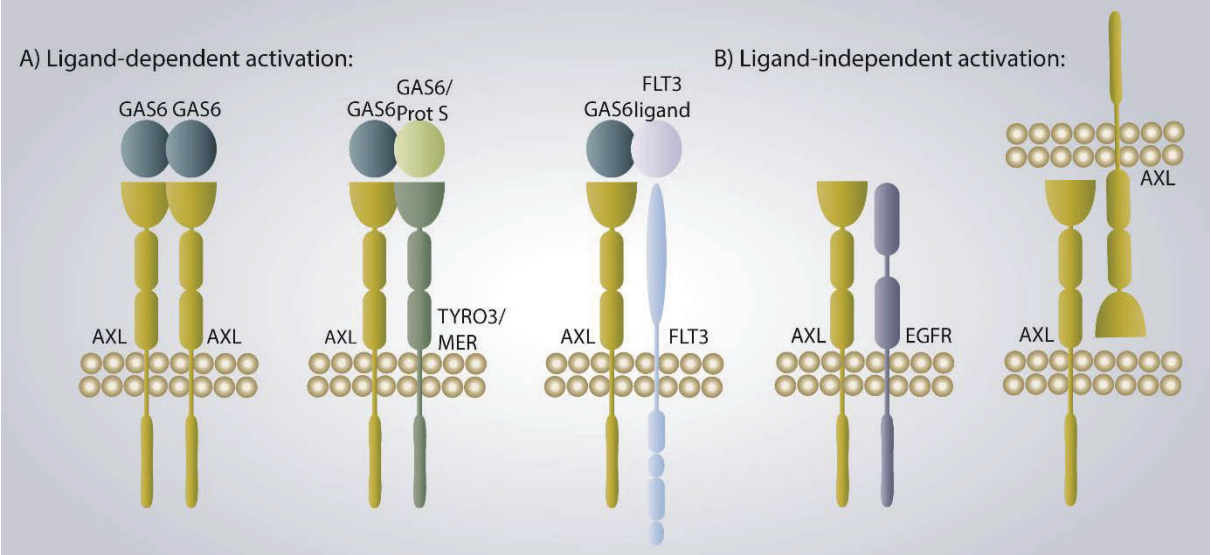

Figure 7. AXL activation. AXL activation may be A) ligand-dependent through dimerization and autophosphorylation with other AXL proteins (left), the other TAM-family members TYRO3 or MER (middle) or other RTKs, such as FLT3 (right) or B) ligand-independent through dimerization with other transmembrane receptors, such as EGFR (left) or AXL proteins present on other cells (right). Prot S - Protein S.

In normal cells and tissues, AXL is universally expressed and is found in endothelial cells, macrophages, platelet cells, skeletal muscle, brain, heart, kidney, liver and testis (42). AXL can be cleaved both on the extracellular and intracellular domain (43, 44). A disintegrin and metalloproteinase domain-containing proteins (ADAM) 10 and 17 are known to cleave AXL on its extracellular domain to yield a soluble isoform (sAXL), which has been found elevated in cancers and vascular and immunogenic diseases (44-49). sAXL has been reported to bind GAS6 present in the blood and may act as an inhibitor of the protein (43). Oppositely, ligand-independent activation through dimerization with the extracellular soluble AXL domain could occur. The intracellular domain is cleaved by γ-secretases and may be transported into the nucleus, a process suggested to play a role in chemoresistance (44).

AXL may activate several pathways important for tumor progression (Figure 8). For instance, AXL activation results in augmented signaling through the MAPK cascades p38/MAPK and ERK/MAPK to increase proliferation and migration (50). In addition, it is shown that the p85 subunits of PI3K interact with AXL by binding to tyrosine 779 and 821 on its intracellular tail (51). Inhibition or reduced expression of AXL results in decreased activation of PI3K (52, 53), which is an important signaling pathway in cell survival, as described previously. In line with this, knockdown of AXL is shown to increase activation of BAD and induce apoptosis (54).

The TAM-family proteins have been found to be important in preventing auto-immunity by dampening pro-inflammatory cytokine production through Toll-like receptors and tumor necrosis factor (TNF)-α signaling (55) (Figure 8). In line with this, TAM-family knockout or inhibition *in vivo* resulted in an over-active immune system through enlarged lymphoid organs and enrichment of immune cells (56), and induced the anti-metastatic potential of natural killer (NK) cells (57). AXL may therefore aid in preventing a successful immune response in cancers. In line with this, AXL inhibition is currently being tested in clinical trials in combination with immunotherapy.

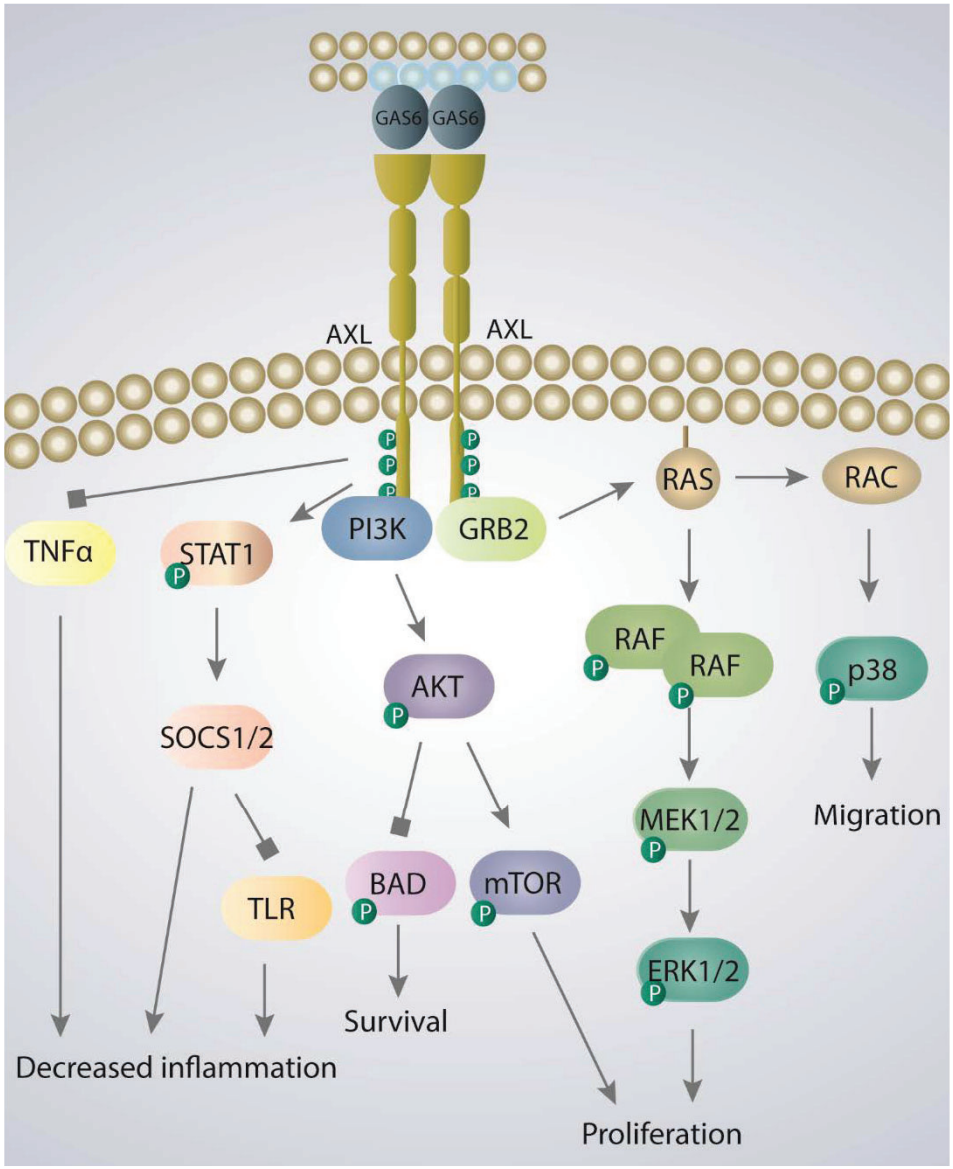

Figure 8. AXL signaling. The figure shows an overview of downstream events of AXL activation by GAS6. TLR – Toll-like receptor. Green circles depict phosphorylation events.

AXL expression is positively correlated with expression of transcription factors of EMT, such as zinc finger protein SNAI1 (SNAIL), zinc finger protein SNAI2 (SLUG), twist-related protein (TWIST) and zinc finger E-box-binding homeobox 2 (ZEB2), and the mesenchymal marker vimentin (58, 59). Furthermore, AXL is inversely linked to microphthalmia-associated transcription factor (MITF) (60), a transcription factor involved with cell differentiation.

Additionally, AXL expression may be induced by treatment and its expression is associated with reduced sensitivity to several inhibitors (61). There are various proposed mechanisms underlying AXL-mediated treatment resistance. For example, AXL contributes to PI3K inhibitor resistance by PI3K-independent mTOR activation through dimerization with EGFR (62). It is further shown that AXL confers treatment resistance to various chemotherapeutic drugs. For instance, AXL expression promoted cisplatin resistance in esophageal cancer by inhibiting tyrosine-protein kinase ABL1 (c-Abl)/tumor protein p73 (p73) signaling (63), doxorubicin resistance in breast cancer by promoting β-catenin expression through AKT/GSK3 signaling (64), and gemcitabine resistance in pancreatic cancer by modulating the immune response (65). Furthermore, inhibition of AXL is shown to result in accumulation of DNA damage (66). It has been reported that small-molecular inhibitors or monoclonal antibodies targeting AXL together with inhibitors targeting BRAF, vascular endothelial growth factor (VEGF), EGFR, WEE1-like protein kinase (WEE1), Poly [ADP-ribose] polymerase (PARP) or chemotherapy result in decreased proliferation compared to corresponding monotherapies (66-71).

AXL is rarely amplified or mutated in cancers, but its protein expression is often upregulated (61). AXL expression is heightened in tumors and is correlated with drug resistance, increased metastatic potential and increased mortality (72-74). Several AXL inhibitors and antibodies are currently in phase I or II clinical trials, alone or in combination with immunotherapy (NCT03184571), EGFR inhibitors (NCT02424617) or chemotherapy (NCT03649321, NCT03607955).

1.4 The cell cycle and DNA damage response

The cell cycle

The essential role of the cell cycle is to accurately copy the chromosomes and precisely segregate the duplicates to yield two identical daughter cells. The cell cycle is divided into four phases; G1, S (DNA synthesis), G2 and M (mitosis), as illustrated in Figure 9. The G1, S and G2 phases are grouped as the interphase, where the cells grow and replicate before cell division in the M phase. In the G1 phase the cells are metabolically active and will grow, but not divide. DNA synthesis occurs in the S phase, while the G2 phase includes continued growth and protein synthesis in preparation for the cell division that takes place in the M phase (75). However, most normal cells reside in a non-dividing state, which may be temporary (quiescence) or permanent (senescence) (76).

The progression through the cell cycle needs to be heavily regulated to prevent uncontrolled cell division and is managed by both external and internal signals. There are various regulatory points throughout the cell cycle that determine if the progression is as intended. The major cell cycle checkpoint is the restriction point, occurring in late G1, which controls the progression to the S phase (77). Unfavorable conditions in the gap phases (G1 and G2), may halt the progression into the next phase, turn cells quiescent or senescent, or lead to apoptosis (78).

In addition to being controlled by extracellular growth factors and nutrient demands, the cell cycle is administered by internal signals that make sure all the events occur at the intended time and order. Flaws in the cell cycle progression, such as an incompletely replicated genome or damaged chromosomes, arrest the cell cycle until the error has been amended (79). Central to the regulation of the cell cycle are the cyclin-dependent kinases (CDKs). The CDKs themselves are tightly regulated by phosphorylation, by binding of their activating partners, the cyclins, and their inhibitors, the cyclin-dependent kinase inhibitors (CKIs) (75). Overview of central CDKs, cyclins and CKIs are displayed in Figure 9.

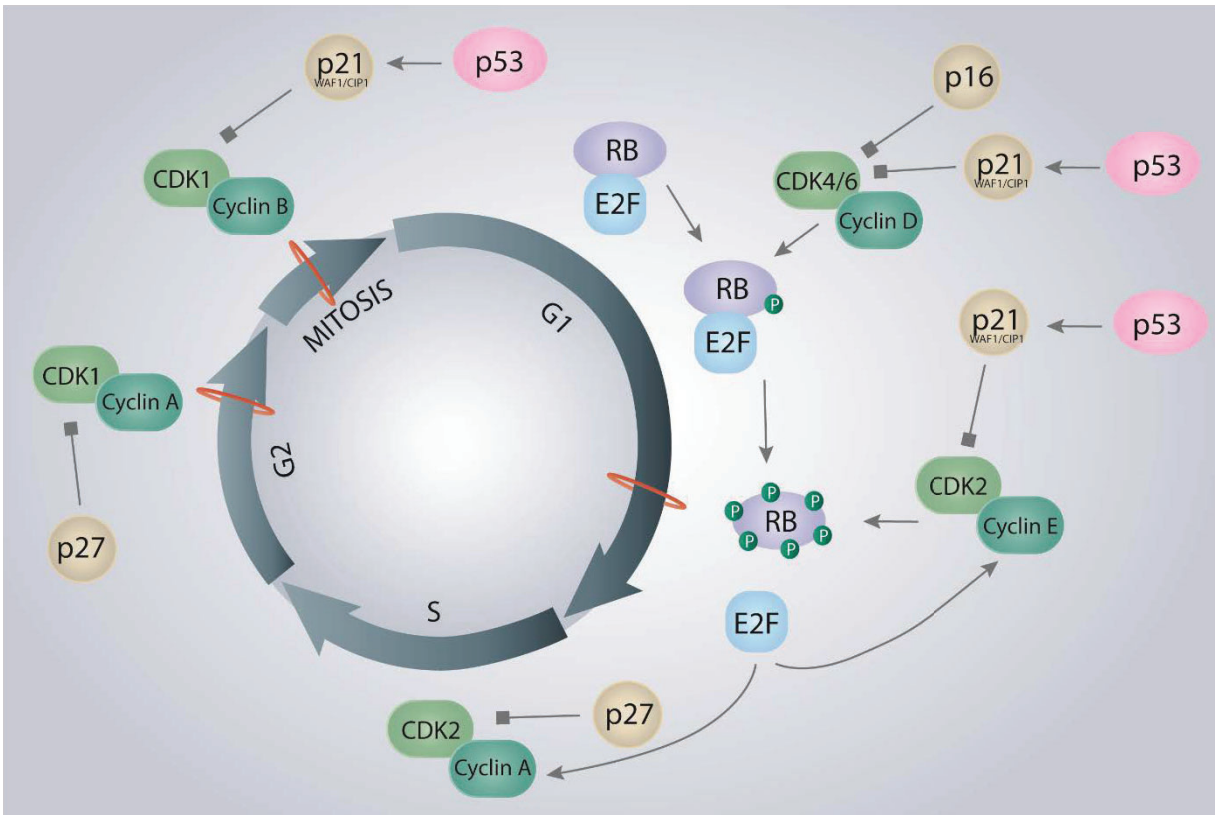

Figure 9. The cell cycle and its regulation. An overview of the cell cycle with central cyclins, CDKs and CKIs. Additional regulators are p53 that may activate $p21^{WAF1/CIP1}$ and retinoblastoma (RB) that binds the transcription factor E2F. Phosphorylation of RB by cyclin D/CDK4/6 and cyclin E/CDK2 releases E2F, resulting in the transcription of genes coding for instance for cyclin A and cyclin E. Square arrowheads depict inhibition, the three red rings illustrate the major checkpoints in the cell cycle and green circles depict phosphorylation events.

Furthermore, the tumor-suppressor p53, often termed "the guardian of the genome", is a transcription factor that responds to various stress signals, such as DNA damage and oncogenic activity (80). Many of its target genes are involved with processes such as cell cycle arrest and/or apoptosis. For example, p53 may increase expression of $p21^{WAF1/CIP1}$ (inhibitor of CDK4/6, CDK2 and CKD1 binding to their respective cyclins) to promote G1 or M arrest. In addition, p53 may activate the pro-apoptotic protein BAX which results in the release of cytochrome c from the mitochondria (81). This in turn, can result in the cleavage and activation of caspases, proteases that are a vital part of apoptosis by degrading cellular components.

DNA damage response

The cells are continuously exposed to variables that can lead to DNA damage. These events may be external, such as ultraviolet radiation or chemical exposure, or internal, such as accumulation of reactive oxygen species (82). Coping with DNA damage is crucial to maintain genomic integrity. Thus, cells contain several proteins that detect and activate pathways in response to DNA damage that lead to DNA repair, cell cycle arrest or apoptosis. Inadequate regulation of the DNA damage response (DDR) may lead to accumulation of DNA damage in the daughter cells, which is common in cancer (83). Maintaining genomic instability is one of the enabling characteristics in the hallmarks of cancer (5). DNA damage may present itself in various manners, such as base modifications and single or double-stranded breaks, which result in the activation of different repair and signaling pathways (84). Of these, DNA double-stranded breaks might be the most obstructing as it incapacitates processes such as DNA replication and may cause chromosomal translocations (85). DNA double-stranded breaks are often caused by ionizing radiation. In response to DNA damage, the ataxia-telangiectasia mutated (ATM) and ATM- and Rad3-Related (ATR) kinases activate serine/threonine-protein kinase CHK (CHK) 1 and CHK2 (83). While there is substantial crosstalk between the ATM and ATR pathways, ATM is mainly activated in response to double-stranded breaks caused by radiation and genotoxicity and activates CHK2, while ATR activates CHK1 in response to for instance oxidative damage and blocked replication (86). Within minutes of double-stranded breaks, ATM may additionally phosphorylate H2A histone family member X (H2AX), which attracts DNA repair proteins to the damaged site and induce a positive feedback loop that activates other H2AX and ATM proteins (87). In parallel, downstream effects of ATM and ATR signaling through CHK1 and CHK2 may include activation of p53 and inhibition of M-phase inducer phosphatase 3 (CDC25C) activity to induce apoptosis or cell cycle arrest (88).

Using DDR inhibitors to treat cancer patients may seem counter-intuitive, as obstructing mutations in central genes of the DDR pathways is found in several types of cancers (89). Additionally, a predisposition for cancer is seen in individuals with germline mutations in principal components of DNA repair and the DDR pathways (90). While genomic instability by excluding one of the two DDR pathways may offer evolutionary advantages for cancer cells, it also makes them heavily reliant on the other. Thus, inhibiting the remaining DDR pathway can lead to cell death in cancer cells, while normal cells that have both DDR pathways intact are able to survive. This phenomenon is an example of synthetic lethality (Figure 10). This

principle is exploited for example in the use of PARP inhibitors for *BRCA1/2* mutated breast and ovarian cancers. *BRCA1/2* mutations render the cells deficient in homologous repair, while inhibition of PARP result in an inability to facilitate DNA repair, and thus, inhibition of PARP in *BRCA1/2* mutated cells may result in cell death (91).

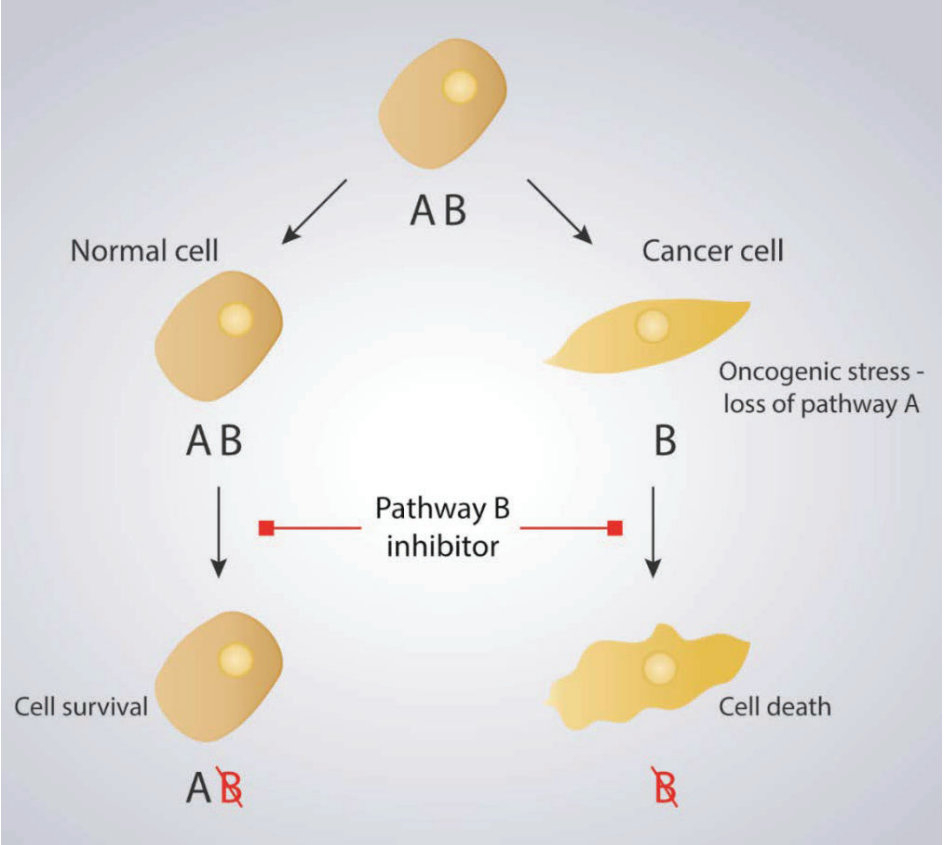

Figure 10. Synthetic lethality in cancer cells. Oncogenic stress may lead to the loss of DNA damage response (DDR) pathways (depicted as A in the figure) that can be exploited to induce synthetic lethality by inhibiting the remaining DDR pathway (depicted B), which may result in cell death. Figure inspired by O'Connor M.J., *Molecular Cell,* 2015 (92).

Additional targets of the DDR pathway include blockade of the ATM/ATR-CHK1/CHK2 pathways (93). For instance, ATR inhibitor VE-822, is currently in clinical trials alone (NCT02487095) or in combination with chemotherapy (NCT02723864). Although treatment with CHK1 inhibitor LY2603618 in combination with chemotherapy increased progression-free survival (but not overall survival) compared to chemotherapy alone in non-small cell lung cancer (NSCLC), continued treatment was halted due to adverse effects (94). Likewise, treatment with CHK1/CHK2 inhibitor AZD7762 resulted in cardiac toxicity (95). Further, LY2603618 in combination with chemotherapy did not improve overall survival compared to chemotherapy alone in pancreatic cancer (96).

1.5 Immune system and cancer

Parts of this chapter is based on the following reviews: Flem-Karlsen et al., B7-H3 in Cancer - Beyond Immune Regulation. *Trends in Cancer*, 2018 (97) and Flem-Karlsen et al., B7-H3 immune checkpoint protein in human cancer. *Current Medicinal Chemistry*, 2019 (98).

The immune system protects the body from pathogens and stress. Additionally, the immune system is crucial in battling cancer, where inflammation and immune evasion has emerged as hallmarks of cancer progression (5). The immune system consists of an intricate system of cells and soluble factors that work together to maintain or restore body homeostasis. Especially important in cancers are the T cells, especially T cell surface glycoprotein CD8 positive ($CD8^+$) cytotoxic T cells that detect and eliminate malignant cells (99).

Naïve T cells are activated when the major histocompatibility complex (MHC) on antigen-presenting cells (APC) bind the T cell receptor. This interaction is regulated by immune checkpoint proteins that administer a secondary activation or inhibition signal. Several of these signals can be provided by proteins of the B7 family present on APCs. B7 family binding either act inhibitory or stimulatory on the T cells depending on the B7 family member and which receptor it binds (100). For instance, the T lymphocyte activation antigens CD80 (B7-1) and CD86 (B7-2) may bind T cell-specific surface glycoprotein CD28 (CD28) on the T cell to induce a co-stimulatory signal to activate the immune system. Oppositely, the same proteins can bind cytotoxic T lymphocyte protein 4 (CTLA-4) resulting in an inhibition of T cell activity (101). In the past few years, therapeutic focus for many cancers has been on developing inhibitors that target several immune checkpoint proteins. The aim of this treatment is to remove the breaks on T cell activation, leading to a mobilized immune response that may improve the detection and destruction of cancer cells by the immune system. To date, the focus has principally been on targeting programmed cell death protein 1 (PD-1) and CTLA-4, transmembrane proteins present on T cells that may bind B7 family members to regulate T cell activation (102), in addition to targeting B7 family member programmed cell death 1 ligand 1 (PD-L1, also known as B7-H1). PD-1 inhibitory antibodies prevent the PD-1 immunosuppressive role by blocking its binding to both PD-L1 and programmed cell death 1 ligand 2 (PD-L2, also known as B7-DC), while PD-L1 inhibitory antibodies prevent immunosuppression by blocking PD-1/PD-L1 interaction. Targeting immune checkpoint proteins has been demonstrated to be a successful therapeutic strategy in many forms of cancer,

with some patients obtaining long-lasting responses. Favorable outcomes of immune checkpoint inhibitors are especially prominent in cancers with a high degree of somatic mutations, such as melanoma and lung cancer (103), However, many patients experience little beneficial effects, and/or develop resistance to immunotherapy, emphasizing the need to find clear biomarkers to distinguish patients who will respond to this treatment (104).

B7 family of immune checkpoint proteins

The B7 family is part of the immunoglobulin (Ig) superfamily. It consists of ten known members that contains Ig constant- (IgC) and Ig variable- (IgV) like domains, a transmembrane domain and a cytoplasmic tail (105). Many of the B7 family proteins are found to bind receptors of the CD28/CTLA-4 family through their Ig-like domains (101). Figure 11 shows the B7 family members present on APCs and their co-inhibitory receptors on T cells.

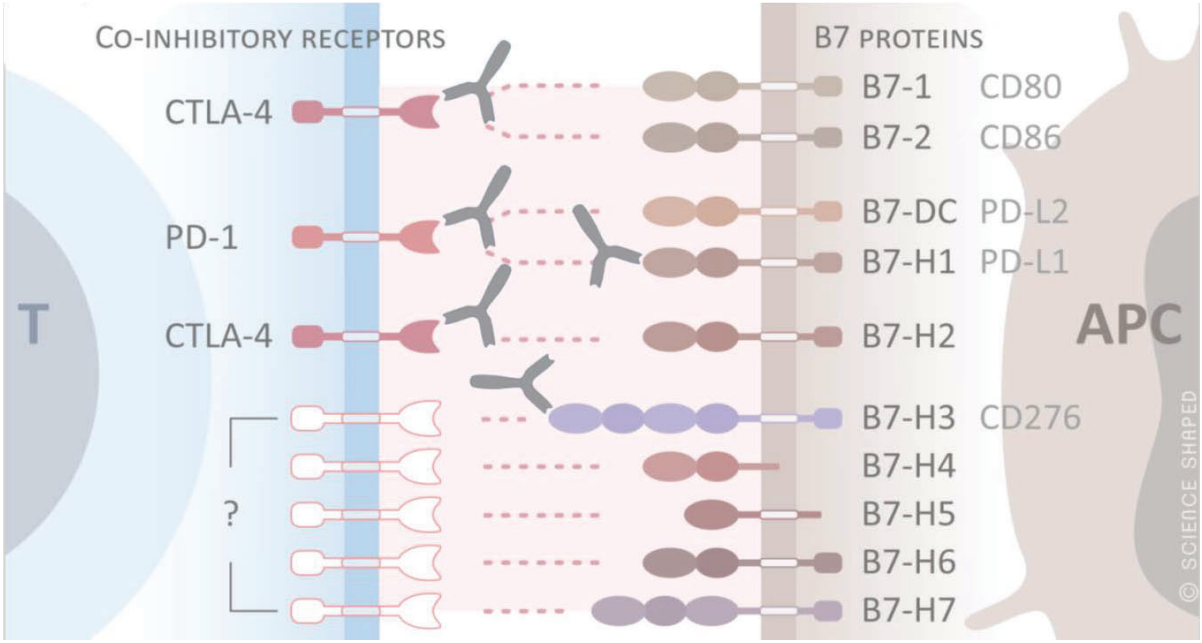

Figure 11. B7 family and their co-inhibitory receptors on T cells. The figure illustrates the B7 family members present on antigen-presenting cells (APC) and their co-inhibitory receptors on T cells. Current immunotherapeutic antibodies in clinical use (targeting CTLA-4, PD-1 and PD-L1) or clinical trials (targeting B7-H3) are indicated with a grey antibody molecule. The figure is modified with permission from Flem-Karlsen, K. *et al,* Curr Med Chem, 2019 (98).

B7-H3: an immunoregulatory and pro-oncogenic protein

In normal cells, B7-H3 messenger ribonucleic acid (RNA) (mRNA) is present in most tissues. However, the protein is expressed at low levels, suggesting a tight post-transcriptional regulation (106). B7-H3 is mainly present on the cell surface but is also detected in the cell nucleus (107). Furthermore, we have previously observed B7-H3 expression in intracellular and extracellular vesicles (108). The protein has been observed as a soluble isoform (sB7-H3) generated from alternative splicing (109) or cleavage by matrix metalloproteinases (MMP) of the membrane-bound protein (110).

B7-H3 is proposed to have an immune regulatory role and is expressed on APCs, T cells, NK cells, macrophages and dendritic cells (106, 111, 112). The binding partner(s) of B7-H3 are currently unknown. B7-H3 has been found to bind activated T cell surface glycoprotein CD4 positive ($CD4^+$) and $CD8^+$ T cells and is proposed as both a T cell co-stimulatory and co-inhibitory protein (113). This suggests that B7-H3 may have at least two binding partners on the T cells and that the opposing regulation of the immune response may depend on which protein it binds. In line with this, B7-H3 is found to both enhance inflammation (114) and suppress the immune response (115). This interpretation is strengthened by the fact that other B7 family members can act both co-inhibitory and co-stimulatory.

B7-H3 expression is increased in cancer cells and B7-H3 is emerging as a pro-tumorigenic protein independently of its immune regulatory roles. Apart from a few opposing results, reports state an association between high expression of B7-H3 and increased metastasis and tumor grade, and thus reduced overall survival (98). Overexpression of B7-H3 *in vitro* and *in vivo* has resulted in increased cell proliferation, migration and invasion, while the opposite is observed when B7-H3 expression is decreased or when cells are treated with an inhibitory B7-H3 monoclonal antibody (116-118). B7-H3 expression is found to induce activation and signaling through major cancer pathways such as PI3K and signal transducer and activator of transcription 3 (STAT3) (119, 120) (Figure 12).

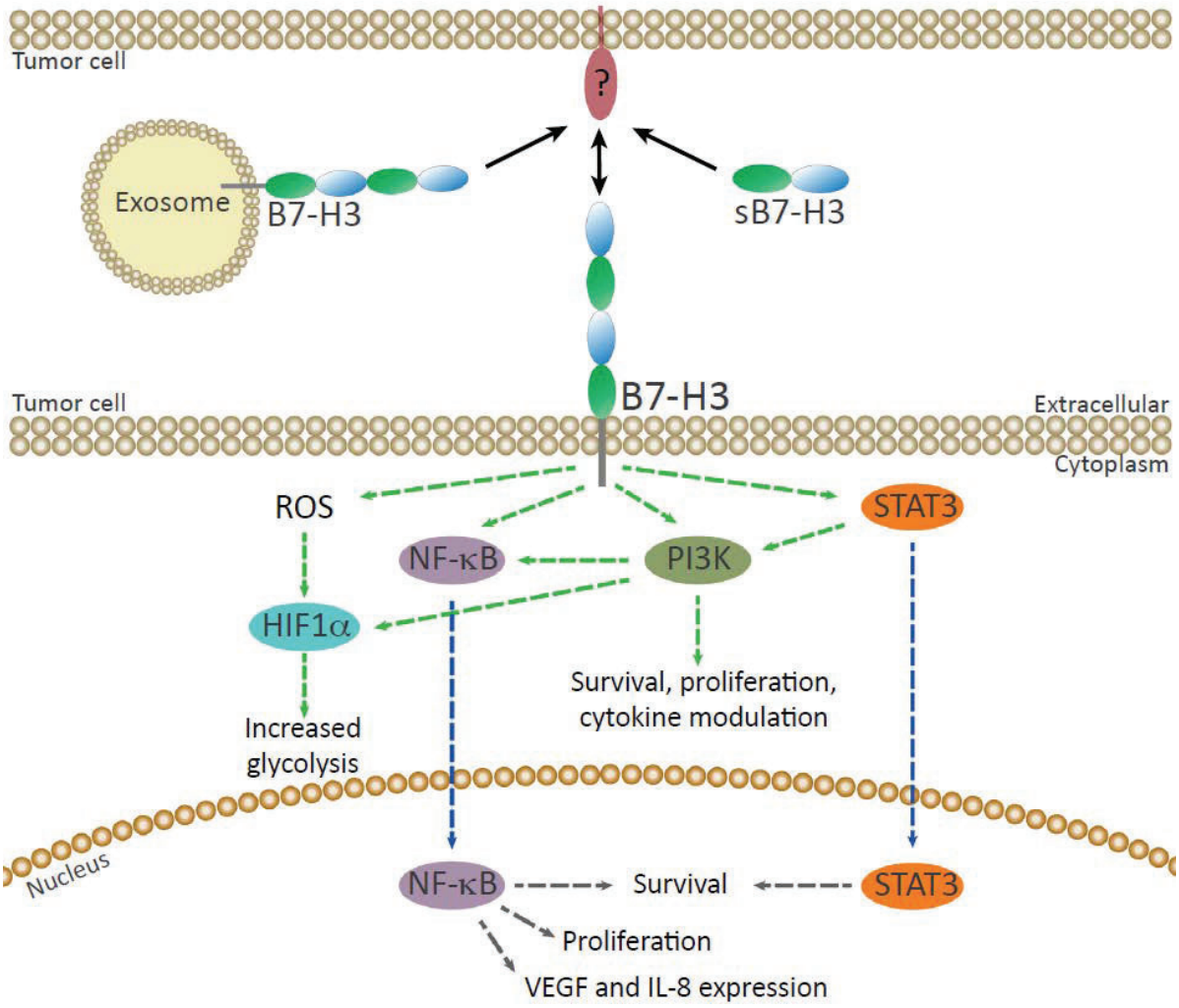

Figure 12. B7-H3 signaling. The figure illustrates the interaction between B7-H3 and its unknown ligand(s) in addition to downstream signaling. sB7-H3 – soluble B7-H3, ROS – reactive oxygen species. The figure is reused with permission from Flem-Karlsen, K. *et al,* Trends Cancer, 2018 (97).

Furthermore, B7-H3 expression has been associated with treatment resistance to chemotherapy and targeted therapies (98). We have previously demonstrated that abolished B7-H3 expression increases sensitivity to dacarbazine (DTIC) chemotherapy and ERK/MAPK and PI3K inhibitors in melanoma cells, and PI3K inhibitors in breast cancer cells (108, 121). B7-H3 is shown to mediate paclitaxel chemotherapy resistance in breast cancer cells by upregulating the tyrosine protein kinase JAK (JAK)2/STAT3 pathway. Additionally, B7-H3 is reported to mediate chemoresistance to oxaliplatin chemotherapy in colorectal cancer cells by upregulating aerobic glycolytic enzyme hexokinase 2 through STAT3 signaling (122). Others and we have shown that B7-H3 expression is associated with a higher glycolytic rate (108, 121, 123). B7-H3 may induce aerobic glycolysis by upregulating reactive oxygen species and stabilizing hypoxia-induced factor 1 (HIF-1) (124).

B7-H3 may promote EMT by activating the transcription factors mothers against decapentaplegic homolog 1 (SMAD1) and SLUG through PI3K and JAK/STAT3 signaling (125, 126). B7-H3 can also regulate expression of cytokines and metalloproteinases that promote metastasis, such as interleukin (IL)-8, MMP-2, TIMP metalloproteinase inhibitor (TIMP)-1 and TIMP-2 (116, 127).

Due to its high expression on cancer cells compared to normal cells, B7-H3 represents a potential biomarker as well as a therapeutic target. B7-H3 monoclonal and bi-specific antibodies are currently in phase I/II clinical trials in patients with B7-H3 positive cancer cells, alone or in combination with CTLA-4 antibody ipilimumab (NCT02381314) or PD-1 antibody MGA012 (NCT03729596) or pembrolizumab (NCT02475213). Further, recent studies have shown potential for B7-H3 chimeric antigen receptor (CAR) T cell therapy (128). In line with this, a phase I/II clinical trial utilizing B7-H3 CARs has been initiated (NCT04077866).

1.6 Melanoma

Melanoma is a type of cancer that develops from melanocytes, which are melanin-producing cells primarily located in the skin. Melanocytes produce melanin to protect cell nuclei from ultraviolet radiation (129). Once produced, melanin is contained in organelles called melanosomes, which can be transported to nearby keratinocytes, the predominant cell in the outer layer of the skin, resulting in skin pigmentation (129). In many cases, excess ultraviolet radiation (or in some cases, somatic mutations or inherited genes) turn melanocytes malignant, resulting in the formation of a tumor type, melanoma, which if it spreads, is notorious for its heterogeneity and treatment resistance. Melanomas are classified according to the TNM system, which considers characteristics of the tumor and the number and location of metastases, if any, to determine stage (130). The clinical stage groups range from 0-IV, where stage III and IV comprise cases where the cancer has metastasized to regional lymph nodes or distant sites, respectively (Figure 13).

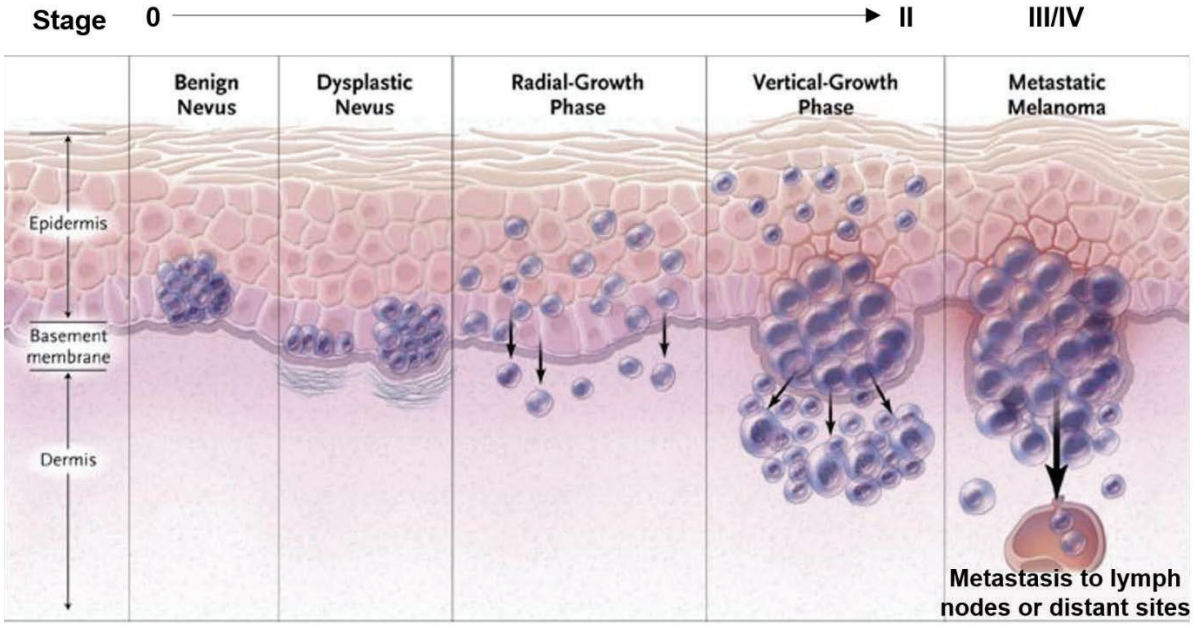

Figure 13. Progression of melanoma. The development from a benign nevus to metastatic melanoma. The figure is modified with permission from Miller, A. J., Mihm, M.C., N Engl J Med, 2006 (131), copyright Massachusetts Medical Society.

Epidemiology and risk factors

Norway has one of the highest melanoma incidences in the world, with over 2000 new cases per year (2). The Norwegian Cancer Registry reports a 20% increase in melanoma cases in the last five-year period (2013-2017) compared to the previous one (2008-2012) and the incidence is expected to rise (Figure 14) (132).

Several factors contribute to the development of melanoma, with the most prevalent being exposure to ultraviolet radiation through natural sunlight and tanning beds and increased age (131). While many cancers arise among older adults and the elderly, melanomas have a high incidence among young adults (2). Especially how an individual respond to ultraviolet radiation plays a role in the risk of developing melanoma, which depends on factors such as skin pigmentation and number of nevi. Additionally, around 5-10% of melanomas are mainly caused by inherited germline mutations, most notably in *CDKN2A* and *CDK4* (133). This also includes mutations in *MC1R*, which may lead to fair skin and red hair and alter the pigment production, which increases sensitivity to ultraviolet radiation (133).

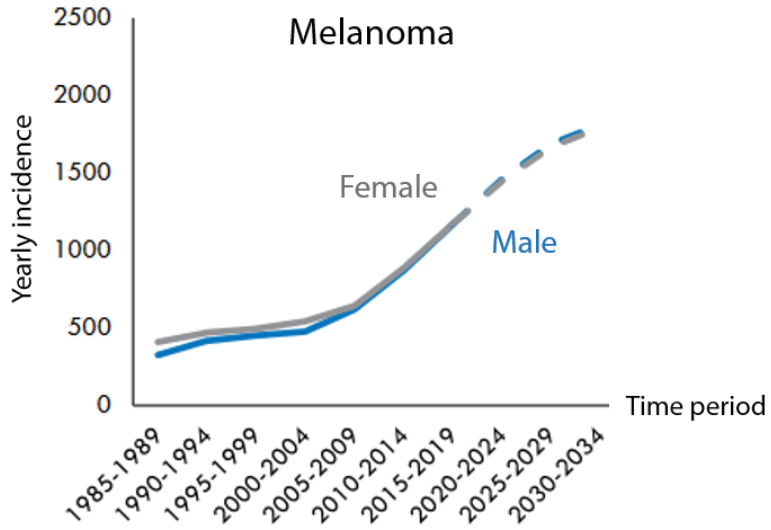

Figure 14. Past and projected yearly incidence of melanoma in Norway. The Figure shows 5-year intervals of the yearly incidence of melanoma from 1985-2019 and the projected yearly incidence from 2020-2034 based on gender. The projected incidence is calculated by Oslo Economics using data from the Cancer Registry of Norway. The figure is modified from (134) with permission by the authors.

An important prognostic factor of melanoma is the vertical depth of the primary tumor (Breslow depth) (131). If operated, patients with primary melanomas below 1 mm Breslow thickness and no metastasis have a high survival rate (Table 1). Additional prognostic factors include lactate dehydrogenase (LDH) levels, ulceration and mitotic number (130). However, the most important prognostic factor is metastasis, particularly if the melanoma cells have spread to distant organs. Five-year survival grouped by metastatic spread is presented in Table 1.

Table 1. Five-year relative survival in melanoma

	Relative survival, %	
Stage	**Female**	**Male**
Localized	95.1	91.0
Regional	67.1	67.1
Distant	39.8	22.9
Uknown	74.0	57.2
Overall	91.7	85.5

Table 1. Five-year relative survival in melanoma. The table list the percentage five-year relative survival in melanoma patients in Norway grouped the spread of the cancer and by gender. Data is from the Cancer Registry of Norway (2).

Molecular classification and signaling

Melanomas have a high prevalence of mutations, where most are due to mutagenic exposure from ultraviolet radiation (135). There have currently been suggested four molecular subtypes of advanced melanoma, based on mutations in oncogenes or tumor-suppressor genes resulting in cell proliferation. The molecular subtypes are based on mutations in *BRAF*, *NRAS*, *NF1,* or none of these genes (136).

About half of melanoma patients harbor a mutation in the *BRAF* gene, which codes for a protein that is part of the signaling cascade ERK/MAPK, as described in section 1.3. About 90% of the *BRAF* mutations are at position 600 ($BRAF^{V600}$), which is part of the activation segment of the kinase domain (137). The most common of these is substitution of valine (V) to glutamic acid (E) ($BRAF^{V600E}$), while substitutions to lysine ($BRAF^{V600K}$), aspartate ($BRAF^{V600D}$) or arginine ($BRAF^{V600R}$) are also found. These mutations result in a constitutively active protein, leading to increased kinase activity and increased ERK/MAPK signaling (138). Further, approximately 20% of melanoma patients have a mutation in the *NRAS* gene, also resulting in a constitutively active ERK/MAPK signaling pathway, where the most commonly mutated site is the glutamine in position 61 ($NRAS^{Q61}$) (136). It was long thought that the *BRAF* and *NRAS* mutations were mutually exclusive. However, sequencing efforts have identified incidences where both these mutations preside in the same tumors, even within the same cell (139). Another important signaling pathway is PI3K, and *PIK3CA* (activator of the PI3K pathway) is mutated in 6% of melanomas (140)*. Additionally, mutations in the tumor-suppressors *TP53* (encoding p53), *PTEN* (negative AKT regulator) and *NF1* (negative RAS regulator) are found in 17%, 15% and 17% of melanomas, respectively (140)*. Mutations in *NF1* may coexist with *BRAF* or *NRAS* mutations (141).

In addition to these common mutations, transcriptional profiling of melanoma cells has generated two groups based on their molecular signatures. The groups are defined by one having a high proliferative ability and a low invasive rate (proliferative phenotype), while the other displaying a low proliferative rate and a high invasive capacity (invasive phenotype) (142). The proliferative phenotype is characterized by high expression of MITF and its target genes, such as transcription factor SOX-10 (SOX10) and melanoma antigen recognized by T cells 1 (MELAN-A) (143).

*Data from the skin cutaneous melanoma datasets from TCGA (PanCancer Atlas) and Broad (Cell 2012) as presented in cbioportal.org.

Oppositely, the invasive phenotype has a high expression of the WNT inhibitors WNT5A, Dickkopf-related protein (DKK) 1 and DKK3, and a reduced expression of WNT/β-catenin target genes, such as MITF (144). Additionally, the invasive phenotype shows upregulation of RTKs, including AXL (145). It has been shown that melanoma cells are able to switch between these two phenotypes, facilitating the cells' needs to grow or invade or as a response to cellular stress, such as hypoxia and treatment (142). Thus, phenotype switching has been found to be important in therapy resistance, where either intrinsically or acquired high levels of AXL and WNT5A and low levels of MITF result in reduced response to MAPK inhibitors (60, 146). Interestingly, while most treatment-naïve melanoma biopsies in a study demonstrated $MITF^{high}$/AXL^{low} expression (57%), followed by $MITF^{low}$/AXL^{high} expression (26%), a subset showed $MITF^{high}$/AXL^{high} expression (17%) (147), suggesting a high population of treatment resistant cells in the two latter populations.

Furthermore, efforts have been made to profile melanomas by gene expression signatures to predict clinical outcome (148). For example, Jönsson *et al* characterized four subtypes in stage IV melanomas. These were termed high immune, proliferative, pigmented and normal-like that had distinct expression of genes involved with high or low expression of immune response genes, melanin synthesis or epidermis development, respectively (149). These gene expression profiles were later adjusted to two groups in primary melanomas, were the proliferative/pigmented subtypes had lower survival compared to the high immune/normal-like (150). Although not currently employed in the clinic, genetic signatures like these may aid in determining prognosis and clinical-decision making, in line with PAM50 profiling recently approved in Norway for luminal B breast cancers.

Treatment

Melanoma patients with operable melanomas receive treatment in the form of complete resection of the tumor. If the primary tumor is over 0.8 mm in diameter or is ulcerated, sentinel node diagnostics is performed and the draining lymph nodes are resected. In cases where the sentinel node tumor is equal to or larger than 1 mm, complete resection of the lymph nodes is performed. Recently, adjuvant treatment with PD-1 inhibitor pembrolizumab or nivolumab or BRAF and MEK inhibition using dabrafenib and trametinib was approved for treatment in Norway for stage III melanoma patients with completely resected tumors. This decision was

based on studies showing increased progression-free survival in patients receiving such adjuvant treatment (151-153).

If inoperable stage III melanoma or in the case of distant metastases, the treatment options for melanoma patients have been limited. Historically, the principal therapy has been the chemotherapy drug DTIC, which has a low response rate (154). However, DTIC may still be administered today in the event of relapse or contraindications of current first- and second-line therapies.

Introduction of the $BRAF^{V600}$ inhibitors vemurafenib and dabrafenib, approved by the Food and Drug Administration (FDA) in 2011 and 2013, respectively, have improved treatment responses in *BRAF* mutated metastatic melanomas. Though the initial response is often monumental, nearly all patients relapse within twelve months (155, 156). To increase the efficiency and remission period, BRAF inhibition is currently given in combination with MEK inhibition. There are currently three combinations of BRAF and MEK inhibitors approved for clinical use. The response and survival rates of these drug combinations, as depicted from the COMBI-v/COMBI-d (157), coBRIM (158) and COLOMBUS (159, 160) studies, are listed in Table 2.

Table 2. BRAF and MEK inhibitors in clinical use

Study name	BRAF inhibitor	MEK inhibitor	Overall response	PFS, months	OS, months	2-year survival	5-year survival
COMBI-v/-d	Dabrafenib	Trametinib	68%	11,4	25,6	52,0%	34,0%
coBRIM	Vemurafenib	Cobimetinib	70%	12,3	22,3	48,3%	N/A
COLOMBUS	Encorafenib	Binimetinib	63%*	14,9	33,6	57,6%	N/A

Table 2. BRAF and MEK inhibitors in clinical use. The table describes the overall response and survival rates of the BRAF and MEK inhibitor combinations in clinical use. PFS - Progression-free survival, OS - Overall survival, N/A - Not available. *Number from blinded independent committee review, overall response by local review was 75%.

BRAF inhibition is not suitable for patients lacking a *BRAF* mutation. The drug may lead to a paradoxical activation of the ERK/MAPK pathway through dimerization of BRAF to CRAF, which can lead to tumor growth. Even kinase-dead BRAF or BRAF lacking the RAS binding site due to alternative splicing may dimerize with other RAF proteins to drive ERK/MAPK signaling (161). In fact, it is shown that the BRAF/CRAF heterodimers may activate MEK to a larger degree than homodimers (162).

Currently, first-line treatment for metastatic melanomas is immunotherapy using immune checkpoint inhibitors, which is applicable for patients regardless of *BRAF* mutation status. Due to their immunogenic nature caused by a high degree of somatic mutations (163), melanomas are particularly suitable for immunotherapy and this treatment has shown promising results, with seemingly lasting results for a portion of the patients (164). Immunotherapy show response later than small-molecular inhibitors, meaning that BRAF inhibition as first-line treatment may be applicable for *BRAF* mutated patients presenting with a high tumor-burden.

Ipilimumab, a monoclonal antibody targeting CTLA-4, was approved for treatment of melanoma by the FDA in 2011 as the first immunotherapy to be used in the clinic, and showed increased survival compared to DTIC chemotherapy. Long-term follow up data show an overall survival of 26% (164). Furthermore, targeting PD-1 using pembrolizumab or nivolumab demonstrated increased survival compared to CTLA-4 blockade (165, 166), and these inhibitors are the first-line treatment option in Norway today for inoperable or metastatic melanoma. Combined treatment with ipilimumab and nivolumab in stage IV melanoma patients has demonstrated additional improved response rates and longer survival compared to nivolumab monotreatment, but at the cost of increased toxicity (164). Although immunotherapy has improved response and survival rates, not all patients respond to the treatment and a subset of patients initially responding develop resistance. Additionally, immunotherapy not suitable for patients with certain diseases, such as serious autoimmune disorders, highlighting the necessity of alternative therapy options for patients ineligible for current first- and/or second-line treatment options.

Treatment resistance

A challenge in melanoma treatment is that the cancer cells do not respond or become resistant to therapy. The resistance mechanisms may be innate or acquired, meaning that the cells harbor intrinsic characteristics that prevent the treatment from working or develop resistance mechanisms after a period of treatment response, respectively.

Around 30% of melanoma patients treated with BRAF and MEK inhibitors do not show objective response (Table 2). Innate ERK/MAPK inhibitor resistance can be mediated by copy number alterations in *CCND1* (encoding cyclin D1) (167), and loss of *PTEN* or *NF1* (168, 169) in addition to mutations in *AKT3*, *PI3KCA*, *RAC* and *CDKN2A* (168, 170, 171) (Figure 15).

Overexpression of AXL, MITF and COT has also been conferred with innate BRAF resistance (60).

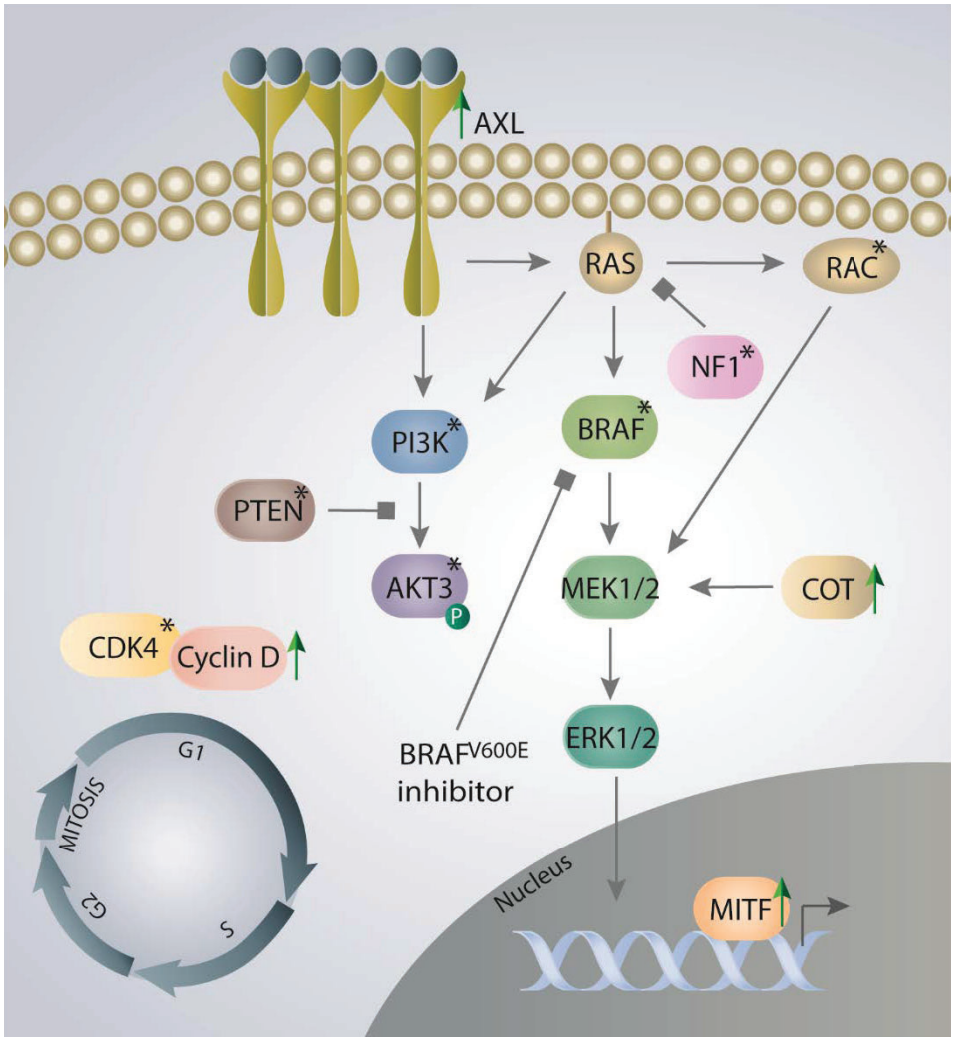

Figure 15. Innate resistance to BRAF inhibition. The figure illustrates innate mechanisms of resistance to BRAF inhibition and includes mutations (*) in *PI3K, AKT3, PTEN, CCND1, CDKN2A, RAC* and *CDK4* in addition to upregulation (green arrow) of AXL, cyclin D1, MITF, and COT.

During treatment with ERK/MAPK inhibitors, the cells may adapt and alter in various ways to induce resistance (Figure 16), leading to a great degree of heterogeneity in resistance mechanisms, both intratumorally and between patients (172). Mechanisms of acquired resistance may be reliant on genetic alterations. These can be within the ERK/MAPK pathway to reactivate ERK/MAPK signaling, such as *NRAS*, *MEK* or *NF1* mutations or alternative splicing or amplification of mutant *BRAF* (173, 174). Additionally, mutations in the PI3K pathway or overexpression of MITF may increase survival in BRAF inhibited cells (172). Further, upregulation of serine/threonine protein kinase COT or RTKs, such as EGFR, platelet-

derived growth factor receptor β (PDGFRβ), insulin-growth factor 1 receptor (IGF1R) and AXL may lead to activation of the MAPK pathway despite the presence of MAPK inhibitors (173, 175).

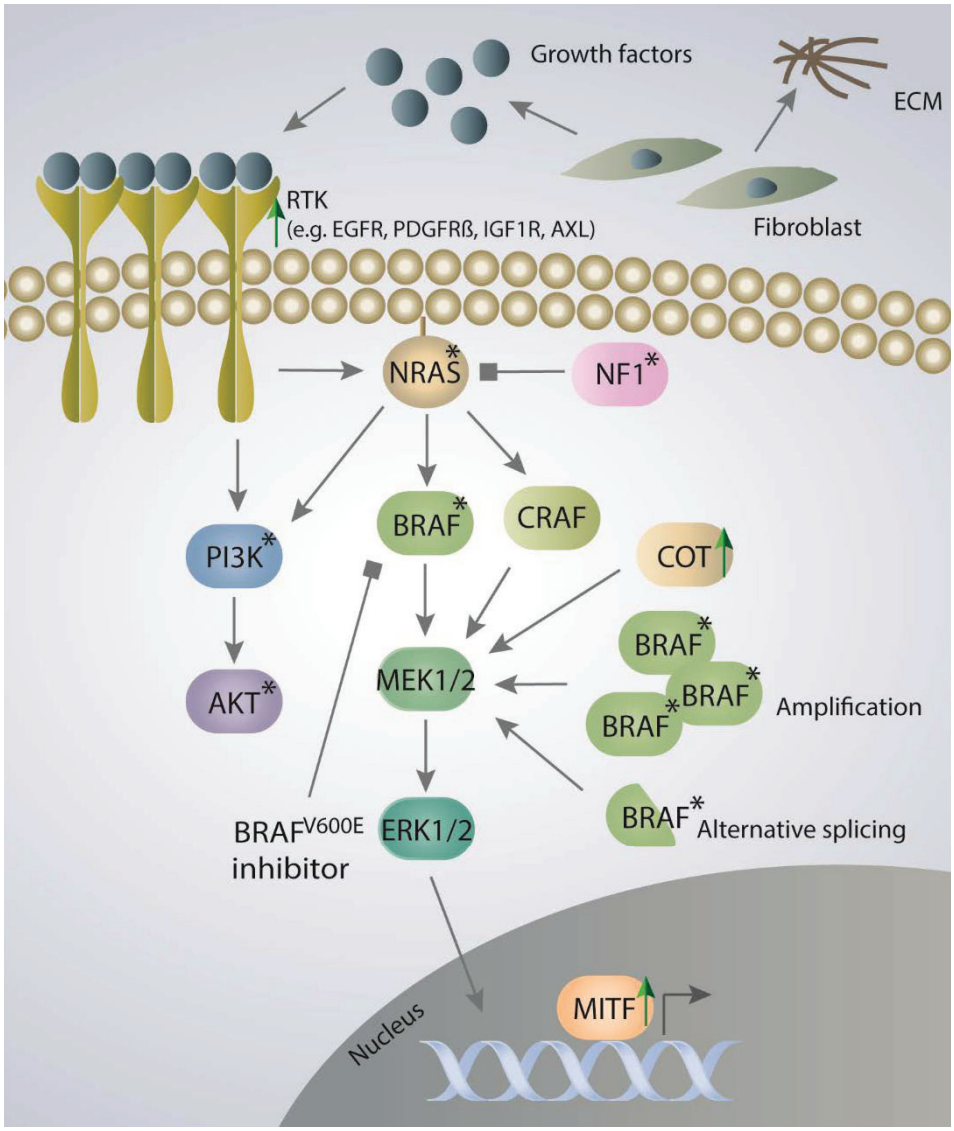

Figure 16. Acquired resistance to BRAF inhibition. The figure illustrates mechanisms of acquired resistance to BRAF inhibition and includes mutations (*) in *NRAS, NF1, PI3K* or *AKT*, upregulation (green arrow) of receptor tyrosine kinases (RTK), MITF or COT or alternative splicing or amplification of *BRAF*. Additionally, extracellular factors such as changes in the extracellular matrix (ECM) and growth factors released from fibroblasts may aid in BRAF inhibition resistance.

Acquired resistance towards ERK/MAPK inhibitors can also depend on cell extrinsic and microenvironmental changes. An example of this is cancer-associated fibroblasts that secrete growth factors that reduce the ERK/MAPK response in cancer cells (176). Further, fibroblasts

may promote alterations in the matrix stiffness, leading to niches of melanoma cells and cancer-associated fibroblasts that develop resistance to BRAF inhibitors (177).

Around 40% of melanoma patients do not show objective response to treatment with nivolumab and ipilimumab (164). For the immune system to successfully target and kill the tumor cells, several criteria must be met, as depicted in the cancer immunity cycle (Figure 17). Briefly, the immune cells must be able to distinguish and detect the antigens presented on the cancerous cells to activate the T cells. Further, the T cells must be transported to the proximity of the tumor and be able to infiltrate the tumor area and sufficiently kill the tumor cells, even within a microenvironment that may be immune inhibitory.

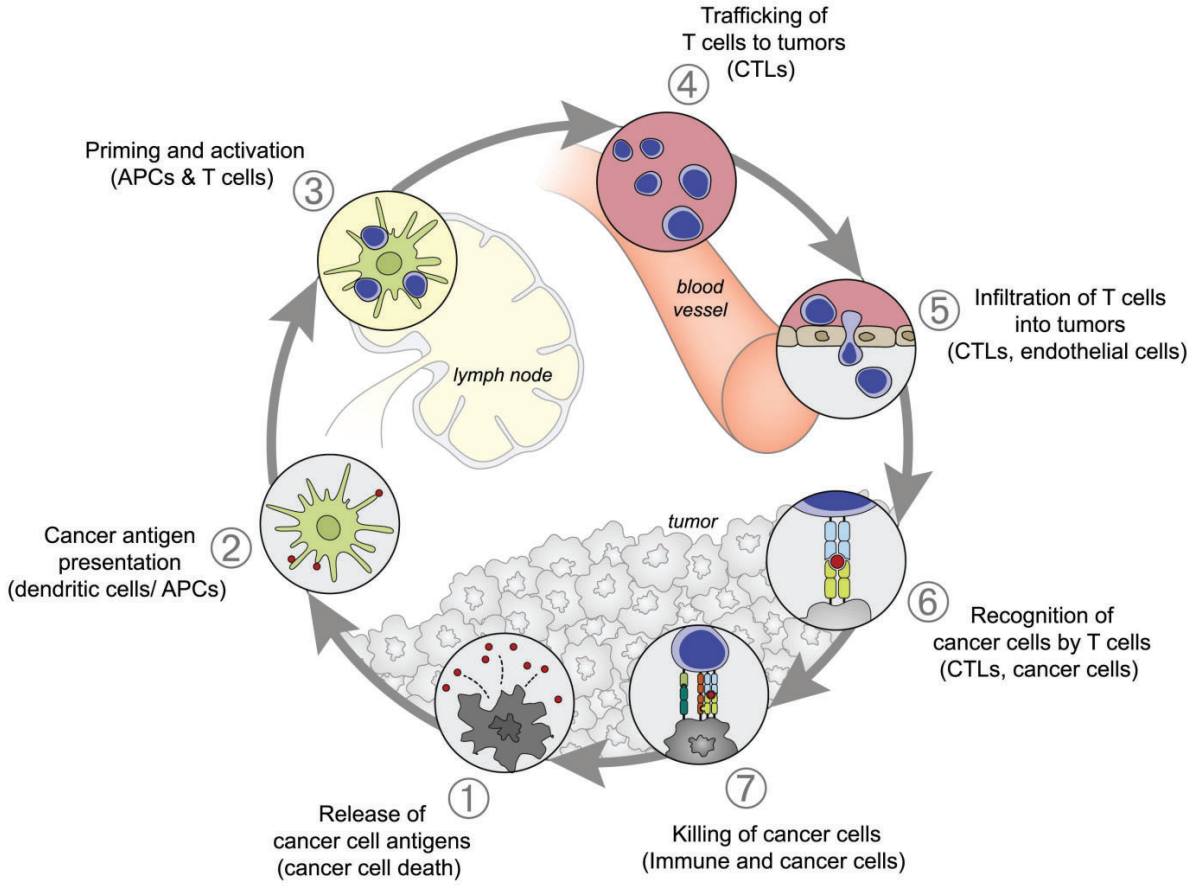

Figure 17. The cancer immunity cycle. The figure illustrates the events that must take place for successful recognition and killing of cancer cells by the immune system, divided into seven major steps. The parentheses indicate the cell types and biological processes involved in each step. The figure is reused with permission from Chen D.S. and Mellmann I., Immunity, 2013 (178). APC – Antigen presenting cells, CTL – cytotoxic T lymphocytes.

There are proposed innate and acquired mechanisms of resistance towards immunotherapy related to each step of the cancer immune cycle. Innate mechanisms include lack of antigen-presentation to the immune cells and can occur for instance through deletion of genes coding for MHC proteins (179). Patients that did not respond to ipilimumab had loss of genes in the interferon (IFN)-γ pathway (180). Further, ERK/MAPK, PI3K or β-catenin signaling may result in decreased response to immunotherapies (181-183). Additional factors that have been associated with innate resistance is a lack of lymphocytes and/or macrophages in the tumor vicinity caused by lack of chemokines essential for T cell functioning or a high expression of immunosuppressive cells, such as T regulatory cells or immune suppressive macrophages (184-186). In line with this, studies have found that patients with a high quantity of $CD8^+$ T cells present in the tumor vicinity have favorable response to PD-1 monoclonal antibody treatment (187). Further, a high mutational burden has been suggested as a positive predictive biomarker of immunotherapy response (188).

The mechanisms of acquired immunotherapy resistance consist in many cases of similar examples as those of innate resistance, for instance mutations in *JAK* leading to lack of IFN-γ signaling (189). It is shown that immunotherapy resistant cells have upregulated levels of immune checkpoint markers in addition to the presence of immunosuppressive cells that aid in turning a tumor "cold" (i.e. lacking immune cell infiltration). For example, T cell function is shown to be exhausted by upregulation of T cell immunoglobulin and mucin domain-containing molecule 3 (TIM3) in NSCLC patients resistant to PD-1 antibody therapy (190). Additionally, expression of T cell regulatory proteins V-domain Ig suppressor of T cell activation (VISTA, also known as B7-H5) and PD-L1 is found to be upregulated after ipilimumab treatment (191). It has further been suggested that targeting T cell inhibitory protein lymphocyte-activation gene 3 (LAG-3) in combination with nivolumab is beneficial for melanoma patients who have progressed on anti-PD-1/PD-L1 treatment (192) and this combination is currently in clinical trials (NCT01968109).

2 Aims

The main aims of this thesis was to develop patient-derived preclinical models to predict responses to targeted therapies in melanoma and elucidate the potential of novel treatment strategies.

The specific aims of the study were:

- To develop an *ex vivo* drug efficacy assay (Paper I) and investigate its potential to determine targeted treatment responses in cells harvested directly from melanoma patient lymph node metastases or patient-derived xenografts (Paper I and Paper II).
- To investigate whether AXL contributes to proliferation, migration and signaling in melanoma cell lines (Paper II) and correlate the levels of its soluble isoform in blood samples harvested from melanoma patients to clinical outcomes (Paper III).
- To examine the impact of reduced expression or activity of AXL in combination with inhibitors of the DNA damage response pathway (Paper II).
- To delineate the molecular mechanisms of how B7-H3 expression contributes to chemotherapy resistance (Paper IV).

3 Summary of publications

3.1 Paper I

A three-dimensional *ex vivo* viability assay reveals a strong correlation between response to targeted inhibitors and mutation status in melanoma lymph node metastases.

Flørenes VA, Flem-Karlsen K, McFadden E, Bergheim IR, Nygaard V, Nygård V, Farstad IN, Øy GF, Emilsen E, Giller-Fleten K, Ree AH, Flatmark K, Gullestad HP, Hermann R, Ryder T, Wernhoff P, Mælandsmo GM.

Translational Oncology. 2019 Jul;12(7):951-958.

In this study, we established a three-dimensional *ex viv*o drug efficacy assay to examine drug response in 38 freshly harvested melanoma lymph node metastases and 21 patient-derived xenografts. A strong correlation was observed between BRAF inhibitor response and *BRAF* mutations status. Furthermore, five of thirteen *NRAS* mutated tumors demonstrated increased growth potential when treated with BRAF inhibition. Importantly, two tumors that were diagnosed as *BRAF* wild-type by routine diagnostics exhibited a strong response to BRAF inhibition. Upon re-evaluation and next-generation sequencing, one tumor was found to carry a complex $BRAF^{V600E}$ mutation, while the other harbored a $BRAF^{V600E/K601N}$ double mutation. In an effort to unravel genes involved with innate resistance to treatment, we sequenced 21 patient samples and one patient-derived xenograft, but observed no mechanisms of resistance apart from NRAS mutated tumors being resistant to BRAF inhibition. Further, with the *ex vivo* drug efficacy assay, we were able to demonstrate concordance between *ex vivo* drug response in patient material and tissue from patient-derived xenografts, showing the potential of using patient-derived xenografts and the *ex vivo* drug efficacy assay as models for personalized cancer treatment.

3.2 Paper II

Targeting AXL and the DNA damage response pathway as a novel therapeutic strategy in melanoma.

Flem-Karlsen K, McFadden E, Omar N, Haugen MH, Øy GF, Ryder T, Gullestad HP, Hermann R, Mælandsmo GM, Flørenes VA.

Manuscript in second revision, Molecular Cancer Therapeutics.

Upregulated receptor tyrosine kinase AXL has been found in various forms of cancer and is correlated with metastasis and treatment resistance. In this study, we observed reduced proliferation and ERK/MAPK and PI3K signaling in cells treated with small-molecular inhibitor of AXL, BGB324, or in cells with transiently reduced AXL expression.

Currently, AXL is being studied as a relevant therapeutic target and small-molecular inhibitors targeting AXL are currently in clinical trials. Interestingly, recent studies have shown that AXL expression reduces sensitivity to chemotherapy and PARP inhibition (69, 193, 194). Based on these studies, we investigated the combined targeting of AXL and the DNA damage response pathway, mainly CHK1 and CHK2 proteins. In melanoma cell lines, we observed that combining BGB324 with small-molecular inhibitors of CHK1/CHK2 (AZD7762) or ATR (VE-822) resulted in reduced proliferation, results that were verified using transiently knocked down models of either AXL or CHK1/CHK2. This effect was also observed when inhibiting AXL and CHK1/CHK2 in the *ex vivo* drug efficacy assay demonstrated in Paper I and *in vivo*. Further, combined inhibition of AXL and CHK1/CHK2 resulted in cell cycle arrest and increased apoptosis in addition to downregulation of DNA damage response proteins. These results indicate that targeting AXL and the DNA damage response pathway may be therapeutically beneficial and should be further investigated.

3.3 Paper III

Soluble AXL as a marker of disease progression and survival in melanoma.

Flem-Karlsen K, Nyakas M, McFadden E, Wernhoff P, Farstad IN, Flørenes VA, Mælandsmo GM.

Manuscript in second revision, PLOS ONE.

Receptor tyrosine kinase AXL can be cleaved by the metalloproteinases ADAM 10 and ADAM 17, which results in a soluble isoform of 80-85 kDa. Soluble AXL is present in human blood and is found to be elevated in cancers, such as hepatocellular and renal cell carcinoma and in inflammatory diseases. We have previously observed that soluble AXL levels were increased in effusions from ovarian carcinoma, malignant mesothelioma and breast cancer patients compared to benign effusions.

In this study, we aimed to examine the levels of soluble AXL in blood samples drawn from patients and relate these levels to disease progression and survival. Further, we investigated soluble AXL levels in the media of melanoma cell lines in response to small-molecular inhibitors targeting AXL or ERK/MAPK proteins. In line with what was observed in Paper II, higher cellular AXL expression in response to AXL inhibition was observed, while in this paper, we found that this was coupled with reduced soluble AXL levels. We demonstrated that AXL inhibition stabilized the protein, thus resulting in increased cellular expression and decreased soluble levels. Interestingly, soluble AXL levels mirrored the cellular expression, and could thus potentially be used to examine AXL expression in tumors. Additionally, soluble AXL levels were increased in stage IV compared to stage III melanoma patients, showing that soluble AXL could be related to disease burden. Soluble AXL levels was associated with survival in stage IV patients treated with anti-CTLA-4 antibody ipilimumab for seven weeks. However, blood samples drawn before treatment initiation and at week four of treatment did not show correlation between soluble AXL levels and survival. Measuring soluble AXL levels may thus be an easily available method to predict AXL tumor expression, which may be associated with aggressive cancer characteristics, such as increased stage and metastases.

3.4 Paper IV

p38 MAPK activation through B7-H3-mediated DUSP10 repression promotes chemoresistance.

Flem-Karlsen K, Tekle C, Øyjord T, Flørenes VA, Mælandsmo GM, Fodstad Ø, Nunes-Xavier CE.

Scientific Reports. 2019 April;9(1):5839.

B7-H3 is an immune checkpoint protein of the B7 family, is upregulated in cancer and is associated with poor survival. We have previously observed that B7-H3 expression increases proliferation and the glycolytic levels in melanoma cells. Additionally, we demonstrated that melanoma cells with stably reduced B7-H3 expression or treated with an inhibitory B7-H3 antibody had increased sensitivity to DTIC chemotherapy and to small-molecule inhibitors targeting ERK/MAPK or PI3K pathways: vemurafenib (BRAF inhibitor), binimetinib (MEK inhibitor), everolimus (mTOR inhibitor), or triciribidine (AKT inhibitor).

In this study, we examined how B7-H3 is associated with chemotherapy resistance in melanoma cells. To do so, we treated melanoma cells with the chemotherapeutic drugs DTIC and cisplatin and observed that B7-H3 knockdown cells had increased sensitivity to the treatment *in vitro* and *in vivo* compared to B7-H3 expressing cells. Importantly, reduced B7-H3 expression in DTIC-resistant melanoma cells resensitized the cells to DTIC treatment. By gene expression analysis, we identified that B7-H3 knockdown cells had increased expression of DUSP10 as compared to B7-H3 expressing cells. DUSP10 is a phosphatase that dephosphorylates and inactivates p38/MAPK. In line with this, B7-H3 knockdown cells treated with chemotherapy had decreased p38/MAPK activation. p38/MAPK is a crucial pathway to uphold cell survival in response to cellular stress, such as genotoxicity. Decreasing DUSP10 expression in shB7-H3 cells resulted in higher p38/MAPK activation and less sensitivity to DTIC. These results indicate that B7-H3 mediates chemoresistance by reducing DUSP10 levels to induce p38/MAPK signaling.

4 Methodological considerations

Within its natural habitat, cell behavior is dependent on many factors that are difficult to recapitulate. The sterile and rigorous setting of a laboratory is not always representative for the diverse and complex properties of a cell. To highlight this, many drugs that seem to function in a preclinical setting do not make it to final development. In fact, only 3.4% of oncologic drugs proceed through preclinical and clinical testing to approval (195). In this chapter, pitfalls and strengths of the various model and experimental systems employed in the articles will be discussed.

4.1 Model systems

In vitro cultures and alterations to cell lines

Much of the work in this thesis is performed on melanoma cell lines grown as monolayers. Cancer cell lines are established by expanding cancer cells of solid tumors in culture flasks or wells in appropriate growth mediums and are often used in cancer research as an accessible, affordable and easy model to monitor mechanisms and investigate the effect of treatment. Cell lines may be propagated effortlessly, which gives researchers material for large-scale analyses. Additionally, by using *in vitro* cultures, researchers can reduce the number of animals employed for *in vivo* experiments.

However, using *in vitro* cultures comes with a number of challenges. In its natural habitat, cancer cells have established complex relationships with each other and the body's immune system, which is difficult to replicate within a laboratory setting. *In vitro* cultures lack surrounding structure and only provide cell-cell interaction in a two-dimensional form. Many cell types, such as fibroblasts and endothelial cells, have shown to interact with tumors to alter and refine signaling and treatment response (196), processes that are lost in cell culture flasks. For example, studies in our lab have shown that co-culturing cancer cells with fibroblasts result in less sensitivity towards BRAF inhibitors (197). Additionally, no forms of hormonal impulses or interaction with the immune system is present. Thus, many of the phenotypic characteristics of the tumor are lost.

Melanomas are known for being heterogeneous, however, growing cells *in vitro* highly selects for the cells that are most capable to adapting to this kind of growth, thus losing the natural diversity within the tumor. In line with this, it has been shown that melanoma cell lines have a higher degree of *BRAF* or *RAS* mutations compared to patient tumors (198). The homogeneity within a cell line may also be an advantage, as it standardizes the cell line and should make experiments easy to replicate. However, studies have shown that cell lines evolve and develop new mutations in culture (199). Additionally, cell-line misidentification and cross-contamination are an issue. For example, the cell line MDA-MB-435 was long thought to be a breast cancer cell line but is now known to be derived from the melanoma cell line M14 (200). These disadvantages may also be illustrated by the HeLa cell line, the first human cell line to be established from the cervical tumor of Henrietta Lacks in 1951. HeLa cells grow rapidly, are widely employed and have been found to contaminate a range of other cell lines. A recent study demonstrated high heterogeneity in HeLa cells collected from thirteen different labs (201), indicating genetic drift of the cells. Alterations in *in vitro* cultures may be one of the factors contributing to the low reproducibility between laboratories. To minimize these challenges, maintaining strict culture conditions is vital. Additionally, using cells at a low passage number to prevent genetic drift, checking the cells for mycoplasma contamination and short tandem repeat fingerprinting to ensure the use of the correct cell line is good practice.

Several of the cell lines used in the articles have been established in-house and originate from patient melanoma metastases surgically removed at the Norwegian Radium Hospital. Most of the in-house cell lines have been harvested from lymph node metastases, while Melmet 1 originate from a subcutaneous metastasis. The FEMX-1 cell line corresponds to cells harvested from a mouse engrafted with a patient melanoma metastasis, while FEMX-V corresponds to the fifth passage in mice injected intravenously (202, 203). Patient material is employed with patient consent and the patient material used in these studies are approved by the Regional Committee for Medical Research Ethics of South-East Norway.

In Paper IV, we employed established lines with short hairpin knocked down B7-H3 expression (119). Additionally, we have transiently knocked down expression of AXL, CHK1, CHK2 (Paper II) and DUSP10 (Paper IV) using small interfering RNAs (siRNA). The transfection procedure may alter signaling and produce off-target effects (204). Therefore, we used two different siRNAs targeting the same protein and performed the same procedure with control cells, except with a non-targeting control. Although the control conditions are thought to have

negligible effects, it is likely that these manipulations have an impact on the cells. An example of this is demonstrated in Paper III, where the control knock down cells showed a large decrease in proliferation when they were treated with CHK1 and CHK2 inhibitor AZD7762. We hypothesize that this is due to the toxic nature of the reagents necessary for transient transfection, and that targeting the DDR pathway in addition to the transfection resulted in reduced proliferation. In retrospect, establishing stably knocked down expression of all our most studied proteins (e.g. AXL) would be beneficial, although this process is time consuming.

Cells that were going to be used for immunoblots of phosphorylated AXL (pAXL) expression were treated with AXL ligand GAS6 and vitamin K for one hour before cell lysis. Without this pre-treatment, pAXL expressions were too low for visualization on the immunoblot. Due to the cost of the ligand, continuously treating cells for all AXL-related experiments with GAS6 and vitamin K was not feasible, although it would be more biologically relevant. As GAS6 is released from fibroblasts, co-culturing the cancer cells with fibroblasts could have been an approach to establish a stable supply of GAS6.

Spheroid models

Cells may be cultured as three-dimensional spheroids. This solves some of the issues with two-dimensional culturing, as cells will retain a three-dimensional structure and cell-cell contact, which is more physiologically relevant. Importantly, structure-specific factors such as nutrient and oxygen levels are maintained, which will yield populations within the spheroid that are not present in monolayers, for example areas of hypoxic cells (205). Spheroids are shown to be more resistant to chemotherapy compared to monolayers (206), which may be caused by the quiescent cell populations that are less sensitive to treatment, but remain an important cell population for cancer relapse. It has been shown that spheroids with a diameter over 500 µM structures into a necrotic rim with a surrounding layer of quiescent cells and an outer rim of proliferating cells (207). By plating 15.000-20.000 cells per well, we generated spheroids that were around 1000 µM in diameter (data not shown), which would indicate that the spheroids could acquire these tumor-like structures. However, due to the short plating time in the *ex* vivo assay (5 days), these areas most likely do not develop. Cell suspensions may be promoted to form spheroids by using low-adhesion plates, hanging drop plates or gravitational approaches (e.g. spinner flasks) (208). These methods rely on the self-aggregation of the cells, meaning that the spheroid structure and size may vary between different cells. Scaffolds such as matrigel

or collagen mimic the extracellular matrix to stimulate spheroid formation (209). Scaffolds allows the researcher to add growth factors and other molecules to resemble the microenvironment of the tissue of interest. However, output assays may not be compatible with the scaffold system. In our articles, we have cultured established cell lines and disaggregated lymph node metastases harvested directly from patients operated at the Norwegian Radium Hospital as spheroids in a scaffold-free system. Using round-bottom wells, we have generated spheroids to determine treatment response to relevant drugs. We chose to employ round-bottom wells as they are relatively affordable, allow for culturing of a chosen number of cells, are easy to treat with drugs and are compatible with cell viability assays. Figure 18 shows an overview of the workflow of the *ex vivo* drug efficacy assay.

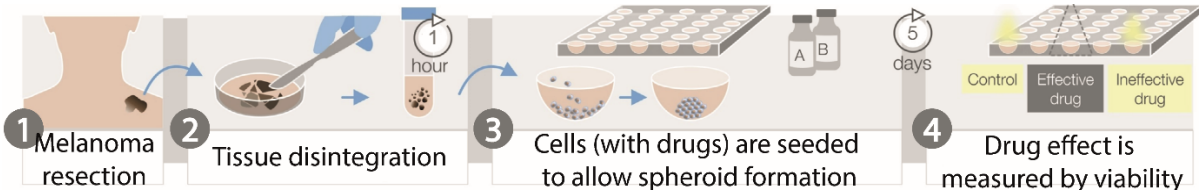

Figure 18. Workflow of the *ex vivo* drug efficacy assay. The figure illustrates the workflow of the *ex vivo* drug efficacy assay from disintegration of the resected melanoma lymph node metastasis to the measurement of cell viability to determine drug effect. Figure by Science Shaped ©.

From the surgical removal of the lymph node metastases, a varying number of cells surrounding the tumor may be excised and thus cultured together with the cancer cells. Importantly, immune cells in the tumor vicinity may be present in the samples. However, the extent of non-malignant cells that are present will be diverse between each patient sample and may depend on the practice of the surgeon and location of the tumor. Further, the cells most able to adapt to the changed surrounding will grow the fastest. Thus, many of the non-malignant cells might perish quickly and be outgrown by the proliferative cancer cells. In our *ex vivo* drug efficacy assay, we have added small-molecular inhibitors at the same time as the cells. This was done to ensure penetrance of the drug to the cells. However, by adding inhibitors after the spheroids have formed, the *ex vivo* drug efficacy assay may have more closely mimicked the biological approach. The drug efficiency of these two approaches should be further explored.

Further discussion and focus on the results of the spheroid drug sensitivity assay can be found in Section 5.1.

In vivo models

Utilizing the lives of other animals and causing them discomfort to conduct research is not something that should be taken lightly, and thus, all animal experiments should be carefully planned and based on data from experiments in cell cultures or spheroid models. *In vivo* models may be used to demonstrate the effect of a treatment in a living organism. In our studies, we have employed mice with diminished immune systems, which increases the chance of tumor growth and allows for rapid development of tumors. However, using immune-deficient mice means that not all aspects of the tumor microenvironment is mimicked and that drugs could be processed differently or have other pharmacokinetic differences compared to mice with competent immune systems. In addition, the cells implanted into the mouse are human cells while the microenvironment is that of the mouse. Melanoma cells were injected or implanted subcutaneously, thus forming artificial tumors into the flanks of the mice. In some of our treatment experiments, we only utilized one flank, while in others both flanks were engrafted. Although injecting cells into both flanks to simulate two separate tumors can reduce the number of animals, the experience within the department is that in some instances, only one tumor will grow. Growing tumors subcutaneously does not reproduce the tumors natural metastatic cascade and is in many cases not the 'natural' place for these cells. Although orthotopic engraftments are thought to better replicate the human tumor, subcutaneous models are easier to engraft and monitor. However, a recent study demonstrated close genetic similarity between the subcutaneous and orthotopic models, even though the DNA methylation pattern varied somewhat between them (210).

To establish PDXs in Paper I we employed female NOD scid gamma (NSG) mice, which carries the NOD.*Cg-Prkdc*^{scid}*Il2rg*^{tm1Wjl}/SzJI strain. This makes them the most immunodeficient mouse strain available with absent or defective production of cells within the adaptive and innate immune system. Patient lymph node metastases were surgically removed and subcutaneously engrafted onto the flanks of mice. The success rate of our melanoma engraftments was 77%, which is in line with what others have previously experienced (211). Compared to engraftments of cell lines, PDXs have the asset that they maintain the tumor heterogeneity. For instance, it is shown that the cell population in neuroblastoma PDXs remain stable and resemble the original tumor for up to eight passages (212). As shown with cell lines, melanoma PDX models also have increased mutational rate of *BRAF* and *NRAS* compared to the original tumor (198). Additionally, this study observed divergent mutations in the same PDX model expanded in

different mice, suggesting that intratumoral heterogeneity can result in the growth of varying clones. In line with this, we observed contrasting melanin content and response rates to treatment in the *ex vivo* drug efficacy assay of the same tumor sample passaged into two mice (Figure 19).

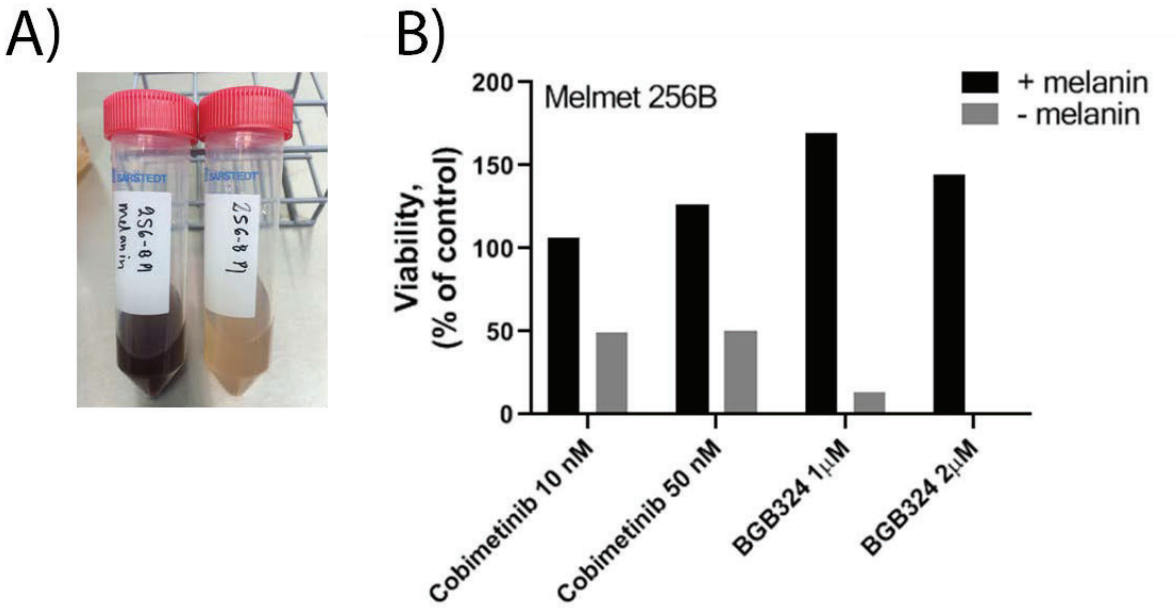

Figure 19. Melanin content and drug response in Melmet 256B. Patient-derived lymph node Melmet 256B was passaged into two NSG mice that subsequently resulted in divergent A) melanin content and B) cell viability in response to small-molecular inhibitor treatment in the *ex vivo* drug efficacy assay (unpublished data).

This indicates that which part of the tumor that is propagated in mice is meaningful for tumor signaling and growth pattern. Further, the rapidly proliferating zones may more often be chosen as the necrotic areas are discarded. This may also suggest that engrafting PDX models for several passages may result in genetic drift and that PDX tumors should be employed at a relatively low passage number. In line with this, we observe a decrease in the number of days the tumor required until it was around 1000 mm^3 and thus ready to passage from the first passage to the ones following (Figure 20). After the first passage, however, the time to passage stayed relatively consistent. It has been shown that PDX tumors up to five passages demonstrated similar histological and morphological phenotypes, even under the influence of BRAF inhibition (213). Additionally, there has been observed similar histology between the original tumor biopsy and the second passage of a head and neck squamous cell carcinoma xenograft (214). This indicates that PDX models used at a low passage sufficiently recapitulates patient tumors.

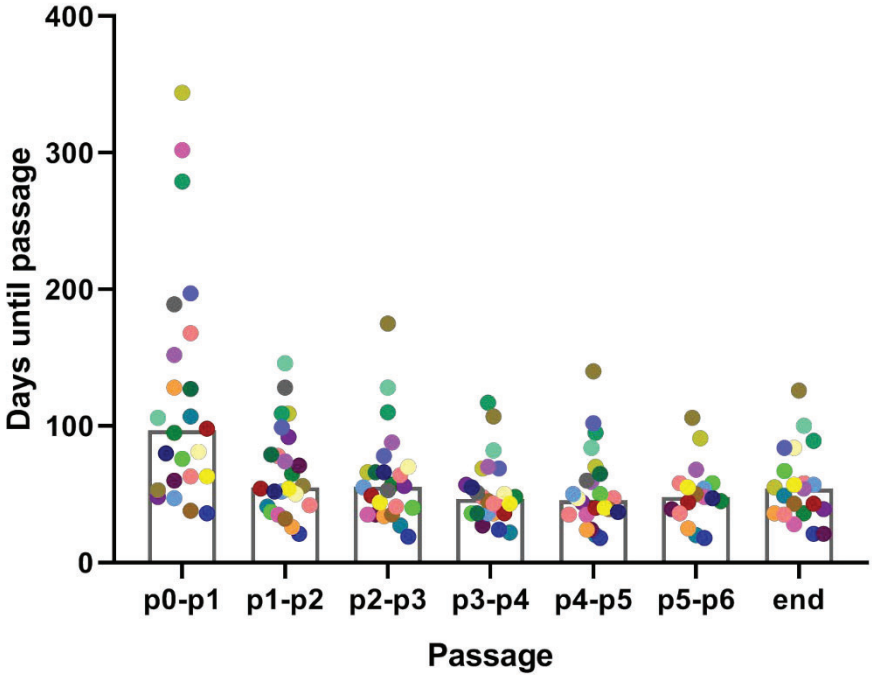

Figure 20. Time to passage of PDXs in NSG mice. The figure illustrates how many days until the tumor was passaged onto new mice (unpublished data). The mean tumor volume at passage was 1000m^3. Each dot represents the mice with the tumor passaged and the bars represent the median value of the group. The color corresponds to a certain PDX model. End means the last passage before the model was considered established and tumor samples stored in a biobank.

For the *in vivo* treatment studies, female athymic nude foxn1^{nu} mice were chosen. Through breeding, these mice have a loss of the *FOXN1* gene, resulting in loss of the adaptive immune system as the T cell maturation in the thymus is removed, while the innate immune system is retained. However, established cell lines and PDX models that have grown in NSG mice generally show a good take in nude mice. In our experiments, we observed a high take rate (from 77% and upwards) in established cell lines and previously passaged PDX models from NSG mice. Nude mice have the advantage of being hairless and have a calm disposition, allowing for easier handling and monitoring of the tumors.

4.2 Experimental systems

Treatment with small-molecular inhibitors and chemotherapy

To determine the effect of inhibiting the activity of the proteins of interest, we have employed small-molecular inhibitors targeting AXL (BGB324), CHK1 and CHK2 (AZD7762), ATR (VE-822), BRAF (vemurafenib) and MEK (cobimetinib). Treating cells with small-molecular inhibitors may inactivate the target efficiently and rapidly and can thus be a straightforward approach to investigate the effect of blocked activation of a protein. However, the pharmacology of the inhibitors must be examined; the inhibitors might have off-target effects, and how they act might be influenced by cell specific factors such as membrane permeability. To exclude the possibility of off-target effects, we supplemented the results using the most prominent inhibitors with experiments where the targets were transiently knocked down. This is especially important for inhibitors that still are still being investigated in clinical trials and are used at high concentrations, such as BGB324. In Paper II, we were troubled by the fact that CHK1/CHK2 inhibitor AZD7762 displayed some selectivity towards AXL (215). A publication has even called for using AZD7762 as a AXL inhibitor (216). In line with this, in Paper II, we found that AZD7762 reduces pAXL expression. However, treatment with ATR inhibitor VE-822 also reduced pAXL signaling, indicating a general mechanism of targeting the ATM/ATR-CHK1/CHK2 pathway. Additionally, short exposure (10 minutes) to AZD7762 and VE-822 did not reduce pAXL levels to the extent of BGB324 treatment, indicating that the inhibitors do not affect AXL activity directly.

Drugs are often diluted in dimethyl sulfoxide (DMSO), which may be toxic to the cells. To account for this toxicity, control cells were treated with the same amount of DMSO as the treated cells. In paper IV, we used the chemotherapeutic agents DTIC and cisplatin to treat melanoma cells. Chemotherapy treatment is rarely employed in the treatment of melanoma nowadays, however, chemotherapy treatment allowed us to induce stress signaling pathway p38/MAPK in the melanoma cells. This was utilized as a method to observe alterations in the cellular stress response to modifications in B7-H3 expression.

Measurements of cell viability and proliferation

Cell viability/proliferation assays may be used to determine cell sensitivity towards treatments. Many cell viability assays rely on the measurement of energy molecules, such as ATP (Cell Titer Glo) or NAD(P)H (MTS), to give rise to luminetric or colometric changes which may be measured using light absorbance. The assumption behind these assays is that there is a direct correlation between the amount of energy molecules and the number of viable cells. The assays are easy to employ and relatively affordable, but they are toxic to the cells and must be utilized at the endpoint of an experiment. Further, the assays are heavily reliant upon the metabolic activity of cells, and is thus best used in highly metabolic cells. The assays do not provide information to why the metabolic activity of the cells have changed, and further analysis measuring factors such as cell cycle progression and apoptosis should be explored. In addition, the compounds themselves are yellow-colored which may yield signals that must be accounted for in the read-out. Finally, drugs used to treat cells may interact with the dye to give incorrect measurements.

A non-toxic method is to measure cell proliferation in response to cell variations or drugs by continuous photographs of the cell culture plates by the Incucyte FLR and Incucyte Zoom instruments. The corresponding program determines cell confluence by calculating the percentage of the well that is covered by cells. However, as the measurement is highly dependent on the morphology of the cells, using the Incucyte system is best when comparing changes or treatments within the same cell line.

Protein detection

To analyze differences in protein expression, we have employed several protein analysis methods, such as western blotting, simple western technology, immunohistochemistry and enzyme-linked immunosorbent assays (ELISA). A common drawback with all these methods is that they are heavily reliant on the quality of the antibodies used. Additionally, the output of these methods is static in that they only show the protein expression in a sample at a single time. This can be circumvented by running several samples in a time-dependent manner; however, these samples could thus be subjected to technical errors that misrepresent the results.

One of the most common molecular biology methods is western blotting, which is an accessible, although time-consuming approach, to detect protein expression. The method is affordable and

allows for analysis of many samples simultaneously. However, researchers are unable to detect heterogeneity within the samples, as only the average protein expression will be shown. Thus, western blotting can be supplemented with immunofluorescence, immunohistochemistry or flow cytometry to investigate alterations in protein expressions throughout the cell population. In addition, the output of western blotting can be very subjective, as it might be difficult to interpret small changes between groups when the bands are visualized. To limit subjective interpretation, bands can be quantified by image processing programs.

4.3 Statistical analyses

In science, it is common to calculate the p value of a certain quantitative measurement. This value will determine how likely it is if the observed result is simply due to chance or if there is a valid effect. A p value of 0.05, meaning that there is a 5% possibility of the observed result being merely due to chance, is an arbitrary value that is considered the threshold for determining statistically significant results. The use of the p value is deeply integrated into the scientific community. However, many researchers now call for a change in the practice of how p values are used (217). It is believed that the p values often are over-fitted and misinterpreted. Additionally, in biological systems, small differences may be crucial, while big differences may be irrelevant and the p value does not account for this. Thus, to determine if a change is real, using several methods to observe the same outcome is good practice.

In Paper II, we calculated the synergistic effect of BGB324 and AZD7762. To do so, we employed the Chou-Talay method, which is based on a median-effect equation of drug response (218). Drug combination effects can be antagonistic, additive or synergistic, reflected by a score of >1, 1 or <1, respectively. Antagonism means that the drugs have less response together than the added effect of the monotherapies, while synergy means that the effect of the drug combination is greater. Additive effect means that the drug responses are equal to that of the drugs independently added together. To determine the synergy using Chou-Talay, a dose-curve for each drug is added. Determining IC50 values for BGB324 was challenging, as inhibiting the protein at the top non-toxic level (2μM) did not lead to more than 20-30% decrease in proliferation. This is line with what other researchers at our lab has observed (data not shown). However, increasing the concentration to 3μM dramatically decreased cell viability, likely explained by off-target effects and was thus not inserted into the equation. In hindsight, measuring cell viability at several BGB324 concentrations between 2μM and 3μM would be

beneficial to yield the most optimal dose-response curve to calculate its synergistic effect with AZD7762.

4.4 Ethical considerations

In the studies included in this thesis, there are two main ethical considerations; the harvesting of patient material and subsequent use of patient information and the use of animal models.

In regards of patient material, we employed the use of melanoma lymph node metastases harvested from patients operated at the Norwegian Radium Hospital. In parallel, patient information was collected. Before the surgery, the patients receive a written agreement form stating the objectives of the study. The patients have the opportunity to not be included in the study and this is clearly stated in the agreement form. Patients are a vulnerable group and it is important to inform them of their rights regarding their participation. In addition, the patients have the opportunity to withdraw their agreement without any questions asked, at any time. It is also clearly stated that participation in the study will not affect their treatment options. The patient information is kept in restricted files at the hospital network where a limited number of people involved with the project have access. Patient information that is to be used is made anonymous and is not presented in a way where anyone can track the information back to the patient.

The project also employs mice models. It is unfortunate to utilize living beings in the name of research. However, there is to date no other satisfactory alternative method that can compete with this whole-body testing of treatments. All experiments are carefully and thoroughly planned and investigated *in vitro* before the experimental set-up is moved to animals. In this manner, we aim to minimize the amount of animal experiments. All animal studies have been approved by The Norwegian Animal Research Authority and kept according to the Norwegian Welfare Act. The animals are monitored several times a week and weighed at least once a week before treatment, and at least twice a week on treatment. Any animals showing signs of distress or weight loss over 15% are immediately euthanized to minimize suffering. To increase the animals' quality of life they are never kept in cages alone and are given stimulating objects such as paper tissues and cardboard houses.

5 Discussion

5.1 Personalized cancer treatment

Personalized cancer treatment refers to the aim of tailoring therapy regimen for a patient by considering factors such as genetic or phenotypic profiles, tumor site and other characteristics. By these factors, clinicians can subgroup patients, which may guide treatment strategies and reduce side effects and costs of suboptimal drugs. Personalized treatment has been employed for many years, for example through blood type matched transfusions or Herceptin treatment for receptor tyrosine-protein kinase erbB-2 (HER2) positive breast cancer patients. With new methods, such as genomic analyses, the field of personalized treatment has gained increased potential. A challenge with personalized cancer treatment is to balance the wish to perform analyses with the cost and time of doing them. For example, next generation sequencing of tumors could identify oncogenic drivers, but the observed aberrations may not be actionable targets and may thus be an unnecessary cost. A recent study illustrated that targeted therapy by repurposing anticancer drugs may have a clinical benefit (219), and show the potential of subgrouping therapy based on the driver mutations and not strictly by cancer type. Furthermore, the vast amount of data collected for each patient will have to be handled appropriately, maintaining patient confidentiality. Together, the patient data will accumulate to large-scale biological databases, which requires massive storage capacity, in addition to personnel capable of analyzing the data.

At present, rather few diagnostic elements are considered when determining prognosis and treatment decisions for melanoma patients. Many of these are descriptive of the tumor, such as histological type, tumor depth, infiltration level, mitotic numbers and ulceration. Melanomas have a high number of somatic mutations compared to other cancers (135), but some commonly mutated genes that act as cancer drivers have been identified (136). Today, routine diagnostics examine resected tumors for *BRAF* and *NRAS* mutations, which may guide clinical decisions. Importantly, mutational discrepancy intratumorally and between primary tumor and metastases has been found (220) and thus, a single biopsy might not provide full view of the mutational status of the tumor. First-line treatment for metastatic melanomas today is immunotherapy, but if tumors regress or patients are ineligible for immunotherapy, BRAF inhibition together with MEK inhibition is the preferred therapy for patients with $BRAF^{V600E/K}$ mutated tumors.

In Paper I, we observed that two patients who were diagnosed with wild-type *BRAF* by the routine diagnostic in-house polymerase chain reaction (PCR) assay responded well to BRAF inhibition in the *ex vivo* assay. Upon further analyses, it was revealed that the tumor cells indeed harbored *BRAF* mutations. One had a double $BRAF^{V600E/K601N}$ mutation. Based on the $BRAF^{V600E}$ mutation, it suggests a constitutively active BRAF and that this patient would benefit from BRAF inhibition, in line with the results from the *ex vivo* assay. The $BRAF^{K601N}$ mutation is associated with a RAS-independent oncogenic BRAF protein, and cells that contain this class of BRAF proteins are suggested to be sensitive MEK inhibition (221). It may be possible that a BRAF inhibitor would not bind the protein if the mutated lysine to arginine on codon 601 interferes with the drug. However, both lysine and arginine have positively charged side chains of relatively same size and this suggests that BRAF inhibition would still be eligible for this patient. The other patient had tumor cells with a complex $BRAF^{V600E}$ mutation. Instead of the common codon alteration from GTG to GAG due to nucleotide changes at base pair 1799, these cells had a rare variant where both base pair 1799 and 1800 were altered to alanines, resulting in a GAA codon. GAA also corresponds to an alteration to a glutamine (as is the case for the $BRAF^{V600E}$ mutation), indicating that BRAF maintains its oncogenic properties and that BRAF inhibition would be a valid treatment option for this patient, which is in line with the results obtained from the *ex vivo* assay. These examples highlight cases where patients might benefit from a higher degree of precision diagnostics and personalized cancer treatment. Additionally, it shows that utilizing an *ex vivo* drug efficacy assay may supplement molecular testing of the tumors.

Identifying other common mutations in melanomas, such as *NRAS* or *NF1*, does not currently yield actionable targets and may be done to subgroup patients for clinical trials. However, *NRAS* mutations are associated with decreased survival (222) and may be an indicator of the need of increased follow-up. In addition, mutations in *CDKN2A* and loss of *PTEN* are associated with treatment resistance and lower response to BRAF inhibitors and may thus be examined to identify patients that may need increased follow-up.

Using patient-derived xenografts and *ex vivo* assays to guide clinical decisions.

By the use of preclinical models, the aim is to predict patient response to therapy and foresee the trajectory of the patient tumor. Establishing such models could help guide and support clinical decisions and limit side effects by reducing administration of unneeded drugs. However, this is difficult, due to factors such as genetic drift and lack of complete recapitulation of the tumor microenvironment. Two examples of models that have been established to investigate patient response to treatment is the use of PDXs and *ex vivo* assays.

PDX models are shown to recapitulate the patient's response to several treatment regimens (223), highlighting its potential as a model to determine treatment response. However, as discussed in Section 4.1, PDX models face many challenges such as lack of a functional immune system. Further, time to engraftment may be long, and in many cases, patients do not have sufficient time to wait for PDX results before treatment initiation. We have observed a variation in primary engraftment time from 36 to 344 days, with a median of 97 days (passage 0-1, Figure 20). This suggests that most patients will commence treatment before the PDX tumor is established in mice. However, a study observed that many PDXs from stage IIIC and IV melanomas reached the third passage in mice before patients succumbed from the disease (224), highlighting a potential for PDX-based treatment models to aid in recruitment for clinical trials. Furthermore, another study mentions that 5.3% of their engrafted tumors were established within two weeks (225). In this study, the authors engrafted tumor cells from a patient with clear cell adenocarcinoma and managed to predict response to both first-line and second-line treatment prior to the occurrence in the patient.

We have exclusively engrafted stage III melanoma cells in our studies. The recently approved adjuvant treatment regiments for this patient group suggest that PDX models may have time to engraft before treatment initiation. However, using PDX models for treatment predictions in melanoma is challenging as the models are established in immunocompromised mice and will thus not respond to immunotherapy. Efforts to generate mice that carry a functional human immune system (i.e. humanized mice) are currently in progress, although facing challenges such as graft-versus-host disease (226).

Utilizing an *ex vivo* assay to predict treatment response can limit some of the issues with PDX models, such as long engraftment periods and animal welfare concerns. Of the 71 patient

samples we have investigated in the *ex vivo* assay, 15 did not yield an adequate signal in the cell viability assay, resulting in an establishment rate of 79% (data not shown). Additionally, some tumors were discarded before plating in the *ex vivo* assay, due to the absence of viable cells. In Paper I and II, we demonstrated that there was generally good concordance between the *ex vivo* drug efficacy assay and the PDX models, showing that the *ex vivo* assay may be a valid replacement for PDX models. Still, the issue with lacking immune system is a problem in the *ex vivo* assay. An approach to solve this issue could be to plate immune cells harvested from patient blood together with the tumor cells or co-culture the patient tumor with established immune cell lines, although these approaches would have to be further studied and optimized.

Utilizing patient-derived material in drug efficacy assays has been proposed as a method to identify response to various chemotherapeutic drugs (214). For instance, it has been demonstrated less response to chemotherapy in patient-derived breast cancer spheroids harvested from patients who did not show pathological complete response to the treatment (227). Further, a recent article predicted chemotherapy response in ovarian cancer and correctly demonstrated response in 26 of 35 patients (228). However, four patients were projected as non-responders in the drug efficacy assay but had clinical benefit of the chemotherapy. It has been suggested that it is improbable that a drug will have effect in a patient if the patient's tumor cells do not respond to the treatment when directly exposed to the drug at high concentrations (229). Therefore, incorporating *ex vivo* drug efficacy assays in the clinic may aid in determining patients who will <u>not</u> respond to certain therapies and thus reduce unnecessary side effects and treatment costs. In line with this, an *ex vivo* assay accurately predicted a melanoma patient that did not respond to BRAF inhibition by measuring phosphorylated ERK1/2 expression (230). However, this study also demonstrated reduced phosphorylated ERK1/2 levels in four patients who neither did respond to BRAF inhibition. This highlights the need for large prospective studies to determine if *ex vivo* drug efficacy assays are specific enough to be implemented in the clinic. Additionally, establishing the optimal culturing conditions and read-out methods of treatment response is needed to advance the spheroid assays.

In our studies we have employed low-adhesion plates to generate spheroids to be used in the *ex vivo* drug assay. Another three-dimensional culture type is organoids, which can be established from cells with stem cell-like properties, including cells from some types of cancer (e.g. epithelial and neural cancers). Organoids have been shown to recapitulate tumors genetically

and structurally (231) and have the advantage that they can be kept in culture long-term. As they are established through developmental processes, they may be used to examine cancer progression and is shown to better recapitulate the original tumor compared to spheroids (232). Cell viability assays using organoids have been established in 384- or 1536-well plates (231), even as co-cultures with fibroblasts (233), allowing for screening of a large number of drugs and concentrations simultaneously . However, melanomas are not epithelial-based and do not form organoids. Thus, generating spheroids is currently the favorable method for melanomas and other solid, non-epithelial tumors for drug discovery *ex vivo*.

5.2 Therapeutic relevance of targeting AXL

AXL expression is often upregulated in cancers and is associated with lower overall survival and aggressive cancer characteristics as described in Section 1.3. Thus, AXL poses as a potential therapeutic target in several cancers, including melanoma, and several small-molecular inhibitors and antibodies have been engineered to target AXL (234-236). Interestingly, AXL has gained focus as an important contributor to phenotype switching (or EMT in epithelial-derived cancers), which is associated with treatment resistance (237). A mechanism of resistance towards targeted therapy is overexpression of RTKs to overcome treatment pressure by reactivating or bypassing the inhibited pathway. Examples include induced expression of receptor tyrosine-protein kinase erbB-3 (HER3) in response to PI3K inhibition in breast cancer (238) and induced EGFR expression in response to MAPK inhibitors in colorectal cancer (239). AXL has been found to dimerize with HER3 and especially, EGFR (62). Further, AXL overexpression has shown to result in less sensitivity towards EGFR inhibitors (240, 241). Thus, targeting AXL and EGFR together may be beneficial. However, it has been stated that melanomas are less reliant on EGFR signaling compared to other cancers (e.g. colorectal cancer) and in a panel of ten melanoma cell lines only three expressed EGFR (242). However, in Paper II, we demonstrated that only three out of ten melanoma cell lines expressed AXL as well. Two cell lines overlap between the panels and the expression of EGFR and AXL coincide in these cells. This could indicate that a subset of melanomas display high expression of these RTKs and may indicate mesenchymal-like treatment resistant cells. AXL is inversely correlated with MITF and studies have found that also a high MITF expression was correlated with innate resistance to MAPK inhibitors. In line with this, treatment with a MITF inhibitor has shown to increase sensitivity to MAPK inhibitors (243). Although loss of MITF

results in increased AXL, it is not known if the inverse relationship is true. In Paper II, we observed lower invasion in cells treated with an AXL inhibitor, indicating a less invasive phenotype. However, we also observed slightly decreased proliferation, suggesting that the cells do not accumulate MITF to yield the proliferative phenotype. A $MITF^{low}/AXL^{high}$ expression is associated with the invasive and treatment resistance phenotype and low response to MAPK inhibitors (60). This rather suggests an option for treatment with a combination of AXL and MAPK inhibitors for patients with low MITF expression. Accordingly, a clinical trial is investigating the combination of AXL inhibition together with MAPK inhibitors in melanoma (NCT02872259).

Current experience from clinical trials indicate that BGB324 is very well tolerated by patients alone or in combination with pembrolizumab or erlotinib ((244, 245) and personal communication with Dr. Marta Nyakas), meaning that even small benefit to survival from combining BGB324 treatment with standard therapy would argue for using AXL inhibitors in the clinic.

Combined inhibition of AXL and the DNA damage response pathway

Inhibition of AXL signaling increases DNA damage and reduces the expression of proteins involved with DNA repair (69) and the accumulation of CHK1 in the nucleus (70). AXL expression has further been suggested to protect cancer cells from fork collapse, a process mediated through the DDR pathway (66). These data indicate that AXL contribute to cell survival by managing DNA repair or the DDR. In line with this, in Paper II we observed downregulated expression of proteins involved with DDR following combined treatment with AXL and CHK1/2 inhibitors. In addition, AXL expression has been shown to reduce sensitivity to chemotherapies, PARP and WEE1 inhibitors (69, 70, 193, 194). These data suggest that targeting AXL in combination with these therapies might be clinically beneficial. A question is whether the resistance towards chemotherapies, cell cycle and DNA repair inhibitors is mediated by phenotype switching (or EMT for epithelial-based cancers) or if it is an AXL-specific mechanism. In support of the first, transcriptional changes demonstrating EMT and induced AXL expression was observed in cisplatin resistant NSCLC cells (246). Overexpression of AXL has been suggested to be the driving force of EMT in breast cancer cells and suppression of AXL heightened chemotherapy response (247). However, another

report state that EMT-derived therapy resistance is independent of AXL, despite demonstrating that AXL inhibition increases sensitivity to taxanes and inhibitors of aurora kinase and polo-like kinase 1 in mescenchymal cells (194). Furthermore, in Paper II we observed reduced AXL phosphorylation in response to inhibition of DDR proteins (CHK1/2 and ATR). It has been suggested that CHK1/2 inhibitor AZD7762 also has affinity for AXL and may thus be employed as an AXL inhibitor (216). However, as we also observed reduced phosphorylation of AXL in ATR inhibited cells, and found similar proliferation responses in knock down cells as in inhibited cells, it indicates that there may be a currently unexplored mechanism that downregulated AXL activation in response to DDR inhibition.

5.3 Soluble AXL levels as a biomarker of cancer aggressiveness

Studies have shown that AXL ligand GAS6 may bind sAXL in human plasma and serum (248). This would indicate that shedding of sAXL results in decreased AXL signaling as it sequesters the activating ligand and that increased sAXL would be associated with a favorable outcome. Additionally, studies employing an engineered AXL extracellular domain with increased binding affinity for GAS6 have shown that the variant binds GAS6 and results in decreased therapy resistance (249). On the other hand, elevated sAXL levels are associated with increased cancer stage and lower survival (47, 49). We recently reported that sAXL levels were increased in patient effusions from ovarian carcinoma, malignant mesothelioma and breast cancer compared to benign reactive effusions (250). In line with this, a prominent increase in sAXL levels was observed in blood samples when comparing stage III and stage IV melanoma patients in Paper III. Currently, disease relapse is observed through computerized tomography (CT) scans. CT scans expose the patients to x-rays and its use has been shown to attribute to radiation-induced cancer (251). Thus, to limit its use would be beneficial. In paper III, sAXL levels showed good sensitivity and specificity as a biomarker of stage IV melanoma and could thus further be studied as a marker of progressive disease. However, the blood samples of the stage IV melanoma patients were first drawn at the start of treatment. It would be beneficial to study the sAXL levels over time, starting with stage III melanoma patients, to identify if sAXL measurements in blood samples could substitute or supplement CT scans to measure disease progression.

There are currently no approved biomarkers of immunotherapy response in melanoma, although PD-L1 expression in the tumor and a high mutational burden has been suggested as predictive markers (252). However, due to complex signaling and alterations in tumor-immune interactions, it has been suggested that dynamic biomarkers (i.e. biomarkers measured over time) may be more accurate in determining immunotherapy response (253). In Paper III, we measured sAXL levels in the blood of stage IV melanoma patients before or on treatment with ipilimumab to examine if sAXL levels could be associated with survival. A correlation between increased sAXL and lower survival was observed only after 7 weeks of ipilimumab treatment, and not at earlier time points (before treatment and at 4 weeks of treatment). This indicates that a threshold level of sAXL needs to be exceeded and highlights the importance of dynamic biomarkers. The difference in sAXL levels associated with survival was not dramatic. Therefore, categorizing patients based only on sAXL levels would be difficult due to somewhat overlap between the two groups. Thus, sAXL could potentially be used in a panel with other markers to increase the specificity and sensitivity of the assay.

A question is whether testing AXL expression as a biomarker could have been performed by quantitative PCR (qPCR) of tumor cells instead of by enzyme-linked immunosorbent assays (ELISA) of blood samples. qPCR-based methods are already employed in routine diagnostics for melanoma to test for *BRAF* and *NRAS* mutations, and would therefore be a cost-effective and convenient method. However, this method is restricted as it cannot easily measure biomarkers over time. Additionally, AXL mRNA expression has been found to not correlate with AXL protein expression in dendritic cells and macrophages (254). In line with this, we observed dissimilarities in the mRNA and protein expression in cells harvested from patients (data not shown). These data suggest that AXL is post-transcriptionally regulated and that measuring sAXL levels are more accurate to determine AXL cellular expression compared to mRNA expression approaches.

5.4 Therapeutic relevance of targeting B7-H3

Expression of B7-H3 is commonly detected in cancers and is associated with a negative prognostic impact, as described in Section 1.5. Importantly, B7-H3 is usually not detected in normal cells, highlighting its potential as a specific target of cancer cells and indicating that targeting B7-H3 may have few side effects. On the other hand, B7-H3 expression is suggested to be induced in response to inflammation in non-cancerous cells (255). Cancer cells may

release factors to induce an inflammatory microenvironment (256), implying that B7-H3 expression may be upregulated in normal cells in cancer patients. Although monoclonal and bispecific antibodies targeting B7-H3 has been generated and tested in phase I/II clinical trials, final results are yet to be communicated. However, interim reports have stated that a B7-H3 monoclonal antibody was tolerated well in patients, with no dose-limiting toxicities (257). Interestingly, recent studies demonstrated that B7-H3 CAR T cells had antitumor efficacy in several cancer types (128, 258, 259), highlighting B7-H3 as a potential target using CAR T cell therapy. Accordingly, a clinical trial using B7-H3 CAR T cells for recurrent or refractory glioblastoma is expected to commence soon (NCT04077866).

B7-H3 has been proposed to have both immune regulatory and pro-oncogenic functions. In the models employed in Paper IV, the immune system is lacking, thus we have examined the tumor-promoting role of B7-H3 independent of the immune system. Previously, we have observed that inhibited or knocked down expression of B7-H3 results in increased sensitivity to ERK/MAPK and PI3K pathway inhibitors and chemotherapy (108), indicating that targeting B7-H3 together with these inhibitors may be beneficial. In Paper IV, we explored the stress response through p38/MAPK signaling associated with chemotherapy and observed that expression of B7-H3 accentuates p38/MAPK signaling through repression of p38/MAPK phosphatase DUSP10. Interestingly, the p38/MAPK pathway may be activated through T cell receptor signaling (260). In line with this, B7-H3 augments p38/MAPK signaling in the brain tissue of mice with bacterial meningitis (261). Thus, examining B7-H3 activation of p38/MAPK in immune competent mice would be interesting.

As chemotherapy is rarely employed in treatment of melanomas, p38/MAPK activation through B7-H3 signaling should be examined in cancers that are more relevant. This may be especially important as B7-H3 is shown to decrease drug sensitivity to a range of chemotherapeutic drugs and small-molecular inhibitors with various mechanisms of actions, indicating a general mechanism of B7-H3 signaling to mediate therapy resistance.

Furthermore, B7-H3 may promote EMT and is shown to induce invasion (262) and expression of the mesenchymal signature (N-cadherin, vimentin) and decrease expression of the epithelial marker E-cadherin (263, 264). B7-H3 is found to increase the stem cell population through activation of MEK1/2 by binding the major vault protein (MVP) (265). EMT is found to induce a stem-cell like population, highlighting the role of B7-H3 in EMT. It is found that B7-H3 mediates resistance to chemotherapies through the JAK2/STAT3 (119) and PI3K pathways

(266, 267), in addition to p38/MAPK as demonstrated in Paper IV. Upregulation of these pathways are associated with EMT (268, 269), indicating that drug resistance mediated through B7-H3 expression could be a measure of the mesenchymal-like phenotype. Studies of B7-H3 in phenotype switching or EMT would be beneficial to determine if B7-H3 is involved in these processes.

Sensitization to various treatments through inhibited activity or reduced expression of B7-H3 indicates the potential of targeting B7-H3 to enhance therapeutic responses. Interestingly, in Paper IV we observed resensitization to DTIC in resistant cells with knocked down expression of B7-H3. This suggests that B7-H3 may be an important target in treatment resistant tumors and this potential should be further studied in melanoma as well as other cancers.

6 Concluding remarks and future perspectives

New treatment options in the past decade have revolutionized melanoma therapy resulting in longer survival and better patient care. Despite this, many patients do not respond to, are not eligible for or develop resistance towards the current treatment options. Thus, it is important to detect ways to enhance the benefit of the available treatment options and investigate biomarkers or other indicators that can predict responders and non-responders. Additionally, discovering new therapeutic targets and new combinations to augment treatment responses and ways to overcome resistance mechanisms is essential. The use of preclinical models, such as *ex vivo* assays and PDXs, may be important for this work and could be implemented to aid in identifying therapeutic responses.

In Paper I, we aimed to examine the competency of using an *ex vivo* drug efficacy assay to predict treatment response to vemurafenib in tumor cells harvested from stage III melanoma patients with surgical resection of their lymph node metastases. We found that there was a good concordance between vemurafenib response and BRAF mutation status. Additionally, we detected a subset of BRAF mutated cells that did not respond to vemurafenib, although we did not expose mutations associated with innate resistance. However, this work was only performed on a group level, and it would be interesting to associate a patient's clinical response to treatment response in the *ex vivo* assay to evaluate the feasibility of the *ex vivo* assay as a treatment predictor. This approach has recently gained interest since stage III melanoma patients with complete resection of their lymph node metastases from August 2019 receive adjuvant treatment with immunotherapy or targeted therapy. Most patients will receive immunotherapy as first-line treatment, thus developing the *ex vivo* assay to distinguish immune responses will benefit the assay. Either co-culturing the tumor cells with immune cell lines or adding immune cells from the respective patients' blood may be approaches to evaluate. Additionally, expanding the assay to 384- or 1536-well plates (compared to the current 96-well plates) would allow for screening of more drugs, combinations and concentrations and could be useful for drug discovery and preclinical research.

By using the *ex vivo* drug efficacy assay to examine new targeted treatment combinations, we demonstrated in Paper II that cells harvested from patients had a slight decrease in viability after treatment with AXL inhibitor BGB324, and more prominent decrease in viability after the

combination of BGB324 and CHK1/2 inhibitor AZD7762. It would be particularly compelling to examine the effect of AXL inhibition on DNA damage, as we did not detect the link between AXL inhibition and H2AX activity that others have reported. This may be caused by the fact that different methodological approaches have been utilized (i.e. we used flow cytometry and immunoblot compared to others that used immunofluorescence) or that there are cancer-type or cell-type specific mechanisms. However, we did observe inhibited CDC25C activity after BGB324 treatment, indicating DNA damage. Furthermore, it could also be of interest to examine the effect of AXL and DDR inhibition related to phenotype switching.

In Paper III, we demonstrated that sAXL levels were detected in plasma and serum from stage III and IV melanoma patients. We detected higher sAXL levels with increased stage, highlighting a potential to employ sAXL levels a biomarker of cancer aggressiveness. To warrant this, sAXL levels should be measured at several time points in stage III melanoma patients who are thus followed to determine if sAXL levels can be employed as a biomarker of disease progression. Additionally, sAXL levels were correlated with survival in patients after seven weeks of ipilimumab treatment. However, if sAXL should have any potential as a biomarker of ipilimumab response, it should probably be included in a panel with other markers to increase sensitivity and specificity.

In paper IV, we detected decreased sensitivity to DTIC and cisplatin in B7-H3 expressing cells, indicating that B7-H3 aids in treatment resistance to chemotherapy. We found that B7-H3 knockdown results in the upregulation of p38/MAPK phosphatase DUSP10. It would be interesting to determine the molecular mechanism underlying this regulation. Further, DUSP10 may also negatively regulate the JNK pathway, thus examining JNK signaling in regards to B7-H3 expression and stress signaling is compelling. Especially, it would be important to investigate how B7-H3 mediates stress response in an immune competent setting. Crucial to understanding B7-H3 biology is to identify its binding partner(s). This could unravel the molecular mechanisms underlying B7-H3 tumor promoting and immune stimulatory and inhibitory functions.

7 References

1. Mehlen P, Puisieux A. Metastasis: a question of life or death. Nat Rev Cancer. 2006;6:449.
2. Cancer in Norway 2018 - Cancer incidence, mortality, survival and prevalence in Norway. Oslo: Cancer Registry of Norway, 2018.
3. Public Health Report: Health Status in Norway 2018. Oslo: Norwegian Institute of Public Health, 2018.
4. Bailey MH, Tokheim C, Porta-Pardo E, Sengupta S, Bertrand D, Weerasinghe A, et al. Comprehensive Characterization of Cancer Driver Genes and Mutations. Cell. 2018;174(4):1034-5.
5. Hanahan D, Weinberg RA. Hallmarks of cancer: the next generation. Cell. 2011;144(5):646-74.
6. Floor SL, Dumont JE, Maenhaut C, Raspe E. Hallmarks of cancer: of all cancer cells, all the time? Trends Mol Med. 2012;18(9):509-15.
7. Tsoi J, Robert L, Paraiso K, Galvan C, Sheu KM, Lay J, et al. Multi-stage Differentiation Defines Melanoma Subtypes with Differential Vulnerability to Drug-Induced Iron-Dependent Oxidative Stress. Cancer Cell. 2018;33(5):890-904 e5.
8. Luzzi KJ, MacDonald IC, Schmidt EE, Kerkvliet N, Morris VL, Chambers AF, et al. Multistep nature of metastatic inefficiency: dormancy of solitary cells after successful extravasation and limited survival of early micrometastases. Am J Pathol. 1998;153(3):865-73.
9. Paget S. The distribution of secondary growths in cancer of the breast. 1889. Cancer Metastasis Rev. 1989;8(2):98-101.
10. Kaplan RN, Riba RD, Zacharoulis S, Bramley AH, Vincent L, Costa C, et al. VEGFR1-positive haematopoietic bone marrow progenitors initiate the pre-metastatic niche. Nature. 2005;438(7069):820-7.
11. Peinado H, Zhang H, Matei IR, Costa-Silva B, Hoshino A, Rodrigues G, et al. Pre-metastatic niches: organ-specific homes for metastases. Nat Rev Cancer. 2017;17:302.
12. Turajlic S, Swanton C. Metastasis as an evolutionary process. Science. 2016;352(6282):169-75.
13. Anderson RL, Balasas T, Callaghan J, Coombes RC, Evans J, Hall JA, et al. A framework for the development of effective anti-metastatic agents. Nat Rev Clin Oncol. 2019;16(3):185-204.
14. Skrypek N, Goossens S, De Smedt E, Vandamme N, Berx G. Epithelial-to-Mesenchymal Transition: Epigenetic Reprogramming Driving Cellular Plasticity. Trends Genet. 2017;33(12):943-59.
15. Lemmon MA, Schlessinger J. Cell signaling by receptor tyrosine kinases. Cell. 2010;141(7):1117-34.
16. Caunt CJ, Keyse SM. Dual-specificity MAP kinase phosphatases (MKPs): shaping the outcome of MAP kinase signalling. FEBS J. 2013;280(2):489-504.
17. Zhang W, Liu HT. MAPK signal pathways in the regulation of cell proliferation in mammalian cells. Cell Res. 2002;12(1):9-18.
18. Buday L, Downward J. Many faces of Ras activation. Biochim Biophys Acta. 2008;1786(2):178-87.
19. Durrant DE, Morrison DK. Targeting the Raf kinases in human cancer: the Raf dimer dilemma. Br J Cancer. 2018;118(1):3-8.
20. Cox AD, Der CJ, Philips MR. Targeting RAS Membrane Association: Back to the Future for Anti-RAS Drug Discovery? Clin Cancer Res. 2015;21(8):1819-27.

21. Leicht DT, Balan V, Kaplun A, Singh-Gupta V, Kaplun L, Dobson M, et al. Raf kinases: function, regulation and role in human cancer. Biochim Biophys Acta. 2007;1773(8):1196-212.
22. Ashwell JD. The many paths to p38 mitogen-activated protein kinase activation in the immune system. Nat Rev Immunol. 2006;6(7):532-40.
23. Cuenda A, Rousseau S. p38 MAP-kinases pathway regulation, function and role in human diseases. Biochim Biophys Acta. 2007;1773(8):1358-75.
24. Wagner EF, Nebreda AR. Signal integration by JNK and p38 MAPK pathways in cancer development. Nat Rev Cancer. 2009;9(8):537-49.
25. Eferl R, Wagner EF. AP-1: a double-edged sword in tumorigenesis. Nat Rev Cancer. 2003;3(11):859-68.
26. Thorpe LM, Yuzugullu H, Zhao JJ. PI3K in cancer: divergent roles of isoforms, modes of activation and therapeutic targeting. Nat Rev Cancer. 2015;15(1):7-24.
27. Manning BD, Cantley LC. AKT/PKB signaling: navigating downstream. Cell. 2007;129(7):1261-74.
28. Mendoza MC, Er EE, Blenis J. The Ras-ERK and PI3K-mTOR pathways: cross-talk and compensation. Trends Biochem Sci. 2011;36(6):320-8.
29. Cheung M, Sharma A, Madhunapantula SV, Robertson GP. Akt3 and mutant V600E B-Raf cooperate to promote early melanoma development. Cancer Res. 2008;68(9):3429-39.
30. O'Bryan JP, Frye RA, Cogswell PC, Neubauer A, Kitch B, Prokop C, et al. axl, a transforming gene isolated from primary human myeloid leukemia cells, encodes a novel receptor tyrosine kinase. Mol Cell Biol. 1991;11(10):5016-31.
31. Hafizi S, Dahlback B. Gas6 and protein S. Vitamin K-dependent ligands for the Axl receptor tyrosine kinase subfamily. FEBS J. 2006;273(23):5231-44.
32. Schoumacher M, Burbridge M. Key Roles of AXL and MER Receptor Tyrosine Kinases in Resistance to Multiple Anticancer Therapies. Curr Oncol Rep. 2017;19(3):19.
33. Wu G, Ma Z, Hu W, Wang D, Gong B, Fan C, et al. Molecular insights of Gas6/TAM in cancer development and therapy. Cell Death Dis. 2017;8(3):e2700.
34. Nagata K, Ohashi K, Nakano T, Arita H, Zong C, Hanafusa H, et al. Identification of the product of growth arrest-specific gene 6 as a common ligand for Axl, Sky, and Mer receptor tyrosine kinases. J Biol Chem. 1996;271(47):30022-7.
35. Lemke G, Burstyn-Cohen T. TAM receptors and the clearance of apoptotic cells. Ann N Y Acad Sci. 2010;1209:23-9.
36. Hasanbasic I, Rajotte I, Blostein M. The role of gamma-carboxylation in the anti-apoptotic function of gas6. J Thromb Haemost. 2005;3(12):2790-7.
37. Lew ED, Oh J, Burrola PG, Lax I, Zagorska A, Traves PG, et al. Differential TAM receptor-ligand-phospholipid interactions delimit differential TAM bioactivities. Elife. 2014;3.
38. Tsou WI, Nguyen KQ, Calarese DA, Garforth SJ, Antes AL, Smirnov SV, et al. Receptor tyrosine kinases, TYRO3, AXL, and MER, demonstrate distinct patterns and complex regulation of ligand-induced activation. J Biol Chem. 2014;289(37):25750-63.
39. Park IK, Trotta R, Yu J, Caligiuri MA. Axl/Gas6 pathway positively regulates FLT3 activation in human natural killer cell development. Eur J Immunol. 2013;43(10):2750-5.
40. Scaltriti M, Elkabets M, Baselga J. Molecular Pathways: AXL, a Membrane Receptor Mediator of Resistance to Therapy. Clin Cancer Res. 2016;22(6):1313-7.
41. Burchert A, Attar EC, McCloskey P, Fridell YW, Liu ET. Determinants for transformation induced by the Axl receptor tyrosine kinase. Oncogene. 1998;16(24):3177-87.
42. Linger RM, Keating AK, Earp HS, Graham DK. TAM receptor tyrosine kinases: biologic functions, signaling, and potential therapeutic targeting in human cancer. Adv Cancer Res. 2008;100:35-83.

43. O'Bryan JP, Fridell YW, Koski R, Varnum B, Liu ET. The transforming receptor tyrosine kinase, Axl, is post-translationally regulated by proteolytic cleavage. J Biol Chem. 1995;270(2):551-7.
44. Lu Y, Wan J, Yang Z, Lei X, Niu Q, Jiang L, et al. Regulated intramembrane proteolysis of the AXL receptor kinase generates an intracellular domain that localizes in the nucleus of cancer cells. FASEB J. 2017;31(4):1382-97.
45. Orme JJ, Du Y, Vanarsa K, Mayeux J, Li L, Mutwally A, et al. Heightened cleavage of Axl receptor tyrosine kinase by ADAM metalloproteases may contribute to disease pathogenesis in SLE. Clin Immunol. 2016;169:58-68.
46. Miller MA, Oudin MJ, Sullivan RJ, Wang SJ, Meyer AS, Im H, et al. Reduced Proteolytic Shedding of Receptor Tyrosine Kinases Is a Post-Translational Mechanism of Kinase Inhibitor Resistance. Cancer Discov. 2016;6(4):382-99.
47. Dengler M, Staufer K, Huber H, Stauber R, Bantel H, Weiss KH, et al. Soluble Axl is an accurate biomarker of cirrhosis and hepatocellular carcinoma development: results from a large scale multicenter analysis. Oncotarget. 2017;8(28):46234-48.
48. Staufer K, Dengler M, Huber H, Marculescu R, Stauber R, Lackner C, et al. The non-invasive serum biomarker soluble Axl accurately detects advanced liver fibrosis and cirrhosis. Cell Death Dis. 2017;8(10):e3135.
49. Reichl P, Fang M, Starlinger P, Staufer K, Nenutil R, Muller P, et al. Multicenter analysis of soluble Axl reveals diagnostic value for very early stage hepatocellular carcinoma. Int J Cancer. 2015;137(2):385-94.
50. Korshunov VA. Axl-dependent signalling: a clinical update. Clin Sci (Lond). 2012;122(8):361-8.
51. Braunger J, Schleithoff L, Schulz AS, Kessler H, Lammers R, Ullrich A, et al. Intracellular signaling of the Ufo/Axl receptor tyrosine kinase is mediated mainly by a multi-substrate docking-site. Oncogene. 1997;14(22):2619-31.
52. Keating AK, Kim GK, Jones AE, Donson AM, Ware K, Mulcahy JM, et al. Inhibition of Mer and Axl receptor tyrosine kinases in astrocytoma cells leads to increased apoptosis and improved chemosensitivity. Mol Cancer Ther. 2010;9(5):1298-307.
53. Kirane A, Ludwig KF, Sorrelle N, Haaland G, Sandal T, Ranaweera R, et al. Warfarin Blocks Gas6-Mediated Axl Activation Required for Pancreatic Cancer Epithelial Plasticity and Metastasis. Cancer Res. 2015;75(18):3699-705.
54. Papadakis ES, Cichon MA, Vyas JJ, Patel N, Ghali L, Cerio R, et al. Axl promotes cutaneous squamous cell carcinoma survival through negative regulation of pro-apoptotic Bcl-2 family members. J Invest Dermatol. 2011;131(2):509-17.
55. Rothlin CV, Ghosh S, Zuniga EI, Oldstone MB, Lemke G. TAM receptors are pleiotropic inhibitors of the innate immune response. Cell. 2007;131(6):1124-36.
56. Lu Q, Lemke G. Homeostatic regulation of the immune system by receptor tyrosine kinases of the Tyro 3 family. Science. 2001;293(5528):306-11.
57. Paolino M, Choidas A, Wallner S, Pranjic B, Uribesalgo I, Loeser S, et al. The E3 ligase Cbl-b and TAM receptors regulate cancer metastasis via natural killer cells. Nature. 2014;507(7493):508-12.
58. Gjerdrum C, Tiron C, Hoiby T, Stefansson I, Haugen H, Sandal T, et al. Axl is an essential epithelial-to-mesenchymal transition-induced regulator of breast cancer metastasis and patient survival. Proc Natl Acad Sci U S A. 2010;107(3):1124-9.
59. Vuoriluoto K, Haugen H, Kiviluoto S, Mpindi JP, Nevo J, Gjerdrum C, et al. Vimentin regulates EMT induction by Slug and oncogenic H-Ras and migration by governing Axl expression in breast cancer. Oncogene. 2011;30(12):1436-48.

60. Muller J, Krijgsman O, Tsoi J, Robert L, Hugo W, Song C, et al. Low MITF/AXL ratio predicts early resistance to multiple targeted drugs in melanoma. Nat Commun. 2014;5:5712.
61. Gay CM, Balaji K, Byers LA. Giving AXL the axe: targeting AXL in human malignancy. Br J Cancer. 2017;116(4):415-23.
62. Elkabets M, Pazarentzos E, Juric D, Sheng Q, Pelossof RA, Brook S, et al. AXL mediates resistance to PI3Kalpha inhibition by activating the EGFR/PKC/mTOR axis in head and neck and esophageal squamous cell carcinomas. Cancer Cell. 2015;27(4):533-46.
63. Hong J, Peng D, Chen Z, Sehdev V, Belkhiri A. ABL regulation by AXL promotes cisplatin resistance in esophageal cancer. Cancer Res. 2013;73(1):331-40.
64. Wang C, Jin H, Wang N, Fan S, Wang Y, Zhang Y, et al. Gas6/Axl Axis Contributes to Chemoresistance and Metastasis in Breast Cancer through Akt/GSK-3beta/beta-catenin Signaling. Theranostics. 2016;6(8):1205-19.
65. Ludwig KF, Du W, Sorrelle NB, Wnuk-Lipinska K, Topalovski M, Toombs JE, et al. Small-Molecule Inhibition of Axl Targets Tumor Immune Suppression and Enhances Chemotherapy in Pancreatic Cancer. Cancer Res. 2018;78(1):246-55.
66. Kariolis MS, Miao YR, Diep A, Nash SE, Olcina MM, Jiang D, et al. Inhibition of the GAS6/AXL pathway augments the efficacy of chemotherapies. J Clin Invest. 2017;127(1):183-98.
67. Boshuizen J, Koopman LA, Krijgsman O, Shahrabi A, van den Heuvel EG, Ligtenberg MA, et al. Cooperative targeting of melanoma heterogeneity with an AXL antibody-drug conjugate and BRAF/MEK inhibitors. Nat Med. 2018;24(2):203-12.
68. Ye X, Li Y, Stawicki S, Couto S, Eastham-Anderson J, Kallop D, et al. An anti-Axl monoclonal antibody attenuates xenograft tumor growth and enhances the effect of multiple anticancer therapies. Oncogene. 2010;29(38):5254-64.
69. Balaji K, Vijayaraghavan S, Diao L, Tong P, Fan Y, Carey JP, et al. AXL Inhibition Suppresses the DNA Damage Response and Sensitizes Cells to PARP Inhibition in Multiple Cancers. Mol Cancer Res. 2017;15(1):45-58.
70. Sen T, Tong P, Diao L, Li L, Fan Y, Hoff J, et al. Targeting AXL and mTOR Pathway Overcomes Primary and Acquired Resistance to WEE1 Inhibition in Small-Cell Lung Cancer. Clin Cancer Res. 2017;23(20):6239-53.
71. Oien DB, Garay T, Eckstein S, Chien J. Cisplatin and Pemetrexed Activate AXL and AXL Inhibitor BGB324 Enhances Mesothelioma Cell Death from Chemotherapy. Front Pharmacol. 2017;8:970.
72. Hutterer M, Knyazev P, Abate A, Reschke M, Maier H, Stefanova N, et al. Axl and growth arrest-specific gene 6 are frequently overexpressed in human gliomas and predict poor prognosis in patients with glioblastoma multiforme. Clin Cancer Res. 2008;14(1):130-8.
73. Gjerdrum C, Tiron C, Høiby T, Stefansson I, Haugen H, Sandal T, et al. Axl is an essential epithelial-to-mesenchymal transition-induced regulator of breast cancer metastasis and patient survival. Proc Natl Acad Sci U S A. 2010;107(3):1124.
74. Quinn JM, Greenwade MM, Palisoul ML, Opara G, Massad K, Guo L, et al. Therapeutic Inhibition of the Receptor Tyrosine Kinase AXL Improves Sensitivity to Platinum and Taxane in Ovarian Cancer. Mol Cancer Ther. 2019;18(2):389-98.
75. Harashima H, Dissmeyer N, Schnittger A. Cell cycle control across the eukaryotic kingdom. Trends Cell Biol. 2013;23(7):345-56.
76. Childs BG, Baker DJ, Kirkland JL, Campisi J, van Deursen JM. Senescence and apoptosis: dueling or complementary cell fates? EMBO Rep. 2014;15(11):1139-53.
77. Johnson A, Skotheim JM. Start and the restriction point. Curr Opin Cell Biol. 2013;25(6):717-23.

78. Pietenpol JA, Stewart ZA. Cell cycle checkpoint signaling: cell cycle arrest versus apoptosis. Toxicology. 2002;181-182:475-81.
79. Barnum KJ, O'Connell MJ. Cell cycle regulation by checkpoints. Methods Mol Biol. 2014;1170:29-40.
80. Riley T, Sontag E, Chen P, Levine A. Transcriptional control of human p53-regulated genes. Nat Rev Mol Cell Biol. 2008;9(5):402-12.
81. Schuler M, Bossy-Wetzel E, Goldstein JC, Fitzgerald P, Green DR. p53 induces apoptosis by caspase activation through mitochondrial cytochrome c release. J Biol Chem. 2000;275(10):7337-42.
82. Ou HL, Schumacher B. DNA damage responses and p53 in the aging process. Blood. 2018;131(5):488-95.
83. Roos WP, Thomas AD, Kaina B. DNA damage and the balance between survival and death in cancer biology. Nat Rev Cancer. 2016;16(1):20-33.
84. Chatterjee N, Walker GC. Mechanisms of DNA damage, repair, and mutagenesis. Environ Mol Mutagen. 2017;58(5):235-63.
85. Mehta A, Haber JE. Sources of DNA double-strand breaks and models of recombinational DNA repair. Cold Spring Harb Perspect Biol. 2014;6(9):a016428.
86. Marechal A, Zou L. DNA damage sensing by the ATM and ATR kinases. Cold Spring Harb Perspect Biol. 2013;5(9).
87. Podhorecka M, Skladanowski A, Bozko P. H2AX Phosphorylation: Its Role in DNA Damage Response and Cancer Therapy. J Nucleic Acids. 2010;2010(pii: 920161):9.
88. Awasthi P, Foiani M, Kumar A. ATM and ATR signaling at a glance. J Cell Sci. 2015;128(23):4255-62.
89. Knijnenburg TA, Wang L, Zimmermann MT, Chambwe N, Gao GF, Cherniack AD, et al. Genomic and Molecular Landscape of DNA Damage Repair Deficiency across The Cancer Genome Atlas. Cell Rep. 2018;23(1):239-54 e6.
90. Hoeijmakers JH. Genome maintenance mechanisms for preventing cancer. Nature. 2001;411(6835):366-74.
91. Farmer H, McCabe N, Lord CJ, Tutt AN, Johnson DA, Richardson TB, et al. Targeting the DNA repair defect in BRCA mutant cells as a therapeutic strategy. Nature. 2005;434(7035):917-21.
92. O'Connor MJ. Targeting the DNA Damage Response in Cancer. Mol Cell. 2015;60(4):547-60.
93. Weber AM, Ryan AJ. ATM and ATR as therapeutic targets in cancer. Pharmacol Ther. 2015;149:124-38.
94. Wehler T, Thomas M, Schumann C, Bosch-Barrera J, Segarra NV, Dickgreber NJ, et al. A randomized, phase 2 evaluation of the CHK1 inhibitor, LY2603618, administered in combination with pemetrexed and cisplatin in patients with advanced nonsquamous non-small cell lung cancer. Lung Cancer. 2017;108:212-6.
95. Sausville E, LoRusso P, Carducci M, Carter J, Quinn MF, Malburg L, et al. Phase I dose-escalation study of AZD7762, a checkpoint kinase inhibitor, in combination with gemcitabine in US patients with advanced solid tumors. Cancer Chemother Pharmacol. 2014;73(3):539-49.
96. Laquente B, Lopez-Martin J, Richards D, Illerhaus G, Chang DZ, Kim G, et al. A phase II study to evaluate LY2603618 in combination with gemcitabine in pancreatic cancer patients. BMC Cancer. 2017;17.
97. Flem-Karlsen K, Fodstad O, Tan M, Nunes-Xavier CE. B7-H3 in Cancer - Beyond Immune Regulation. Trends Cancer. 2018;4(6):401-4.
98. Flem-Karlsen K, Fodstad Y, Nunes-Xavier CE. B7-H3 immune checkpoint protein in human cancer. Curr Med Chem. 2019.

99. Thommen DS, Schumacher TN. T Cell Dysfunction in Cancer. Cancer Cell. 2018;33(4):547-62.
100. Ceeraz S, Nowak EC, Noelle RJ. B7 family checkpoint regulators in immune regulation and disease. Trends Immunol. 2013;34(11):556-63.
101. Sharpe AH, Freeman GJ. The B7-CD28 superfamily. Nat Rev Immunol. 2002;2(2):116-26.
102. Zou W, Chen L. Inhibitory B7-family molecules in the tumour microenvironment. Nat Rev Immunol. 2008;8(6):467-77.
103. Zou W, Wolchok JD, Chen L. PD-L1 (B7-H1) and PD-1 pathway blockade for cancer therapy: Mechanisms, response biomarkers, and combinations. Sci Transl Med. 2016;8(328):328rv4.
104. Seidel JA, Otsuka A, Kabashima K. Anti-PD-1 and Anti-CTLA-4 Therapies in Cancer: Mechanisms of Action, Efficacy, and Limitations. Front Oncol. 2018;8:86.
105. Hansen JD, Du Pasquier L, Lefranc MP, Lopez V, Benmansour A, Boudinot P. The B7 family of immunoregulatory receptors: a comparative and evolutionary perspective. Mol Immunol. 2009;46(3):457-72.
106. Chapoval AI, Ni J, Lau JS, Wilcox RA, Flies DB, Liu D, et al. B7-H3: a costimulatory molecule for T cell activation and IFN-gamma production. Nat Immunol. 2001;2(3):269-74.
107. Ingebrigtsen VA, Boye K, Tekle C, Nesland JM, Flatmark K, Fodstad O. B7-H3 expression in colorectal cancer: nuclear localization strongly predicts poor outcome in colon cancer. Int J Cancer. 2012;131(11):2528-36.
108. Flem-Karlsen K, Tekle C, Andersson Y, Flatmark K, Fodstad O, Nunes-Xavier CE. Immunoregulatory protein B7-H3 promotes growth and decreases sensitivity to therapy in metastatic melanoma cells. Pigment Cell Melanoma Res. 2017;30(5):467-76.
109. Chen W, Liu P, Wang Y, Nie W, Li Z, Xu W, et al. Characterization of a soluble B7-H3 (sB7-H3) spliced from the intron and analysis of sB7-H3 in the sera of patients with hepatocellular carcinoma. PLoS One. 2013;8(10):e76965.
110. Zhang G, Hou J, Shi J, Yu G, Lu B, Zhang X. Soluble CD276 (B7-H3) is released from monocytes, dendritic cells and activated T cells and is detectable in normal human serum. Immunology. 2008;123(4):538-46.
111. Steinberger P, Majdic O, Derdak SV, Pfistershammer K, Kirchberger S, Klauser C, et al. Molecular characterization of human 4Ig-B7-H3, a member of the B7 family with four Ig-like domains. J Immunol. 2004;172(4):2352-9.
112. Suh WK, Gajewska BU, Okada H, Gronski MA, Bertram EM, Dawicki W, et al. The B7 family member B7-H3 preferentially down-regulates T helper type 1-mediated immune responses. Nat Immunol. 2003;4(9):899-906.
113. Castellanos JR, Purvis IJ, Labak CM, Guda MR, Tsung AJ, Velpula KK, et al. B7-H3 role in the immune landscape of cancer. Am J Clin Exp Immunol. 2017;6(4):66-75.
114. Zhang G, Wang J, Kelly J, Gu G, Hou J, Zhou Y, et al. B7-H3 augments the inflammatory response and is associated with human sepsis. J Immunol. 2010;185(6):3677-84.
115. Veenstra RG, Flynn R, Kreymborg K, McDonald-Hyman C, Saha A, Taylor PA, et al. B7-H3 expression in donor T cells and host cells negatively regulates acute graft-versus-host disease lethality. Blood. 2015;125(21):3335-46.
116. Tekle C, Nygren MK, Chen YW, Dybsjord I, Nesland JM, Maelandsmo GM, et al. B7-H3 contributes to the metastatic capacity of melanoma cells by modulation of known metastasis-associated genes. Int J Cancer. 2012;130(10):2282-90.
117. Kasten BB, Arend RC, Katre AA, Kim H, Fan J, Ferrone S, et al. B7-H3-targeted 212Pb radioimmunotherapy of ovarian cancer in preclinical models. Nucl Med Biol. 2017;47:23-30.

118. Seaman S, Zhu Z, Saha S, Zhang XM, Yang MY, Hilton MB, et al. Eradication of Tumors through Simultaneous Ablation of CD276/B7-H3-Positive Tumor Cells and Tumor Vasculature. Cancer Cell. 2017;31(4):501-15 e8.
119. Liu H, Tekle C, Chen YW, Kristian A, Zhao Y, Zhou M, et al. B7-H3 silencing increases paclitaxel sensitivity by abrogating Jak2/Stat3 phosphorylation. Mol Cancer Ther. 2011;10(6):960-71.
120. Li Y, Guo G, Song J, Cai Z, Yang J, Chen Z, et al. B7-H3 Promotes the Migration and Invasion of Human Bladder Cancer Cells via the PI3K/Akt/STAT3 Signaling Pathway. J Cancer. 2017;8(5):816-24.
121. Nunes-Xavier CE, Karlsen KF, Tekle C, Pedersen C, Oyjord T, Hongisto V, et al. Decreased expression of B7-H3 reduces the glycolytic capacity and sensitizes breast cancer cells to AKT/mTOR inhibitors. Oncotarget. 2016;7(6):6891-901.
122. Shi T, Ma Y, Cao L, Zhan S, Xu Y, Fu F, et al. B7-H3 promotes aerobic glycolysis and chemoresistance in colorectal cancer cells by regulating HK2. Cell Death Dis. 2019;10(4):308.
123. Zuo J, Wang B, Long M, Gao Z, Zhang Z, Wang H, et al. The type 1 transmembrane glycoprotein B7-H3 interacts with the glycolytic enzyme ENO1 to promote malignancy and glycolysis in HeLa cells. FEBS Lett. 2018;592(14):2476-88.
124. Lim S, Liu H, Madeira da Silva L, Arora R, Liu Z, Phillips JB, et al. Immunoregulatory Protein B7-H3 Reprograms Glucose Metabolism in Cancer Cells by ROS-Mediated Stabilization of HIF1alpha. Cancer Res. 2016;76(8):2231-42.
125. Jiang B, Zhang T, Liu F, Sun Z, Shi H, Hua D, et al. The co-stimulatory molecule B7-H3 promotes the epithelial-mesenchymal transition in colorectal cancer. Oncotarget. 2016;7(22):31755-71.
126. Kang FB, Wang L, Jia HC, Li D, Li HJ, Zhang YG, et al. B7-H3 promotes aggression and invasion of hepatocellular carcinoma by targeting epithelial-to-mesenchymal transition via JAK2/STAT3/Slug signaling pathway. Cancer Cell Int. 2015;15:45.
127. Xu L, Ding X, Tan H, Qian J. Correlation between B7-H3 expression and matrix metalloproteinases 2 expression in pancreatic cancer. Cancer Cell Int. 2013;13(1):81.
128. Majzner RG, Theruvath JL, Nellan A, Heitzeneder S, Cui Y, Mount CW, et al. CAR T Cells Targeting B7-H3, a Pan-Cancer Antigen, Demonstrate Potent Preclinical Activity Against Pediatric Solid Tumors and Brain Tumors. Clin Cancer Res. 2019;25(8):2560-74.
129. Ando H, Niki Y, Ito M, Akiyama K, Matsui MS, Yarosh DB, et al. Melanosomes are transferred from melanocytes to keratinocytes through the processes of packaging, release, uptake, and dispersion. J Invest Dermatol. 2012;132(4):1222-9.
130. Gershenwald JE, Scolyer RA, Hess KR, Sondak VK, Long GV, Ross MI, et al. Melanoma staging: Evidence-based changes in the American Joint Committee on Cancer eighth edition cancer staging manual. CA Cancer J Clin. 2017;67(6):472-92.
131. Miller AJ, Mihm MC, Jr. Melanoma. N Engl J Med. 2006;355(1):51-65.
132. Cancer in Norway 2017 - Cancer incidence, mortality, survival and prevalence in Norway. Oslo: Cancer Registry of Norway, 2018.
133. Ransohoff KJ, Jaju PD, Tang JY, Carbone M, Leachman S, Sarin KY. Familial skin cancer syndromes: Increased melanoma risk. J Am Acad Dermatol. 2016;74(3):423-34; .
134. Fremtidens kreftkostnader. Oslo Economics. 2019.
135. Alexandrov LB, Nik-Zainal S, Wedge DC, Aparicio SA, Behjati S, Biankin AV, et al. Signatures of mutational processes in human cancer. Nature. 2013;500(7463):415-21.
136. Cancer Genome Atlas N. Genomic Classification of Cutaneous Melanoma. Cell. 2015;161(7):1681-96.

137. Long GV, Menzies AM, Nagrial AM, Haydu LE, Hamilton AL, Mann GJ, et al. Prognostic and clinicopathologic associations of oncogenic BRAF in metastatic melanoma. J Clin Oncol. 2011;29(10):1239-46.
138. Dankner M, Rose AAN, Rajkumar S, Siegel PM, Watson IR. Classifying BRAF alterations in cancer: new rational therapeutic strategies for actionable mutations. Oncogene. 2018;37(24):3183-99.
139. Raaijmakers MI, Widmer DS, Narechania A, Eichhoff O, Freiberger SN, Wenzina J, et al. Co-existence of BRAF and NRAS driver mutations in the same melanoma cells results in heterogeneity of targeted therapy resistance. Oncotarget. 2016;7(47):77163-74.
140. Cerami E, Gao J, Dogrusoz U, Gross BE, Sumer SO, Aksoy BA, et al. The cBio cancer genomics portal: an open platform for exploring multidimensional cancer genomics data. Cancer Discov. 2012;2(5):401-4.
141. Cirenajwis H, Lauss M, Ekedahl H, Torngren T, Kvist A, Saal LH, et al. NF1-mutated melanoma tumors harbor distinct clinical and biological characteristics. Mol Oncol. 2017;11(4):438-51.
142. Li FZ, Dhillon AS, Anderson RL, McArthur G, Ferrao PT. Phenotype switching in melanoma: implications for progression and therapy. Front Oncol. 2015;5:31.
143. Hoek KS, Eichhoff OM, Schlegel NC, Dobbeling U, Kobert N, Schaerer L, et al. In vivo switching of human melanoma cells between proliferative and invasive states. Cancer Res. 2008;68(3):650-6.
144. Kaur A, Webster MR, Weeraratna AT. In the Wnt-er of life: Wnt signalling in melanoma and ageing. Br J Cancer. 2016;115(11):1273-9.
145. Sensi M, Catani M, Castellano G, Nicolini G, Alciato F, Tragni G, et al. Human cutaneous melanomas lacking MITF and melanocyte differentiation antigens express a functional Axl receptor kinase. J Invest Dermatol. 2011;131(12):2448-57.
146. Wellbrock C, Arozarena I. Microphthalmia-associated transcription factor in melanoma development and MAP-kinase pathway targeted therapy. Pigment Cell Melanoma Res. 2015;28(4):390-406.
147. Smith MP, Rana S, Ferguson J, Rowling EJ, Flaherty KT, Wargo JA, et al. A PAX3/BRN2 rheostat controls the dynamics of BRAF mediated MITF regulation in MITF(high) /AXL(low) melanoma. Pigment Cell Melanoma Res. 2019;32(2):280-91.
148. Gerami P, Cook RW, Wilkinson J, Russell MC, Dhillon N, Amaria RN, et al. Development of a prognostic genetic signature to predict the metastatic risk associated with cutaneous melanoma. Clin Cancer Res. 2015;21(1):175-83.
149. Jonsson G, Busch C, Knappskog S, Geisler J, Miletic H, Ringner M, et al. Gene expression profiling-based identification of molecular subtypes in stage IV melanomas with different clinical outcome. Clin Cancer Res. 2010;16(13):3356-67.
150. Harbst K, Staaf J, Lauss M, Karlsson A, Masback A, Johansson I, et al. Molecular profiling reveals low- and high-grade forms of primary melanoma. Clin Cancer Res. 2012;18(15):4026-36.
151. Hauschild A, Dummer R, Schadendorf D, Santinami M, Atkinson V, Mandala M, et al. Longer Follow-Up Confirms Relapse-Free Survival Benefit With Adjuvant Dabrafenib Plus Trametinib in Patients With Resected BRAF V600-Mutant Stage III Melanoma. J Clin Oncol. 2018:JCO1801219.
152. Eggermont AMM, Blank CU, Mandala M, Long GV, Atkinson V, Dalle S, et al. Adjuvant Pembrolizumab versus Placebo in Resected Stage III Melanoma. N Engl J Med. 2018;378(19):1789-801.
153. Weber J, Mandala M, Del Vecchio M, Gogas HJ, Arance AM, Cowey CL, et al. Adjuvant Nivolumab versus Ipilimumab in Resected Stage III or IV Melanoma. N Engl J Med. 2017;377(19):1824-35.

154. Crosby T, Fish R, Coles B, Mason MD. Systemic treatments for metastatic cutaneous melanoma. Cochrane Database Syst Rev. 2000(2):CD001215.
155. Long GV, Flaherty KT, Stroyakovskiy D, Gogas H, Levchenko E, de Braud F, et al. Dabrafenib plus trametinib versus dabrafenib monotherapy in patients with metastatic BRAF V600E/K-mutant melanoma: long-term survival and safety analysis of a phase 3 study. Ann Oncol. 2017;28(7):1631-9.
156. Daud A, Gill J, Kamra S, Chen L, Ahuja A. Indirect treatment comparison of dabrafenib plus trametinib versus vemurafenib plus cobimetinib in previously untreated metastatic melanoma patients. J Hematol Oncol. 2017;10(1):3.
157. Robert C, Grob JJ, Stroyakovskiy D, Karaszewska B, Hauschild A, Levchenko E, et al. Five-Year Outcomes with Dabrafenib plus Trametinib in Metastatic Melanoma. N Engl J Med. 2019.
158. Ascierto PA, McArthur GA, Dreno B, Atkinson V, Liszkay G, Di Giacomo AM, et al. Cobimetinib combined with vemurafenib in advanced BRAF(V600)-mutant melanoma (coBRIM): updated efficacy results from a randomised, double-blind, phase 3 trial. Lancet Oncol. 2016;17(9):1248-60.
159. Dummer R, Ascierto PA, Gogas HJ, Arance A, Mandala M, Liszkay G, et al. Encorafenib plus binimetinib versus vemurafenib or encorafenib in patients with BRAF-mutant melanoma (COLUMBUS): a multicentre, open-label, randomised phase 3 trial. Lancet Oncol. 2018;19(5):603-15.
160. Dummer R, Ascierto PA, Gogas HJ, Arance A, Mandala M, Liszkay G, et al. Overall survival in patients with BRAF-mutant melanoma receiving encorafenib plus binimetinib versus vemurafenib or encorafenib (COLUMBUS): a multicentre, open-label, randomised, phase 3 trial. Lancet Oncol. 2018;19(10):1315-27.
161. Poulikakos PI, Persaud Y, Janakiraman M, Kong X, Ng C, Moriceau G, et al. RAF inhibitor resistance is mediated by dimerization of aberrantly spliced BRAF(V600E). Nature. 2011;480(7377):387-90.
162. Rushworth LK, Hindley AD, O'Neill E, Kolch W. Regulation and role of Raf-1/B-Raf heterodimerization. Mol Cell Biol. 2006;26(6):2262-72.
163. Castle JC, Uduman M, Pabla S, Stein RB, Buell JS. Mutation-Derived Neoantigens for Cancer Immunotherapy. Front Immunol. 2019;10:1856.
164. Larkin J, Chiarion-Sileni V, Gonzalez R, Grob JJ, Rutkowski P, Lao CD, et al. Five-Year Survival with Combined Nivolumab and Ipilimumab in Advanced Melanoma. N Engl J Med. 2019.
165. Topalian SL, Sznol M, McDermott DF, Kluger HM, Carvajal RD, Sharfman WH, et al. Survival, durable tumor remission, and long-term safety in patients with advanced melanoma receiving nivolumab. J Clin Oncol. 2014;32(10):1020-30.
166. Ribas A, Hamid O, Daud A, Hodi FS, Wolchok JD, Kefford R, et al. Association of Pembrolizumab With Tumor Response and Survival Among Patients With Advanced Melanoma. JAMA. 2016;315(15):1600-9.
167. Smalley KS, Lioni M, Dalla Palma M, Xiao M, Desai B, Egyhazi S, et al. Increased cyclin D1 expression can mediate BRAF inhibitor resistance in BRAF V600E-mutated melanomas. Mol Cancer Ther. 2008;7(9):2876-83.
168. Whittaker SR, Theurillat JP, Van Allen E, Wagle N, Hsiao J, Cowley GS, et al. A genome-scale RNA interference screen implicates NF1 loss in resistance to RAF inhibition. Cancer Discov. 2013;3(3):350-62.
169. Paraiso KH, Xiang Y, Rebecca VW, Abel EV, Chen YA, Munko AC, et al. PTEN loss confers BRAF inhibitor resistance to melanoma cells through the suppression of BIM expression. Cancer Res. 2011;71(7):2750-60.

170. Watson IR, Li L, Cabeceiras PK, Mahdavi M, Gutschner T, Genovese G, et al. The RAC1 P29S hotspot mutation in melanoma confers resistance to pharmacological inhibition of RAF. Cancer Res. 2014;74(17):4845-52.
171. Irvine M, Stewart A, Pedersen B, Boyd S, Kefford R, Rizos H. Oncogenic PI3K/AKT promotes the step-wise evolution of combination BRAF/MEK inhibitor resistance in melanoma. Oncogenesis. 2018;7(9):72.
172. Johnson DB, Menzies AM, Zimmer L, Eroglu Z, Ye F, Zhao S, et al. Acquired BRAF inhibitor resistance: A multicenter meta-analysis of the spectrum and frequencies, clinical behaviour, and phenotypic associations of resistance mechanisms. Eur J Cancer. 2015;51(18):2792-9.
173. Shi H, Hugo W, Kong X, Hong A, Koya RC, Moriceau G, et al. Acquired resistance and clonal evolution in melanoma during BRAF inhibitor therapy. Cancer Discov. 2014;4(1):80-93.
174. Rizos H, Menzies AM, Pupo GM, Carlino MS, Fung C, Hyman J, et al. BRAF inhibitor resistance mechanisms in metastatic melanoma: spectrum and clinical impact. Clin Cancer Res. 2014;20(7):1965-77.
175. Nazarian R, Shi H, Wang Q, Kong X, Koya RC, Lee H, et al. Melanomas acquire resistance to B-RAF(V600E) inhibition by RTK or N-RAS upregulation. Nature. 2010;468(7326):973-7.
176. Straussman R, Morikawa T, Shee K, Barzily-Rokni M, Qian ZR, Du J, et al. Tumour micro-environment elicits innate resistance to RAF inhibitors through HGF secretion. Nature. 2012;487(7408):500-4.
177. Hirata E, Girotti MR, Viros A, Hooper S, Spencer-Dene B, Matsuda M, et al. Intravital imaging reveals how BRAF inhibition generates drug-tolerant microenvironments with high integrin beta1/FAK signaling. Cancer Cell. 2015;27(4):574-88.
178. Chen DS, Mellman I. Oncology meets immunology: the cancer-immunity cycle. Immunity. 2013;39(1):1-10.
179. Havel JJ, Chowell D, Chan TA. The evolving landscape of biomarkers for checkpoint inhibitor immunotherapy. Nat Rev Cancer. 2019;19(3):133-50.
180. Gao J, Shi LZ, Zhao H, Chen J, Xiong L, He Q, et al. Loss of IFN-gamma Pathway Genes in Tumor Cells as a Mechanism of Resistance to Anti-CTLA-4 Therapy. Cell. 2016;167(2):397-404 e9.
181. Spranger S, Bao R, Gajewski TF. Melanoma-intrinsic beta-catenin signalling prevents anti-tumour immunity. Nature. 2015;523(7559):231-5.
182. Liu C, Peng W, Xu C, Lou Y, Zhang M, Wargo JA, et al. BRAF inhibition increases tumor infiltration by T cells and enhances the antitumor activity of adoptive immunotherapy in mice. Clin Cancer Res. 2013;19(2):393-403.
183. Peng W, Chen JQ, Liu C, Malu S, Creasy C, Tetzlaff MT, et al. Loss of PTEN Promotes Resistance to T Cell-Mediated Immunotherapy. Cancer Discov. 2016;6(2):202-16.
184. Harlin H, Meng Y, Peterson AC, Zha Y, Tretiakova M, Slingluff C, et al. Chemokine expression in melanoma metastases associated with CD8+ T-cell recruitment. Cancer Res. 2009;69(7):3077-85.
185. Strauss L, Bergmann C, Szczepanski M, Gooding W, Johnson JT, Whiteside TL. A unique subset of CD4+CD25highFoxp3+ T cells secreting interleukin-10 and transforming growth factor-beta1 mediates suppression in the tumor microenvironment. Clin Cancer Res. 2007;13(15 Pt 1):4345-54.
186. Cassetta L, Kitamura T. Targeting Tumor-Associated Macrophages as a Potential Strategy to Enhance the Response to Immune Checkpoint Inhibitors. Front Cell Dev Biol. 2018;6:38.

187. Daud AI, Loo K, Pauli ML, Sanchez-Rodriguez R, Sandoval PM, Taravati K, et al. Tumor immune profiling predicts response to anti-PD-1 therapy in human melanoma. J Clin Invest. 2016;126(9):3447-52.
188. Samstein RM, Lee CH, Shoushtari AN, Hellmann MD, Shen R, Janjigian YY, et al. Tumor mutational load predicts survival after immunotherapy across multiple cancer types. Nat Genet. 2019;51(2):202-6.
189. Zaretsky JM, Garcia-Diaz A, Shin DS, Escuin-Ordinas H, Hugo W, Hu-Lieskovan S, et al. Mutations Associated with Acquired Resistance to PD-1 Blockade in Melanoma. N Engl J Med. 2016;375(9):819-29.
190. Koyama S, Akbay EA, Li YY, Herter-Sprie GS, Buczkowski KA, Richards WG, et al. Adaptive resistance to therapeutic PD-1 blockade is associated with upregulation of alternative immune checkpoints. Nat Commun. 2016;7:10501.
191. Gao J, Ward JF, Pettaway CA, Shi LZ, Subudhi SK, Vence LM, et al. VISTA is an inhibitory immune checkpoint that is increased after ipilimumab therapy in patients with prostate cancer. Nat Med. 2017;23(5):551-5.
192. Ascierto PA, Melero I, Bhatia S, Bono P, Sanborn RE, Lipson EJ, et al. Initial efficacy of anti-lymphocyte activation gene-3 (anti–LAG-3; BMS-986016) in combination with nivolumab (nivo) in pts with melanoma (MEL) previously treated with anti–PD-1/PD-L1 therapy. J Clin Oncol. 2017;35(15_suppl):9520-.
193. Brand TM, Iida M, Stein AP, Corrigan KL, Braverman CM, Coan JP, et al. AXL Is a Logical Molecular Target in Head and Neck Squamous Cell Carcinoma. Clin Cancer Res. 2015;21(11):2601-12.
194. Wilson C, Ye X, Pham T, Lin E, Chan S, McNamara E, et al. AXL Inhibition Sensitizes Mesenchymal Cancer Cells to Antimitotic Drugs. Cancer Res. 2014;74(20):5878-90.
195. Wong CH, Siah KW, Lo AW. Estimation of clinical trial success rates and related parameters. Biostatistics. 2019;20(2):273-86.
196. Hanahan D, Coussens Lisa M. Accessories to the Crime: Functions of Cells Recruited to the Tumor Microenvironment. Cancer Cell. 2012;21(3):309-22.
197. Seip K, Fleten KG, Barkovskaya A, Nygaard V, Haugen MH, Engesaeter BO, et al. Fibroblast-induced switching to the mesenchymal-like phenotype and PI3K/mTOR signaling protects melanoma cells from BRAF inhibitors. Oncotarget. 2016;7(15):19997-20015.
198. Garman B, Anastopoulos IN, Krepler C, Brafford P, Sproesser K, Jiang Y, et al. Genetic and Genomic Characterization of 462 Melanoma Patient-Derived Xenografts, Tumor Biopsies, and Cell Lines. Cell Rep. 2017;21(7):1936-52.
199. Ben-David U, Siranosian B, Ha G, Tang H, Oren Y, Hinohara K, et al. Genetic and transcriptional evolution alters cancer cell line drug response. Nature. 2018;560(7718):325-30.
200. Prasad VVTS, Gopalan ROG. Continued use of MDA-MB-435, a melanoma cell line, as a model for human breast cancer, even in year, 2014. Npj Breast Cancer. 2015;1:15002.
201. Liu Y, Mi Y, Mueller T, Kreibich S, Williams EG, Van Drogen A, et al. Multi-omic measurements of heterogeneity in HeLa cells across laboratories. Nat Biotechnol. 2019;37(3):314-22.
202. Fodstad O, Kjonniksen I, Aamdal S, Nesland JM, Boyd MR, Pihl A. Extrapulmonary, tissue-specific metastasis formation in nude mice injected with FEMX-I human melanoma cells. Cancer Res. 1988;48(15):4382-8.
203. Xi Y, Riker A, Shevde-Samant L, Samant R, Morris C, Gavin E, et al. Global comparative gene expression analysis of melanoma patient samples, derived cell lines and corresponding tumor xenografts. Cancer Genom Proteom. 2008;5(1):1-35.

204. Stepanenko AA, Heng HH. Transient and stable vector transfection: Pitfalls, off-target effects, artifacts. Mutat Res. 2017;773:91-103.
205. Khaitan D, Chandna S, Arya MB, Dwarakanath BS. Establishment and characterization of multicellular spheroids from a human glioma cell line; Implications for tumor therapy. J Transl Med. 2006;4:12.
206. Uematsu N, Zhao YX, Kiyomi A, Yuan B, Onda K, Tanaka S, et al. Chemo-sensitivity of Two-dimensional Monolayer and Three-dimensional Spheroid of Breast Cancer MCF-7 Cells to Daunorubicin, Docetaxel, and Arsenic Disulfide. Anticancer Res. 2018;38(4):2101-8.
207. Alvarez-Perez J, Ballesteros P, Cerdan S. Microscopic images of intraspheroidal pH by H-1 magnetic resonance chemical shift imaging of pH sensitive indicators. Magn Reson Mater Phy. 2005;18(6):293-301.
208. Kim JB. Three-dimensional tissue culture models in cancer biology. Semin Cancer Biol. 2005;15(5):365-77.
209. Cui X, Hartanto Y, Zhang H. Advances in multicellular spheroids formation. J R Soc Interface. 2017;14(127).
210. Jun E, Hong SM, Yoo HJ, Kim MB, Won JS, An S, et al. Genetic and metabolic comparison of orthotopic and heterotopic patient-derived pancreatic-cancer xenografts to the original patient tumors. Oncotarget. 2018;9(8):7867-81.
211. Krepler C, Sproesser K, Brafford P, Beqiri M, Garman B, Xiao M, et al. A Comprehensive Patient-Derived Xenograft Collection Representing the Heterogeneity of Melanoma. Cell Rep. 2017;21(7):1953-67.
212. Braekeveldt N, von Stedingk K, Fransson S, Martinez-Monleon A, Lindgren D, Axelson H, et al. Patient-Derived Xenograft Models Reveal Intratumor Heterogeneity and Temporal Stability in Neuroblastoma. Cancer Res. 2018;78(20):5958-69.
213. Krepler C, Xiao M, Sproesser K, Brafford PA, Shannan B, Beqiri M, et al. Personalized Preclinical Trials in BRAF Inhibitor-Resistant Patient-Derived Xenograft Models Identify Second-Line Combination Therapies. Clin Cancer Res. 2016;22(7):1592-602.
214. Majumder B, Baraneedharan U, Thiyagarajan S, Radhakrishnan P, Narasimhan H, Dhandapani M, et al. Predicting clinical response to anticancer drugs using an ex vivo platform that captures tumour heterogeneity. Nat Commun. 2015;6:6169.
215. Zabludoff SD, Deng C, Grondine MR, Sheehy AM, Ashwell S, Caleb BL, et al. AZD7762, a novel checkpoint kinase inhibitor, drives checkpoint abrogation and potentiates DNA-targeted therapies. Mol Cancer Ther. 2008;7(9):2955-66.
216. Park JS, Lee C, Kim HK, Kim D, Son JB, Ko E, et al. Suppression of the metastatic spread of breast cancer by DN10764 (AZD7762)-mediated inhibition of AXL signaling. Oncotarget. 2016;7(50):83308-18.
217. Kim J, Bang H. Three common misuses of P values. Dent Hypotheses. 2016;7(3):73-80.
218. Chou TC. Theoretical basis, experimental design, and computerized simulation of synergism and antagonism in drug combination studies. Pharmacol Rev. 2006;58(3):621-81.
219. van der Velden DL, Hoes LR, van der Wijngaart H, van Berge Henegouwen JM, van Werkhoven E, Roepman P, et al. The Drug Rediscovery protocol facilitates the expanded use of existing anticancer drugs. Nature. 2019;574(7776):127-31.
220. Grzywa TM, Paskal W, Wlodarski PK. Intratumor and Intertumor Heterogeneity in Melanoma. Transl Oncol. 2017;10(6):956-75.
221. Johnson DB, Dahlman KB. Class Matters: Sensitivity of BRAF-Mutant Melanoma to MAPK Inhibition. Clin Cancer Res. 2018;24(24):6107-9.

222. Jakob JA, Bassett RL, Jr., Ng CS, Curry JL, Joseph RW, Alvarado GC, et al. NRAS mutation status is an independent prognostic factor in metastatic melanoma. Cancer. 2012;118(16):4014-23.
223. Izumchenko E, Paz K, Ciznadija D, Sloma I, Katz A, Vasquez-Dunddel D, et al. Patient-derived xenografts effectively capture responses to oncology therapy in a heterogeneous cohort of patients with solid tumors. Ann Oncol. 2017;28(10):2595-605.
224. Einarsdottir BO, Bagge RO, Bhadury J, Jespersen H, Mattsson J, Nilsson LM, et al. Melanoma patient-derived xenografts accurately model the disease and develop fast enough to guide treatment decisions. Oncotarget. 2014;5(20):9609-18.
225. Vargas R, Gopal P, Kuzmishin GB, DeBernardo R, Koyfman SA, Jha BK, et al. Case study: patient-derived clear cell adenocarcinoma xenograft model longitudinally predicts treatment response. NPJ Precis Oncol. 2018;2:14.
226. Meraz IM, Majidi M, Meng F, Shao R, Ha MJ, Neri S, et al. An Improved Patient-Derived Xenograft Humanized Mouse Model for Evaluation of Lung Cancer Immune Responses. Cancer Immunol Res. 2019;7(8):1267-79.
227. Halfter K, Ditsch N, Kolberg HC, Fischer H, Hauzenberger T, von Koch FE, et al. Prospective cohort study using the breast cancer spheroid model as a predictor for response to neoadjuvant therapy--the SpheroNEO study. BMC Cancer. 2015;15:519.
228. Shuford S, Wilhelm C, Rayner M, Elrod A, Millard M, Mattingly C, et al. Prospective Validation of an Ex Vivo, Patient-Derived 3D Spheroid Model for Response Predictions in Newly Diagnosed Ovarian Cancer. Sci Rep. 2019;9(1):11153.
229. Blom K, Nygren P, Larsson R, Andersson CR. Predictive Value of Ex Vivo Chemosensitivity Assays for Individualized Cancer Chemotherapy: A Meta-Analysis. SLAS Technol. 2017;22(3):306-14.
230. Schayowitz A, Bertenshaw G, Jeffries E, Schatz T, Cotton J, Villanueva J, et al. Functional Profiling of Live Melanoma Samples Using a Novel Automated Platform. Plos One. 2012;7(12).
231. van de Wetering M, Francies HE, Francis JM, Bounova G, Iorio F, Pronk A, et al. Prospective derivation of a living organoid biobank of colorectal cancer patients. Cell. 2015;161(4):933-45.
232. Kondo J, Inoue M. Application of Cancer Organoid Model for Drug Screening and Personalized Therapy. Cells. 2019;8(5).
233. Kenny HA, Lal-Nag M, White EA, Shen M, Chiang CY, Mitra AK, et al. Quantitative high throughput screening using a primary human three-dimensional organotypic culture predicts in vivo efficacy. Nat Commun. 2015;6:6220.
234. Holland SJ, Pan A, Franci C, Hu Y, Chang B, Li W, et al. R428, a Selective Small Molecule Inhibitor of Axl Kinase, Blocks Tumor Spread and Prolongs Survival in Models of Metastatic Breast Cancer. Cancer Res. 2010;70(4):1544-54.
235. Jeon JY, Park I-K, Buelow DR, Whatcott C, Warner SL, Blum W, et al. TP-0903, a Novel Axl Inhibitor with Activity in Drug Resistant FLT3-ITD+ AML through a Mechanism That Includes FLT3 Inhibition. Blood. 2017;130(Suppl 1):2522-.
236. Leconet W, Chentouf M, du Manoir S, Chevalier C, Sirvent A, Aït-Arsa I, et al. Therapeutic Activity of Anti-AXL Antibody against Triple-Negative Breast Cancer Patient-Derived Xenografts and Metastasis. Clin Cancer Res. 2017;23(11):2806-16.
237. Antony J, Huang RY. AXL-Driven EMT State as a Targetable Conduit in Cancer. Cancer Res. 2017;77(14):3725-32.
238. Chakrabarty A, Sanchez V, Kuba MG, Rinehart C, Arteaga CL. Feedback upregulation of HER3 (ErbB3) expression and activity attenuates antitumor effect of PI3K inhibitors. Proc Natl Acad Sci U S A. 2012;109(8):2718-23.

239. Prahallad A, Sun C, Huang S, Di Nicolantonio F, Salazar R, Zecchin D, et al. Unresponsiveness of colon cancer to BRAF(V600E) inhibition through feedback activation of EGFR. Nature. 2012;483(7387):100-3.
240. Brand TM, Iida M, Stein AP, Corrigan KL, Braverman CM, Luthar N, et al. AXL mediates resistance to cetuximab therapy. Cancer Res. 2014;74(18):5152-64.
241. Giles KM, Kalinowski FC, Candy PA, Epis MR, Zhang PM, Redfern AD, et al. Axl mediates acquired resistance of head and neck cancer cells to the epidermal growth factor receptor inhibitor erlotinib. Mol Cancer Ther. 2013;12(11):2541-58.
242. Laurenzana A, Margheri F, Biagioni A, Chilla A, Pimpinelli N, Ruzzolini J, et al. EGFR/uPAR interaction as druggable target to overcome vemurafenib acquired resistance in melanoma cells. EBioMedicine. 2019;39:194-206.
243. Aida S, Sonobe Y, Tanimura H, Oikawa N, Yuhki M, Sakamoto H, et al. MITF suppression improves the sensitivity of melanoma cells to a BRAF inhibitor. Cancer Lett. 2017;409:116-24.
244. Lorens J, Arce-Lara CE, Arriola E, Brunsvig P, Carcereny Costa E, Domine M, et al. Phase II open-label, multi-centre study of bemcentinib (BGB324), a first-in-class selective AXL inhibitor, in combination with pembrolizumab in patients with advanced NSCLC. J Clin Oncol. 2018;36(15_suppl):3078-.
245. Byers L, Gold K, Peguero J, Johnson M, Nieva J, Harb W, et al. P2.13-10 Ph I/II Study of Oral Selective AXL Inhibitor Bemcentinib (BGB324) in Combination with Erlotinib in pts with EGFRm NSCLC. J Thorac Oncol. 2018;13(10):S801-S2.
246. Kurokawa M, Ise N, Omi K, Goishi K, Higashiyama S. Cisplatin influences acquisition of resistance to molecular-targeted agents through epithelial–mesenchymal transition-like changes. Cancer Sci. 2013;104(7):904-11.
247. Asiedu MK, Beauchamp-Perez FD, Ingle JN, Behrens MD, Radisky DC, Knutson KL. AXL induces epithelial-to-mesenchymal transition and regulates the function of breast cancer stem cells. Oncogene. 2014;33(10):1316-24.
248. Ekman C, Stenhoff J, Dahlback B. Gas6 is complexed to the soluble tyrosine kinase receptor Axl in human blood. J Thromb Haemost. 2010;8(4):838-44.
249. Kariolis MS, Miao YR, Diep A, Nash SE, Olcina MM, Jiang D, et al. Inhibition of the GAS6/AXL pathway augments the efficacy of chemotherapies. J Clin Invest. 2017;127(1):183-98.
250. Flem Karlsen K, McFadden E, Florenes VA, Davidson B. Soluble AXL is ubiquitously present in malignant serous effusions. Gynecol Oncol. 2018.
251. Mathews JD, Forsythe AV, Brady Z, Butler MW, Goergen SK, Byrnes GB, et al. Cancer risk in 680,000 people exposed to computed tomography scans in childhood or adolescence: data linkage study of 11 million Australians. BMJ. 2013;346:f2360.
252. Gibney GT, Weiner LM, Atkins MB. Predictive biomarkers for checkpoint inhibitor-based immunotherapy. Lancet Oncol. 2016;17(12):e542-e51.
253. Lesterhuis WJ, Bosco A, Millward MJ, Small M, Nowak AK, Lake RA. Dynamic versus static biomarkers in cancer immune checkpoint blockade: unravelling complexity. Nat Rev Drug Discov. 2017;16(4):264-72.
254. Zagorska A, Traves PG, Lew ED, Dransfield I, Lemke G. Diversification of TAM receptor tyrosine kinase function. Nat Immunol. 2014;15(10):920-8.
255. Veenstra RG, Flynn R, Kreymborg K, McDonald-Hyman C, Saha A, Taylor PA, et al. B7-H3 expression in donor T cells and host cells negatively regulates acute graft-versus-host disease lethality. Blood. 2015;125(21):3335-46.
256. Mantovani A, Allavena P, Sica A, Balkwill F. Cancer-related inflammation. Nature. 2008;454(7203):436-44.

257. Powderly J, Cote G, Flaherty K, Szmulewitz RZ, Ribas A, Weber J, et al. Interim results of an ongoing Phase I, dose escalation study of MGA271 (Fc-optimized humanized anti-B7-H3 monoclonal antibody) in patients with refractory B7-H3-expressing neoplasms or neoplasms whose vasculature expresses B7-H3. J Immunother Cancer. 2015;3(Suppl 2):O8-O.
258. Du H, Hirabayashi K, Ahn S, Kren NP, Montgomery SA, Wang X, et al. Antitumor Responses in the Absence of Toxicity in Solid Tumors by Targeting B7-H3 via Chimeric Antigen Receptor T Cells. Cancer Cell. 2019;35(2):221-37 e8.
259. Tang X, Zhao S, Zhang Y, Wang Y, Zhang Z, Yang M, et al. B7-H3 as a Novel CAR-T Therapeutic Target for Glioblastoma. Mol Ther Oncolytics. 2019;14:279-87.
260. Rudd CE. MAPK p38: alternative and nonstressful in T cells. Nat Immunol. 2005;6(4):368-70.
261. Chen X, Li Y, Blankson S, Liu M, Huang D, Redmond HP, et al. B7-H3 Augments Inflammatory Responses and Exacerbates Brain Damage via Amplifying NF-κB p65 and MAPK p38 Activation during Experimental Pneumococcal Meningitis. PLoS ONE. 2017;12(1):e0171146.
262. Lemke D, Pfenning PN, Sahm F, Klein AC, Kempf T, Warnken U, et al. Costimulatory protein 4IgB7H3 drives the malignant phenotype of glioblastoma by mediating immune escape and invasiveness. Clin Cancer Res. 2012;18(1):105-17.
263. Jiang B, Zhang T, Liu F, Sun Z, Shi H, Hua D, et al. The co-stimulatory molecule B7-H3 promotes the epithelial-mesenchymal transition in colorectal cancer. Oncotarget. 2016.
264. Yu TT, Zhang T, Lu X, Wang RZ. B7-H3 promotes metastasis, proliferation, and epithelial-mesenchymal transition in lung adenocarcinoma. Onco Targets Ther. 2018;11:4693-700.
265. Liu Z, Zhang W, Phillips JB, Arora R, McClellan S, Li J, et al. Immunoregulatory protein B7-H3 regulates cancer stem cell enrichment and drug resistance through MVP-mediated MEK activation. Oncogene. 2019;38(1):88-102.
266. Zhang P, Chen Z, Ning K, Jin J, Han X. Inhibition of B7-H3 reverses oxaliplatin resistance in human colorectal cancer cells. Biochem Biophys Res Commun. 2017;490(3):1132-8.
267. Jiang B, Liu F, Liu Z, Zhang T, Hua D. B7-H3 increases thymidylate synthase expression via the PI3k-Akt pathway. Tumour Biol. 2016.
268. Wendt MK, Balanis N, Carlin CR, Schiemann WP. STAT3 and epithelial-mesenchymal transitions in carcinomas. JAKSTAT. 2014;3(1):e28975.
269. Gonzalez DM, Medici D. Signaling mechanisms of the epithelial-mesenchymal transition. Sci Signal. 2014;7(344):re8.

I

Translational Oncology
www.transonc.com

Volume 12 Number 7 July 2019 pp. 951–958 951

A Three-dimensional *Ex Vivo* Viability Assay Reveals a Strong Correlation Between Response to Targeted Inhibitors and Mutation Status in Melanoma Lymph Node Metastases[1]

Vivi Ann Flørenes[*], Karine Flem-Karlsen[*,†], Erin McFadden[*], Inger Riise Bergheim[‡], Vigdis Nygaard[§], Vegard Nygård[¶], Inger Nina Farstad[*,†], Geir Frode Øy[§], Elisabeth Emilsen[*], Karianne Giller-Fleten[§], Anne Hansen Ree[#,†], Kjersti Flatmark[†,§,], Hans Petter Gullestad[††], Robert Hermann[††], Truls Ryder[††], Patrik Wernhoff[*,2] and Gunhild Mari Mælandsmo[§,‡‡,2]**

[*]Department of Pathology, Norwegian Radium Hospital, Oslo University Hospital, N-0310 Oslo, Norway; [†]Institute for Clinical Medicine, Faculty of Medicine, University of Oslo, Norway; [‡]Department of Cancer Genetics, Institute for Cancer Research, Norwegian Radium Hospital, Oslo University Hospital, N-0310 Oslo, Norway; [§]Department of Tumor Biology, Institute for Cancer Research, Norwegian Radium Hospital, Oslo University Hospital, N-0310 Oslo, Norway; [¶]Department of Core Facilities, Institute for Cancer Research, Norwegian Radium Hospital, Oslo University Hospital, N-0310 Oslo, Norway; [#]Department of Oncology, Akershus University Hospital, N-1478 Lørenskog, Norway; [**]Department of Gastroenterological Surgery, Norwegian Radium Hospital, Oslo University Hospital, N-0310 Oslo, Norway; [††]Department of Plastic and Reconstructive Surgery, Norwegian Radium Hospital, Oslo University Hospital, N-0310 Oslo, Norway; [‡‡]Institute of Medical Biology, Faculty of Health Sciences, UiT-Arctic University of Norway, Tromsø, Norway

Abstract

Although clinical management of melanoma has changed considerably in recent years, intrinsic treatment resistance remains a severe problem and strategies to design personal treatment regimens are highly warranted. We have applied a three-dimensional (3D) *ex vivo* drug efficacy assay, exposing disaggregated cells from 38 freshly harvested melanoma lymph node metastases and 21 patient derived xenografts (PDXs) to clinical relevant drugs for 7 days, and examined its potential to evaluate therapy response. A strong association between Vemurafenib response and BRAF mutation status was achieved ($P < .0001$), while enhanced viability was seen in some NRAS mutated tumors. BRAF and NRAS mutated tumors responded comparably to the MEK inhibitor Cobimetinib. Based on the *ex vivo* results, two tumors diagnosed as BRAF wild-type by routine pathology examinations had to be re-evaluated; one was subsequently found to have a complex V600E mutation, the other a double BRAF mutation (V600E/K601 N). No BRAF inhibitor resistance mechanisms were identified, but PIK3CA and

Address all correspondence to: Gunhild M. Mælandsmo, Department of Tumor Biology, Norwegian Radium Hospital, Oslo University Hospital, PO Box 4950 Nydalen, 0424 Oslo, Norway. E-mail: gunhild.mari.malandsmo@rr-research.no

[1] Acknowledgements: This work was supported by South-Eastern Norway Regional Health Authority (KFK, EM, PW) and Research Council of Norway under the program from Publicly Initiated Clinical Trial Studies (grant number 218325VN, IRB) and the Cancer Society of Norway (IRB).

[2] Authors have contributed equally.

Received 6 December 2018; Revised 28 March 2019; Accepted 1 April 2019

1936-5233/19
https://doi.org/10.1016/j.tranon.2019.04.001

NF1 mutations were identified in two highly responsive tumors. Concordance between *ex vivo* drug responses using tissue from PDXs and corresponding patient tumors demonstrate that PDX models represent an indefinite source of tumor material that may allow *ex vivo* evaluation of numerous drugs and combinations, as well as studies of underlying molecular mechanisms. In conclusion, we have established a rapid and low cost *ex vivo* drug efficacy assay applicable on tumor tissue from patient biopsies. The 3D/spheroid format, limiting the influence from normal adjacent cells and allowing assessment of drug sensitivity to numerous drugs in one week, confirms its potential as a supplement to guide clinical decision, in particular in identifying non-responding patients.

Translational Oncology (2019) 12, 951–958

Introduction

Clinical management of melanomas has changed noticeably in recent years due to development of small-molecular inhibitors (BRAFi) targeting the $BRAF^{V600E}$ mutated protein and the use of immunotherapy [1]. Unfortunately, whereas initial responses are frequently observed in patients eligible to BRAFi treatment, nearly all relapse within one year [2,3]. Intrinsic BRAFi resistance is seen in approximately 20% of the patients and is associated with overexpression of cyclin D1 and COT, loss of PTEN and NF1, stromal expression of hepatocyte growth factor and RAC1 and HOXD8 mutations [4]. Reports have also indicated co-existence of clones harboring either BRAF or NRAS mutation [5,6] or BRAF/NRAS double-mutations within the same cells [7]. The majority of mechanisms of acquired BRAFi resistance include NRAS and MEK1/2 mutations, $BRAF^{V600E}$ amplification and alternative splicing of BRAF. In addition, dysregulation of PI3-kinase/Akt signaling and overexpression of receptor tyrosine kinases have been shown to have an impact [3]. To overcome acquired resistance, patients have been offered BRAFi in combination with MEK inhibitors (MEKi). Although progression-free survival is improved, most patients will, however, eventually experience disease progression [2,8,9].

Tumor cell lines grown as monolayer cultures (2D) have traditionally been used as a first step to evaluate the efficacy of anticancer therapies. This approach does, however, not adequately recapitulate the complex biology of the tumors [10–13]. To date, the use of patient derived xenograft (PDX) models have been recognized as the cornerstone for evaluating the potential of novel anti-cancer therapy [14,15] and several studies have demonstrated a strong correlation between treatment responses in PDXs and patient outcome [14,16,17]. The use of PDX models has, however, its limitations and is not well suited as routine assays of response prediction in individual patients. Most importantly, variability in engraftment and latency time clearly exceed what can be accepted in a clinical setting. Likewise, loss of human tumor environment and immune responses, costs and ethical considerations, limit extensive use of PDXs in routine diagnostics [18,19].

As a compromise between 2D-cultures and PDXs, several studies have demonstrated that growth as 3D-cultures more accurately mimic tumor tissue architecture, development of hypoxia, and expression of genes associated with tumorigenesis and therapy response [13,20,21] and thus outperform drug response predictions in 2D assays. One example is the use of organoids, established from patient tumor tissue, which has emerged as promising preclinical models to study drug efficacy, in particular in cancers of epithelial origin [22–24]. In melanomas, the use of human cell lines grown in 2D or 3D cultures [22,25,26], as well as animal models, have been the standard assays to evaluate the performance of novel drugs, and to our knowledge, no assays have been developed where patient tumor cells are utilized for drug sensitivity assessments (review in [27]). In the present study, we have developed and demonstrated clinical feasibility of an *ex vivo* drug sensitivity assay using fresh tumor tissue from melanoma lymph node metastases. The cells were kept in 3D, avoiding influences from stromal cells, and drug responses were evaluated after one-week exposure. Proof-of-principles was demonstrated by evaluating the sensitivity to BRAF-MEK–ERK inhibitors, and comparing the output with molecular data. Based on data from the drug sensitivity test, two tumors were found misclassified as BRAFwt according to routine diagnostic examinations. Upon subsequent NGS, both tumors were confirmed to have less common BRAF mutations. In conclusion, we have demonstrated that the *ex vivo* drug sensitivity assay is a fast and low-cost method showing potential to provide functional information that can supplement the molecular data. Ultimately this may enhance the diagnostic precision and assist in clinical decision-making.

Materials and Methods

Patients

Randomly collected treatment naïve melanoma lymph node metastases, resected at the Norwegian Radium Hospital, Oslo University Hospital were included. The study was approved by the Regional Committee for Medical Research Ethics of South-East Norway (2014/2208, 2015/2434). Informed consent was obtained from all patients according to national guidelines.

Ex vivo Drug Response Assay

Patient tumor tissue and PDXs were mechanically disaggregated and treated with collagenase (125 U/ml) and 2.5 mg/ml DNase (Sigma Aldrich, St. Louis, MO, USA) for one hour. To remove debris and large cell clumps the suspensions were filtered through 100 µm nylon Cell Strainer (BD Falcon, Franklin Lakes, NJ, US) and washed in ice-cold PBS. If required, red blood cells were removed by ACK lysis buffer (Lonza, Verviers, Belgium). The cells were washed in cold PBS and re-suspended in RPMI-1640 medium (Lonza) supplemented with 5% fetal calf serum (FCS) (Sigma Aldrich), 2 mM L-glutamine, and penicillin/streptavidin (50 U/ml of each) (Lonza). To analyze for drug response, approximately 20,000 viable cells (assessed by Trypan Blue exclusion), resuspended in RPMI-1640 containing 5% FCS and antibiotics, were plated per well in 96-wells round

bottom low adhesion plates, allowing spheroids to form (Nunc A/S, Roskilde, Denmark). Drugs were added immediately after seeding. After 5 days of treatment with Vemurafenib (Selleck Chemicals, Houston, TX, USA) and/or Cobimetinib (Selleck Chemicals), effect on viability was assessed using the CellTiter-Glo® Luminescent Cell Viability Assay (Promega, Madison, WI, USA) and reported as percentage viable cells in treated as compared to untreated control samples. For each patient sample, three technical replicates were analyzed. Several drug concentrations were initially applied, (data not shown), and 2 μM Vemurafenib and 50 nM Cobimetinib, were chosen as standard. Of the obtained tumor tissue, approximately 30% had to be discarded due to lack of viable cells in the biopsy, little material or lack of viability in control cells after analyses. However, PDX models could still be made from some of the latter and used in the *ex vivo* drug efficacy assay.

Molecular Analyses

DNA was extracted from 21 melanoma lymph node metastases and one PDX by the AllPrep DNA/RNA Mini Kit and AllPrep DNA/RNA/miRNA Universal kit (Qiagen, Hilden, Germany). Prior to extraction, cryo-sections were made and stained with hematoxylin/eosin. Only samples with >10% tumor cells were subjected to molecular analysis. The Ion Torrent PGM™ was used for sequencing with two different panels: the Ion AmpliSeq™ Cancer Hotspot Panel v2 covering ~2800 hotspot mutations in 50 genes, and the Oncomine Comprehensive Panel covering hotspot mutations in 73 genes, full exon coverage of 26 genes and copy number aberrations in 49 genes (Thermo Fisher Scientific, Inc., San Francisco, CA, USA).

The Torrent Suite Variant Caller version 5.0 was run using panel-optimized parameters from AmpliSeq.com for Ion AmpliSeq Cancer Hotspot Panel v2. Using hg19 as reference, single nucleotide substitutions that exceeded a 5% variant allele frequency threshold were identified. The variants were functionally annotated with ANNOVAR, using RefSeq as the underlying gene model [28] and using information from the 1000 Genomes Project [1000genomes.org] and the Catalogue of Somatic Mutations in Cancer [cancer.sanger.ac.uk/cosmic]. Detected mutations were in addition checked using the Integrative Genomics Viewer (IGV) [29]. $BRAF^{V600E/K}$ and NRAS mutation status were additionally established for all samples by an in-house PCR based assay used in routine diagnostics. Data supporting the findings are stored at Services for sensitive data (TSD) – University of Oslo. Access can be arranged by contacting the corresponding author (VAF) upon request.

In vivo Studies

To establish PDX models, melanoma lymph node metastases obtained from surgery were implanted subcutaneously into NOD SCID gamma mice (success rate 77%). Briefly, tumor tissue was cut into pieces of about 2 mm^3 and implanted subcutaneously in the flanks of >6 months old female mice. The first passage was named P0. Totally 21 PDX models have been established, of which 16 were from patient tumors analyzed for drug effects *ex vivo*.

Prior to *in vivo* treatment, the PDXs were re-implanted in the flanks of 6–8-week-old female atymic nude *foxn1*^{nu} mice and underwent two additional passages before treatment was initiated with bilateral implantation into new mice. After four weeks, the mice were randomized into a control (6 mice) and a treatment group (8 mice) each having an average tumor –volume distribution of 135 mm^3. The latter group was given 50 mg/kg Vemurafenib twice daily by oral gavage for 14 days. Controls were given 10% DMSO in 0,5% methylcellulose orally for the duration of the treatment. Tumor diameters were measured twice a week by digital calipers and tumor volume calculated by the formula 0.5 x length x $width^2$. Data is presented as average tumor volume ± standard error of the mean (S.E.M.). All mice were bred at the Department of Comparative Medicine, The Norwegian Radium Hospital and kept according to regulations of the Norwegian Welfare Act. Experiments involving animals were approved by the Norwegian Animal Research Authority (FOTS application number 8554).

Statistical Analysis

Statistical significance was determined by the Student's two-tailed *t*-test using GraphPad Prism version 7.0 (GraphPad Software, San Diego, CA, USA).

Results

Ex Vivo Assessment of Patients Own Tumor for Response to Vemurafenib Reveals A Close Correlation to Known BRAF/NRAS Mutation Status in Metastatic Melanoma

Here we aimed to establish a 3D *ex vivo* drug efficacy assay using freshly harvested melanoma tissue samples. As a proof of concept, the BRAFi Vemurafenib was chosen as test drug and the results correlated to BRAF mutation status. Tissue from 38 treatment naïve melanoma lymph node metastases were disaggregated and cells plated as spheroids in the presence or without 2 μM Vemurafenib for five days before viability was assessed. 50% reduction in viability was chosen as a stringent cutoff to discriminate between responders/non-responders. As shown in Figure 1, the assay verified a strong association between response and diagnostically detected BRAF mutation status ($P < .0001$). Of the 21 $BRAF^{V600E}$ mutated tumors, 12 (57%) were clearly responsive, whereas three were borderline responsive (Melmets-326, –376, –363), and six did not respond to the treatment. These numbers are in agreement with clinical experiences demonstrating an objective response to BRAF inhibition in approximately 50% of patients with metastatic melanoma [30]. None of the BRAF wild-type tumors responded to Vemurafenib while several of the BRAFwt/NRASmut tumors (in particular Melmets-328, –349, –365,), showed a marked increase in viability when tested in the *ex vivo* assay (Figure 1).

It is not expected that BRAF wild-type and NRAS mutated tumors will benefit from BRAFi treatment. Therefore we also tested the effect of the MEKi Cobimetinib. The effect of Vemurafenib and Cobimetinib was overall comparable in the BRAF mutated tumors (10 cases), but two tumors (Melmet-363, Melmet-376) that were borderline responsive to Vemurafenib, responded to Cobimetinib. Of the NRAS mutated tumors, four of seven clearly responded to Cobimetinib. Surprisingly, in two NRAS mutated (Melmel-388, Melmet-432), and to a minor extent in one BRAF mutated tumor (Melmet-397), the effect of MEKi was reversed when combined with BRAFi (Table 1).

Comparable Ex Vivo Treatment Responses in Patient Derived Tumor Cells And Corresponding PDXs

It has been previously documented that melanoma PDXs reliably reflect treatment responses seen in patients [14,31]. We therefore aimed to examine whether therapy effects using patient tumor cells and cells derived from the corresponding PDXs (n = 16) were

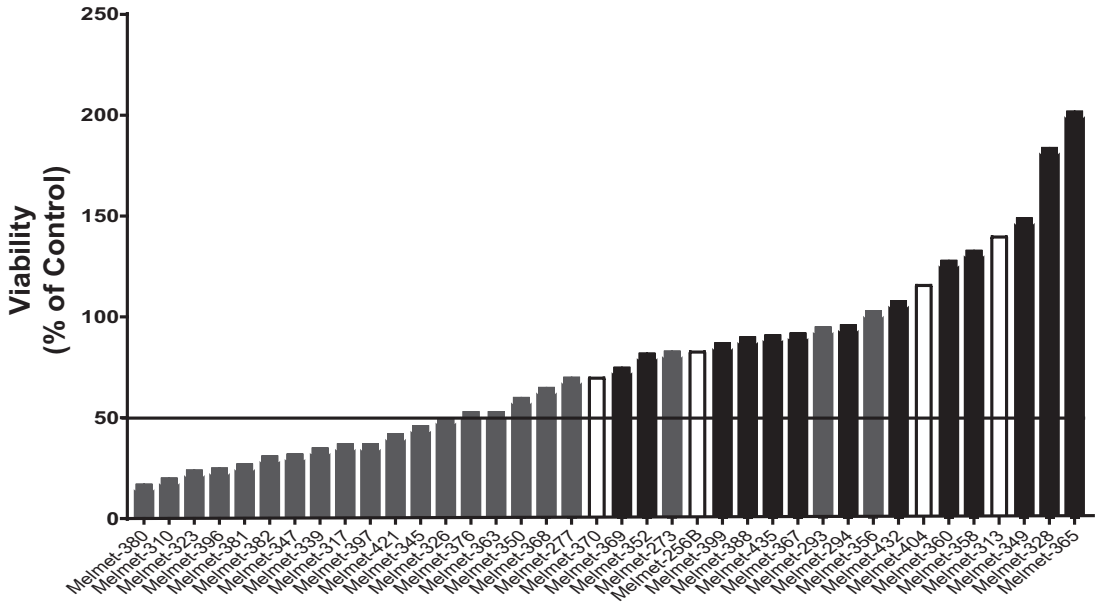

Figure 1. Viability of patient derived melanoma samples analyzed *ex vivo* for response to Vemurafenib. Lymph node metastases from 38 patients were disaggregated and cells plated and exposed to 2 μM Vemurafenib for 5 days as described in "Materials and Methods". Viability was assessed using CellTiter-Glo® Luminescent Cell viability assay and results presented as percentage viable cells compared to untreated controls and correlated to BRAF mutation status ($P < 0.0001$, Student's two-tailed *t*-test). 50% reduction in viability was chosen as cutoff for response/non-response. Gray bars; BRAF mutated, black bars; NRAS mutated, white bars; Double wild-type.

comparable in the *ex vivo* assay. In addition, five PDXs where patient tumors had not been analyzed were included. The PDX tumors were handled and exposed to treatment *ex vivo* as the patient samples. Despite minor variations, a good concordance was maintained throughout PDX-passages (Table 2 and data not shown). For some PDXs, however, later passages seemed to respond more similar to cells derived directly from the patient's tumor (Melmet-347, Melmet-381). Furthermore, in two cases (Melmets-350 and -356) several PDX passages showed no sign of viability in the controls when cultivated *ex vivo*.

Table 1. Relative viability of melanoma lymph node metastases analyzed ex vivo after treatment with Vemurafenib and/or Cobimetinib

Patient No.	Mutation	Relative viability (% of control) [1]		
		Vemurafenib (2 μM)	Cobimetinib (50 nM)	Vemurafenib/Cobimetinib (2 μM + 50 nM)
Melmet-339	*BRAF*	34	38	n.a.*
Melmet-347	*BRAF*	31	29	n.a.
Melmet-363	*BRAF*	52	39	n.a.
Melmet-368	*BRAF*	64	52	n.a.
Melmet-376	*BRAF*	52	40	n.a.
Melmet-380	*BRAF*	16	16	14
Melmet-381	*BRAF*	26	10	16
Melmet-382	*BRAF*	30	35	29
Melmet-396	*BRAF*	24	17	20
Melmet-397	*BRAF*	36	32	48
Melmet-352	*NRAS*	81	78	n.a.
Melmet-360	*NRAS*	127	55	n.a.
Melmet-367	*NRAS*	91	117	n.a.
Melmet-369	*NRAS*	74	40	n.a.
Melmet-388	*NRAS*	89	48	83
Melmet-399	*NRAS*	86	49	55
Melmet-432	*NRAS*	108	42	73
Melmet-370	*Wt/Wt*	70	92	n.a.

[1] Percentage survival.
* n.a. = Not analyzed.

Table 2. Viability of melanoma lymph node metastases and PDXs analyzed ex vivo after treatment with Vemurafenib (2 μM)

Patient No.	Mutation	Relative viability (% of control)[1]				
		Lymph node	PDX passage[2,3]			
			Lowest		Highest	
Melmet-334	*BRAF*	n.a.*	52	(4)	-	(n.a.)**
Melmet-347	*BRAF*	31	64	(1)	13	(3)
Melmet-350	*BRAF*	59	-	(0)	-	(1)
Melmet-351	*BRAF*	n.a.	57	(2)	56	(6)
Melmet-356	*BRAF*	102	-	(0)	-	(4)
Melmet-363	*BRAF*	52	43	(7)	28	(8)
Melmet-376	*BRAF*	52	33	(2)	43	(6)
Melmet-380	*BRAF*	16	26	(0)	42	(3)
Melmet-381	*BRAF*	30	87	(4)	11	(7)
Melmet-382	*BRAF*	35	17	(2)	18	(5)
Melmet-389	*BRAF*	n.a.	61	(0)	12	(6)
Melmet-393	*BRAF*	n.a.	30	(3)	20	(6)
Melmet-358	*NRAS*	132	86	(0)	107	(5)
Melmet-365	*NRAS*	201	122	(1)	116	(5)
Melmet-367	*NRAS*	91	118	(7)	n.a.	(n.a.)
Melmet-369	*NRAS*	74	169	(0)	271	(3)
Melmet-388	*NRAS*	89	67	(0)	125	(7)
Melmet-256	*Wt/Wt*	83	86	(0)	80	(7)
Melmet-370	*Wt/Wt*	70	98	(1)	103	(10)
Melmet-374	*Wt/Wt*	n.a.	79	(3)	103	(5)
Melmet-404	*Wt/Wt*	116	77	(0)	103	(1)

[1] Percentage survival.
[2] Number of passages in parentheses.
[3] PDX for Melmet-350, -356 not analyzed due to control sample not growing.
* n.a. = Not analyzed due to limited tumor material available.
** Only one PDX passage analyzed.

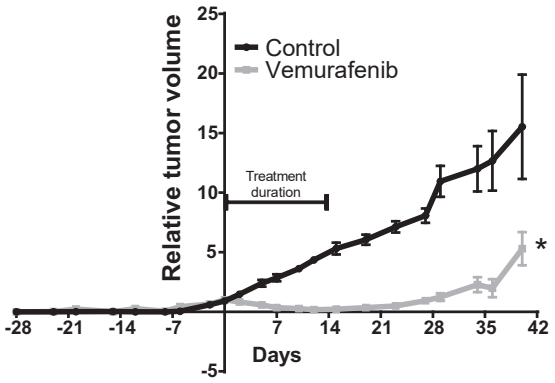

Figure 2. Antitumor efficacy of Vemurafenib *in vivo*. Melmet-382 PDX was treated with Vemurafenib (50 mg/kg) given twice daily by oral gavage for 14 days. Control mice were given 10% DMSO in 0,5% methylcellulose orally. Tumor volume was measured twice a week and results presented as relative volume related to tumor volume at initiation of the treatment. Error bars represent ±S.E.M.

As a final confirmation step, PDX of Melmet-382 (passage 4) was examined *in vivo* for response to Vemurafenib. As was observed in the *ex vivo* assay performed on patient- and PDX-derived material, a strong significant response was achieved (Figure 2).

Targeted Sequencing of Patient Tumor Samples Combined with Ex Vivo Drug Sensitivity Assessment Provide Precise Diagnostic Information

In attempt to reveal molecular mechanisms of treatment response, targeted sequencing (IonTorrent™ Oncomine and/or Cancer Hotspot Panel) was performed on 21 of the patient samples and one PDX. The sequence data were filtered against databases for common mutations (1000 Genomes) and known cancer mutations (COSMIC). Following variant calling, non-synonymous mutations were reported (Figure 3 and Table S1 for complete list of mutations). As expected, $BRAF^{V600E}$ (62%) was the most common mutation followed by CDKN2A (33%) and NRAS (29%). It appeared that the mutation load was higher in NRAS compared to BRAF mutated tumors. The Melmet-323 tumor, found highly responsive to BRAFi (viability, 25% of control) was shown to have a rare dinucleotide BRAF mutation yielding a complex V600E variant (c.1799_1800TG > AA). This tumor had previously been diagnosed as BRAF/NRAS wild-type by a PCR based assay routinely used for diagnostic evaluation. Likewise, the PDX from Melmet-389 (patient tissue not analyzed) diagnosed as BRAF wild-type showed remarkable response to Vemurafenib when analyzed *ex vivo*. In this case, targeted sequencing revealed a double BRAF mutation (V600E and K601 N). Two other tumors carrying double BRAF mutations, $BRAF^{V600E/K601E}$ (Melmet-363) and $BRAF^{V600E/S605R}$ (Melmet-273), were found borderline sensitive and resistant, respectively.

Interestingly, despite that aberrations in the PI3K/Akt pathway and NF1 mutations have been associated with BRAFi resistance, two highly responsive $BRAF^{V600E}$ mutated tumors (Melmet-380, Melmet-381) were shown to have a PIK3CA (p.H1047R) or NF1 mutation (Melmet-380). Other candidate genes with suggested impact on treatment response [32,33] and found affected included three TP53, two IDH1 and one EZH2 mutations (Figure 3 and Table S1).

Discussion

Despite promising molecular anti-cancer targets, lack of model systems and/or biomarkers identifying responders have clearly limited the success of targeted therapy. Melanoma is one of the most heterogeneous cancer forms and differences in BRAF mutation status have been observed between primary tumors and corresponding metastases, between different metastases as well as intra-tumorally [34,35]. This makes it difficult to identify patients likely to benefit from targeting therapy based solely on molecular screening of a single biopsy. During the last decades, various 3D-culture systems [36,37] and organoid models, the latter in particular from epithelial derived cancers [23], have been developed to assess response to anti-cancer treatment. However, no *ex vivo* assay based on the patient's own tumor cells has, to the best of our knowledge, so far been established in routine diagnostics [23,38]. In the current study, we applied a modified version of the ATP-based tumor sensitivity- [39] and extreme drug resistance assays [40] that we previously successfully have used to predict primary platinum resistance in ovarian cancer patients [41]. Here, when melanoma lymph node metastases were analyzed for response to Vemurafenib *ex vivo*, two important observations were made. First, a strong correlation between response and verified BRAF status were achieved in the sense that all patients that responded to the treatment harbored a BRAF mutation, whereas this was not the case for any of the NRAS or BRAF wild-type tumors. Second, and in agreement with intrinsic resistance seen in the clinic, not all BRAF mutated tumors responded to the treatment. Furthermore, *ex vivo* analysis of tumor material harvested from various passages of corresponding PDXs retained the response profile

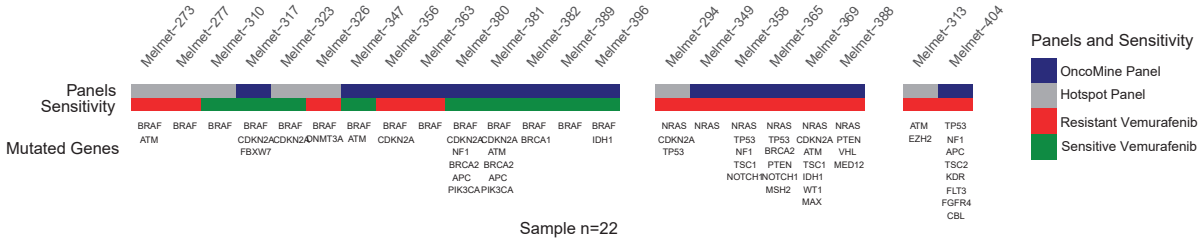

Figure 3. Distribution of mutations in 21 melanoma lymph node metastases and one PDX (melmet 389). Sequencing was performed using IonTorrent Oncomine (blue and cancer Hotspot (gray) panels. Mutation analysis was performed using the Torrent Suite Variant Caller version 5.9 and annotated using ANNOVAR as described in Materials and Methods. Response to Vemurafenib is shown in bottom bar; sensitive (green), resistant (red).

seen in the matching patient tumor samples, as was also seen when treating the PDX *in vivo*.

Numerous studies have concluded that permanent cancer cell lines grown as adherent 2D-cultures poorly reflect the complexity of a solid tumor [12]. Furthermore, most melanoma cell lines have been derived from highly proliferative tumors [42], exposed to high selection pressure due to BRAF or NRAS mutations and loss of CDKN2A [43],. This may partly explain the high failure rate of novel targeted therapy since the test system usually has been based on the use of such cell lines. During the course of this study, we aimed to establish adherent *in vitro* cell lines from some of the tumors and PDXs. In cases where we successfully were able to establish permanent cell lines, they all seemed to be highly proliferative (personal observation) and to harbor BRAF or NRAS mutations. In addition, we experienced, as also has been reported by others [42], that the primary cultures were easily over-grown by fibroblasts. In contract, stromal cells will not grow anchorage-independently making the 3D assay superior to the more time consuming establishment of stably growing cell cultures in 2D.

Studies have suggested that assay-guided therapy more accurately identifies ineffective than effective drugs [44,45]. Using the stringent 50% reduction in viability as cutoff to discriminate between responders and non-responders [46], all NRAS mutated or wild-type tumors were resistant to Vemurafenib, and some showed increased viability as compared to controls. The latter is in accordance with studies showing paradoxical reactivation of MAPK signaling and increased proliferation when wild-type or NRAS mutated tumors are treated with BRAFi [47].

In accordance with clinical observations [48], approximately 60% of the BRAF mutated tumors responded in the 3D assay. In agreement with a recent study, in which melanoma tissue was cultured as micro tumor fragments [49], complete loss of viability following BRAF or MEK inhibition was, however, not achieved, a finding that may be explained by intra-tumor heterogeneity and/or the presence of normal cell infiltration.

Both pre-clinical and clinical studies have demonstrated that combined BRAF and MEK inhibition may be beneficial for patients with BRAF mutated tumors. Moreover, selective MEK inhibition has shown efficacy in NRAS mutated melanoma (reviewed in [49]). In the current study, response of BRAF mutated tumors to Vemurafenib and/or Cobimetinib was in most cases comparable, and in accordance with previous studies [50], half of the NRAS mutated tumors responded to MEK inhibition. Response to MEK inhibition was, however, less pronounced in NRAS mutated tumors than response to BRAF inhibition in BRAF mutated tumors. Of particular note, in a recent study [51], BRAFi were shown to amplify the effect of MEKi in NRAS mutated melanomas whereas in another study [49], an antagonistic effect of combining MEK and mutated BRAF inhibition was observed. In support of the latter, in three cases (two NRAS and one BRAF mutated) the combined treatment was less efficient than the mono-treatments. Taken together this clearly demonstrates that there is a need to extend the current molecular examinations with functional tests reporting on drug sensitivity to provide precise diagnostics for guidance of clinical treatment decisions.

Two tumors, originally diagnosed as BRAF wild-type by PCR-based in-house routine pathology examination, showed excellent response to Vemurafenib in the *ex vivo* assay. Based on this, targeted sequencing was performed and both were found to be BRAF mutated. Several reasons may explain the discrepancy such as the sensitivity of the molecular analyses or intra-tumoral heterogeneity. In support of the former, one tumor was found to harbor a complex BRAF mutation that was not analyzed for in the diagnostic assay. Furthermore, in support of heterogeneity, a study by Saint-Jean et al. [52] demonstrated that seven percent of melanomas diagnosed as BRAF wild-type by the first biopsy examination, revealed BRAF mutations following analysis of repeated biopsies. Likewise, a recent meta-analysis revealed intra-tumoral discrepancy in BRAF status among patients with metastatic melanoma [53]. The current cohort of samples consisted exclusively of stage III lymph node metastases that were not offered treatment besides removal of the malignant lesion. Some, however, developed distant metastases (stage IV) and five of these (two sensitive and three resistant from the *ex vivo* assay) received BRAFi treatment. In contrast to responses observed in the *ex vivo* assay the general clinical response was in all cases poor. For three patients a mixed response was observed; some metastases declined whereas some grew progressively, a finding strongly supporting melanoma heterogeneity. Together, these results strongly suggest more thorough molecular analysis of cases where discrepancy between *ex vivo* viability results and clinical diagnosis is observed and underscores the necessity, in a diagnostic setting, to examine multiple biopsies from each tumor [34]. The *ex vivo* assay will, however, to some extent account for intra-tumor heterogeneity as a larger fraction of the lesion is disaggregated and examined for drug sensitivity. It should be mentioned also that a meta-analysis comprising more than 15,000 tumors demonstrated that drug resistance could be foreseeable with high accuracy using various assays, whereas sensitivity, on the other hand, was less predictable [38], as also supported by our findings.

Except for mutated NRAS being strongly associated with BRAFi resistance, no other mechanisms of resistance were revealed. Aberrations in the PI3K/Akt pathway as well as NF1 mutations have been associated with BRAFi resistance [4]. This is in contrast to our findings demonstrating co-existence of PIK3CA mutations and one NF1 mutation in two of the most BRAFi responsive tumors. In agreement with our findings, however, it has been claimed that oncogenic PIK3CA mutation does not play a major role in Vemurafenib resistance [54], and a study by Krauthammer et al. suggested that loss of NF1 not necessarily is associated with BRAFi resistance [55].

The high success rate of establishing melanoma PDX models, and their ability to reliably recapitulate patient tumor architecture, genotype and response to treatment, have made them powerful tools to develop new and improved therapeutic strategies [14,56,57]. In a study by Einarsdottir et al. [58], PDX models in passage three were claimed to develop fast enough to guide treatment decisions. Although the use of PDXs in routine diagnostic may not be a realistic goal due to variability in engraftment, latency period, number of animals required and costs [14], they may provide an unlimited resource of tumor cells for both small-scale as well as large-scale *ex vivo* drug screening. Here we demonstrated that PDXs assessed for treatment responses using the *ex vivo* assay show a high degree of concordance with results observed when analyzing the corresponding patient tumors directly, or when treating PDXs *in vivo,* supporting previous observations that early PDX passages resemble the original tumor [59]. In agreement with our findings, short-time *ex vivo* cultures of breast cancer PDXs were recently found to predict *in vivo* drug responses [60]. When analyzing several PDX passages for treatment response *ex vivo*, concordance was in most cases achieved, indicating PDX stability [61]. Notably, although cells from the

parental tumors in general were easy to cultivate *ex vivo*, serial PDX-passages from two of the tumors showed no sign of viability, suggesting dependence of factors provided by the host or tumor stromal cells. However, in general, in cases where the amount of tumor material is scarce, PDX models may be established and used as an indefinite source of tumor material for *ex vivo* drug testing.

In conclusion, the presented data strongly support the potential of the *ex vivo* assay to provide valuable functional information in the patient tumor. The fast and reliable analyses, combined with the low cost, make the assay attractive to supplement molecular data in clinical decisions. Furthermore, the findings underscore the importance of considering intra-tumor heterogeneity as well as heterogeneity between various metastases in the individual patients when analyzing drug effects *ex vivo*. Finally, we hypothesize that analyzing drug effects *ex vivo* will be of particular importance in pinpointing patients that are not likely to respond to targeted therapy.

Supplementary data to this article can be found online at https://doi.org/10.1016/j.tranon.2019.04.001.

References

[1] Shah DJ and Dronca RS (2014). Latest advances in chemotherapeutic, targeted, and immune approaches in the treatment of metastatic melanoma. *Mayo Clin Proc* **89**(4), 504–519.

[2] Long GV, Stroyakovskiy D, Gogas H, Levchenko E, de Braud F, Larkin J, Garbe C, Jouary T, Hauschild A, and Grob JJ, et al (2014). Combined BRAF and MEK inhibition versus BRAF inhibition alone in melanoma. *N Engl J Med* **371**(20), 1877–1888.

[3] Sullivan RJ and Flaherty KT (2013). Resistance to BRAF-targeted therapy in melanoma. *Eur J Cancer* **49**(6), 1297–1304.

[4] Manzano JL, Layos L, Buges C, de Los Llanos Gil M, Vila L, Martinez-Balibrea E, and Martinez-Cardus A (2016). Resistant mechanisms to BRAF inhibitors in melanoma. *Ann Transl Med* **4**(12), 237.

[5] Jovanovic B, Egyhazi S, Eskandarpour M, Ghiorzo P, Palmer JM, Bianchi Scarra G, Hayward NK, and Hansson J (2010). Coexisting NRAS and BRAF mutations in primary familial melanomas with specific CDKN2A germline alterations. *J Invest Dermatol* **130**(2), 618–620.

[6] Sensi M, Nicolini G, Petti C, Bersani I, Lozupone F, Molla A, Vegetti C, Nonaka D, Mortarini R, and Parmiani G, et al (2006). Mutually exclusive NRASQ61R and BRAFV600E mutations at the single-cell level in the same human melanoma. *Oncogene* **25**(24), 3357–3364.

[7] Raaijmakers MI, Widmer DS, Narechania A, Eichhoff O, Freiberger SN, Wenzina J, Cheng PF, Mihic-Probst D, Desalle R, and Dummer R, et al (2016). Co-existence of BRAF and NRAS driver mutations in the same melanoma cells results in heterogeneity of targeted therapy resistance. *Oncotarget* **7**(47), 77163–77174.

[8] Johnson DB, Flaherty KT, Weber JS, Infante JR, Kim KB, Kefford RF, Hamid O, Schuchter L, Cebon J, and Sharfman WH, et al (2014). Combined BRAF (Dabrafenib) and MEK inhibition (Trametinib) in patients with BRAFV600-mutant melanoma experiencing progression with single-agent BRAF inhibitor. *J Clin Oncol* **32**(33), 3697–3704.

[9] Welsh SJ, Rizos H, Scolyer RA, and Long GV (2016). Resistance to combination BRAF and MEK inhibition in metastatic melanoma: Where to next? *Eur J Cancer* **62**, 76–85.

[10] Das V, Bruzzese F, Konecny P, Iannelli F, Budillon A, and Hajduch M (2015). Pathophysiologically relevant in vitro tumor models for drug screening. *Drug Discov Today* **20**(7), 848–855.

[11] Gillet JP, Calcagno AM, Varma S, Marino M, Green LJ, Vora MI, Patel C, Orina JN, Eliseeva TA, and Singal V, et al (2011). Redefining the relevance of established cancer cell lines to the study of mechanisms of clinical anti-cancer drug resistance. *Proc Natl Acad Sci U S A* **108**(46), 18708–18713.

[12] Mitra A, Mishra L, and Li S (2013). Technologies for deriving primary tumor cells for use in personalized cancer therapy. *Trends Biotechnol* **31**(6), 347–354.

[13] Zeeberg K, Cardone RA, Greco MR, Saccomano M, Nohr-Nielsen A, Alves F, Pedersen SF, and Reshkin SJ (2016). Assessment of different 3D culture systems to study tumor phenotype and chemosensitivity in pancreatic ductal adenocarcinoma. *Int J Oncol* **49**(1), 243–252.

[14] Byrne AT, Alferez DG, Amant F, Annibali D, Arribas J, Biankin AV, Bruna A, Budinska E, Caldas C, and Chang DK, et al (2017). Interrogating open issues in cancer medicine with patient-derived xenografts. *Nat Rev Cancer* **17**(10), 632.

[15] Cassidy JW, Caldas C, and Bruna A (2015). Maintaining Tumor Heterogeneity in Patient-Derived Tumor Xenografts. *Cancer Res* **75**(15), 2963–2968.

[16] Kemper K, Krijgsman O, Cornelissen-Steijger P, Shahrabi A, Weeber F, Song JY, Kuilman T, Vis DJ, Wessels LF, and Voest EE, et al (2015). Intra- and inter-tumor heterogeneity in a vemurafenib-resistant melanoma patient and derived xenografts. *EMBO Mol Med* **7**(9), 1104–1118.

[17] Kemper K, Krijgsman O, Kong X, Cornelissen-Steijger P, Shahrabi A, Weeber F, van der Velden DL, Bleijerveld OB, Kuilman T, and Kluin RJC, et al (2016). BRAF(V600E) Kinase Domain Duplication Identified in Therapy-Refractory Melanoma Patient-Derived Xenografts. *Cell Rep* **16**(1), 263–277.

[18] Aparicio S, Hidalgo M, and Kung AL (2015). Examining the utility of patient-derived xenograft mouse models. *Nat Rev Cancer* **15**(5), 311–316.

[19] Hidalgo M, Amant F, Biankin AV, Budinska E, Byrne AT, Caldas C, Clarke RB, de Jong S, Jonkers J, and Maelandsmo GM, et al (2014). Patient-derived xenograft models: an emerging platform for translational cancer research. *Cancer Discov* **4**(9), 998–1013.M Hidalgo, F Amant, AV Biankin, E Budinska, AT Byrne, C Caldas, RB Clarke, S de Jong, J Jonkers, GM Maelandsmo, et al., Patient-derived xenograft models: an emerging platform for translational cancer research. Cancer Discov, 2014. 4(9): p. 998-1013.

[20] Nath S and Devi GR (2016). Three-dimensional culture systems in cancer research: Focus on tumor spheroid model. *Pharmacol Ther* **163**, 94–108.S Nath and GR Devi, Three-dimensional culture systems in cancer research: Focus on tumor spheroid model. Pharmacol Ther, 2016. 163: p. 94-108.

[21] Onion D, Argent RH, Reece-Smith AM, Craze ML, Pineda RG, Clarke PA, Ratan HL, Parsons SL, Lobo DN, and Duffy JP, et al (2016). 3-Dimensional Patient-Derived Lung Cancer Assays Reveal Resistance to Standards-of-Care Promoted by Stromal Cells but Sensitivity to Histone Deacetylase Inhibitors. *Mol Cancer Ther* **15**(4), 753–763.

[22] Beaumont KA, Anfosso A, Ahmed F, Weninger W, and Haass NK (2015). Imaging- and Flow Cytometry-based Analysis of Cell Position and the Cell Cycle in 3D Melanoma Spheroids. *J Vis Exp* **106**e53486.

[23] Weeber F, Ooft SN, Dijkstra KK, and Voest EE (2017). Tumor Organoids as a Pre-clinical Cancer Model for Drug Discovery. *Cell Chem Biol* **24**(9), 1092–1100.

[24] Xu H, Lyu X, Yi M, Zhao W, Song Y, and Wu K (2018). Organoid technology and applications in cancer research. *J Hematol Oncol* **11**(1), 116.

[25] Spoerri L, Beaumont KA, Anfosso A, and Haass NK (2017). Real-Time Cell Cycle Imaging in a 3D Cell Culture Model of Melanoma. *Methods Mol Biol* **1612**, 401–416.

[26] Haass NK, Sproesser K, Nguyen TK, Contractor R, Medina CA, Nathanson KL, Herlyn M, and Smalley KS (2008). The mitogen-activated protein/extracellular signal-regulated kinase kinase inhibitor AZD6244 (ARRY-142886) induces growth arrest in melanoma cells and tumor regression when combined with docetaxel. *Clin Cancer Res* **14**(1), 230–239.

[27] Marconi A, Quadri M, Saltari A, and Pincelli C (2018). Progress in melanoma modelling in vitro. *Exp Dermatol* **27**(5), 578–586.

[28] Wang K, Li M, and Hakonarson H (2010). ANNOVAR: functional annotation of genetic variants from high-throughput sequencing data. *Nucleic Acids Res* **38** (16), e164.

[29] Robinson JT, Thorvaldsdottir H, Winckler W, Guttman M, Lander ES, Getz G, and Mesirov JP (2011). Integrative genomics viewer. *Nat Biotechnol* **29**(1), 24–26.

[30] Chapman PB, Hauschild A, Robert C, Haanen JB, Ascierto P, Larkin J, Dummer R, Garbe C, Testori A, and Maio M, et al (2011). Improved survival with vemurafenib in melanoma with BRAF V600E mutation. *N Engl J Med* **364** (26), 2507–2516.

[31] Gao H, Korn JM, Ferretti S, Monahan JE, Wang Y, Singh M, Zhang C, Schnell C, Yang G, and Zhang Y, et al (2015). High-throughput screening using patient-derived tumor xenografts to predict clinical trial drug response. *Nat Med* **21**(11), 1318–1325.

[32] Kunz M and Holzel M (2017). The impact of melanoma genetics on treatment response and resistance in clinical and experimental studies. *Cancer Metastasis Rev* **36**(1), 53–75.

[33] Mahmoud F, Shields B, Makhoul I, Hutchins LF, Shalin SC, and Tackett AJ (2016). Role of EZH2 histone methyltrasferase in melanoma progression and metastasis. *Cancer Biol Ther* **17**(6), 579–591.

[34] Grzywa TM, Paskal W, and Wlodarski PK (2017). Intratumor and Intertumor Heterogeneity in Melanoma. *Transl Oncol* **10**(6), 956–975.
[35] Yancovitz M, Litterman A, Yoon J, Ng E, Shapiro RL, Berman RS, Pavlick AC, Darvishian F, Christos P, and Mazumdar M, et al (2012). Intra- and inter-tumor heterogeneity of BRAF(V600E)mutations in primary and metastatic melanoma. *PLoS One* **7**(1)e29336.
[36] Fang Y and Eglen RM (2017). Three-Dimensional Cell Cultures in Drug Discovery and Development. *SLAS Discov* **22**(5), 456–472.
[37] Friedrich J, Seidel C, Ebner R, and Kunz-Schughart LA (2009). Spheroid-based drug screen: considerations and practical approach. *Nat Protoc* **4**(3), 309–324.
[38] Volm M and Efferth T (2015). Prediction of Cancer Drug Resistance and Implications for Personalized Medicine. *Front Oncol* **5**, 282.
[39] Konecny G, Crohns C, Pegram M, Felber M, Lude S, Kurbacher C, Cree IA, Hepp H, and Untch M (2000). Correlation of drug response with the ATP tumorchemosensitivity assay in primary FIGO stage III ovarian cancer. *Gynecol Oncol* **77**(2), 258–263.
[40] Kim HS, Kim TJ, Chung HH, Kim JW, Kim BG, Park NH, Song YS, Bae DS, and Kang SB (2009). In vitro extreme drug resistance assay to taxanes or platinum compounds for the prediction of clinical outcomes in epithelial ovarian cancer: a prospective cohort study. *J Cancer Res Clin Oncol* **135**(11), 1513–1520.
[41] Hetland TE, Kaern J, Skrede M, Sandstad B, Trope C, Davidson B, and Florenes VA (2012). Predicting platinum resistance in primary advanced ovarian cancer patients with an in vitro resistance index. *Cancer Chemother Pharmacol* **69**(5), 1307–1314.
[42] Raaijmakers MI, Widmer DS, Maudrich M, Koch T, Langer A, Flace A, Schnyder C, Dummer R, and Levesque MP (2015). A new live-cell biobank workflow efficiently recovers heterogeneous melanoma cells from native biopsies. *Exp Dermatol* **24**(5), 377–380.
[43] Garman B, Anastopoulos IN, Krepler C, Brafford P, Sproesser K, Jiang Y, Wubbenhorst B, Amaravadi R, Bennett J, and Beqiri M, et al (2017). Genetic and Genomic Characterization of 462 Melanoma Patient-Derived Xenografts, Tumor Biopsies, and Cell Lines. *Cell Rep* **21**(7), 1936–1952.
[44] Fruehauf JP and Alberts DS (2005). In vitro drug resistance versus chemosensitivity: two sides of different coins. *J Clin Oncol* **23**(15), 3641–3643 author reply 3646-3648.
[45] Kreahling JM and Altiok S (2015). Special Technologies for Ex Vivo Analysis of Cancer. *Cancer Control* **22**(2), 226–231.
[46] Santo VE, Rebelo SP, Estrada MF, Alves PM, Boghaert E, and Brito C (2017). Drug screening in 3D in vitro tumor models: overcoming current pitfalls of efficacy read-outs. *Biotechnol J* **12**(1).
[47] Vu HL and Aplin AE (2016). Targeting mutant NRAS signaling pathways in melanoma. *Pharmacol Res* **107**, 111–116.
[48] Eroglu Z and Ribas A (2016). Combination therapy with BRAF and MEK inhibitors for melanoma: latest evidence and place in therapy. *Ther Adv Med Oncol* **8**(1), 48–56.
[49] Seidel D, Rothe R, Kirsten M, Jahnke HG, Dumann K, Ziemer M, Simon JC, and Robitzki AA (2019). A multidimensional impedance platform for the real-time analysis of single and combination drug pharmacology in patient-derived viable melanoma models. *Biosens Bioelectron* **123**, 185–194.
[50] Solit DB, Garraway LA, Pratilas CA, Sawai A, Getz G, Basso A, Ye Q, Lobo JM, She Y, and Osman I, et al (2006). BRAF mutation predicts sensitivity to MEK inhibition. *Nature* **439**(7074), 358–362.
[51] Niessner H, Sinnberg T, Kosnopfel C, Smalley KSM, Beck D, Praetorius C, Mai M, Beissert S, Kulms D, and Schaller M, et al (2017). BRAF Inhibitors Amplify the Proapoptotic Activity of MEK Inhibitors by Inducing ER Stress in NRAS-Mutant Melanoma. *Clin Cancer Res* **23**(20), 6203–6214.
[52] Saint-Jean M, Quereux G, Nguyen JM, Peuvrel L, Brocard A, Vallee A, Knol AC, Khammari A, Denis MG, and Dreno B (2014). Is a single BRAF wild-type test sufficient to exclude melanoma patients from vemurafenib therapy? *J Invest Dermatol* **134**(5), 1468–1470.
[53] Valachis A and Ullenhag GJ (2017). Discrepancy in BRAF status among patients with metastatic malignant melanoma: A meta-analysis. *Eur J Cancer* **81**, 106–115.
[54] Romano E, Pradervand S, Paillusson A, Weber J, Harshman K, Muehlethaler K, Speiser D, Peters S, Rimoldi D, and Michielin O (2013). Identification of multiple mechanisms of resistance to vemurafenib in a patient with BRAFV600E-mutated cutaneous melanoma successfully rechallenged after progression. *Clin Cancer Res* **19**(20), 5749–5757.
[55] Krauthammer M, Kong Y, Bacchiocchi A, Evans P, N Pornputtapong C Wu, McCusker JP, Ma S, Cheng E, and Straub R, et al (2015). Exome sequencing identifies recurrent mutations in NF1 and RASopathy genes in sun-exposed melanomas. *Nat Genet* **47**(9), 996–1002.
[56] Krepler C, Sproesser K, Brafford P, Beqiri M, Garman B, Xiao M, Shannan B, Watters A, Perego M, and Zhang G, et al (2017). A Comprehensive Patient-Derived Xenograft Collection Representing the Heterogeneity of Melanoma. *Cell Rep* **21**(7), 1953–1967.
[57] Krepler C, Xiao M, Sproesser K, Brafford PA, Shannan B, Beqiri M, Q Liu W Xu, Garman B, and Nathanson KL, et al (2016). Personalized Preclinical Trials in BRAF Inhibitor-Resistant Patient-Derived Xenograft Models Identify Second-Line Combination Therapies. *Clin Cancer Res* **22**(7), 1592–1602.
[58] Einarsdottir BO, Bagge RO, Bhadury J, Jespersen H, Mattsson J, Nilsson LM, Truve K, Lopez MD, Naredi P, and Nilsson O, et al (2014). Melanoma patient-derived xenografts accurately model the disease and develop fast enough to guide treatment decisions. *Oncotarget* **5**(20), 9609–9618.
[59] Hartsough EJ and Aplin AE (2016). Of Mice and Melanoma: PDX System for Modeling Personalized Medicine. *Clin Cancer Res* **22**(7), 1550–1552.
[60] Bruna A, Rueda OM, Greenwood W, Batra AS, Callari M, Batra RN, Pogrebniak K, Sandoval J, Cassidy JW, and Tufegdzic-Vidakovic A, et al (2016). A Biobank of Breast Cancer Explants with Preserved Intra-tumor Heterogeneity to Screen Anticancer Compounds. *Cell* **167**(1), 260–274 e222.
[61] Sia D, Moeini A, Labgaa I, and Villanueva A (2015). The future of patient-derived tumor xenografts in cancer treatment. *Pharmacogenomics* **16**(14), 1671–1683.

Table S1. Mutations identified in 21 melanoma lymph node metastases and one PDX by IonTorrent Cancer Hotspot and Oncomine Comprehensive Panel.

Patient ID	Chromosome	Start	Stopp	Reference	Variant	Gene	Mutation type	Amino acid change	rsID
Melmet-273	7	140453136	140453136	A	T	*BRAF*	missense	V600E	rs113488022
Melmet-273	7	140453120	140453120	A	T	*BRAF*	missense	S605R	-
Melmet-273	11	108119823	108119823	T	C	*ATM*	missense	V410A	rs56128736
Melmet-277	7	140453136	140453136	A	T	*BRAF*	missense	V600E	rs113488022
Melmet-294	1	115256530	115256530	G	T	*NRAS*	missense	Q61K	rs121913254
Melmet-294	9	21971116	21971116	G	A	*CDKN2A*	missense	P81L	rs11552823
Melmet-294	17	7574003	7574003	G	A	*TP53*	nonsense	R342X	rs730882029
Melmet-310	7	140453136	140453136	A	T	*BRAF*	missense	V600E	rs113488022
Melmet-313	7	148506464	148506464	G	A	*EZH2*	missense	T683I	-
Melmet-313	11	108138003	108138003	T	C	*ATM*	missense	F858L	rs1800056
Melmet-317	9	21974679	21974679	G	A	*CDKN2A*	nonsense	Q50X	rs864622636
Melmet-317	7	140453136	140453136	A	T	*BRAF*	missense	V600E	rs113488022
Melmet-317	4	153268161	153268161	T	C	*FBXW7*	missense	N216S	rs746085490
Melmet-323	7	140453135	140453135	CA	TT	*BRAF*	missense	V600E	-
Melmet-323	9	21971133	21971133	GGGGT	AGGA	*CDKN2A*	frameshift del.	D74fs	-
Melmet-326	2	25463245	25463245	G	A	*DNMT3A*	missense	P750S	-
Melmet-326	7	140453136	140453136	A	T	*BRAF*	missense	V600E	rs113488022
Melmet-347	7	140453136	140453136	A	T	*BRAF*	missense	V600E	rs113488022
Melmet-347	11	108106513	108106513	C	T	*ATM*	missense	L150F	-
Melmet-347	11	108235849	108235849	C	T	*ATM*	missense	P2964L	-
Melmet-349	1	115256529	115256529	T	C	*NRAS*	missense	Q61R	rs11554290
Melmet-356	9	21971158	21971158	C	-	*CDKN2A*	frameshift del.	G67fs	-
Melmet-356	7	140453136	140453136	A	T	*BRAF*	missense	V600E	rs113488022
Melmet-358	9	139413102	139413102	C	T	*NOTCH1*	missense	G347D	-
Melmet-358	17	29486093	29486093	G	-	*NF1*	frameshift del.	L90fs	-
Melmet-358	1	115258745	115258745	C	G	*NRAS*	missense	G13R	rs121434595
Melmet-358	17	7578263	7578263	G	-	*TP53*	frameshift del.	R196fs	-
Melmet-358	9	135782198	135782198	G	A	*TSC1*	missense	S453F	-
Melmet-363	7	140453134	140453134	T	C	*BRAF*	missense	K601E	rs121913364
Melmet-363	7	140453136	140453136	A	T	*BRAF*	missense	V600E	rs113488022
Melmet-365	2	47698157	47698157	A	T	*MSH2*	missense	E572G	-
Melmet-365	9	139405696	139405696	G	C	*NOTCH1*	missense	P832R	-
Melmet-365	13	32913306	32913306	-	T	*BRCA2*	frameshift ins.	V1605fs	-
Melmet-365	10	89653814	89653814	C	T	*PTEN*	missense	P38S	rs587780004
Melmet-365	10	89692976	89692976	T	A	*PTEN*	missense	F154I	-
Melmet-365	17	7578520	7578520	A	T	*TP53*	missense	p.L137Q	-
Melmet-365	1	115256529	115256529	T	C	*NRAS*	missense	Q61R	rs11554290

Melmet-369	11	108143509	108143509	T	C	*ATM*	missense	E1072K	-
Melmet-369	9	135782729	135782729	C	A	*TSC1*	missense	C431F	-
Melmet-369	14	65544712	65544712	G	A	*MAX*	nonsense	Q72X	-
Melmet-369	9	21971159	21971159	CGTGGAGCAG	-	*CDKN2A*	frameshift del.	L64fs	-
Melmet-369	11	32413577	32413577	C	T	*WT1*	missense	R441Q	-
Melmet-369	2	209113113	209113113	G	A	*IDH1*	missense	R132C	rs121913499
Melmet-369	1	115256529	115256529	T	C	*NRAS*	missense	Q61R	rs11554290
Melmet-380	13	32911074	32911074	A	-	*BRCA2*	frameshift del.	Q861fs	-
Melmet-380	17	29677244	29677244	-	A	*NF1*	frameshift ins.	L2455fs	-
Melmet-380	9	21971054	21971054	-	C	*CDKN2A*	frameshift ins.	A102fs	-
Melmet-380	3	178952085	178952085	A	G	*PIK3CA*	missense	H1047R	rs121913279
Melmet-380	7	140453136	140453136	A	T	*BRAF*	missense	V600E	rs113488022
Melmet-380	5	112178772	112178772	C	T	*APC*	missense	S2494F	-
Melmet-381	11	108117732	108117732	-	T	*ATM*	frameshift ins.	N314fs	-
Melmet-381	13	32899285	32899285	-	T	*BRCA2*	frameshift ins.	V130fs	-
Melmet-381	9	21971054	21971054	-	C	*CDKN2A*	frameshift ins.	A102fs	-
Melmet-381	3	178952085	178952085	A	G	*PIK3CA*	missense	H1047R	rs121913279
Melmet-381	5	112178772	112178772	C	T	*APC*	missense	S2494F	-
Melmet-381	7	140453136	140453136	A	T	*BRAF*	missense	V600E	rs113488022
Melmet-382	17	41246457	41246457	G	A	*BRCA1*	missense	P364L	-
Melmet-382	17	41246061	41246061	C	T	*BRCA1*	missense	R496H	rs28897677
Melmet-382	7	140453136	140453136	A	T	*BRAF*	missense	V600E	rs113488022
Melmet-388	3	10191555	10191555	C	T	*VHL*	missense	S183L	rs5030823
Melmet-388	X	70339253	70339253	G	A	*MED12*	missense	G44S	rs199469669
Melmet-388	1	115256530	115256530	G	T	*NRAS*	missense	Q61K	rs121913254
Melmet-388	10	89693008	89693008	GG	AA	*PTEN*	frameshift ins.	-	-
Melmet-389[1]	7	140453132	140453132	T	A	*BRAF*	missense	K601N	rs121913365
Melmet-389	7	140453136	140453136	A	T	*BRAF*	missense	V600E	rs113488022
Melmet-396	2	209113113	209113113	G	A	*IDH1*	missense	R132C	rs121913499
Melmet-396	7	140453136	140453136	AC	TT	*BRAF*	frameshift ins.	V600K	rs121913227
Melmet-404	4	55962506	55962506	C	T	*KDR*	missense	G873E	rs780022671
Melmet-404	5	112154922	112154922	A	G	*APC*	missense	K398R	rs145912662
Melmet-404	17	7578553	7578553	T	G	*TP53*	missense	Y126S	-
Melmet-404	16	2103448	2103448	G	A	*TSC2*	missense	G111R	-
Melmet-404	5	176517541	176517541	G	A	*FGFR4*	missense	G81D	-
Melmet-404	17	29508446	29562746	C	T	*NF1*	missense	R1276X	-
Melmet-404	11	119149241	119149241	C	T	*CBL*	missense	P417S	rs867564832
Melmet-404	13	28610124	28610124	C	T	*FLT3*	missense	G456R	-

[1] Analysed only on PDX for Melmet-389

II

Title: **Targeting AXL and the DNA damage response pathway as a novel therapeutic strategy in melanoma**

Running title: Dual inhibition of AXL and CHK1/2 in melanoma

Authors: **Karine Flem-Karlsen[1,2*], Erin McFadden[1], Nasrin Omar[3], Mads H Haugen[3], Geir Frode Øy[3], Truls Ryder[4], Hans Petter Gullestad[4], Robert Hermann[4], Gunhild Mari Mælandsmo[3,5], Vivi Ann Flørenes[1]**

[1] Department of Pathology, The Norwegian Radium Hospital, Oslo University Hospital, Oslo, Norway.

[2] Institute for Clinical Medicine, Faculty of Medicine, University of Oslo, Oslo, Norway.

[3] Department of Tumor Biology, Institute for Cancer Research, The Norwegian Radium Hospital, Oslo University Hospital, Oslo, Norway.

[4] Department of Plastic and Reconstructive Surgery, The Norwegian Radium Hospital, Oslo University Hospital, Oslo, Norway.

[5]Institute of Medical Biology, Faculty of Health Sciences, UiT – Arctic University of Norway, Tromsø, Norway

***Corresponding author:** Karine Flem-Karlsen, Department of Pathology, Oslo University Hospital, Oslo, Norway. P.O. Box 4950 Nydalen, 0424 Oslo. Email: kaflem@rr-research.no

Abstract:

Receptor tyrosine kinase AXL is found upregulated in various types of cancer, including melanoma, and correlates with an aggressive cancer phenotype, inducing cell proliferation and epithelial-to-mesenchymal transition. Additionally, AXL has recently been linked to chemotherapy resistance and inhibition of AXL is found to increase DNA damage and reduce expression of DNA repair proteins. In light of this, we aimed to investigate if targeting AXL together with DNA damage response proteins would be therapeutically beneficial. Using melanoma cell lines, we observed that combined reduction of AXL and CHK1/CHK2 signaling decreased proliferation, deregulated cell cycle progression, increased apoptosis and reduced expression of DNA damage response proteins. Enhanced therapeutic effect of combined- as compared to mono-treatments was further observed in a patient-derived xenograft model and, of particular interest, when applying a three-dimensional *ex vivo* spheroid drug-sensitivity assay on tumor cells harvested directly from 27 patients with melanoma lymph node metastases.

Together, these results indicate that targeting AXL together with the DNA damage response pathway could be a promising treatment strategy in melanoma and that further investigations in patient groups lacking treatment alternatives should be pursued.

Keywords: AXL Receptor Protein Tyrosine Kinase, Targeted Molecular Therapy, DNA Damage, CHK1, CHK2, Melanoma

Introduction:

The incidence of melanoma is increasing worldwide (1). While the prognosis of early stage disease is very good, once the cancer progress survival drops dramatically, with over 20 000 melanoma-related deaths in Europe annually (2). Approximately 50% of all melanomas harbor activating BRAF mutations, with $BRAF^{V600E}$ being the most prevalent. The development of $BRAF^{V600}$ inhibitors vemurafenib and dabrafenib has led to targeted treatment options for patients with these mutations. However, almost all patients develop resistance within a year, often due to reactivation of the MAPK pathway or other receptor tyrosine kinases independently of BRAF (3,4). Lately, immune checkpoint inhibitors, like monoclonal antibodies targeting PD-1 and CTLA-4, have shown promising therapeutic effects (5). Yet, only a portion of the patients respond, signifying the importance to identify alternative therapeutic strategies.

The receptor tyrosine kinase AXL; a 138 kDa single-pass transmembrane protein of the TYRO3, AXL, MERTK (TAM)-family, has been found overexpressed, both as mRNA and protein, in a wide range of cancers (6-8), including melanoma (9). AXL is reported to play a role in cancer progression, and has been shown to promote cell proliferation, migration, invasion and epithelial-to-mesenchymal transition (EMT) (10-13). Additionally, AXL is shown to mediate resistance to BRAF and MEK inhibitors (14,15), as well as immunotherapy (16). All the TAM-family members are activated by the vitamin K-dependent ligand Growth arrest-specific protein 6 (GAS6), with AXL having the highest affinity for the ligand (17). In addition, AXL can be activated independently of GAS6 through aggregation of the protein or by heterodimerization with non-TAM receptor tyrosine kinases (18). Activated AXL undergoes homodimerization and autophosphorylation to induce downstream effects that activate proteins involved in the PI3K, MAPK14 (p38/MAPK) and MAPK1 (ERK/MAPK) pathways (12,13,19).

Recently AXL expression was found to reduce the sensitivity to chemotherapies, as well as to PARP inhibitors (20-22). In ovarian cancer cell lines, an association between AXL and cisplatin resistance has been observed (23). Additionally, inhibited AXL expression has been found to induce DNA damage and reduce the expression of DNA damage repair proteins (21). Together, these data suggest a link between AXL and the DNA damage response (DDR) pathway. Central to the DDR are the serine/threonine specific kinases CHK1 and CHK2 that are activated by ATR or ATM, respectively, in response to single-stranded (ATR) or double-stranded (ATM) DNA-breaks. CHK1 and CHK2 transduce signals to effectors such as TP53 (p53), CDC25C, BRCA1 and RAD51, ultimately leading to DNA repair, cell cycle arrest and/or apoptosis (24).

In this study, we assessed how dual inhibition of AXL and CHK1/CHK2 altered proliferation, signal transduction, apoptosis and cell cycle distribution in melanomas. We discovered that targeting or inhibiting expression of AXL and CHK1/CHK2 in combination reduced cell proliferation and induced

cell cycle arrest and apoptosis. We further showed that the combined treatment was superior to mono-treatment in a patient-derived xenograft (PDX) model and when analyzing drug sensitivity utilizing cells harvested directly from melanoma lymph node metastases in a 3D *ex-vivo* drug-efficacy assay. Together, these data suggest that dual targeting of AXL and DDR pathway is a promising treatment strategy for melanomas that should be further investigated in patients having developed resistance and where few treatment alternatives are available.

Materials and methods:

Cell lines and patient material

Melanoma cell lines were established from subcutaneous (Melmet 1) or lymph node (Melmet 5, FEMX-1 and HHMS) metastatic lesions of patients treated at the Norwegian Radium Hospital, Oslo University Hospital (25,26). WM115, WM902B, WM983 and WM1366 cells were a kind gift from Meenhard Herlyn, the Wistar cell line collection (Philadelphia, PA, USA). The melanoma cell lines MDA-MB-435 and MeWo were obtained from American Type Culture Collection (Manassas, VA, USA). All cells were routinely checked for mycoplasma by PCR in-house. Melmet 1 and WM1366 cell lines were STR fingerprinted (April 2018) by Genetica Cell Line Testing (Burlington, NC, USA). The melanoma cells were grown in RPMI-1640 (Sigma Aldrich, St. Louis, MO, USA) supplemented with 5% fetal bovine serum (FBS) (Sigma Aldrich, St. Louis, MO, USA) and 2 mM L-glutamine (Lonza, Basel, Switzerland). Cells were maintained in a humidified incubator at 37°C and with 5% CO_2. All cells were used within 20 passages of thawing.

Melanoma lymph node metastases were obtained from patients operated at the Norwegian Radium Hospital, Oslo University Hospital. Patient material was collected with written informed consent in accordance with the Declaration of Helsinki. The study was approved by the Norway Regional Committee for Medical and Health Research Ethics (approval number 2014/2208 and 2015/2434).

Immunoblot, protein analysis and antibodies

Protein extracts and immunoblots were performed as described (27), with the following exceptions: Proteins were lysed in a buffer containing 1% Triton X-100, 50mM Hepes (pH 7.4), 150mM NaCl, 1.5Mm $MgCl_2$, 1mM EGTA, 100mM NaF, 10mM Na Pyruvate, 1mM Na_3VO_4 and 10% Glycerol, with addition of 10 µL/mL protease and phosphatase inhibitor cocktails (cOmplete Mini and PhosSTOP™, Roche, Mannheim, Germany). Antibodies used were: pAXL (#5724), AXL (#8661), pAKT (#9271), AKT (#9272), pERK (#9101), pp38 (#9211), p38 (#8690), pSRC (#12432), SRC (#2108), pp53 (#9284), p53 (#2524), CDKN1A (p21) (#2947), pCDC25C (#9528), CDC25C (#4688), pCHK1 (#2341), CHK1 (#2360), pCHK2 (#2661), CHK2 (#6334), (all diluted 1:1000, Cell Signaling, Boston, MA, USA), ERK2 (D2) (#sc-1647, 1:1000, Santa Cruz Biotechnology, Dallas, TX, USA) and α-tubulin (DM1A) (#05-829,

1:50 000, Millipore, Burlington, MA, USA). Protein bands were visualized by SuperSignal™ West Dura Extended Duration Substrate (Thermo Fisher Scientific, Waltham, MA, USA) and exposed in a Syngene G Box. If not otherwise specified, protein lysates were made from cells that had been subjected to 400 ng/mL GAS6 (R&D, Minneapolis, MN, USA) and 10 µg/mL Vitamin K (Sigma Aldrich, St. Louis, MO) for 60 minutes. USA Simple Western immunoassay was performed according to the manufacturer protocol and run on the Peggy Sue™ machine (ProteinSimple, San Jose, CA, USA). Antibodies used were AXL (1:100, #8661 Cell Signaling, Boston, MA, USA) and β-actin (1:300, #4967 Cell Signaling, Boston, MA, USA). Data was analyzed using the Compass Software (Protein Simple, San Jose, CA, USA).

Reagents

BGB324 (previously known as R428, first described in (28)) was a kind gift from BerGenBio (Bergen, Norway). AZD7762 (first described in (29)) and VE-822 (first described in (30,31)) was purchased from Selleck Chemicals (Huston, TX, USA). Inhibitors, diluted in DMSO, were used at concentrations and time periods indicated, with controls receiving the same amount of DMSO as the treatment groups.

RNA interference

Cells were transfected with 100 nM siRNA using Lipofectamine® 2000 in Opti-MEM Media (Thermo Scientific, Waltham, MA, USA) according to manufacturers protocol using the following siRNAs targeting AXL: 3 unique 27mer siRNA duplexes (Cat: SR319445, Origene, Rockville, MD, USA) and ON-TARGETplus Human *AXL* siRNA (Cat: J-003104-13-0002, Dharmacon, Lafayette, CO, USA), CHK1: ON-TARGETplus Human *CHEK1* siRNA (Cat: J-003255-10-0002 and J-003255-11-0002, Dharmacon, Lafayette, CO, USA), and CHK2: ON-TARGETplus Human *CHEK2* siRNA (Cat: J-003256-17-0002 and J-003256-18-0002, Dharmacon, Lafayette, CO, USA). ON-TARGETplus Non-targeting Pool Control siRNA (Cat: D-001810-10-05, Dharmacon, Lafayette, CO, USA) was used as control. Cells were left for 48 hours before they were used in further experiments.

***In vitro* proliferation and Caspase-3/7 cleavage**

For analyzing the effect on proliferation, cells were plated at 15-25% confluency in 96-well or 6-well culture plates and left overnight before treatment with drugs for 72 hours. Cell confluence was visualized by IncuCyte FLR or IncuCyte Zoom Kinetic Imaging System (Essen Bioscience, Ann Arbor, MI, USA) light scanning microscopes. For colony formation assays, 500 or 1000 cells were plated in 6-well culture plates overnight before drug-containing media was added. After 21 days, colonies were fixated with ice-cold methanol before being stained with 0.05% crystal violet and counted using the GelCount™ machine (Oxford Optronix, Abingdon, UK).

Caspase-3/7 cleavage was determined using the CellPlayer™ 96-well Caspase-3/7 reagent (Essen Bioscience Ann Arbor, MI, USA) according to manufacturer's protocol. In brief, cells were plated to yield 10-20% confluency. The following day, drugs and 2.5 µM caspase-3/7 reagent was added. Caspase-3/7

cleavage, yielding fluorescent signals, was visualized by IncuCyte FLR or IncuCyte Zoom Kinetic Imaging System (Essen Bioscience, Ann Arbor, MI, USA) light scanning microscopes. Fluorescence was related to the confluence of the respective well at the respective time points.

Flow cytometry

Cells were plated at 30% confluency in 6-well plates overnight before incubation with BGB324 and/or AZD7762 for 24 hours. Control cells were treated with DMSO. Harvested cells were fixated in 70% ice-cold methanol and stored at -20ºC for at least 24 hours. Cells were then labeled with 2.4 µL/mL Hoechst 33258 (Sigma Aldrich, St. Louis, MO, USA) or 500µL propidium iodide Cycloscope™ Reagent (Cytognos, Salamanca, Spain) and incubated for 10 minutes shielded from light. H2AX staining was performed on fixed cells resuspended and blocked in detergent buffer (0.1% Nonidet P40 (Igepal CA-630), 6.5mM Na_2HPO_4, 1.5mM KH_2PO_4, 2.7mM KCL, 137mM NaCl, 0.5mM EDTA PH 7.5 with 4% nonfat milk) before primary incubation with γH2AX antibody (1:500, Abcam, Cambridge, UK) and secondary incubation with Alexa Flour® 647 antibody (1:500, Abcam, Cambridge, UK). Cells were labeled with 2.4 µL/mL Hoechst 33258 (Sigma Aldrich, St. Louis, MO, USA). Analysis was performed using the LSRII flow cytometer (BD Biosciences, San Jose, CA, USA) and analyzed by FlowJo® v10 software (Ashland, OR, USA).

Invasion and migration assays

To measure cell invasion, 50 µg matrigel (BD Biosciences, San Jose, CA, USA) was added to Falcon® Transparent PET Membrane 24-well 8.0 µm cell culture inserts (Corning, Corning, NY, USA). Newly split cells were incubated with 0.1 mCi/mL ^{3}H-Thymidine (Nerliens Mezansky, Oslo, Norway) for 24 hours. Thereafter, 50 000 serum-starved ^{3}H-Thymidine labeled cells/well were plated in the inserts, in RPMI-1640 media (Sigma Aldrich, St. Louis, MO, USA) containing drugs, but without serum. Five percent FBS was added to the bottom well in addition to drugs in the same concentration as the top well. Cells were harvested by scraping from the bottom and top of the matrigel with a cotton swab that was further inserted into tubes containing 4 mL Aquasafe 300 scintillation fluid (Zinsser Analytic, Frankfurt, Germany). The invasive ability was determined by comparing ^{3}H-Thymidine-radioactivity as a measure of number of cells on the bottom of the matrigel membrane divided by the total radioactivity of cells from top and bottom of the membrane.

Migration was measured by plating 50 000 cells/well in 96-well culture plates and scratching the wells the following day by The WoundMaker™ 96-well pin block (Essen Biosciences, Ann Arbord, MI, USA) before adding drug. Cell migration was determined using the Incucyte FLR or Incuzoom Zoom Kinetic Imaging System (Essen Biosciences, Ann Arbor, MI, USA), that scan the cells every three hours, and with the respective software calculating cell confluence.

Ex vivo drug sensitivity assay

Melanoma lymph node metastases obtained following surgery were disaggregated for one hour by 125 units collagenase type 2 (Sigma Aldrich, St. Louis, MO, USA) and 2,5 mg/mL DNase (Sigma Aldrich, St. Louis, MO, USA). To remove aggregates and debris the cell suspensions were filtered through 100 µM filters (WVR, Radnor, PA, USA). If necessary, red blood cells were removed using ACK lysing buffer (Lonza, Basel, Switzerland). Live cells (15.000-20 000 per well) were seeded in Nunc™ 96-Well Polystyrene Round Bottom Microwell plates (Thermo Scientific, Waltham, MA, USA) in RPMI-1640 (Sigma Aldrich, St. Louis, MO, USA) medium supplemented with 5% FBS, 2 mM L-glutamine, 100 units/mL penicillin and 0.1 mg/mL streptomycin (all Lonza, Basel, Switzerland) and allowed to form three-dimensional spheroids. Drugs were added at indicated concentrations immediately after seeding and the cells incubated for 5 days before viability was measured using the CellTiter-Glo® Luminescent Cell Viability Assay (Promega, Madison, WI, USA), and analyzed by Fluoroscan Ascent Fl (Thermo Scientific, Waltham, MA, USA). The *ex-vivo* assay was performed once for each patient sample, with at least three technical replicates per condition.

In vivo studies

Eight week old female athymic (foxn1 nu) nude mice were injected subcutaneously with $2x10^6$ Melmet 1 cells in the right flank. When the tumors reached a volume of approximately 50 mm^3 the mice were randomized into four groups containing 6-8 mice in each group. 50 mg/kg BGB324 diluted in 0.5% Hydroxypropyl Methylcellulose/0.1% Tween-80 was given twice daily by oral gavage and 25 mg/kg AZD7762 diluted in 11.3% (2-Hydroxypropyl)-β-cyclodextrin was given intravenously three times a week. Treatment duration was fourteen days. Groups not receiving BGB324 and/or AZD7762 were administered drug vehicles in the same manner as treatment groups. Treatment toxicity was monitored by weight loss measured twice daily on treatment and twice weekly off treatment. Mice with ≥15% reduced weight were euthanized. Tumor diameters were measured twice a week by digital calipers and tumor volume calculated by the formula 0.5 x length x $width^2$. In line with governmental regulations, the mice were euthanized when the tumors reached a diameter of 16 mm and/or a volume of 2000 mm^3. *In vivo* data is presented as average tumor volume + standard error of the mean (SEM). All mice were bred at the Department of Comparative Medicine, The Norwegian Radium Hospital, housed in rooms with alternating light/dark cycles of 12 hours, had *ad libitum* access to food and water and were kept according to regulations of the Norwegian Animal Welfare Act. Animal experiments were approved by the Norwegian Animal Research Authority (FOTS approval number 8554).

Statistical analysis

All values represent data average + standard deviation (SD) or SEM. Statistical significance was determined by student two-tailed t-test when comparing two groups or one-way ANOVA when comparing three groups. Significance over various time points in the animal experiments was determined by area

under the curve (AUC) analysis. The statistical analyses were performed using GraphPad Prism version 7.0 (GraphPad Software, San Diego, CA, USA). P-values of less than 0.05 were considered significant and marked with asterisks, where $p<0.05$ = *, $p<0.01$ = ** and $p<0.001$ = ***. Synergism was calculated by the CalcuSyn Software (Biosoft, Cambridge, UK) using the Chou-Talalay CI method (32). Experiments were performed at least three times with at least three technical replicates in each experiment, if not otherwise specified. Immunoblots were performed at least twice with independent lysates.

Results:

Decreased expression or inhibition of AXL reduced proliferation and MAPK and PI3K signaling

Ten melanoma cell lines were first examined for AXL expression by Simple Western immunoassay (Supplementary Figure 1A). Of the three AXL expressing cell lines (Melmet 1, WM1366 and MeWo), the two with the highest expression (Melmet 1 and WM1366) were chosen for further studies. The impact of AXL on proliferation was investigated following transfection with two different short interfering RNAs (siRNA). As shown in Figure 1A, silencing AXL decreased proliferation and reduced colony formation as compared to scrambled siRNA control. The effect on proliferation was further confirmed following treatment with the specific small-molecular AXL inhibitor BGB324 (28) (Figure 1B). A BGB324 concentration of 2 μM was chosen as a higher dose (3 μM) drastically reduced proliferation, suggesting off-target effects at this dose (Supplementary Figure 1B). Due to the role of AXL in epithelial-to-mesenchymal transition (EMT) (33), we next investigated the effect of AXL inhibition on migration and invasion. As shown in Supplementary Figure 1C, treatment with BGB324 for 24 hours reduced migration and invasion in both cell lines.

To investigate the effect of targeting AXL on cell signaling, we first confirmed that GAS6 activates AXL, as demonstrated by increased Tyrosine 702 phosphorylation (Supplementary Figure 1D). This phosphorylation site is found responsible for the general activation of the protein (34). BGB324 reduced AXL activation in a dose dependent manner in both cell lines (Figure 1C). Of particular note, BGB324 increased the total AXL protein level, suggesting an attempt to rescue the reduced AXL signaling. Next, the impact of AXL inhibition on downstream signaling pathways was examined. As demonstrated in Figure 1C, BGB324 treatment in GAS6 stimulated cells decreased phosphorylation of AKT, ERK and particularly SRC, but not p38. These effects were confirmed in siAXL transfected cells (Figure 1D).

Combined targeting of AXL and the DNA damage response pathway reduced viability and tumor growth in melanoma cell lines and patient-derived models.

The newly discovered link between AXL signaling and DNA damage response (DDR) (21,35) spurred us to investigate the effect of combined inhibition of AXL and the DDR. As shown in Figure 2A and 2B, co-treatment with BGB324 and the CHK1/2 inhibitor AZD7762 synergistically decreased proliferation in both Melmet 1 and WM1366 cells. The effect was validated using a three-dimensional (spheroid) drug efficacy assay in Melmet 1 cells (Figure 2C). To rule out the possibility of off-target effects, we treated the AXL negative cell line WM115 with BGB324 and/or AZD7762 *in vitro* and using the spheroid drug sensitivity assay and only observed reduced proliferation mediated by the AZD7762 treatment (Figure 2D), suggesting no off-target effects of the BGB324 treatment. Further, reduced proliferation was also observed in siAXL cells treated with AZD7762 compared to treated and untreated scrambled control transfected cells (Figure 2E). The transfected cells were more responsive to AZD7762 than untransfected cells (Figure 2A), possibly due to the added stress of the transfection.

To elucidate if the effect was dependent on either CHK1 or CHK2 signaling, we diminished CHK1 or CHK2 expression by siRNA before treating the cells with BGB324. Reduced expression of CHK1 or CHK2) resulted in slight to no change in proliferation compared to scrambled control transfected cells (Figure 3A and 3B). In both cell lines, siCHK1 transfected cells responded with decreased proliferation in combination with BGB324 compared to BGB324 treated and untreated control transfected cells. This was only significant in cells where CHK1 was completely eradicated (siCHK1 #1), indicating that even a low expression of CHK1 is enough to partly protect the cells from growth inhibition. There was also lower proliferation in siCHK2 transfected cells treated with BGB324 compared to BGB324 treatment alone, however only significant for one of the siRNA molecules (siCHK2 #1). Reducing expression of either CHK1 or CHK2 did not lead to as pronounced decrease in proliferation as AZD7762 treatment, neither alone nor in combination with BGB324, suggesting that signaling through both proteins must be abolished to maximize the response. To examine this hypothesis, we reduced the expression of both CHK1 and CHK2 and observed reduced proliferation in the siCHK1 and siCHK2 cells comparable to AZD7762 mono-treatment (Figure 3C and 3D). The proliferation of the combined siCHK1 and siCHK2 transfected cells was further reduced when the cells were treated with BGB324, yielding results in concordance with cells treated with BGB324 and AZD7762.

Further, we aimed to determine if reduced proliferation was only dependent on diminished activation of the CHK1/2 proteins or if similar effect could be observed when the activation of other DDR proteins was lowered. Thus, we inhibited signaling of ATR, mainly working upstream of CHK1, but also shown to activate CHK2 (36), using the ATR inhibitor VE-822 (30,31) in combination with BGB324 (Figure 3E). In both cell lines, combinatorial treatment with VE-822 and BGB324

significantly inhibited cell proliferation compared to each mono-treatment. This illustrates that other proteins in the DDR pathway also could be targeted together with AXL and cause reduced cell proliferation. Overall, these data demonstrate that inhibiting or reducing the expression of AXL in combination with CHK1 and CHK2 or other proteins in the DDR pathway result in decreased cell viability.

The observed effect on proliferation upon simultaneous targeting of AXL and the DDR encouraged us to examine if this could also reduce proliferation in patient samples. To this end, cells harvested directly from 27 melanoma lymph node metastases were treated with BGB324 and AZD7762 alone or in combination and analyzed for effect on viability using the *ex vivo* drug sensitivity assay. As shown in Figure 4A, the mean effects of the mono-treatments were slightly reduced compared to control, however these results were not significant. BGB324 and AZD7762 in combination, however, significantly decreased the viability compared to either mono-treatment. Of note, cells from three of the patient tumor samples showed increased viability when treated with AZD7762 alone, and in two of them, the viability was not reduced following combined treatment. Finally, the superior effect of the combined treatment was confirmed in the mouse Melmet 1 xenograft model (Figure 4B and 4C). Whereas the mono-treated mice displayed insignificant reductions in tumor volume, mice treated with the combination showed significantly decreased relative tumor volume and prolonged survival time compared to untreated controls or following mono-treatments. No significant weight loss was observed, indicating that the treatments were well tolerated (Supplementary Figure 2).

Combined inhibition of AXL and CHK1/CHK2 leads to cell cycle arrest and increased apoptosis

Due to the observed effects on proliferation and viability we aimed to investigate how reduced AXL and CHK1/2 activity alone and in combination affected cell cycle progression and apoptosis. As shown in Figure 5A and Supplementary Figure 3A, BGB324 treatment had no effect on cell cycle progression in any of the cell lines. AZD7762 treatment, on the other hand, slightly increased the S-phase fraction in Melmet 1 cells at both 24 and 48 hours post-treatment, but had minimal effect in WM1366 cells. Combining the two inhibitors, however, resulted in a considerable S phase arrest in Melmet 1 cells at 24 hours, and S phase and G2/M phase arrest at 48 hours. Co-treatment of WM1366 cells led to G2/M arrest at both 24 hours and 48 hours, whereas S-phase arrest was only observed after 48 hours.

In addition, in both cell lines a marked sub-G1-peak, suggesting apoptosis or necrosis, was observed (Supplementary Figure 3B) following combined treatment with BGB324 and AZD7762. To analyze if this reflected apoptosis, cleavage of CASP3 (caspase-3) and CASP7 (caspase-7) was examined using a kit yielding a fluorescent signal upon cleavage. As shown in Figure 5B, left panels, mono-treatments slightly increased cleavage of caspase-3 and -7, while this was significantly augmented following the combined treatment. Caspase-3 cleavage was further confirmed by western blot analysis (Figure 5B,

right panels), demonstrating caspase-3 cleavage induced by AZD7762 and further increased in cells receiving the combined treatment. However, no caspase-3 cleavage was observed in BGB324 treated cells as examined by western blot. This is in contrast to the BGB324-induced cleavage of caspase-3 and -7 observed by the apoptosis assay, suggesting that caspase-7 cleavage plays a more prominent role following BGB324 treatment.

Further, we investigated the molecular effects of BGB324 and/or AZD7762 treatments by western blot analyses. As seen in Figure 5C, both compounds alone and in combination reduced the phosphorylation of AXL and increased the expression of total AXL. This is in agreement with previous reports demonstrating that AZD7762 may reduce AXL phosphorylation (37). Also in line with previous reports (38), AZD7762 increased phosphorylation of CHK1 and CHK2 in both cell lines, indicating activation of the DDR pathway. In addition, AZD7762 increased Serine 216 phosphorylation of CDC25C, a downstream effector of CHK1 and CHK2. While BGB324 treatment alone did not show any effect on CHK1 and CHK2 phosphorylation compared to control, CDC25C was greatly phosphorylated. Phosphorylation and total expression of CHK1, CHK2 and CDC25C was reduced in the combined treatment.

Previous reports have suggested that BGB324 induces activation and expression of H2AFX (H2AX) (21). This was not evident in our cell lines (Figure 5C). H2AX phosphorylation and expression was, however, observed in AZD7762 treated cells and further increased following combined treatment. The H2AX immunoblot results were verified by flow cytometry for WM1366 cells (Supplementary Figure 3C).

BGB324 alone had no effect on expression of the DDR proteins p53 or CDKN1A ($p21^{WAF1/Cip1}$) in any of the two cell lines, whereas AZD7762 and the combination increased p53 protein levels as well as Serine 15 phosphorylation in Melmet 1 cells (p53 wild-type). Surprisingly, increased Serine 15 phosphorylation of p53 was also observed in the p53 mutated cell line WM1366 after treatment with AZD7762 alone and in combination with BGB324. In both cell lines, AZD7762 increased the expression of $p21^{WAF1/Cip1}$ and this was further augmented when the two inhibitors were combined. While both mono-treatments decreased PI3K and MAPK signaling, enhanced reduction when combined was only seen in PI3K signaling in Melmet 1 cells (Supplementary Figure 3D). These data were also observed in cells treated with BGB324 and/or VE-822 (Supplementary Figure 3E). Importantly, VE-822 treatment reduced pAXL expression (Supplementary Figure 3E), which was also observed in AZD7762 treated cells (Figure 5C). Further, short (10 minutes) exposure to AZD7762 or VE-822 monotherapy did not reduce pAXL expression to the extent of BGB324 treatment (Supplementary Figure 3F).

Together, our data indicates that targeting AXL in combination with the DDR pathway reduces proliferation, leads to downregulation of DDR response proteins and ultimately results in apoptosis. Thus, targeting AXL together with the DDR could be a beneficial treatment option in melanoma.

Discussion

AXL has been observed overexpressed in various types of cancer and linked to aggressive tumor traits, poor prognosis and drug resistance (33,39). In melanoma, acquired resistance to MAPK inhibitors (14,40) and immunotherapy (16) has been associated with increased AXL expression, making AXL an interesting target to overcome treatment resistance. AXL has also emerged as a promising therapeutic strategy in other types of cancers, and currently the AXL inhibitor BGB324 is in phase I/II clinical trials alone or in combination with chemotherapy (NCT02488408), erlotinib (NCT02424617), pembrolizumab (NCT03184558 and NCT03184571) or dabrafenib and trametinib (NCT02872259).

In accordance with a previous report (41), AXL was found expressed in 30% of the examined melanoma cell lines, and reducing (42,43) or inhibiting (20) AXL expression modestly reduced proliferation, migration and invasion. Inhibition of AXL led to decreased AXL-Tyrosine 702 phosphorylation, indicating less activation of the protein (44). Furthermore, AXL has been found to activate the PI3K and MAPK pathways to induce pro-survival and proliferative signals (13). In accordance with this, we observed less proliferation and reduced phosphorylation of SRC, AKT and ERK upon diminished expression or inhibition of AXL. It has been shown that SRC activity is dependent on partnerships with receptor tyrosine kinases such as EGFR and PDGFR (45). These receptor tyrosine kinases are closely related to AXL and the substantial decrease in pSCR expression at even low levels of BGB324 treatment indicate that SRC activity may be dependent on AXL signaling as well. In contrast to what has been observed by others (46), no effect on p38/MAPK signaling was observed, potentially due to cell line or cancer type specific differences in p38/MAPK mediated stress signaling.

Recently, inhibition of AXL signaling was found to induce DNA damage (21,35) and it has also been proposed that AXL protect cancer cells from fork collapse (35), which is mediated by ATR/ATM-CHK1/2 signaling. In the current study, we neither observed activation of H2AX nor CHK1/2 following BGB324 treatment, suggesting that inhibiting AXL does not induce DNA damage in our melanoma cell lines. On the other hand, BGB324 led to increased inhibitory phosphorylation (Serine 216) of CDC25C, implying cell cycle arrest. CHK1/2 signaling was not activated by BGB324 treatment, suggesting that CDC25C is inhibited independently of CHK1/2, for instance through phosphorylation by MARK3 (c-TAK1), p38/MAPK, CAMK2A, and PRKA (AMPK), as has been reported by others (47,48). Additionally, CHK1/2-independent phosphorylation of CDC25C-Serine

216 must also hold true for AZD7762 treated cells as this inhibitor blocks the downstream signaling of CHK1/2 by acting as an ATP competitor (29).

Because of a prior article describing effects of AXL on DDR (21), we speculated whether treatment with BGB324 in combination with a DDR inhibitor could be a beneficial therapeutic strategy in melanoma. In support of this, we found that targeting AXL together with CHK1 and CHK2 inhibited proliferation and viability in cell cultures, PDX models and patient material. Decreased proliferation was coupled with cell cycle deregulation and increased apoptosis. These data are in accordance with a previous finding showing that inhibition of AXL in combination with WEE1, a regulator of cell cycle progression downstream of CHK1/2, reduced tumor growth and increased apoptosis in small cell lung cancer cells (49). While knockdown of CHK1 or CHK2 resulted in reduced proliferation in combination with BGB324, the effect was not as pronounced as when inhibiting or reducing the expression of both CHK1 and CHK2. This suggests that redundancy, crosstalk and overlapping roles of CHK1 and CHK2 (50) protect the cells from growth inhibition when targeting only one of the proteins.

It has previously been shown that AZD7762 treatment reduces AXL phosphorylation (37), a finding in accordance with our results. A direct influence of AZD7762 on AXL phosphorylation might suggest that the inhibitory effect on proliferation when combining the two inhibitors solely is caused by decreased AXL activity. In a kinase screen of AZD7762, the drug also showed selectivity towards AXL, although it was ten times lower for AXL than CHK1/2 (29). To rule out the possibility of AZD7762 affecting AXL signaling, we diminished CHK1 or CHK2 expression, or treated cells with an ATR inhibitor (VE-822), in combination with BGB324. These experiments led to similar results as when using the AZD7762 and BGB324 inhibitors. Importantly, decreased pAXL expression was also observed in cells treated with VE-822, suggesting that there is some unknown mechanism of the DDR pathway that indirectly or directly targets AXL signaling. This interpretation in strengthened by the observation that AZD7762 or VE-822 did not reduce pAXL expression to that of BGB324 treated cells in a short (10 minutes) exposure to the drugs. These data demonstrates that the observed consequences of the combined treatment is not due to off-target effects of the AZD7762 inhibitor. Surprisingly, in the scrambled transfected control cells, we observed lower proliferation when the cells were treated with AZD7762 (Figure 2E) compared to the same treatment in untransfected cells (Figure 2A). This effect was not observed in control transfected cells treated with BGB324 (Figure 3A). We do not know the reason for this, but it is shown that lipofectamine treatment increases DNA damage and induces cellular stress (51,52). Thus, we speculate that DNA damage and cellular stress produced by the transfection will sensitize the cells for the AZD7762 treatment hindering DDR and inducing cellular toxicity. Despite this, cellular proliferation was even further decreased after treatment with AZD7762 in combination with AXL knockdown.

We show here that while AZD7762 treatment resulted in activation and expression of DDR proteins such as CHK1, CHK2 and CDC25C, combined treatment with BGB324 diminished the expression of these proteins, implying that AXL facilitates the DDR. In line with this, AXL inhibition in combination with inhibitors of the DNA repair protein PARP or the cell cycle regulator WEE1 has shown to reduce the expression of DDR and DNA repair proteins (21,49). Further, previous reports have shown that accumulation of p53 and $p21^{WAF1/Cip1}$ following DNA damage is associated with reduced expression of CHK1 (53), CHK2 (54) and CDC25C (55), which was also observed in this study. We do not know, however, if the accumulation of p53 and $p21^{WAF1/Cip1}$ precedes the downregulation of DDR protein expression, or if the downregulation of these proteins promotes increased p53 and $p21^{WAF1/Cip1}$ activation and/or expression. p53 and $p21^{WAF1/Cip1}$ activation and/or expression play a role in triggering apoptosis, and in line with this, we observed that the combined inhibition of AXL and CHK1/2 led to apoptosis through cleavage of caspase-3 and-7. AZD7762 treatment caused a more pronounced increase in caspase-3 cleavage, as assessed by immunoblot, than BGB324 treatment, while the caspase-3 and -7 cleavage was approximately similar in the two mono-treatments as measured by the fluorescent reagent. This indicates that BGB324 activates caspase-7 to a larger degree than AZD7762 treatment.

The observed effects on cell viability upon combined AXL and CHK1/2 targeting in cell lines, was further verified using disaggregated cells from melanoma lymph node metastases in an *ex vivo* drug efficacy assay. The added effect of the combined treatment relative to the mono-treatments was less pronounced in the *ex vivo* assay, probably due to the presence of non-malignant cells in the lymph node metastases or by cells that do not express AXL. Despite this, the assay clearly distinguishes patient-derived tumor cells with different sensitivity to the applied drugs. Previously, we have confirmed platinum chemotherapy resistance in ovarian cancer patients (56), and recently we demonstrated concordance between response to the mutated BRAF inhibitor vemurafenib and *BRAF/NRAS* mutation status when analyzing tumor cells from melanoma lymph node metastases in the *ex vivo* assay (57). Together, these data show that the *ex vivo* assay is able to reflect patient response to various drugs, and should be further evaluated as a supplement to guide treatment in patients having developed resistance against standard treatment regimes.

To conclude, AXL is shown to be upregulated in melanoma and its expression is associated with treatment resistance, making AXL an interesting target to overcome resistance to therapy. In this study, we investigated the effect of targeting AXL together with the DDR and found that this combination resulted in reduced cell proliferation and tumor growth. We show that dual inhibition of AXL and the DDR result in cell cycle retention and increased apoptosis through downregulation of CHK1, CHK2 and CDC25C, suggesting that AXL facilitate the DDR. These data strongly suggest that targeting AXL together with the DDR may be a promising treatment strategy for melanoma and studies to further investigate this possibility is highly warranted.

References:

1. Rigel DS. Epidemiology of melanoma. Seminars in cutaneous medicine and surgery **2010**;29(4):204-9 doi 10.1016/j.sder.2010.10.005.
2. Ferlay J, Steliarova-Foucher E, Lortet-Tieulent J, Rosso S, Coebergh JWW, Comber H*, et al.* Cancer incidence and mortality patterns in Europe: Estimates for 40 countries in 2012. European journal of cancer **2013**;49(6):1374-403.
3. Gibney GT, Messina JL, Fedorenko IV, Sondak VK, Smalley KS. Paradoxical oncogenesis--the long-term effects of BRAF inhibition in melanoma. Nat Rev Clin Oncol **2013**;10(7):390-9 doi 10.1038/nrclinonc.2013.83.
4. Hatzivassiliou G, Song K, Yen I, Brandhuber BJ, Anderson DJ, Alvarado R*, et al.* RAF inhibitors prime wild-type RAF to activate the MAPK pathway and enhance growth. Nature **2010**;464(7287):431-5.
5. Ott PA, Hodi FS, Robert C. CTLA-4 and PD-1/PD-L1 blockade: new immunotherapeutic modalities with durable clinical benefit in melanoma patients. Clinical cancer research : an official journal of the American Association for Cancer Research **2013**;19(19):5300-9 doi 10.1158/1078-0432.CCR-13-0143.
6. Jin G, Wang Z, Wang J, Zhang L, Chen Y, Yuan P*, et al.* Expression of Axl and its prognostic significance in human breast cancer. Oncology letters **2017**;13(2):621-8 doi 10.3892/ol.2016.5524.
7. Sun W, Fujimoto J, Tamaya T. Coexpression of Gas6/Axl in human ovarian cancers. Oncology **2004**;66(6):450-7 doi 10.1159/000079499.
8. Yu H, Liu R, Ma B, Li X, Yen HY, Zhou Y*, et al.* Axl receptor tyrosine kinase is a potential therapeutic target in renal cell carcinoma. British journal of cancer **2015**;113(4):616-25 doi 10.1038/bjc.2015.237.
9. Quong RY, Bickford ST, Ing YL, Terman B, Herlyn M, Lassam NJ. Protein kinases in normal and transformed melanocytes. Melanoma research **1994**;4(5):313-9.
10. Paccez JD, Vasques GJ, Correa RG, Vasconcellos JF, Duncan K, Gu X*, et al.* The receptor tyrosine kinase Axl is an essential regulator of prostate cancer proliferation and tumor growth and represents a new therapeutic target. Oncogene **2013**;32(6):689-98 doi 10.1038/onc.2012.89.
11. Rankin EB, Fuh KC, Taylor TE, Krieg AJ, Musser M, Yuan J*, et al.* AXL is an essential factor and therapeutic target for metastatic ovarian cancer. Cancer research **2010**;70(19):7570-9 doi 10.1158/0008-5472.can-10-1267.
12. Asiedu MK, Beauchamp-Perez FD, Ingle JN, Behrens MD, Radisky DC, Knutson KL. AXL induces epithelial-to-mesenchymal transition and regulates the function of breast cancer stem cells. Oncogene **2014**;33(10):1316-24 doi 10.1038/onc.2013.57.
13. Gay CM, Balaji K, Byers LA. Giving AXL the axe: targeting AXL in human malignancy. British journal of cancer **2017**;116(4):415-23 doi 10.1038/bjc.2016.428.
14. Muller J, Krijgsman O, Tsoi J, Robert L, Hugo W, Song C*, et al.* Low MITF/AXL ratio predicts early resistance to multiple targeted drugs in melanoma. Nature communications **2014**;5:5712 doi 10.1038/ncomms6712.
15. Rambow F, Rogiers A, Marin-Bejar O, Aibar S, Femel J, Dewaele M*, et al.* Toward Minimal Residual Disease-Directed Therapy in Melanoma. Cell **2018**;174(4):843-55 e19.
16. Hugo W, Zaretsky JM, Sun L, Song C, Moreno BH, Hu-Lieskovan S*, et al.* Genomic and Transcriptomic Features of Response to Anti-PD-1 Therapy in Metastatic Melanoma. Cell **2016**;165(1):35-44 doi 10.1016/j.cell.2016.02.065.
17. Zagorska A, Traves PG, Lew ED, Dransfield I, Lemke G. Diversification of TAM receptor tyrosine kinase function. Nature immunology **2014**;15(10):920-8 doi 10.1038/ni.2986.
18. Korshunov VA. Axl-dependent signalling: a clinical update. Clin Sci **2012**;122(7-8):361-8 doi 10.1042/Cs20110411.

19. Rankin EB, Fuh KC, Castellini L, Viswanathan K, Finger EC, Diep AN*, et al.* Direct regulation of GAS6/AXL signaling by HIF promotes renal metastasis through SRC and MET. Proceedings of the National Academy of Sciences of the United States of America **2014**;111(37):13373-8 doi 10.1073/pnas.1404848111.
20. Brand TM, Iida M, Stein AP, Corrigan KL, Braverman CM, Coan JP*, et al.* AXL Is a Logical Molecular Target in Head and Neck Squamous Cell Carcinoma. Clinical Cancer Research **2015**;21(11):2601-12 doi 10.1158/1078-0432.ccr-14-2648.
21. Balaji K, Vijayaraghavan S, Diao L, Tong P, Fan Y, Carey JP*, et al.* AXL Inhibition Suppresses the DNA Damage Response and Sensitizes Cells to PARP Inhibition in Multiple Cancers. Molecular cancer research : MCR **2017**;15(1):45-58 doi 10.1158/1541-7786.MCR-16-0157.
22. Wilson C, Ye X, Pham T, Lin E, Chan S, McNamara E*, et al.* AXL Inhibition Sensitizes Mesenchymal Cancer Cells to Antimitotic Drugs. Cancer research **2014**;74(20):5878-90 doi 10.1158/0008-5472.can-14-1009.
23. Macleod K, Mullen P, Sewell J, Rabiasz G, Lawrie S, Miller E*, et al.* Altered ErbB Receptor Signaling and Gene Expression in Cisplatin-Resistant Ovarian Cancer. Cancer research **2005**;65(15):6789-800 doi 10.1158/0008-5472.can-04-2684.
24. Smith J, Mun Tho L, Xu N, A. Gillespie D. Chapter 3 - The ATM–Chk2 and ATR–Chk1 Pathways in DNA Damage Signaling and Cancer. In: Vande Woude GF, Klein G, editors. Advances in Cancer Research. Volume 108: Academic Press; 2010. p 73-112.
25. Fodstad O, Kjonniksen I, Aamdal S, Nesland JM, Boyd MR, Pihl A. Extrapulmonary, tissue-specific metastasis formation in nude mice injected with FEMX-I human melanoma cells. Cancer research **1988**;48(15):4382-8.
26. Prasmickaite L, Skrbo N, Hoifodt HK, Suo Z, Engebraten O, Gullestad HP*, et al.* Human malignant melanoma harbours a large fraction of highly clonogenic cells that do not express markers associated with cancer stem cells. Pigment cell & melanoma research **2010**;23(3):449-51 doi 10.1111/j.1755-148X.2010.00690.x.
27. Magnussen GI, Holm R, Emilsen E, Rosnes AK, Slipicevic A, Florenes VA. High expression of Wee1 is associated with poor disease-free survival in malignant melanoma: potential for targeted therapy. PloS one **2012**;7(6):e38254 doi 10.1371/journal.pone.0038254.
28. Holland SJ, Pan A, Franci C, Hu Y, Chang B, Li W*, et al.* R428, a Selective Small Molecule Inhibitor of Axl Kinase, Blocks Tumor Spread and Prolongs Survival in Models of Metastatic Breast Cancer. Cancer research **2010**;70(4):1544-54 doi 10.1158/0008-5472.can-09-2997.
29. Zabludoff SD, Deng C, Grondine MR, Sheehy AM, Ashwell S, Caleb BL*, et al.* AZD7762, a novel checkpoint kinase inhibitor, drives checkpoint abrogation and potentiates DNA-targeted therapies. Molecular cancer therapeutics **2008**;7(9):2955-66 doi 10.1158/1535-7163.mct-08-0492.
30. Fokas E, Prevo R, Pollard JR, Reaper PM, Charlton PA, Cornelissen B*, et al.* Targeting ATR in vivo using the novel inhibitor VE-822 results in selective sensitization of pancreatic tumors to radiation. Cell Death Dis **2012**;3:e441.
31. Charrier JD, Durrant SJ, Golec JM, Kay DP, Knegtel RM, MacCormick S*, et al.* Discovery of potent and selective inhibitors of ataxia telangiectasia mutated and Rad3 related (ATR) protein kinase as potential anticancer agents. Journal of medicinal chemistry **2011**;54(7):2320-30 doi 10.1021/jm101488z.
32. Chou TC. Theoretical basis, experimental design, and computerized simulation of synergism and antagonism in drug combination studies. Pharmacological reviews **2006**;58(3):621-81 doi 10.1124/pr.58.3.10.
33. Gjerdrum C, Tiron C, Hoiby T, Stefansson I, Haugen H, Sandal T*, et al.* Axl is an essential epithelial-to-mesenchymal transition-induced regulator of breast cancer metastasis and patient survival. Proceedings of the National Academy of Sciences of the United States of America **2010**;107(3):1124-9 doi 10.1073/pnas.0909333107.

34. Vouri M, Croucher DR, Kennedy SP, An Q, Pilkington GJ, Hafizi S. Axl-EGFR receptor tyrosine kinase hetero-interaction provides EGFR with access to pro-invasive signalling in cancer cells. Oncogenesis **2016**;5(10):e266 doi 10.1038/oncsis.2016.66.
35. Kariolis MS, Miao YR, Diep A, Nash SE, Olcina MM, Jiang D*, et al.* Inhibition of the GAS6/AXL pathway augments the efficacy of chemotherapies. The Journal of clinical investigation **2017**;127(1):183-98 doi 10.1172/JCI85610.
36. Matsuoka S, Rotman G, Ogawa A, Shiloh Y, Tamai K, Elledge SJ. Ataxia telangiectasia-mutated phosphorylates Chk2 in vivo and <em>in vitro</em&gt. Proceedings of the National Academy of Sciences **2000**;97(19):10389 doi 10.1073/pnas.190030497.
37. Park JS, Lee C, Kim HK, Kim D, Son JB, Ko E*, et al.* Suppression of the metastatic spread of breast cancer by DN10764 (AZD7762)-mediated inhibition of AXL signaling. Oncotarget **2016**;7(50):83308-18 doi 10.18632/oncotarget.13088.
38. Isono M, Hoffmann MJ, Pinkerneil M, Sato A, Michaelis M, Cinatl J, Jr.*, et al.* Checkpoint kinase inhibitor AZD7762 strongly sensitises urothelial carcinoma cells to gemcitabine. Journal of experimental & clinical cancer research : CR **2017**;36(1):1 doi 10.1186/s13046-016-0473-1.
39. Liu L, Greger J, Shi H, Liu Y, Greshock J, Annan R*, et al.* Novel Mechanism of Lapatinib Resistance in HER2-Positive Breast Tumor Cells: Activation of AXL. Cancer research **2009**;69(17):6871.
40. Konieczkowski DJ, Johannessen CM, Abudayyeh O, Kim JW, Cooper ZA, Piris A*, et al.* A melanoma cell state distinction influences sensitivity to MAPK pathway inhibitors. Cancer discovery **2014**;4(7):816-27 doi 10.1158/2159-8290.CD-13-0424.
41. Sensi M, Catani M, Castellano G, Nicolini G, Alciato F, Tragni G*, et al.* Human cutaneous melanomas lacking MITF and melanocyte differentiation antigens express a functional Axl receptor kinase. The Journal of investigative dermatology **2011**;131(12):2448-57 doi 10.1038/jid.2011.218.
42. Brand TM, Iida M, Stein AP, Corrigan KL, Braverman CM, Luthar N*, et al.* AXL mediates resistance to cetuximab therapy. Cancer research **2014**;74(18):5152-64 doi 10.1158/0008-5472.CAN-14-0294.
43. Jiang C, Zhou L, Wang H, Zhang Q, Xu Y. Axl Is a Potential Cancer Prognostic Marker for the Migration and Invasion of Nasopharyngeal Carcinoma. Advances in clinical and experimental medicine : official organ Wroclaw Medical University **2016**;25(3):531-7 doi 10.17219/acem/38943.
44. Schoumacher M, Burbridge M. Key Roles of AXL and MER Receptor Tyrosine Kinases in Resistance to Multiple Anticancer Therapies. Current Oncology Reports **2017**;19(3):19 doi 10.1007/s11912-017-0579-4.
45. Irby RB, Yeatman TJ. Role of Src expression and activation in human cancer. Oncogene **2000**;19(49):5636-42 doi 10.1038/sj.onc.1203912.
46. Corno C, Gatti L, Arrighetti N, Carenini N, Zaffaroni N, Lanzi C*, et al.* Axl molecular targeting counteracts aggressiveness but not platinum-resistance of ovarian carcinoma cells. Biochemical pharmacology **2017**;136:40-50.
47. Hutchins JR, Clarke PR. Many fingers on the mitotic trigger: post-translational regulation of the Cdc25C phosphatase. Cell cycle **2004**;3(1):41-5.
48. Shen Y, Sherman JW, Chen X, Wang R. Phosphorylation of CDC25C by AMP-activated protein kinase mediates a metabolic checkpoint during cell-cycle G2/M-phase transition. The Journal of biological chemistry **2018**;293(14):5185-99 doi 10.1074/jbc.RA117.001379.
49. Sen T, Tong P, Diao L, Li L, Fan Y, Hoff J*, et al.* Targeting AXL and mTOR Pathway Overcomes Primary and Acquired Resistance to WEE1 Inhibition in Small-Cell Lung Cancer. Clinical cancer research : an official journal of the American Association for Cancer Research **2017**;23(20):6239-53 doi 10.1158/1078-0432.CCR-17-1284.

50. Bartek J, Lukas J. Chk1 and Chk2 kinases in checkpoint control and cancer. Cancer cell **2003**;3(5):421-9.
51. Fiszer-Kierzkowska A, Vydra N, Wysocka-Wycisk A, Kronekova Z, Jarzab M, Lisowska KM*, et al.* Liposome-based DNA carriers may induce cellular stress response and change gene expression pattern in transfected cells. BMC Mol Biol **2011**;12:27 doi 10.1186/1471-2199-12-27.
52. Irianto J, Xia Y, Pfeifer CR, Athirasala A, Ji J, Alvey C*, et al.* DNA Damage Follows Repair Factor Depletion and Portends Genome Variation in Cancer Cells after Pore Migration. Curr Biol **2017**;27(2):210-23 doi 10.1016/j.cub.2016.11.049.
53. Gottifredi V, Karni-Schmidt O, Shieh S-Y, Prives C. p53 Down-Regulates CHK1 through p21 and the Retinoblastoma Protein. Molecular and cellular biology **2001**;21(4):1066-76 doi 10.1128/MCB.21.4.1066-1076.2001.
54. Matsui T, Katsuno Y, Inoue T, Fujita F, Joh T, Niida H*, et al.* Negative Regulation of Chk2 Expression by p53 Is Dependent on the CCAAT-binding Transcription Factor NF-Y. Journal of Biological Chemistry **2004**;279(24):25093-100 doi 10.1074/jbc.M403232200.
55. Clair SS, Giono L, Varmeh-Ziaie S, Resnick-Silverman L, Liu W-j, Padi A*, et al.* DNA Damage-Induced Downregulation of Cdc25C Is Mediated by p53 via Two Independent Mechanisms: One Involves Direct Binding to the cdc25C Promoter. Molecular cell **2004**;16(5):725-36.
56. Hetland TE, Kaern J, Skrede M, Sandstad B, Trope C, Davidson B*, et al.* Predicting platinum resistance in primary advanced ovarian cancer patients with an in vitro resistance index. Cancer chemotherapy and pharmacology **2012**;69(5):1307-14 doi 10.1007/s00280-012-1835-9.
57. Florenes VA, Flem-Karlsen K, McFadden E, Bergheim IR, Nygaard V, Nygard V*, et al.* A Three-dimensional Ex Vivo Viability Assay Reveals a Strong Correlation Between Response to Targeted Inhibitors and Mutation Status in Melanoma Lymph Node Metastases. Transl Oncol **2019**;12(7):951-8 doi 10.1016/j.tranon.2019.04.001.

Figure legends

Figure 1: Effects of diminished AXL expression or activity on cell proliferation and signaling.

A) Proliferation of Melmet 1 and WM1366 cells with siRNA-mediated silencing of AXL expression measured by IncuCyte Live imaging 72 hours after plating (n=3) (left panels) or by colony formation 21 days after plating (right panels). Colony formation shows an average of two independent experiments for Melmet 1 cells and three independent experiments for WM1366 cells. **B)** Melmet 1 and WM1366 cells treated with 2μM BGB324 (AXL inhibitor) reduced proliferation as measured by the IncuCyte Live imaging system (n=3). Representative immunoblot analysis of indicated proteins following **C)** treatment with indicated concentrations of BGB324 for 24 hours and **D)** siRNA-mediated AXL silencing. Control cells were treated with **C)** DMSO or **D)** scrambled siRNA. Immunoblots were performed at least twice with independent lysates. $p<0.05$ = *, $p<0.01$ = ** and $p<0.001$ = ***.

<u>Figure 2:</u> Inhibition of AXL and CHK1 and CHK2 signaling reduced proliferation in melanoma cell lines.

A) Dual treatment with 2 μM BGB324 and 1 μM AZD7762 reduced average proliferation in Melmet 1 and WM1366 melanoma cell lines. **B)** Combination index (CI) values as estimated by the Chou-Talalay method using average proliferation of indicated doses of BGB324 and AZD7762. CI < 1 indicates synergy. **C)** Proliferation of Melmet 1 cells treated with 2 μM BGB324 and/or 1 μM AZD7762 measured by the 3D spheroid assay correlates to what is observed *in vitro*. **D)** Proliferation measured by Incucyte Live imaging system (left panel) and using the 3D spheroid assay (right panel) in the AXL-negative cell line WM115 treated with BGB324 and/or AZD7762. **E)** Silenced AXL expression in combination with 1 μM AZD7762 reduced proliferation. Δ equals p value = 0.07. Proliferation was measured 72 hours after drug addition by the Incucyte Live imaging system *(in vitro*) or after 5 days using CellTiter-Glo® Luminescent assay (3D spheroid assay). Control cells were treated with DMSO. Experiments show an average of three biological replicates + SEM. $p<0.05$ = *and $p<0.01$ = **.

<u>Figure 3:</u> Treatment with BGB324 and siCHK1 and/or siCHK2 or the ATR inhibitor VE-822 reduced cell proliferation.

A) siRNA-mediated silencing of CHK1 (left panels) or CHK2 (right panels) before treatment with BGB324 reduced proliferation in melanoma cell lines. **B)** Immunoblot of CHK1 or CHK2 protein expression in cells transfected with siRNAs targeting either CHK1 (right panels) or CHK2 (left panels). **C)** Diminished expression of both CHK1 and CHK2 further reduced proliferation in combination with BGB324 treatment. **D)** Immunoblot of CHK1 and CHK2 expression in cells transfected with siCHK1 and siCHK2. **E)** Proliferation after drug addition of BGB324 and indicated doses of the ATR inhibitor VE-822. All proliferation data was measured by Incucyte Live imaging and the data shows average values relative to control cells calculated 72 hours after drug addition of at least three independent experiments + SEM. BGB324: 2 μM. Control cells were treated with DMSO. $p<0.05$ = *, $p<0.01$ = ** and $p<0.001$ = ***. Δ equals p value = 0.0512.

<u>Figure 4:</u> Dual inhibition of AXL and CHK1/2 reduced cell viability in patient tumor samples and inhibited tumor growth *in vivo.*

A) Lymph node metastases from melanoma patients were disaggregated, cells were plated as spheres and treated with 2 μM BGB324 and/or 2μM AZD7762 for five days. Cell viability was measured by CellTiter-Glo® and related to control samples treated with DMSO (n=27 patients). **B)** Tumor volume relative to the volume at day of treatment initiation of Melmet 1 xenografts treated with 50 mg/kg BGB324 twice daily and/or 25 mg/kg AZD7762 three times a week for two weeks. Controls were treated with drug vehicle(s). There were 6-8 mice per group. **C)** Kaplan-Meier survival curve showing

percentage mice in **B)** still alive as function of time. The experiment was terminated at day 62 and all mice still alive (n=9) were censored. $p<0.05$ = *and $p<0.01$ = **.

<u>Figure 5:</u> Combined treatment of BGB324 and AZD7762 leads to cell cycle arrest and apoptosis with reduced expression of cell cycle regulators.

A) Cell cycle distribution of Melmet 1 and WM1366 treated with BGB324 and/or AZD7762 for 24 or 48 hours measured by Hoechst 33258 incorporation and analyzed by Flow Cytometry. The data is shown as average of three independent experiments for 24 hours and two independent experiments for 48 hours + SEM. **B)** Average apoptosis measured by fluorescence staining of a caspase-3/-7 reagent by IncuCyte Live imaging. Fluorescent intensity was related to number of cells in each well and to control 72 hours after treatment with BGB324 and/or AZD7762 (left panels). Apoptosis experiments show an average of three biological experiments + SEM. Protein expression in total lysates of Melmet 1 and WM1366 cells treated with BGB324 and/or AZD7762 as shown by a representative immunoblot for proteins indicated (right panels). **C)** Protein expression in total lysates of Melmet 1 and WM1366 cells treated with BGB324 and/or AZD7762 for 24 hours as shown by a representative immunoblot for proteins indicated. Immunoblots were performed at least twice with independent lysates. In all experiments, control cells were treated with DMSO. Concentration of BGB324: 2 μM and AZD7762: 1 μM. $p<0.05$ = *, $p<0.01$ = ** and $p<0.001$ = ***.

Figure 1

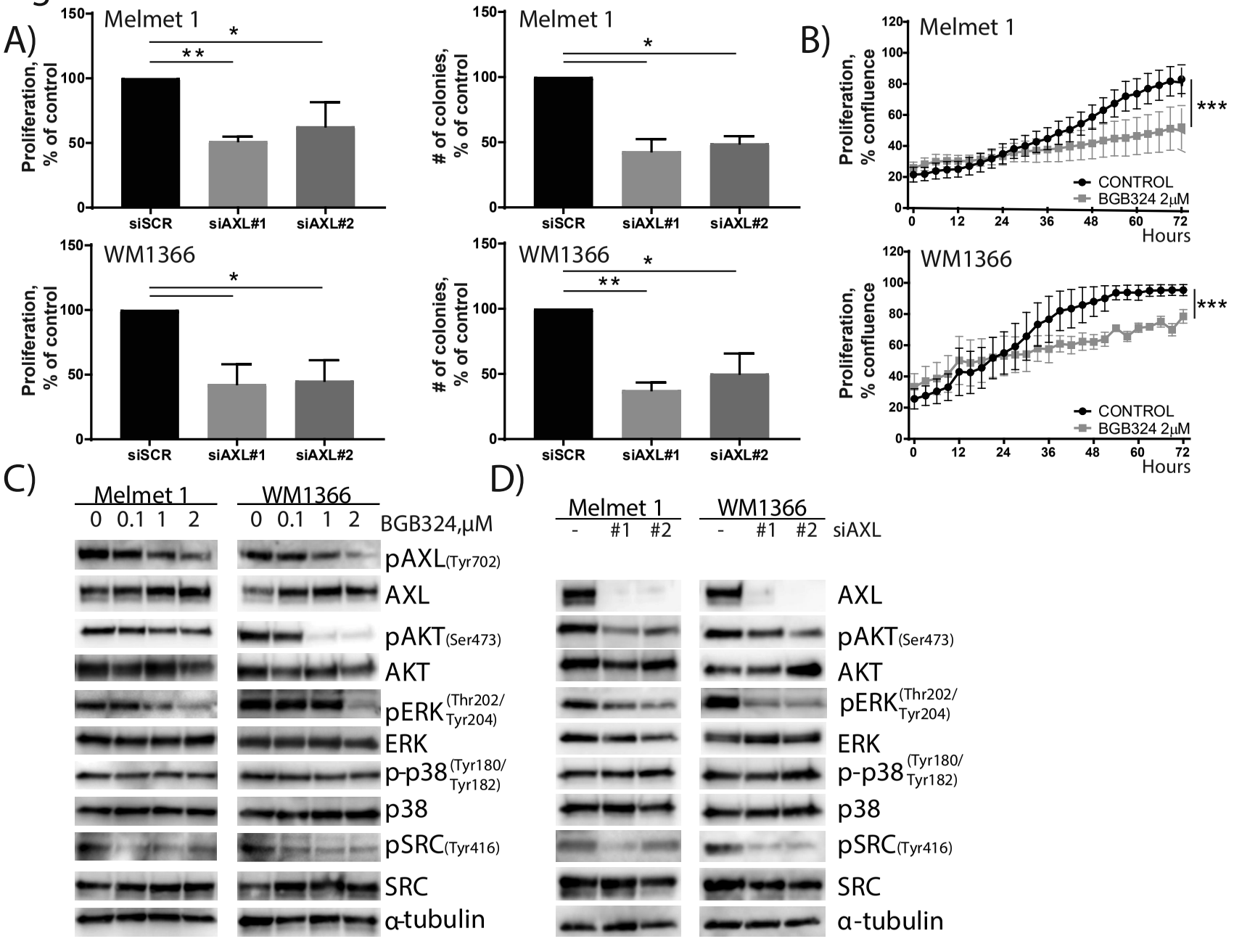
A)
Melmet 1
Proliferation, % of control
# of colonies, % of control
siSCR
siAXL#1
siAXL#2
WM1366
B)
Proliferation, % confluence
CONTROL
BGB324 2μM
Hours
C)
BGB324,μM
0 0.1 1 2
pAXL(Tyr702)
AXL
pAKT(Ser473)
AKT
pERK(Thr202/Tyr204)
ERK
p-p38(Tyr180/Tyr182)
p38
pSRC(Tyr416)
SRC
α-tubulin
D)
siAXL
- #1 #2

Figure 2

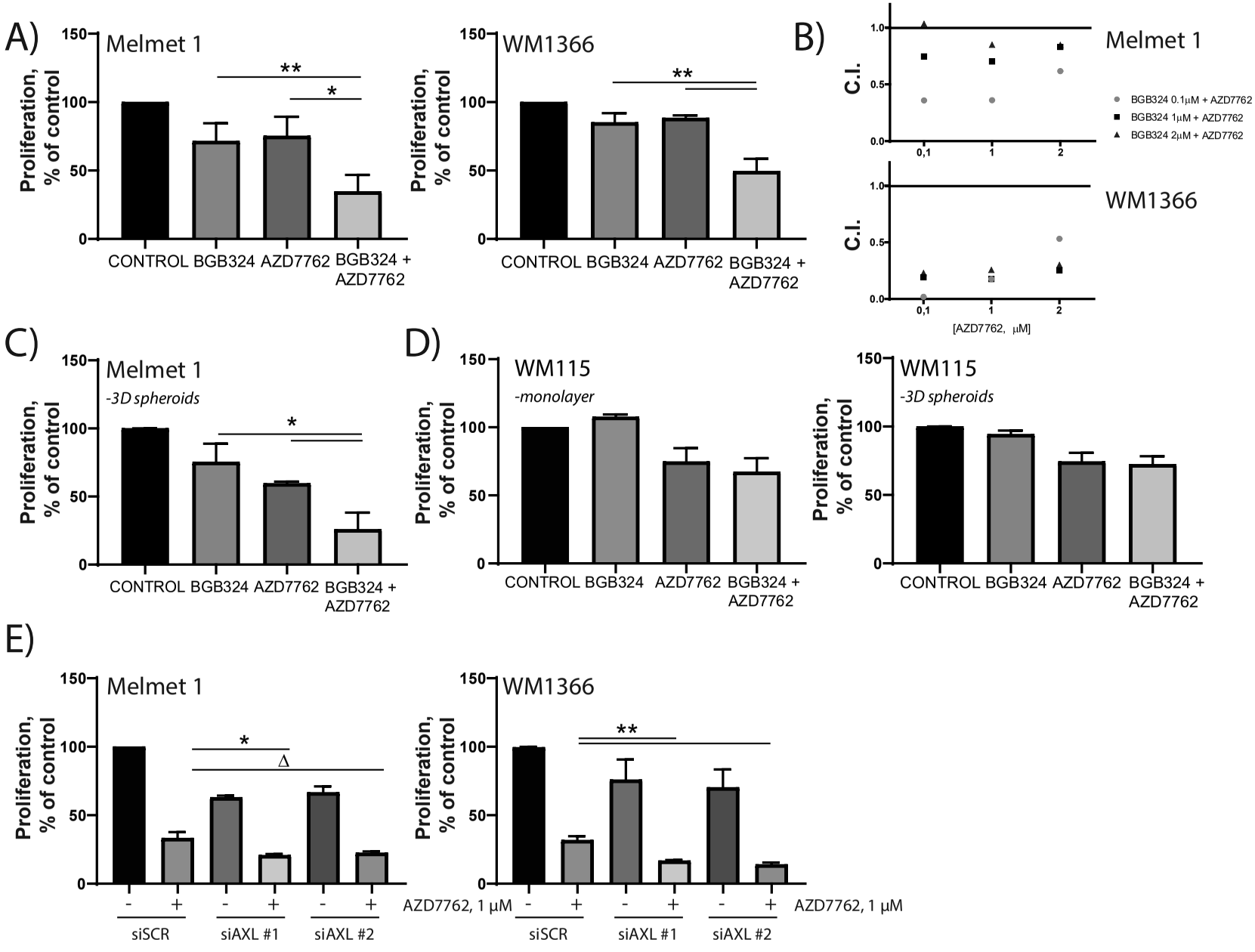
A)
Melmet 1
Proliferation, % of control
150
100
50
0
**
*
CONTROL BGB324 AZD7762 BGB324 + AZD7762
WM1366
Proliferation, % of control
**
CONTROL BGB324 AZD7762 BGB324 + AZD7762
B)
Melmet 1
C.I.
1.0
0.5
0.0
0,1
1
2
BGB324 0.1μM + AZD7762
BGB324 1μM + AZD7762
BGB324 2μM + AZD7762
WM1366
C.I.
[AZD7762, μM]
C)
Melmet 1
-3D spheroids
Proliferation, % of control
*
CONTROL BGB324 AZD7762 BGB324 + AZD7762
D)
WM115
-monolayer
Proliferation, % of control
CONTROL BGB324 AZD7762 BGB324 + AZD7762
WM115
-3D spheroids
Proliferation, % of control
CONTROL BGB324 AZD7762 BGB324 + AZD7762
E)
Melmet 1
Proliferation, % of control
*
Δ
- + - + - +
AZD7762, 1 μM
siSCR siAXL #1 siAXL #2
WM1366
Proliferation, % of control
**
- + - + - +
AZD7762, 1 μM
siSCR siAXL #1 siAXL #2

Figure 3

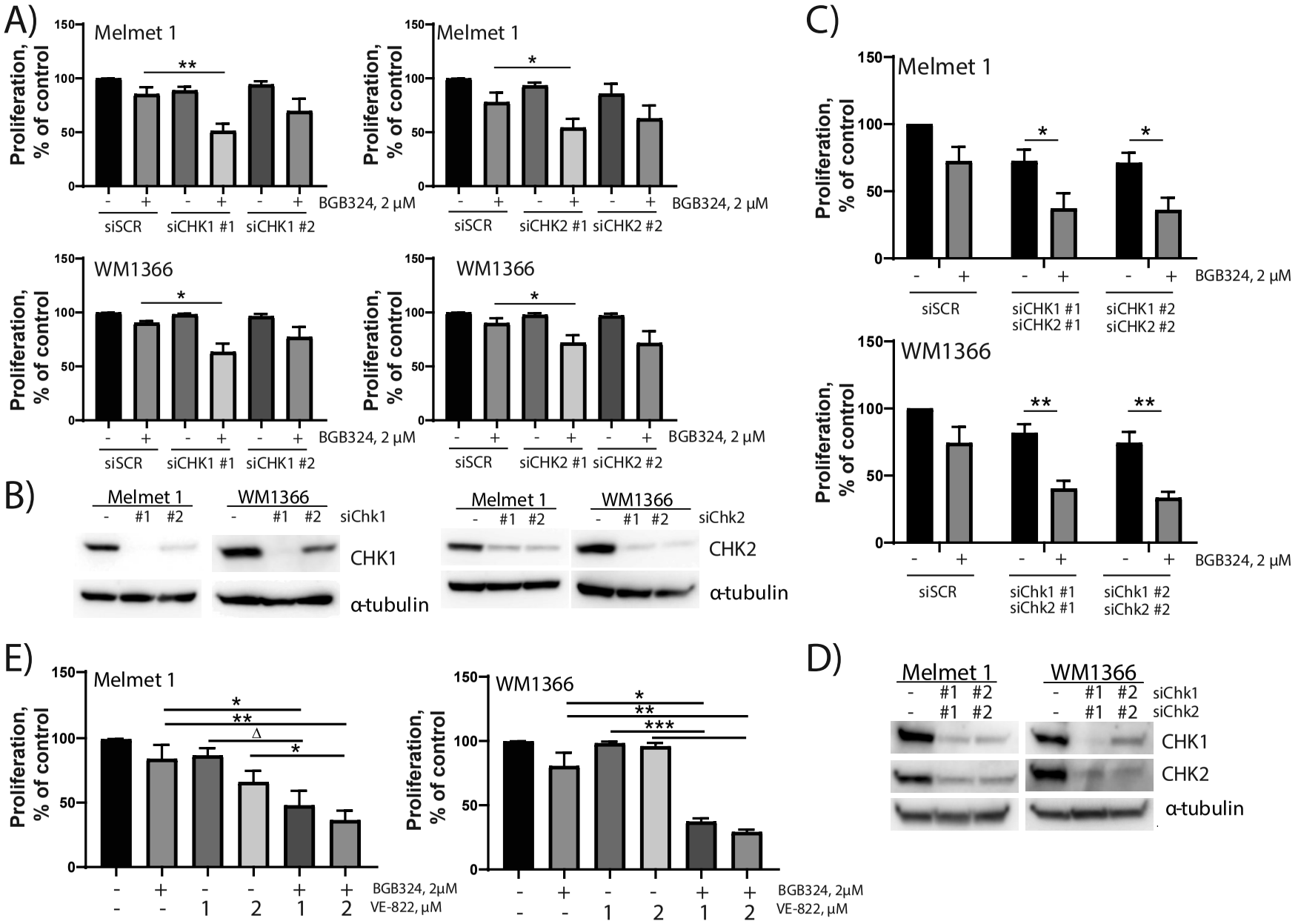
A)
Melmet 1
Proliferation, % of control
BGB324, 2 µM
siSCR
siCHK1 #1
siCHK1 #2
siCHK2 #1
siCHK2 #2
WM1366
B)
siChk1
siChk2
CHK1
CHK2
α-tubulin
C)
siCHK1 #1 siCHK2 #1
siCHK1 #2 siCHK2 #2
siChk1 #1 siChk2 #1
siChk1 #2 siChk2 #2
D)
E)
BGB324, 2µM
VE-822, µM

Figure 4

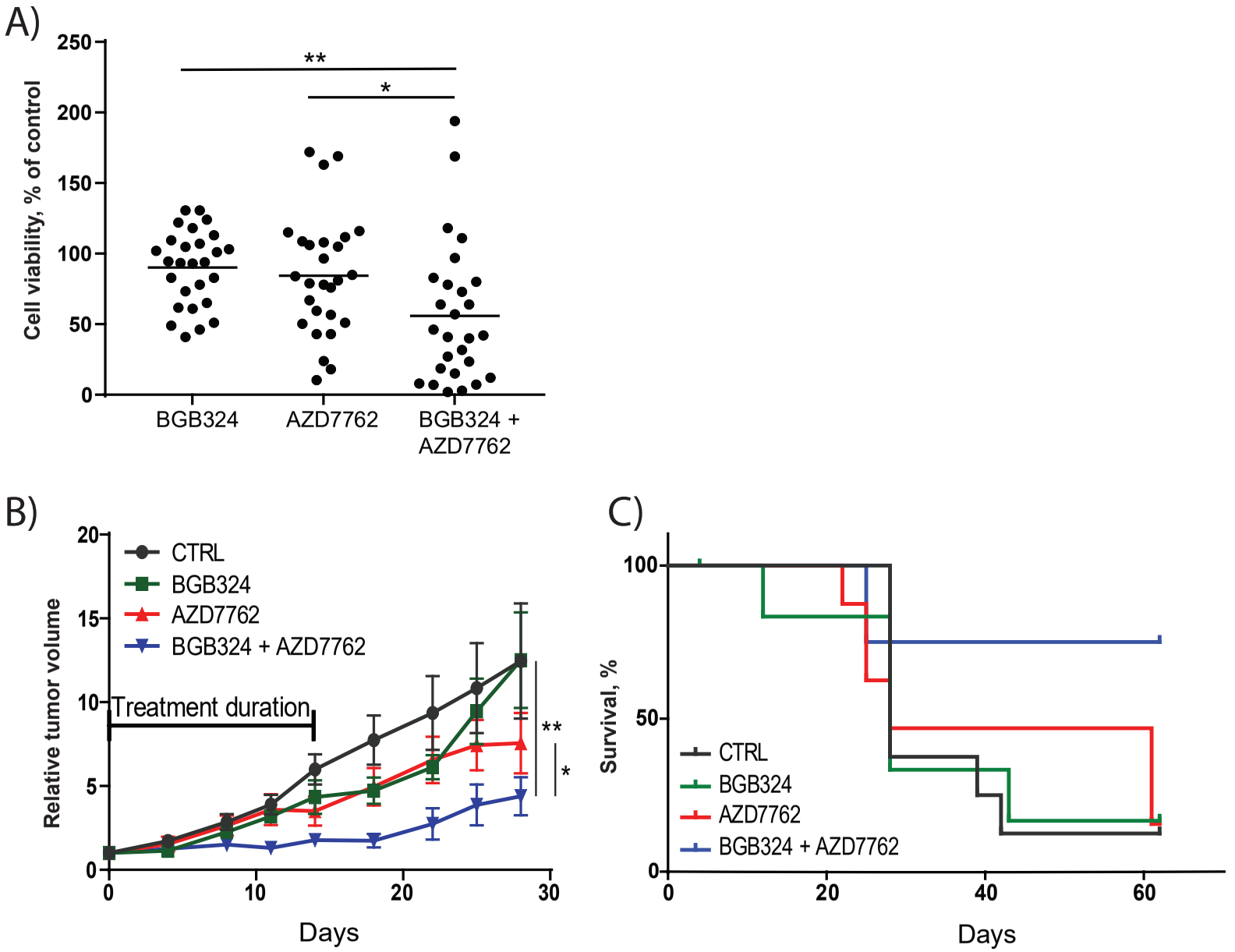
A)
Cell viability, % of control
250
200
150
100
50
0
**
*
BGB324
AZD7762
BGB324 + AZD7762
B)
Relative tumor volume
20
15
10
5
0
CTRL
BGB324
AZD7762
BGB324 + AZD7762
Treatment duration
**
*
0
10
20
30
Days
C)
Survival, %
100
50
0
CTRL
BGB324
AZD7762
BGB324 + AZD7762
0
20
40
60
Days

Figure 5

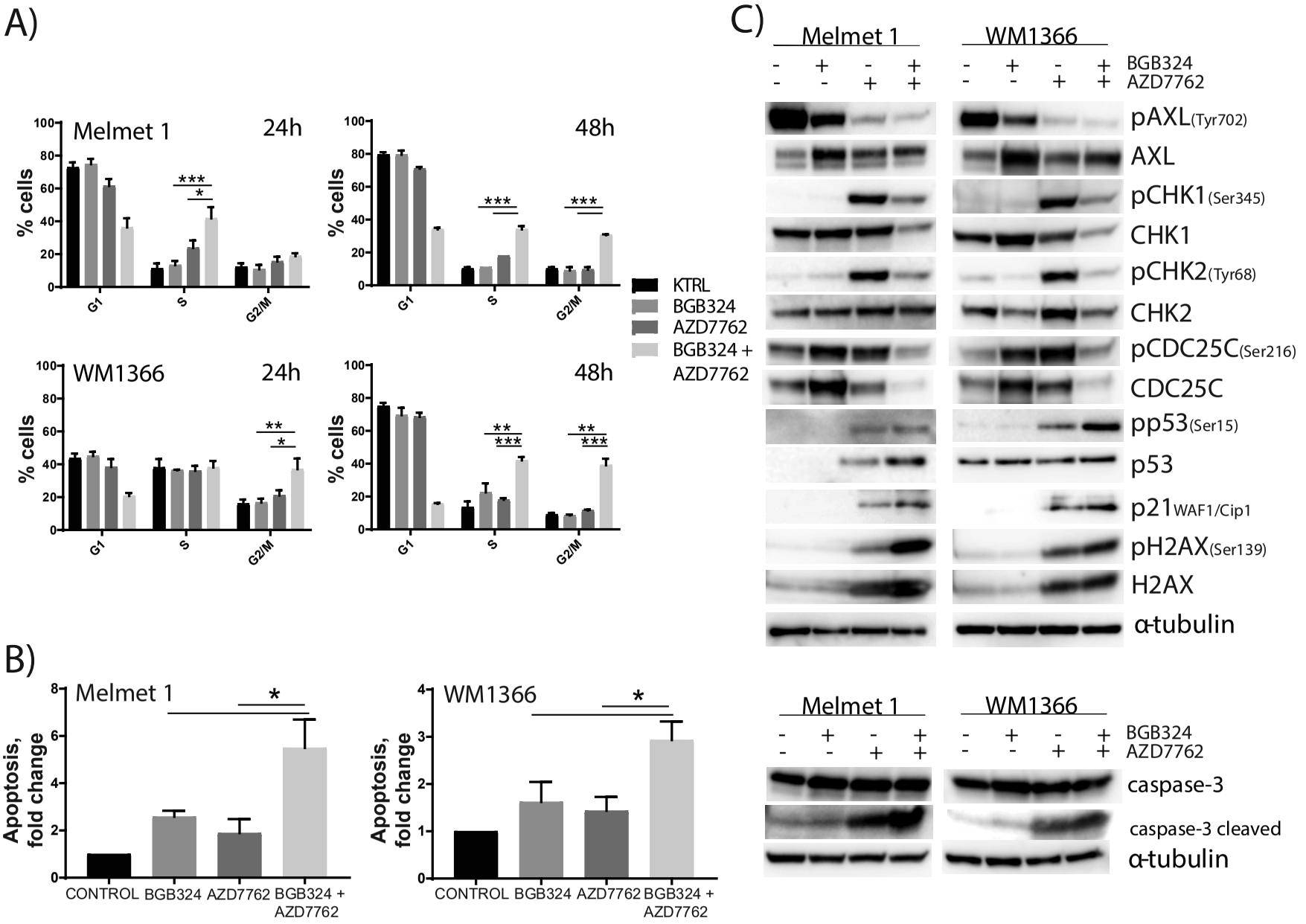
A)
Melmet 1
24h
48h
WM1366
% cells
G1
S
G2/M
KTRL
BGB324
AZD7762
BGB324 + AZD7762
B)
Apoptosis, fold change
CONTROL
BGB324
AZD7762
BGB324 + AZD7762
C)
BGB324
AZD7762
pAXL(Tyr702)
AXL
pCHK1(Ser345)
CHK1
pCHK2(Tyr68)
CHK2
pCDC25C(Ser216)
CDC25C
pp53(Ser15)
p53
p21WAF1/Cip1
pH2AX(Ser139)
H2AX
α-tubulin
caspase-3
caspase-3 cleaved

Supplementary Figure 1

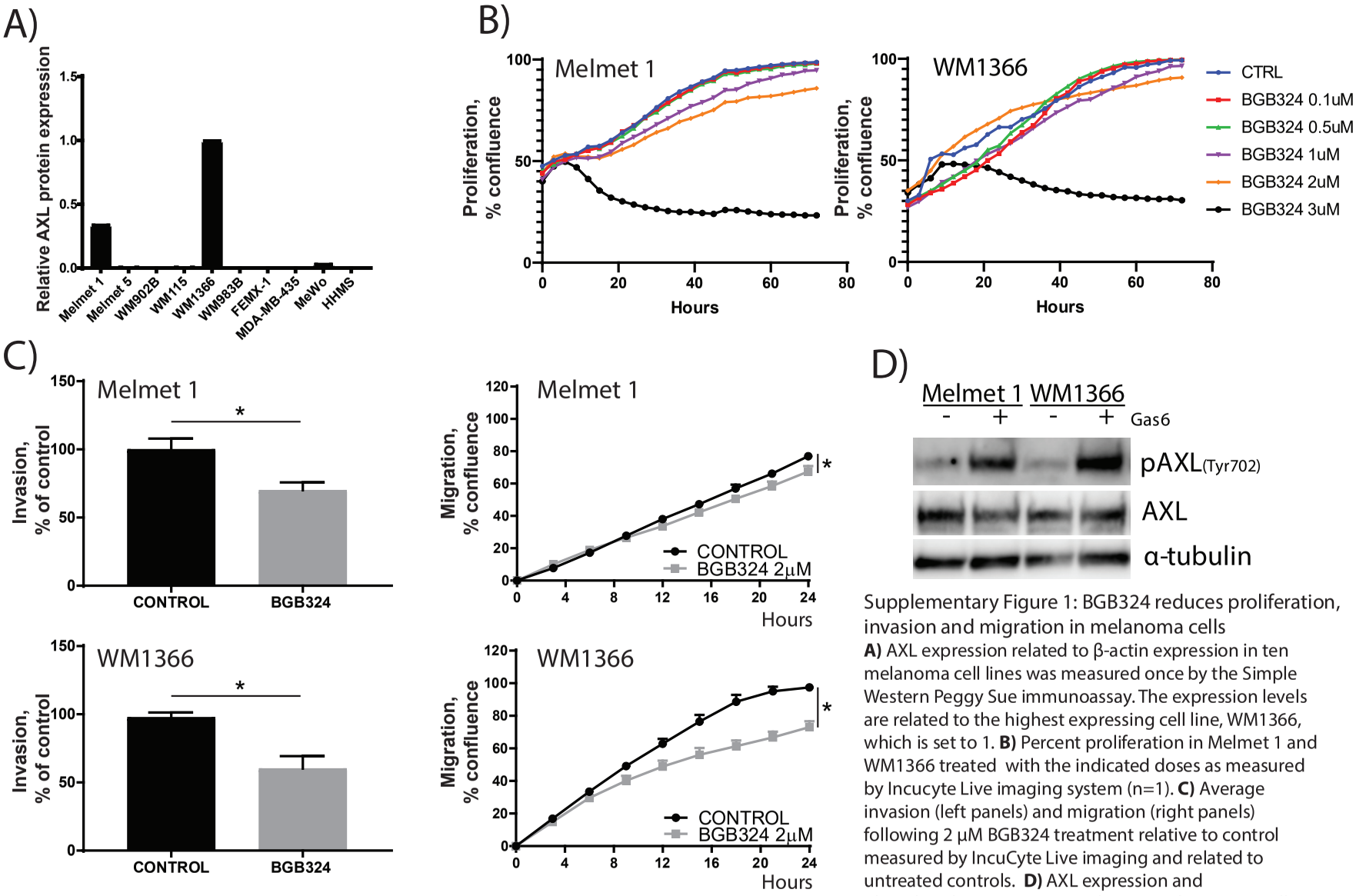

Supplementary Figure 1: BGB324 reduces proliferation, invasion and migration in melanoma cells

A) AXL expression related to β-actin expression in ten melanoma cell lines was measured once by the Simple Western Peggy Sue immunoassay. The expression levels are related to the highest expressing cell line, WM1366, which is set to 1. **B)** Percent proliferation in Melmet 1 and WM1366 treated with the indicated doses as measured by Incucyte Live imaging system (n=1). **C)** Average invasion (left panels) and migration (right panels) following 2 μM BGB324 treatment relative to control measured by IncuCyte Live imaging and related to untreated controls. **D)** AXL expression and phosphorylation status in Melmet 1 and WM1366 cells with or without the presence of GAS6 analyzed by immunoblot. α-tubulin was used as loading control and H2O was used as vehicle control for GAS6. $p<0.05$ = *.

Supplementary Figure 2

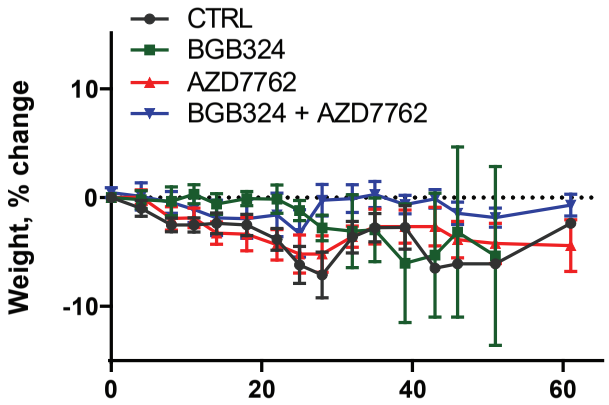

Supplementary Figure 2: In vivo treatment with BGB324 and AZD7762 was well tolerated. Percent weight change in nude mice injected with Melmet 1 cells and treated with 50 mg/kg BGB324 twice daily for two weeks and/or 25 mg/kg AZD7762 three times a week for two weeks. Controls were treated with drug vehicle(s).

Supplementary Figure 3

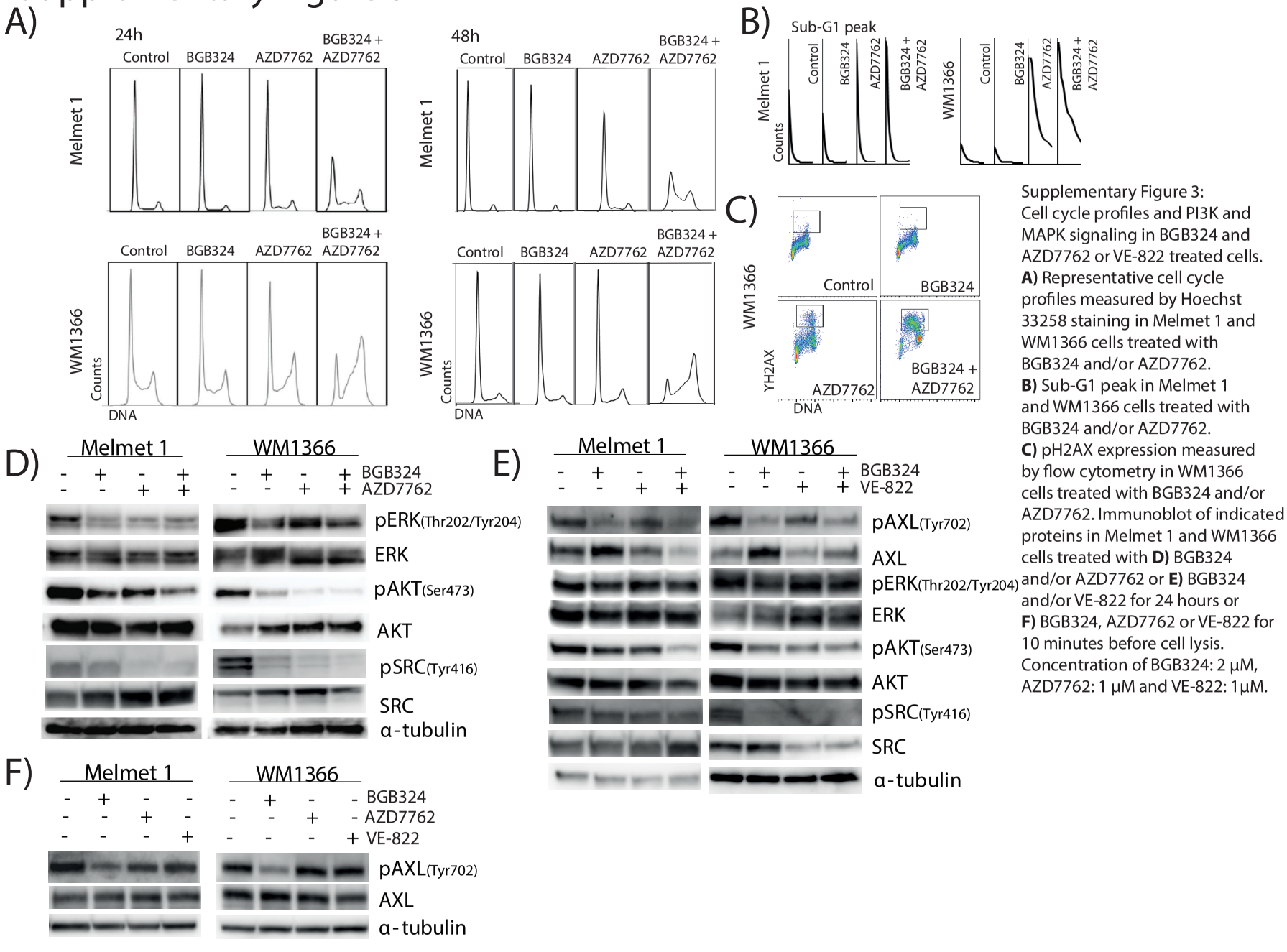

Supplementary Figure 3:
Cell cycle profiles and PI3K and MAPK signaling in BGB324 and AZD7762 or VE-822 treated cells.
A) Representative cell cycle profiles measured by Hoechst 33258 staining in Melmet 1 and WM1366 cells treated with BGB324 and/or AZD7762.
B) Sub-G1 peak in Melmet 1 and WM1366 cells treated with BGB324 and/or AZD7762.
C) pH2AX expression measured by flow cytometry in WM1366 cells treated with BGB324 and/or AZD7762. Immunoblot of indicated proteins in Melmet 1 and WM1366 cells treated with **D)** BGB324 and/or AZD7762 or **E)** BGB324 and/or VE-822 for 24 hours or
F) BGB324, AZD7762 or VE-822 for 10 minutes before cell lysis.
Concentration of BGB324: 2 µM, AZD7762: 1 µM and VE-822: 1µM.

III

Title: Soluble AXL as a marker of disease progression and survival in melanoma

Running title: Soluble AXL in melanoma

Authors: Karine Flem-Karlsen[1,2*], Marta Nyakas [2,3,4], Inger Nina Farstad [1,2], Erin McFadden[1], Patrik Wernhoff[1], Kari Dolven Jacobsen[4], Vivi Ann Flørenes[1], Gunhild Mari Mælandsmo[3,6]

[1] Department of Pathology, The Norwegian Radium Hospital, Oslo University Hospital, Oslo, Norway.

[2] Institute for Clinical Medicine, Faculty of Medicine, University of Oslo, Oslo, Norway.

[3] Department of Tumor Biology, Institute for Cancer Research, The Norwegian Radium Hospital, Oslo University Hospital, Oslo, Norway.

[4] Department of Oncology, The Norwegian Radium Hospital, Oslo University Hospital, Oslo, Norway.

[5]Institute of Medical Biology, Faculty of Health Sciences, UiT – Arctic University of Norway, Tromsø, Norway.

***Corresponding author:** Karine Flem-Karlsen, Department of Pathology, Oslo University Hospital, Oslo, Norway. P.O. Box 4950 Nydalen, 0424 Oslo. Email: kaflem@rr-research.no

Abstract:

Receptor tyrosine kinase AXL is a one-pass transmembrane protein upregulated in cancers and associated with lower survival and therapy resistance. AXL can be cleaved by the A Disintegrin and Metalloproteinases (ADAM)10 and ADAM17, yielding a soluble version of the protein. Elevated soluble AXL (sAXL) has been reported to be associated with disease progression in hepatocellular carcinoma, renal cancer, neurofibromatosis type 1 and inflammatory diseases. In the present work, we analyzed sAXL levels in blood from melanoma patients and showed that sAXL increases with disease progression. Additionally, increased sAXL levels were found correlated with shorter two-year survival in stage IV patients treated with ipilimumab. Furthermore, we showed that sAXL levels were related to the percentage of cells expressing AXL in resected melanoma lymph node metastases. This finding was verified *in vitro*, where sAXL levels in the cell media corresponded to AXL expression in the cells. AXL inhibition using the small-molecular inhibitor BGB324 reduced sAXL levels, while the cellular expression was elevated through increased protein stability. Our findings signify that quantification of sAXL blood levels is a simple and easily assessable method to determine cellular AXL levels and should be further evaluated for its use as a biomarker of disease progression and treatment response.

Introduction:

Melanoma is among the cancers with the highest increase in incidence worldwide (1). Treatment of melanoma is challenging due to high intratumoral heterogeneity and therapy resistance (2-4). Currently, immunotherapies, such as monoclonal antibodies targeting CTLA-4 and PD-1, have become first line treatment. While the response is quite favorable in a fraction of the patients, these treatments are costly and come with significant side effects and there is currently no method for identifying non-responding patients (5). Additionally, small-molecular inhibitors targeting the ERK/MAPK pathway, which comprise BRAF and MEK inhibition may be suitable for patients with BRAF mutated tumors. However, many patients become resistant, leading to disease progression (6). Thus, there is a need for biomarkers to select therapy and monitor treatment resistance and disease recurrence in melanoma patients.

Receptor tyrosine kinase AXL constitutes the TAM family together with TYRO3 and MER (7). The TAM family members share GAS6 as their ligand, although AXL has the highest binding affinity. Upon ligand binding, the receptor dimerizes and autophosphorylates, leading to activation of downstream signaling pathways such as PI3K and ERK/MAPK (8). Induced expression of AXL is observed in several cancer forms and correlates with disease progression and decreased survival (9, 10). Additionally, AXL has been implicated in treatment resistance to immunotherapy, targeted therapies and chemotherapy, where higher expression of AXL is observed in resistant compared to sensitive cells (11-15).

AXL is a one-pass transmembrane protein, with its extracellular portion consisting of two immunoglobulin-like domains and two fibronectin type III domains (16). Proteolytic cleavage of the N-terminal domain of AXL by the metallo-endopeptidases A Disintegrin and Metalloproteinases (ADAM)10 and ADAM17 (17), sheds a ~80-85 kda extracellular fraction (17, 18) known as soluble AXL (sAXL). sAXL is present in human serum and has been

demonstrated to be elevated in hepatocellular (19) and renal cell carcinoma (20). Further, we recently reported that sAXL levels were higher in patient effusions from ovarian carcinoma, malignant mesothelioma and breast cancer compared to benign reactive effusions (21). Additionally, we found that sAXL levels were elevated in effusions from high-grade versus low-grade serous ovarian carcinomas (21). On the other hand, an engineered AXL decoy receptor consisting of the extracellular domain has been found to act as a decoy by binding GAS6, resulting in decreased metastatic potential (22).

We aimed to investigate the feasibility of using sAXL in serum and plasma as a biomarker for disease progression in metastatic melanoma and examine if sAXL levels could be related to tumor burden. We showed that the level of sAXL mirrors the levels of cellular AXL in melanoma cell lines and blood samples, and that treatment with the AXL inhibitor BGB324 or ERK/MAPK inhibitors reduced the levels of sAXL in cell media. Of particular interest, increased sAXL levels in blood samples from melanoma patients were correlated with disease progression. Furthermore, we found that elevated sAXL levels in stage IV melanoma patients treated for seven weeks with ipilimumab significantly correlated with disease progression and reduced survival.

Together, our data suggest that sAXL blood levels may be exploited as an easily assessable marker to monitor cellular AXL expression and that increased levels of sAXL in late-stage patients should be further evaluated as a marker of treatment failure and disease progression.

Results:

sAXL is present in media from melanoma cell lines and the levels are reduced by AXL or MAPK inhibition

We observed sAXL in the media of four melanoma cell lines with AXL protein expression (Fig 1A and B), while no sAXL was detected in the AXL-negative cell line Melmet 369 (S1A and B Fig). The cellular protein expression of AXL reflected the amount of sAXL in the media of the respective cell line. To determine if the level of sAXL detected was expressed as a soluble isoform or contained within extracellular vesicles, we deprived media of extracellular vesicles by ultracentrifugation before measuring sAXL levels (S1C Fig). Following removal of extracellular vesicles, the levels of sAXL were reduced by ~20% indicating that the soluble isoform is the main contributor to sAXL.

Recently, AXL has been found to be cleaved by ADAM10 and ADAM17 to yield sAXL (17). In support of this, treatment with GW280264X, an inhibitor of ADAM10 and ADAM17, abolished the levels of sAXL in Melmet 1 and A375 cell media (Fig 2A) (p value = 0.0104 and 0.0001, respectively), and increased AXL cellular levels, without affecting cell proliferation (S2A and B Fig). To determine if reduced AXL activity altered the amount of sAXL, we treated Melmet 1 and A375 cells with BGB324, a small-molecular inhibitor targeting AXL (23). The results showed increased cellular expression of AXL, while sAXL levels in the media were reduced by 30-40% following BGB324 treatment (Fig 2B and C) (p value Melmet 1 = 0.006 and A375 = 0.004), without affecting proliferation (S2C Fig) The increased cellular expression of AXL was not caused by increased transcription, as no increase in AXL mRNA levels following treatment with BGB324 was observed (S2D Fig). It has been reported that BGB324 induces mRNA expression of the ADAM inhibitor TIMP1 (24). Although this implies that BGB324 may reduce ADAM10/17 activity and thereby cause

less cleavage of AXL and increased membrane expression of the protein, we did not observe increased TIMP1 protein levels upon BGB324 treatment in our cell lines (Fig 2C). Furthermore, it was recently proposed that treatment with an AXL inhibitor could increase the protein stability (25). Accordingly, we observed elevated AXL expression in cells treated with BGB324 and the protein synthesis inhibitor cyclohexemide compared to cyclohexemide alone (Fig 2D). These data showed that inhibiting AXL activity results in increased protein stability and reduced cleavage of the protein.

Reduced sAXL levels were also observed in the media of cells treated with the ERK/MAPK inhibitors vemurafenib or cobimetinib (Fig 3A and B) (p value Melmet 1 = 0.05 and 0.02 and A375 = 0.002 and 0.002, respectively), without having an effect on cell proliferation (S2C Fig). Interestingly, TIMP1 expression was reduced in vemurafenib and cobimetinib treated cells, while AXL cellular levels were unchanged (Fig 3C). This suggests that the reduced sAXL levels in vemurafenib and cobimetinib treated cells are not effectuated by increased TIMP1 expression, in contrast to previous reports (17). When treating cells with BGB324, vemurafenib and cobimetinib in combinations, no change in sAXL levels were observed between mono- and combination therapies (S3 Fig).

sAXL levels increase with disease progression and confers with cellular AXL protein expression

To examine if sAXL could be detected in blood from melanoma patients, we collected blood samples from patients at the time of lymph node resection (stage III disease) or at the start of ipilimumab treatment (stage IV disease) (n=160 and 50, respectively). sAXL was detected in all samples analyzed, with a range of 7.9 to 84.5 ng/mL. Patient characteristics are detailed in Table 1A and 1B. As seen in Fig 4A, mean sAXL expression increased from 26.6 ng/mL

(95% CI = 24.3-28.9 ng/mL) in patients at lymph node resection to 54.1 ng/mL (95% CI = 50.7-57.6 ng/mL) in patients at the start of ipilimumab treatment (p value < 0.0001), with an area under the curve of 0.9256 (S4A Fig). To evaluate whether there were differences in TIMP1 levels between stage III and IV melanoma patients, we analyzed publically available TCGA data and found no change in TIMP1 mRNA levels (S4B Fig). The level of sAXL in stage III patients was not associated with overall survival, Breslow tumor thickness, ulceration, age or gender (S4C Fig and S1 Table). To examine if the level of sAXL coincide with the protein expression of AXL in tumor cells, paraffin embedded sections from 36 lymph node metastases were stained with an AXL antibody (S5 Fig). The immunohistochemistry scores were compared with the respective sAXL levels in the patient blood samples drawn at the same time as lymph node surgery. Of these, 6 of the 36 lymph node metastases showed no AXL staining, while 21, 25 and 11 displayed staining in the membrane, cytoplasm and the nucleus, respectively. The staining localizations were combined and patients with tumors expressing high levels of AXL (expression in ≥10% cells) had a corresponding higher plasma level of sAXL (Fig 4B) (p value = 0.0231). Additionally, we observed higher sAXL levels in patients with NRAS mutation compared to NRAS wild type (Fig 4C) (p value = 0.0143), conferring with a previous report showing higher AXL cellular levels in NRAS mutated melanoma cell lines (26). The data indicate that the levels of sAXL mirror the expression of cellular AXL.

sAXL levels correlate with survival in stage IV melanoma patients treated with ipilimumab

We further analyzed the level of sAXL in serum from patients who underwent ipilimumab treatment. Blood from a total of 53 patients was harvested at three time points; before the start of treatment (baseline), at 4 weeks (second course) and at 7 weeks of treatment (third course) (Table 1B). Of the patients who started ipilimumab treatment, 25 of 50 had received previous

therapy, where dacarbazine was the most prevalent. AXL has been linked to treatment resistance (27, 28), with higher AXL levels in chemotherapy resistant cells (29). Therefore, we analyzed whether there was a change in the baseline sAXL levels in previously untreated versus treated patients. However, no difference was observed between these groups (Fig 5A).

Further, we aimed to examine if sAXL levels were associated with survival in stage IV melanoma patients treated with ipilimumab. There was no change in the expression of sAXL in serum drawn at baseline and week 4 when comparing patient survival two years after start of treatment (Fig 5B and C). Interestingly, in serum drawn from patients at week 7 of ipilimumab treatment (Fig 5D and S6 Fig), sAXL levels were increased in the patients who died within two years (71 ng/mL, 95% CI = 61.4-81.2 ng/mL) compared to those who were still alive (58.1 ng/mL, 95% CI = 51.8 ng/mL-64.4 ng/mL) (p value = 0.03). Higher sAXL levels were additionally observed in patients with more than two (69.0 ng/mL, 95% CI = 61.7-76.3 ng/mL) compared to patients with 0-2 metastases (52.6 ng/mL, 95% CI = 44.0-61.1 ng/mL) (p value = 0.023) (Fig 5E).

In this study, we found that sAXL levels mirror the levels of cellular AXL in melanoma cell lines and patient samples. Further, we showed that sAXL levels increase with disease progression, and that stage IV patients who had higher levels of sAXL at week 7 of ipilimumab treatmenthad shorter two-year survival. Together, these data demonstrated the potential of measuring sAXL in blood as a non-invasive method to monitor cellular AXL levels and showed that sAXL may be used to predict disease progression in melanoma patients.

Discussion:

In the present study, we observed that inhibition of AXL by the small-molecular inhibitor BGB324 resulted in reduced levels of sAXL, and increased the expression of the cellular protein. However, increased expression of AXL was not observed in cells treated with vemurafenib or cobimetinib, despite displaying decreased levels of sAXL. It has been previously reported that the MEK inhibitor PD325901 reduces the catalytic activity of ADAM10 and ADAM17, through increased mRNA expression of TIMP1 (17). Likewise, BGB324 in combination with an EGFR inhibitor has been shown to increase the mRNA expression of TIMP1 in glioblastoma cells (24). In contrast to this, we observed reduced TIMP1 expression in ERK/MAPK inhibited cells. Furthermore, we observed no increase in TIMP1 protein expression after BGB324 treatment, suggesting cell specific mechanisms to be responsible for the AXL cleavage in these cells. For instance, inhibition of ubiquitination and increased protein stability has been reported associated with AXL cell surface accumulation in response to AXL inhibition in breast and lung cancer cells (25). This is in accordance with our results, demonstrating increased AXL expression in cells treated with BGB324 in combination with the protein synthesis inhibitor cycloheximide.

We have previously observed that although the protein expression of AXL is increased in BGB324-treated cells, the activity is decreased compared to control cells (Flem-Karlsen, *in revision*). Thus, the membrane-bound, but kinase inactive, AXL may decrease downstream signaling by binding and sequestering its ligand GAS6. Further, the extracellular domain of AXL may activate the receptor present on other cells ligand-independently (30). Hence, treatment with AXL inhibitors may prevent excessive proliferation not only through downregulation of their respective pathways, but also by decreased activation of AXL on other cells.

The addition of an engineered extracellular domain of AXL has been shown to reduce disease progression and therapy resistance by acting as a decoy of GAS6 (22, 31). However, these studies have generated libraries of AXL mutants with a high affinity for GAS6 to act as an inhibitor of the GAS:AXL pathway. Although sAXL is found to bind GAS6 in serum and plasma, only a fraction of sAXL was bound to GAS6, indicating a surplus of AXL (32). This suggest that excess sAXL may activate membrane-bound AXL through AXL homodimerization. Furthermore, GAS6 activation of AXL has been suggested to play a less dominant role in settings where AXL is overexpressed (33), such as in cancer.

In line with a previous publication in hepatocellular carcinoma (34), we observed a positive correlation between the expression of cellular AXL and the level of sAXL in media from melanoma cell lines. These data indicate that measuring sAXL could be exploited to determine the amount of cellular AXL expressed in the tumor cells. No correlation between sAXL in serum and the mRNA expression in the respective tumor was reported in renal cancer (20). It has additionally been reported that AXL mRNA expression was similar in dendritic cell and macrophages, despite one having abundant, while the other had minimal AXL protein expression (35). This suggests a tight post-transcriptional regulation of the protein, highlighting the necessity to relate sAXL levels to the protein expression of AXL.

AXL expression has been linked to metastasis, treatment resistance and poor survival (8, 28) (36), thus monitoring the levels of AXL in patients may be a tool to determine if the patient tumors display aggressive tumor characteristics. We observed higher sAXL levels in melanoma patients at stage IV compared to stage III. Our observed result is in concordance with others, showing higher sAXL levels in later-stage hepatocellular and renal cancers (19, 20). Currently, disease relapse is monitored through CT scans, which expose the patients to radiation. sAXL levels predicted melanoma stage with good sensitivity and specificity and could be evaluated as a biomarker of disease progression which may reduce the need for CT

scans. sAXL was detected in serum and plasma from stage III and stage IV patients, respectively, meaning that the comparison between these two groups must be done with caution. However, sAXL expression in serum versus plasma from Alzheimer patients has been reported to yield significantly similar levels (37). Additionally, sAXL has been reported to show consistency across a range of parameters, such as different storage conditions, buffer types, freeze/thaw cycles and dilutions, highlighting the stability of this protein in blood (38).

There are currently no approved biomarkers of immunotherapy response in melanoma. In this study, we showed that the level of sAXL in serum samples measured after 7 weeks of treatment (third course) with ipilimumab was higher in patients who died within two years. Additionally, we showed that the levels of sAXL mirror the levels of cellular AXL. Measuring sAXL levels could thus be a measure of the amount of tumor cells that display the treatment resistant AXL^{high} phenotype, highlighting the potential to distinguish patients that have increased stage and less response to treatment. Additionally, AXL is reported to be involved in signaling which leads to immune suppression (39). Thus, the higher sAXL levels in patients with poor prognosis suggest that the patients had lower immune activation and that single-agent immune therapy might not be sufficient. In line with this, AXL inhibition in combination with PD-1 inhibitor pembrolizumab is currently in phase Ib/II clinical trial for treatment of metastatic melanoma (NCT02872259). Our data suggest that measuring sAXL levels may be an easy method to identify patients that need more aggressive treatment regimens and/or closer follow-up. Importantly, sAXL levels may be evaluated from routine blood samples and may be measured over time to monitor alterations in AXL expression. However, it may be difficult to determine treatment response on sAXL levels alone, due to somewhat overlap between the two groups in ipilimumab treated patients at seven weeks. To increase specificity and sensitivity, sAXL should be further studied in a panel together with other markers that are associated with cancer aggressiveness.

In stage III patients, no correlation was observed between sAXL levels and overall survival. In these patients, the levels of sAXL released from the tumor cells may be too low compared to the overall sAXL expression released from normal cells to be able to distinguish patients based on survival. Thus, measuring sAXL levels in combination with other markers may prove more beneficial to increase the assay sensitivity for this group of patients.

In conclusion, we observed higher sAXL levels in late-stage melanoma patients compared to patients at an earlier stage, and sAXL levels were linked to a higher number of metastases and lower survival at week 7 of treatment. Furthermore, we observed a correlation between cellular AXL expression and sAXL levels in melanoma cell lines and patient samples, suggesting that measuring sAXL may be used as an easy assessable marker to determine disease progression and aggressiveness. Thus, monitoring disease progression of both Stage III and IV melanoma patients may reduce the number of required CT scans and thereby, the amount of radiation for each patient over time.

Materials and methods:

Patient material and cell lines

Blood samples were obtained from melanoma patients treated at the Norwegian Radium Hospital, Oslo University Hospital. Samples were either drawn at the time of lymph node metastasis resections, for patients with stage III disease, or before- and at week 4 (at second course) and week 7 (at third course) for stage IV patients treated with 3 mg/kg ipilimumab. Ipilimumab was given every third week up to four courses. Patients with inflammatory diseases were excluded from receiving ipilimumab. Peripheral venous blood was drawn into Vacuette® Na-Citrate 3,2% tubes (Med-Kjemi AS, Asker, Norway) for plasma samples and Vacuette® Serum Gel tubes (Med-Kjemi AS, Asker, Norway) for serum samples. After coagulation at

room temperature, tubes were centrifuged at 2,500 g for 20 minutes for plasma and 1,500 g for 10 minutes for serum, and the samples were stored at -80°C in multiple aliquots. Metastatic lymph node melanoma specimens were obtained from stage III melanoma patients who underwent surgery at the Department of Plastic and Reconstructive Surgery, The Norwegian Radium Hospital, Oslo University Hospital between 1990 and 2016. The histologic diagnosis was based on World Health Organization criteria, and the pathologic staging was performed according to the tumor, node and metastatic classification system AJCC7. Patient material was collected in accordance with the Declaration of Helsinki with informed consent and was approved by the Norway Regional Committee for Medical and Health Research Ethics (application numbers 2014/2208, 2015/2434 and 2013/1518). NRAS and $BRAF^{V600E/K}$ mutations were determined by routine diagnostics by an in-house PCR based assay. Melanoma cell lines Melmet 1, Melmet 369, Melmet 382 and Melmet 388 were established from metastatic lesions of patients treated at the Norwegian Radium Hospital, Oslo University Hospital. A375 was obtained from American Type Culture Collection (Manassas, VA, USA). Melmet 1, A375 and Melmet 382 cells are $BRAF^{V600E}$ mutated, while Melmet 369 and Melmet 388 cells are $NRAS^{Q61}$ mutated. Extensive sequencing data of the tumors Melmet 369, Melmet 382 and Melmet 388 cell lines were generated from are available at Flørenes *et al*, Transl Oncol, 2019 (40). The cell lines were routinely checked for mycoplasma, and Melmet 1 and A375 were STR fingerprinted. Cells were grown in RPMI-1640 (Sigma Aldrich, St. Louis, MO, USA) supplemented with 5% fetal bovine serum (FBS, Sigma Aldrich, St. Louis, MO, USA) and 2 mM L-glutamine (Lonza Bioscience, Basel, Switzerland) and kept at 37°C and 5% CO_2.

Immunoblot and protein analysis

Protein lysates were lysed in a buffer comprising of 1% Triton X-100, 50mM Hepes (pH 7.4), 150mM NaCl, 1.5Mm $MgCl_2$, 1mM EGTA, 100mM NaF, 10mM Na Pyruvate, 1mM Na_3VO_4 and 10% Glycerol, with addition of 10 µL/mL protease and phosphatase inhibitor cocktails (cOmplete Mini and PhosSTOP™, Roche, Mannheim, Germany). Protein quantification was determined by Bradford analysis (Bio-Rad Laboratories AB, Sundbyberg, Sweden). 25µg protein/lane was run on SDS polyacrylamide gel electrophoresis (PAGE) before the protein was transferred to a PDVF immobilon membrane (Millipore, Bedford, MA). Membranes were blocked with 5% non-fat milk in 0.1% TBS-T (150 mM NaCl, 25 mM Tris-Cl, (pH 7.5), 0.01% Tween 20), before incubation with primary antibodies overnight at gentle agitation. Antibodies used were: AXL (#8661) and TIMP1 (D19E6, #8946) (1:1000, Cell Signaling, Boston, MA, USA), and α-tubulin (DM1A) (#05-829, 1:50.000, Millipore, Burlington, MA, USA). The following day, membranes were washed 3x10 minutes in 0.1% TBS-T, hybridized with secondary antibody (HRP-conjugated anti-rabbit or anti-mouse (Promega)) with gentle agitation for one hour at room temperature before 3x10 minutes washes in 0.1% TBS-T. Protein bands were visualized by SuperSignal™ West Dura Extended Duration Substrate (Thermo Fisher Scientific, Waltham, MA, USA) and exposed in a Syngene G Box.

Reagents

BGB324 was a kind gift from BerGenBio (Bergen, Norway). Vemurafenib and cobimetinib were purchased from Selleck Chemicals (Huston, TX, USA) and GW280264X was purchased from Aeobious Inc. (Gloucester, MA, USA). Cycloheximide solution (#C4859) was purchased from Sigma Aldrich (St. Louis, MO, USA). The inhibitors were diluted in DMSO and used at concentrations and time periods as indicated. Control groups received the same amount of DMSO as treated groups.

Cell confluence

To determine the number of cells per well, cells were plated at 15-25% confluency in 96-well or 6-well plates and left overnight before treatment with drugs (or DMSO for control cells) and 400 ng/mL GAS6 and 10 µg/mL Vitamin K for 24 hours. Percent cell confluency was determined by IncuCyte FLR or IncuCyte Zoom Kinetic Imaging System (Essen Biosciences, Ann Arbor, MI, USA).

Immunohistochemistry staining

To determine the protein expression of AXL in the melanoma lymph node metastases standard method immunohistochemistry was performed. Formalin-fixed, paraffin-embedded tissue specimens were deparaffinised with xylene and rehydrated in graded ethanol. Antigen retrieval was performed by boiling for 20 minutes at 97°C in Target Retrieval Solution buffer (pH 6,0: Dako, Glostrup, Denmark) in microwave oven. After quenching endogenous peroxidase with 3% H_2O_2 in methanol for 30 minutes, the slides where incubated over night at 4° with polyclonal antibody against AXL (#AF154, R&D Systems, Minneapolis, MN, USA) and labelled with the Envision Detection System (Dako, Glostrup, Denmark) for 1 hour at room temperature. The slides where developed with 3,3`-ddiaminobenzidine tetrahydrochloride (DAB Plus; Dako, Glostrup, Denmark) and counterstained with 10% Mayer hematoxylin, dehydrated, and mounted. AXL staining was evaluated by a pathologist (INF) blinded to patient characteristics. As no commonly accepted scoring system for *in situ* AXL expression is available, this was done semi-quantitatively with a subjective grading system for the proportion of tumor cells showing a positive reaction. In general, the pattern of AXL expression varied significantly among samples; the AXL protein could be located mostly to the cell membrane, in the cytoplasm or in nuclei, and in some samples, all expression patterns were present. The percentage of tumor cells showing membrane, cytoplasmic and/or nuclear staining was

combined and recorded as <10%, 10-40% and over 50% for each sample. For analysis, AXL expression were divided into high (≥10%) and low (<10%), which generated two equally sized groups, in line with a previous publication (41).

Enzyme-linked immunosorbent assay (ELISA)

The level of soluble AXL was quantified using Human Axl DuoSet® ELISA (Cat no. DY154, R&D Systems, Minneapolis, MN, USA) according to the manufacturer's protocol. Plasma or serum samples were diluted 1:50 in reagent diluents, while cell media was undiluted. Media was removed of cells and apoptotic vesicles by centrifugation at 2000 g for 10 minutes before freezing. Cell culture supernatants abolished of extracellular vesicles were centrifuged at 100.000 g for 70 minutes by a Type Ti70 rotor (Beckman Coulter, Brea, CA, USA). Samples were related to a sample standard of two-fold dilutions from 4000 pg/mL to 62.5 pg/mL and were measured in technical duplicates. Soluble AXL concentrations in Fig 1A were related to cell numbers counted manually by hematocytometer and presented as concentration (pg/mL)/10^6 cells to account for variations in cell numbers. The other ELISA experiments are presented as concentration (ng/mL). The ELISA samples were normalized and quantitated using a second order polynomial standard curve by GraphPad Prism version 7.0 (GraphPad Software, San Diego, CA, USA).

Statistical analysis

Values of cell-based experiments represent average of three independent experiments + standard error of the mean (SEM), if not otherwise noted. Statistical significance was determined by student two-tailed t-test using GraphPad Prism version 7.0 (GraphPad Software, San Diego, CA, USA). P-values of less than 0.05 were considered significant and marked with asterisks, where * = ≤ 0.05, ** = ≤ 0.01 and *** ≤ 0.001. Immunoblots were performed at least

twice with independent lysates. Statistical analysis of patient samples was performed applying the SPSS-PC package (Version 25) using the Mann-Whitney U test (2-tier analyses) or the Kruskal Wallis H test (>2-tier analyses). Overall survival (; OS) was calculated from the date of diagnosis to recurrence or death, respectively. Univariate survival analyses of OS were executed using the Kaplan-Meier log-rank test. sAXL levels were classified as high vs. low based on the median value.

References:

1. Karimkhani C, Green AC, Nijsten T, Weinstock MA, Dellavalle RP, Naghavi M, et al. The global burden of melanoma: results from the Global Burden of Disease Study 2015. The British journal of dermatology. 2017;177(1):134-40.
2. Grzywa TM, Paskal W, Wlodarski PK. Intratumor and Intertumor Heterogeneity in Melanoma. Transl Oncol. 2017;10(6):956-75.
3. Amaral T, Sinnberg T, Meier F, Krepler C, Levesque M, Niessner H, et al. The mitogen-activated protein kinase pathway in melanoma part I - Activation and primary resistance mechanisms to BRAF inhibition. European journal of cancer. 2017;73:85-92.
4. Zaretsky JM, Garcia-Diaz A, Shin DS, Escuin-Ordinas H, Hugo W, Hu-Lieskovan S, et al. Mutations Associated with Acquired Resistance to PD-1 Blockade in Melanoma. The New England journal of medicine. 2016;375(9):819-29.
5. Maio M, Grob JJ, Aamdal S, Bondarenko I, Robert C, Thomas L, et al. Five-year survival rates for treatment-naive patients with advanced melanoma who received ipilimumab plus dacarbazine in a phase III trial. Journal of clinical oncology : official journal of the American Society of Clinical Oncology. 2015;33(10):1191-6.
6. Long GV, Stroyakovskiy D, Gogas H, Levchenko E, de Braud F, Larkin J, et al. Combined BRAF and MEK inhibition versus BRAF inhibition alone in melanoma. The New England journal of medicine. 2014;371(20):1877-88.
7. Graham DK, DeRyckere D, Davies KD, Earp HS. The TAM family: phosphatidylserine sensing receptor tyrosine kinases gone awry in cancer. Nature reviews Cancer. 2014;14(12):769-85.
8. Scaltriti M, Elkabets M, Baselga J. Molecular Pathways: AXL, a Membrane Receptor Mediator of Resistance to Therapy. Clinical cancer research : an official journal of the American Association for Cancer Research. 2016;22(6):1313-7.
9. Hutterer M, Knyazev P, Abate A, Reschke M, Maier H, Stefanova N, et al. Axl and Growth Arrest–Specific Gene 6 Are Frequently Overexpressed in Human Gliomas and Predict Poor Prognosis in Patients with Glioblastoma Multiforme. Clinical Cancer Research. 2008;14(1):130-8.
10. Gjerdrum C, Tiron C, Hoiby T, Stefansson I, Haugen H, Sandal T, et al. Axl is an essential epithelial-to-mesenchymal transition-induced regulator of breast cancer metastasis and patient survival. Proceedings of the National Academy of Sciences of the United States of America. 2010;107(3):1124-9.
11. Zhang Z, Lee JC, Lin L, Olivas V, Au V, LaFramboise T, et al. Activation of the AXL kinase causes resistance to EGFR-targeted therapy in lung cancer. Nature genetics. 2012;44(8):852-60.

12. Hong CC, Lay JD, Huang JS, Cheng AL, Tang JL, Lin MT, et al. Receptor tyrosine kinase AXL is induced by chemotherapy drugs and overexpression of AXL confers drug resistance in acute myeloid leukemia. Cancer letters. 2008;268(2):314-24.
13. Hugo W, Zaretsky JM, Sun L, Song C, Moreno BH, Hu-Lieskovan S, et al. Genomic and Transcriptomic Features of Response to Anti-PD-1 Therapy in Metastatic Melanoma. Cell. 2016;165(1):35-44.
14. Rambow F, Rogiers A, Marin-Bejar O, Aibar S, Femel J, Dewaele M, et al. Toward Minimal Residual Disease-Directed Therapy in Melanoma. Cell. 2018;174(4):843-55 e19.
15. Muller J, Krijgsman O, Tsoi J, Robert L, Hugo W, Song C, et al. Low MITF/AXL ratio predicts early resistance to multiple targeted drugs in melanoma. Nature communications. 2014;5:5712.
16. O'Bryan JP, Frye RA, Cogswell PC, Neubauer A, Kitch B, Prokop C, et al. axl, a transforming gene isolated from primary human myeloid leukemia cells, encodes a novel receptor tyrosine kinase. Molecular and cellular biology. 1991;11(10):5016-31.
17. Miller MA, Oudin MJ, Sullivan RJ, Wang SJ, Meyer AS, Im H, et al. Reduced Proteolytic Shedding of Receptor Tyrosine Kinases Is a Post-Translational Mechanism of Kinase Inhibitor Resistance. Cancer discovery. 2016;6(4):382-99.
18. O'Bryan JP, Fridell YW, Koski R, Varnum B, Liu ET. The transforming receptor tyrosine kinase, Axl, is post-translationally regulated by proteolytic cleavage. The Journal of biological chemistry. 1995;270(2):551-7.
19. Dengler M, Staufer K, Huber H, Stauber R, Bantel H, Weiss KH, et al. Soluble Axl is an accurate biomarker of cirrhosis and hepatocellular carcinoma development: results from a large scale multicenter analysis. Oncotarget. 2017;8(28):46234-48.
20. Gustafsson A, Martuszewska D, Johansson M, Ekman C, Hafizi S, Ljungberg B, et al. Differential Expression of Axl and Gas6 in Renal Cell Carcinoma Reflecting Tumor Advancement and Survival. Clinical Cancer Research. 2009;15(14):4742-9.
21. Flem Karlsen K, McFadden E, Florenes VA, Davidson B. Soluble AXL is ubiquitously present in malignant serous effusions. Gynecologic oncology. 2018.
22. Kariolis MS, Miao YR, Jones DS, 2nd, Kapur S, Mathews, II, Giaccia AJ, et al. An engineered Axl 'decoy receptor' effectively silences the Gas6-Axl signaling axis. Nat Chem Biol. 2014;10(11):977-83.
23. Holland SJ, Pan A, Franci C, Hu Y, Chang B, Li W, et al. R428, a Selective Small Molecule Inhibitor of Axl Kinase, Blocks Tumor Spread and Prolongs Survival in Models of Metastatic Breast Cancer. Cancer research. 2010;70(4):1544-54.
24. Vouri M, Croucher DR, Kennedy SP, An Q, Pilkington GJ, Hafizi S. Axl-EGFR receptor tyrosine kinase hetero-interaction provides EGFR with access to pro-invasive signalling in cancer cells. Oncogenesis. 2016;5(10):e266.
25. Lauter M, Weber A, Torka R. Targeting of the AXL receptor tyrosine kinase by small molecule inhibitor leads to AXL cell surface accumulation by impairing the ubiquitin-dependent receptor degradation. Cell Communication and Signaling. 2019;17(1):59.
26. Sensi M, Catani M, Castellano G, Nicolini G, Alciato F, Tragni G, et al. Human cutaneous melanomas lacking MITF and melanocyte differentiation antigens express a functional Axl receptor kinase. The Journal of investigative dermatology. 2011;131(12):2448-57.
27. Schoumacher M, Burbridge M. Key Roles of AXL and MER Receptor Tyrosine Kinases in Resistance to Multiple Anticancer Therapies. Curr Oncol Rep. 2017;19(3):19.
28. Gay CM, Balaji K, Byers LA. Giving AXL the axe: targeting AXL in human malignancy. British journal of cancer. 2017;116(4):415-23.
29. Lin J-Z, Wang Z-J, De W, Zheng M, Xu W-Z, Wu H-F, et al. Targeting AXL overcomes resistance to docetaxel therapy in advanced prostate cancer. Oncotarget. 2017;8(25):41064-77.
30. Korshunov VA. Axl-dependent signalling: a clinical update. Clin Sci. 2012;122(7-8):361-8.
31. Kariolis MS, Miao YR, Diep A, Nash SE, Olcina MM, Jiang D, et al. Inhibition of the GAS6/AXL pathway augments the efficacy of chemotherapies. The Journal of clinical investigation. 2017;127(1):183-98.

32. Ekman C, Stenhoff J, Dahlback B. Gas6 is complexed to the soluble tyrosine kinase receptor Axl in human blood. J Thromb Haemost. 2010;8(4):838-44.
33. Burchert A, Attar EC, McCloskey P, Fridell YW, Liu ET. Determinants for transformation induced by the Axl receptor tyrosine kinase. Oncogene. 1998;16(24):3177-87.
34. Reichl P, Fang M, Starlinger P, Staufer K, Nenutil R, Muller P, et al. Multicenter analysis of soluble Axl reveals diagnostic value for very early stage hepatocellular carcinoma. International journal of cancer Journal international du cancer. 2015;137(2):385-94.
35. Zagorska A, Traves PG, Lew ED, Dransfield I, Lemke G. Diversification of TAM receptor tyrosine kinase function. Nature immunology. 2014;15(10):920-8.
36. Rankin EB, Giaccia AJ. The Receptor Tyrosine Kinase AXL in Cancer Progression. Cancers. 2016;8(11).
37. Huebinger R. M., Xiao G., Wilhelmsen K. C., Diaz-Arrastia R., Zhang F., O'Bryant S. E., et al. Comparison of protein concentrations in serum versus plasma from Alzheimer's patients. Advances in Alzheimer's Disease. 2012;Vol.1 No.3(2012):8.
38. Dengler M, Huber H, Muller CJ, Zellmer A, Rauch P, Mikulits W. Accurate Determination of Soluble Axl by Enzyme-Linked Immunosorbent Assay. Assay Drug Dev Technol. 2016;14(9):543-50.
39. Myers KV, Amend SR, Pienta KJ. Targeting Tyro3, Axl and MerTK (TAM receptors): implications for macrophages in the tumor microenvironment. Molecular cancer. 2019;18(1):94.
40. Florenes VA, Flem-Karlsen K, McFadden E, Bergheim IR, Nygaard V, Nygard V, et al. A Three-dimensional Ex Vivo Viability Assay Reveals a Strong Correlation Between Response to Targeted Inhibitors and Mutation Status in Melanoma Lymph Node Metastases. Transl Oncol. 2019;12(7):951-8.
41. Tanaka K, Tokunaga E, Inoue Y, Yamashita N, Saeki H, Okano S, et al. Impact of Expression of Vimentin and Axl in Breast Cancer. Clin Breast Cancer. 2016;16(6):520-6 e2.

Figure legends:

Fig 1. sAXL mirrors AXL levels in cell lines

A) Levels of sAXL as measured by ELISA in the media of melanoma cell lines Melmet 1, A375, Melmet 382 and Melmet 388 related to $1*10^6$ cells. Error bars indicate SEM (n=3) and B) Corresponding cellular AXL levels as measured by immunoblot. α-tubulin was used as loading control.

Fig 2. AXL inhibition results in reduced sAXL levels and augmented AXL expression through increased protein stability.

sAXL levels in the media of Melmet 1 and A375 cells treated with A) 3 μM ADAM10/ADAM17 inhibitor GW280264X and B) 2 μM BGB324. sAXL levels were determined by ELISA. For B, the control cells are the same as in Figure 3A and B. The

figures show average sAXL levels + SEM of three independent experiments. Immunoblot analyses showing protein expression of C) AXL and TIMP1 following treatment with 2 μM BGB324 and D) AXL following treatment with 2μM BGB324 and/or 5 μg/mL protein synthesis inhibitor cycloheximide (CHX). Cells were treated with BGB324 for 24 hours and/or CHX for indicated times before harvesting. α-tubulin was used as loading control. * = p value ≤ 0.05, ** = p value ≤ 0.01 and *** = p value ≤ 0.001 calculated using student two-tailed t-test.

Fig 3. MAPKi results in reduced sAXL without affecting AXL expression.

sAXL levels in the media of Melmet 1 and A375 cells treated with A) 1μM vemurafenib and B) 50nM cobimetinib and C) AXL and TIMP1 cellular levels in the corresponding cell lines as visualized by representative immunoblots. Cells were treated with the inhibitors for 24 hours before media or cells were harvested. sAXL levels were determined by ELISA and show average sAXL levels + SEM of three independent experiments. For A and B, the control cells are the same as in Figure 2B. α-tubulin was used as loading control for the immunoblot. * = p value ≤ 0.05 and ** = p value ≤ 0.01 calculated using student two-tailed t-test.

Fig 4. sAXL levels increases during melanoma progression and correlates with cellular AXL levels.

A) sAXL levels measured by ELISA in blood harvested from patients either at time of lymph node resection (stage III) or at the start of ipilimumab treatment (stage IV) (n= 160 and 50, respectively). Error bars represent mean ± 95% confidence interval (CI). B) sAXL levels in 36 plasma samples related to immunohistochemical (IHC) staining of AXL in the respective lymph node metastases. Percent IHC staining expression was divided into two similar sized groups of <10% and ≥10% AXL staining (n= 17 and 19, respectively). C) sAXL levels in plasma drawn from stage III patients at lymph node resection related to NRAS mutation

status. B) and C) are displayed as box and whiskers plot ± range. sAXL levels were determined by ELISA from plasma samples run in technical duplicates, where each point represents one patient. * = p value ≤ 0.05 and *** = p value ≤ 0.001.

Fig 5. sAXL levels are increased in patients with shorter two-year survival after seven weeks of ipilimumab treatment.

A) sAXL levels measured by ELISA in plasma samples in previously treated versus untreated patients at the start of ipilimumab treatment. sAXL levels in serum samples from stage IV patient harvested B) before the start, C) at week 4 or D) at week 7 of ipilimumab treatment grouped according to survival after two years. E) sAXL levels in serum harvested at week 7 of ipilimumab treatment related to number of metastases. sAXL levels were determined by ELISA and run in technical duplicates. The figures are displayed as box and whiskers plot ± range, where each point represents one patient. * = p value ≤ 0.05.

Fig 1

A)

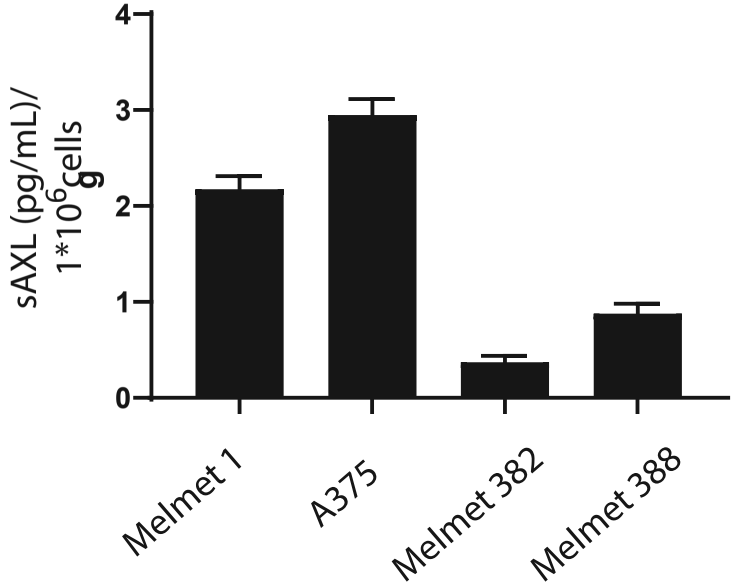
sAXL (pg/mL)/
1*10^6cells
4
3
2
1
0
Melmet 1
A375
Melmet 382
Melmet 388

B)

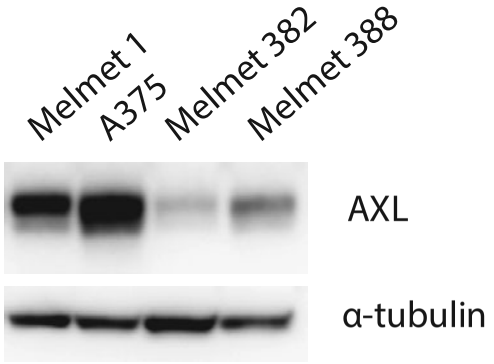
Melmet 1
A375
Melmet 382
Melmet 388
AXL
α-tubulin

Fig 2

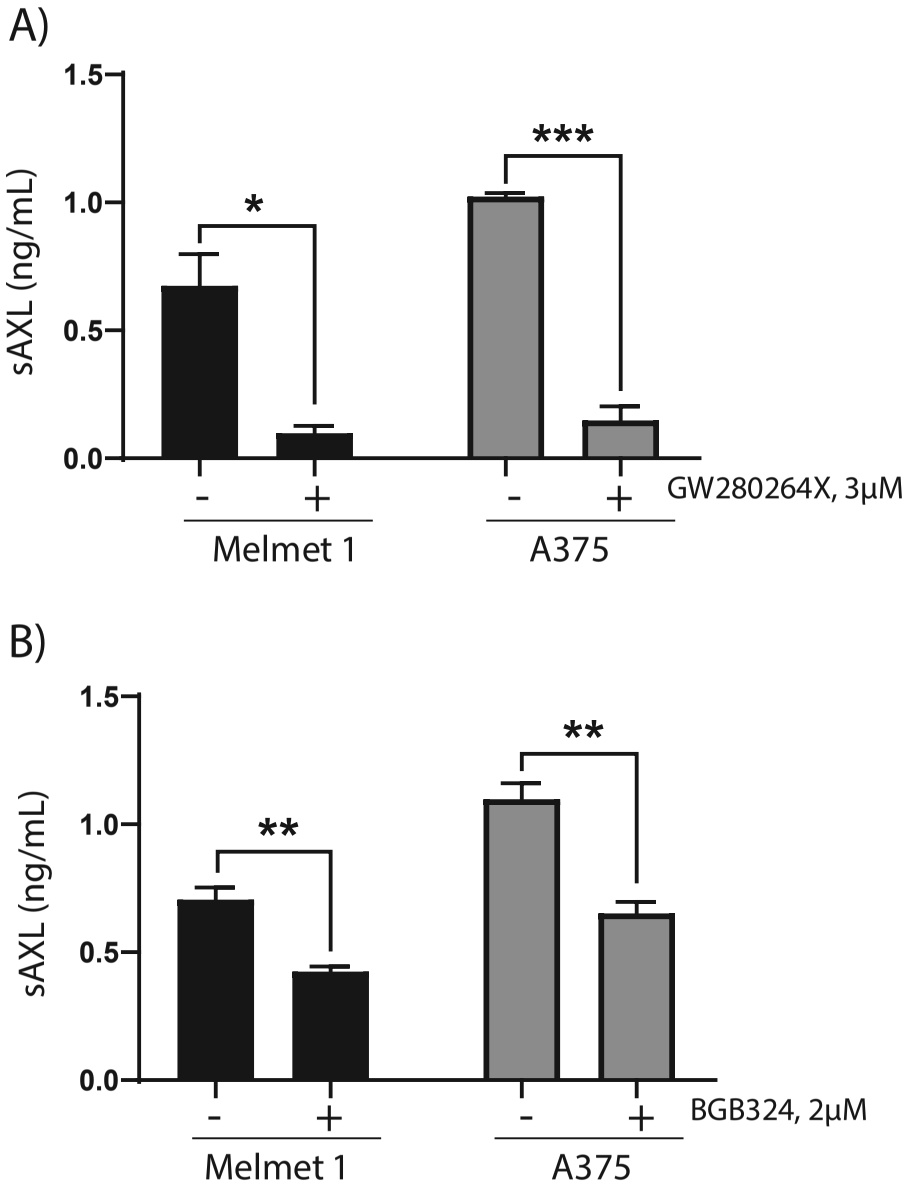
A)
sAXL (ng/mL)
1.5
1.0
0.5
0.0
*
***
- + - +
GW280264X, 3μM
Melmet 1
A375
B)
sAXL (ng/mL)
1.5
1.0
0.5
0.0
**
**
- + - +
BGB324, 2μM
Melmet 1
A375

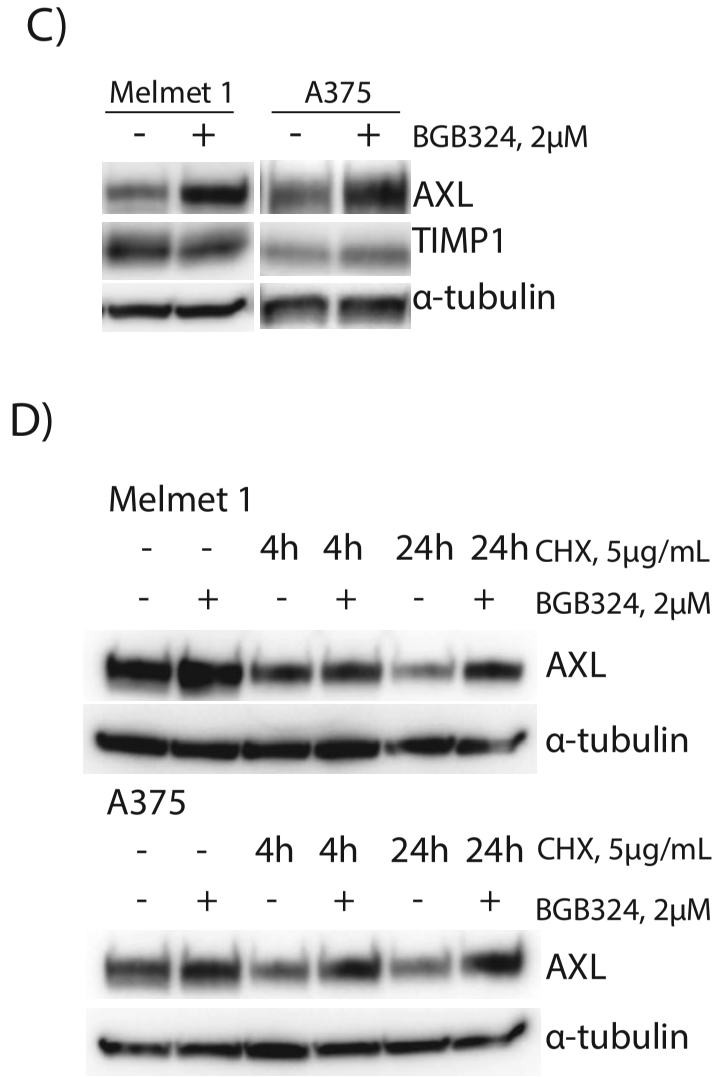
C)
Melmet 1
A375
- + - +
BGB324, 2μM
AXL
TIMP1
α-tubulin
D)
Melmet 1
- - 4h 4h 24h 24h CHX, 5μg/mL
- + - + - + BGB324, 2μM
AXL
α-tubulin
A375
- - 4h 4h 24h 24h CHX, 5μg/mL
- + - + - + BGB324, 2μM
AXL
α-tubulin

Fig 3

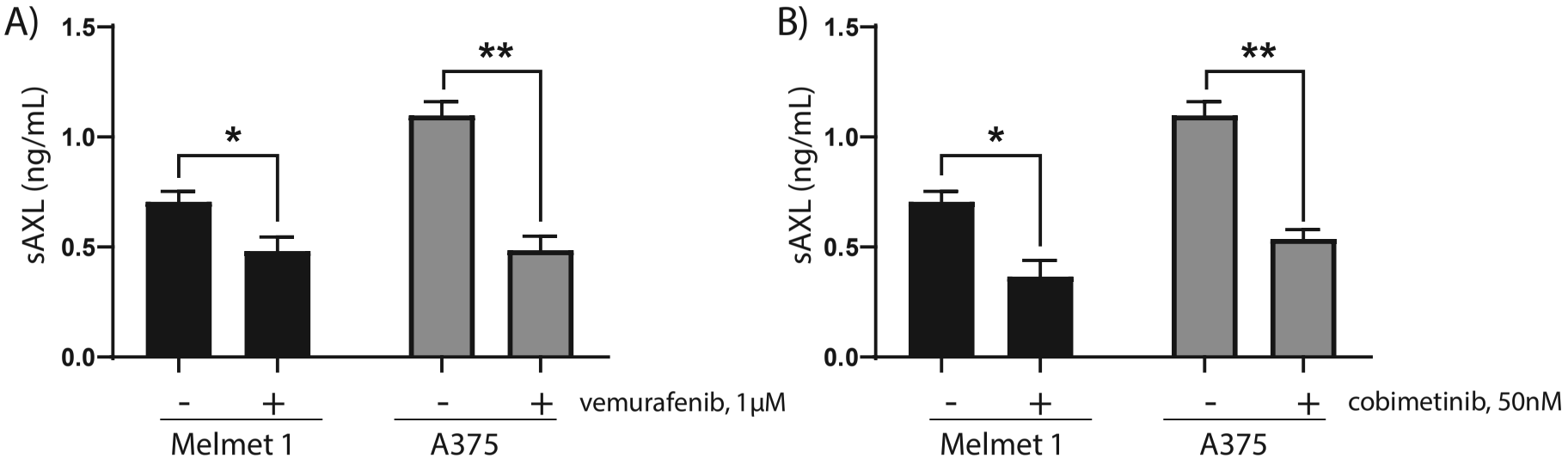
A)
sAXL (ng/mL)
1.5
1.0
0.5
0.0
*
**
- + - +
vemurafenib, 1μM
Melmet 1
A375
B)
sAXL (ng/mL)
1.5
1.0
0.5
0.0
*
**
- + - +
cobimetinib, 50nM
Melmet 1
A375

C)

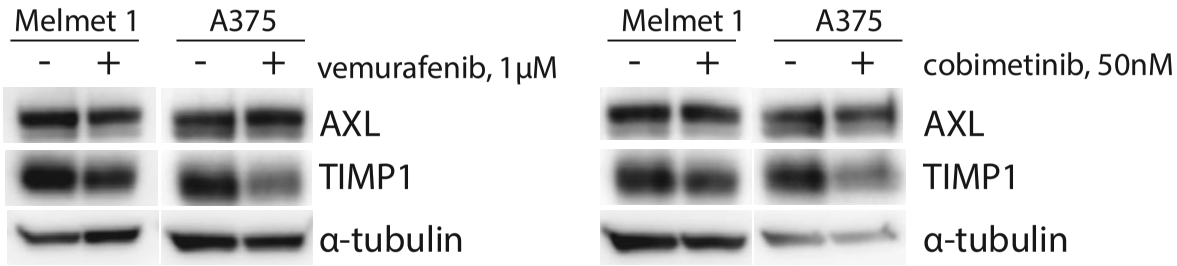
Melmet 1
A375
- + - +
vemurafenib, 1μM
AXL
TIMP1
α-tubulin
Melmet 1
A375
- + - +
cobimetinib, 50nM
AXL
TIMP1
α-tubulin

Fig 4

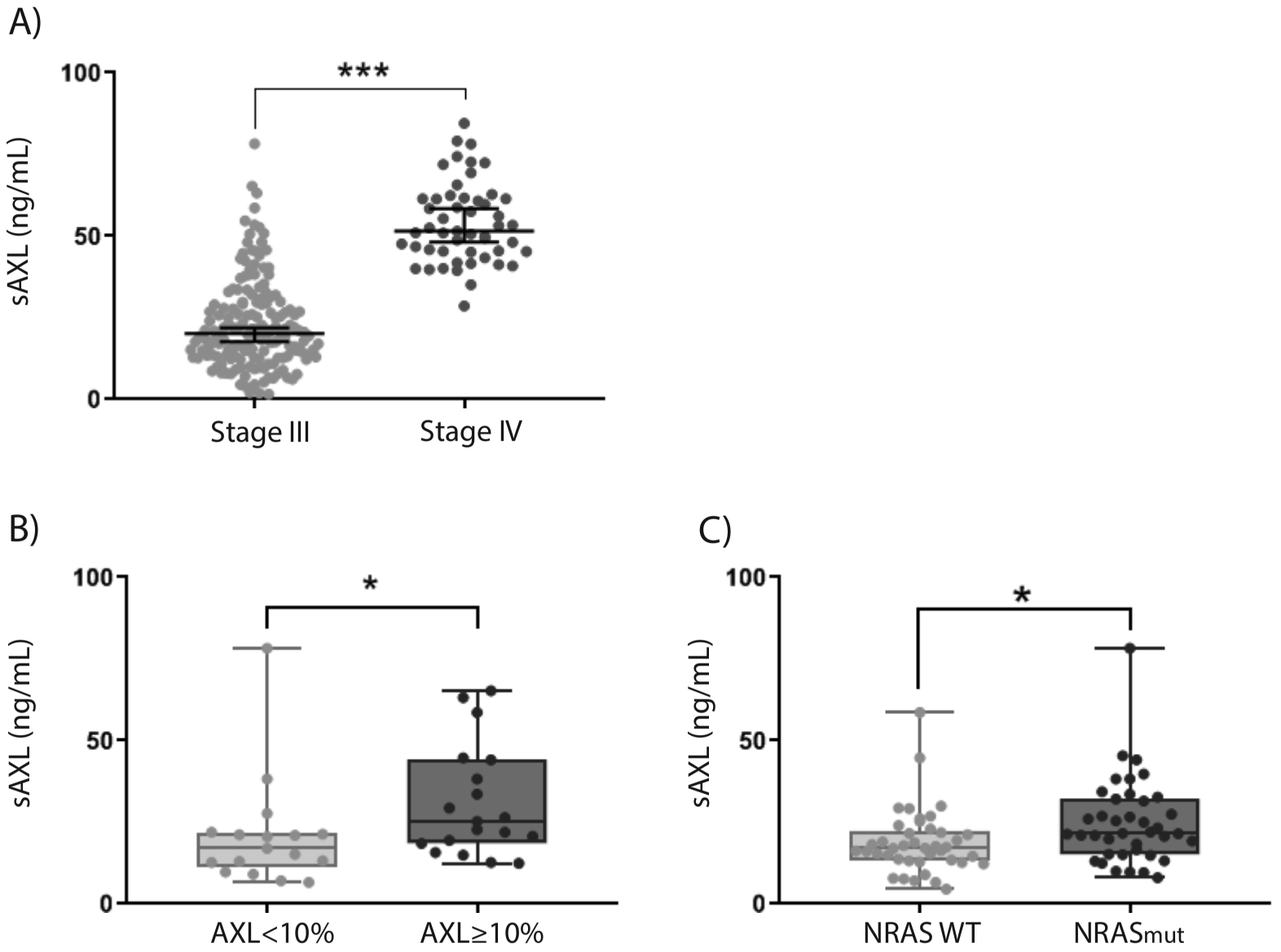
A)
***
100
50
0
sAXL (ng/mL)
Stage III
Stage IV
B)
*
100
50
0
sAXL (ng/mL)
AXL<10%
AXL≥10%
C)
*
100
50
0
sAXL (ng/mL)
NRAS WT
NRASmut

Fig 5

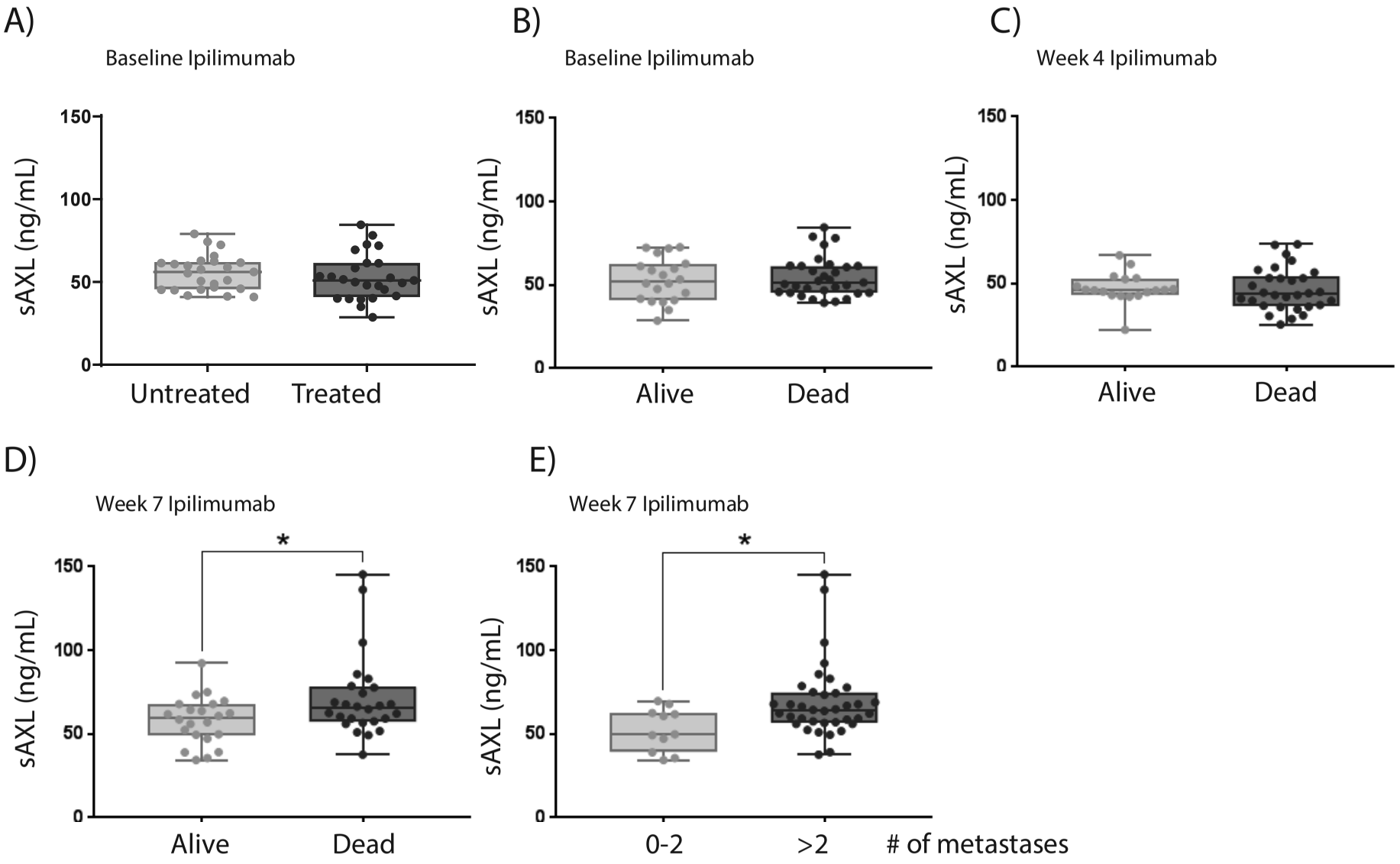
A)
Baseline Ipilimumab
sAXL (ng/mL)
150
100
50
0
Untreated
Treated
B)
Baseline Ipilimumab
sAXL (ng/mL)
150
100
50
0
Alive
Dead
C)
Week 4 Ipilimumab
sAXL (ng/mL)
150
100
50
0
Alive
Dead
D)
Week 7 Ipilimumab
*
sAXL (ng/mL)
150
100
50
0
Alive
Dead
E)
Week 7 Ipilimumab
*
sAXL (ng/mL)
150
100
50
0
0-2
>2
# of metastases

Table 1A. Patient characteristics of the study population stage III disease

		N (%)*
N		160
Gender		
	Male	104 (65.0)
	Female	56 (35.0)
Age, median (range)		65 (25-94)
Melanoma type		
	Superficial spreading	43 (26.9)
	Nodular	42 (26.3)
	Other (acral, desmoplastic)	8 (5.0)
	Unknown	67 (41.9)
Breslow, mm (range)		2.5 (0.4-25)
Ulceration		41 (49.4)**
Mitotic index, pr mm2 (range)		4 (0-37)
BRAF V600 mutation		
	Yes	77 (48.1)
	No	76 (47.5)
	Unknown	7 (4.4)

*Data are shown as number of patients (%) unless otherwise indicated.

** Percentage calculated from known answers.

Table 1B. Clinical characteristics of the study population stage IV disease according to survival

		Survival 2 years (%)	
Total N=53*		Alive	Dead
		22 (41.5)	31 (58.5)
Gender			
	Male	11 (20.8)	21 (39.6)
	Female	11 (20.8)	10 (18.9)
Age, median (range)		60 (27-83)	67 (38-84)
M stage			
	M1a/b	9 (17.0)	4 (7.5)
	M1c	13 (24.5)	27 (50.9)*
Organs involved			
	≤2	15 (28.3)	12 (22.6)
	>2	7 (13.2)	19 (35.8)
BRAF V600 mutation			
	Yes	12 (22.6)	13 (24.5)
	No	7 (13.2)	16 (30.2)
	Unknown	2 (3.8)	3 (5.7)
LDH levels			
	Normal	19 (35.8)	13 (24.5)
	>ULN†	3 (5.7)	18 (34.0)**
Number of other treatments before inclusion			
	0	10 (18.9)	17 (32.1)
	1	9 (17.0)	12 (22.6)
	2	2 (3.8)	1 (1.9)
	3	1 (1.9)	1 (1.9)
Cardiovascular disease			
	No	20 (38)	27 (51)
	Yes	2 (3,5)	4 (7.5)

*Number of patients at baseline = 50, week 4 = 50 and week 7 = 48. Total number of patients accumulates to 53 due to lacking blood samples of six patients at all three time points.

Data are shown as number of patients (%) unless otherwise indicated, †ULN upper limit of normal, *p<0.05, **p<0.01 vs. survivors.

Supplementary Methods:

mRNA expression from TCGA data:

The mRNA expression profiles for TIMP1 and AXL gene were analyzed and compared for stage III and stage IV melanoma using Skin Cutaneous Melanoma data (SKCM) from The Cancer Genome Atlas (TCGA Research Network: https://www.cancer.gov/tcga). SKCM raw count data (n=470) was downloaded from recount2: analysis-ready RNA-seq gene and exon counts datasets (1) and Bioconductor package recount (2). TCGA clinical data, including the melanoma stage III and stage IV information, was retrieved from NIH, National Cancer Institute, GDC Data portal (3). Prior analyze, count data was normalized by log2 transformation (log2 + 1). The mRNA expression profiles in stage III and stage IV were visualized in boxplots (4) and statistically analyzed using Wilcoxon signed-rank test in R (5).

Quantitative real-time PCR:

cDNA was purified by QIAquick PCR Purification Kit (Qiagen) following the manufacturer's instructions. qPCR reaction was run in duplicates using 8.8 ng cDNA, 300 nM primer, 200 nM FAM490 labeled probe (Roche) and 1x PerfeCTa q-PCR SuperMix (Quanta BioSciences). Bio-Rad CFX Connect™ Real Time PCR machine (Bio-Rad) was used to perform the PCR and data was analyzed by the Bio-Rad CFX Manager software. AXL mRNA levels were related to housekeeping gene YARS.

References:

1. Collado-Torres L, Nellore A, Kammers K, Ellis SE, Taub MA, Hansen KD, et al. Reproducible RNA-seq analysis using recount2. Nature biotechnology. 2017;35(4):319-21.
2. Collado-Torres L, Nellore A, Jaffe AE. recount workflow: Accessing over 70,000 human RNA-seq samples with Bioconductor. F1000Res. 2017;6:1558.

3. Grossman RL, Heath AP, Ferretti V, Varmus HE, Lowy DR, Kibbe WA, et al. Toward a Shared Vision for Cancer Genomic Data. The New England journal of medicine. 2016;375(12):1109-12.
4. Wickham H. ggplot2: Elegant Graphics for Data Analysis: Springer International Publishing; 2016.
5. R Core Team. R: A language and environment for statistical computing. R Foundation for Statistical Computing, Vienna, Austria Available online at https://wwwR-projectorg/. 2018.

Supplementary figure legends:

S1 Fig. sAXL levels mirror AXL cellular levels and is not primarily contained within extracellular vesicles.

A) sAXL levels in the media of Melmet 369, Melmet 382 and Melmet 388 +SEM, and **B)** the corresponding AXL protein expression measured by immunoblot (N=2). GAPDH was used as loading control. **C)** AXL levels in the media of Melmet 1 and A375 cells with or without depletion of extracellular vesicles by ultracentrifugation + SEM (n=3). sAXL levels were measured by ELISA.

S2 Fig. Treatments does not alter proliferation or mRNA expression in melanoma cells.

A) Proliferation measured by Incucyte and **B)** Representative immunoblot of AXL protein expression of Melmet 1 and A375 cells treated with 3μM ADAM10/17 inhibitor GW280264X. α-tubulin was used as loading control for the immunoblot. B) Proliferation in Melmet 1 (top panel) and A375 (bottom panel) cells treated with 2 μM BGB324, 1 μM vemurafenib or 50 nM cobimetinib. Proliferation is measured by the Incucyte imaging system. C) Relative mRNA levels of AXL in Melmet 1 and A375 cells treated with 2μM AXL inhibitor BGB324. The data shows average values related to untreated control cells + SEM of three independent experiments. Cells were treated with the inhibitors for 24 hours before they were harvested.

S3 Fig. Combinations of BGB324, vemurafenib and cobimetinib does not alter sAXL expression compared to monotherapies

sAXL levels in Melmet 1 (left panel) and A375 (right panel) cells treated with 2 μM BGB324, 1 μM vemurafenib and/or 50 nM cobimetinib for 24 hours. Control cells and monotreatment of BGB324, vemurafenib and cobimetinib are the same as the ones presented in Figures 2B, 3A and 3B. sAXL levels were determined by ELISA and show average values + SEM of three independent experiments.

S4 Fig. sAXL levels increase with disease progression.

A) Area under the curve (AUC) comparison between the levels of sAXL in patients at the start of ipilimumab treatment and at the time of lymph node resection. **B)** TIMP1 mRNA expression in stage III and IV melanomas from publically available TCGA data. **C)** Kaplan Meier plot of sAXL levels in blood divided in sAXL low (n=80 and high (n=80) from patients with stage III melanoma correlated with overall survival.

S5 Fig. Immunohistochemistry staining of AXL.

IHC staining showing examples of <10%, 10-50% and >50% AXL positive tumor cells in sections from stage III melanoma patients. <10%: Some cells in the lymph node metastasis (middle and right part of the picture) show faint cytoplasmic or nuclear staining. Stronger staining is seen in endothelial cells of lymphatic vessels (orig. magnif. X200). 10-50%: More cells in the metastasis (left part) show stronger staining, mainly cytoplasmic (orig. magnif. x100). >50%: More than half the cells in the metastatic node show relatively strong cytoplasmic and membrane staining (orig. magnify. X100).

S6 Fig. sAXL levels are increased in patients with shorter two-year survival.

AUC comparison between the levels of sAXL in patients who were alive or dead two years after ipilimumab treatment

S1 Fig

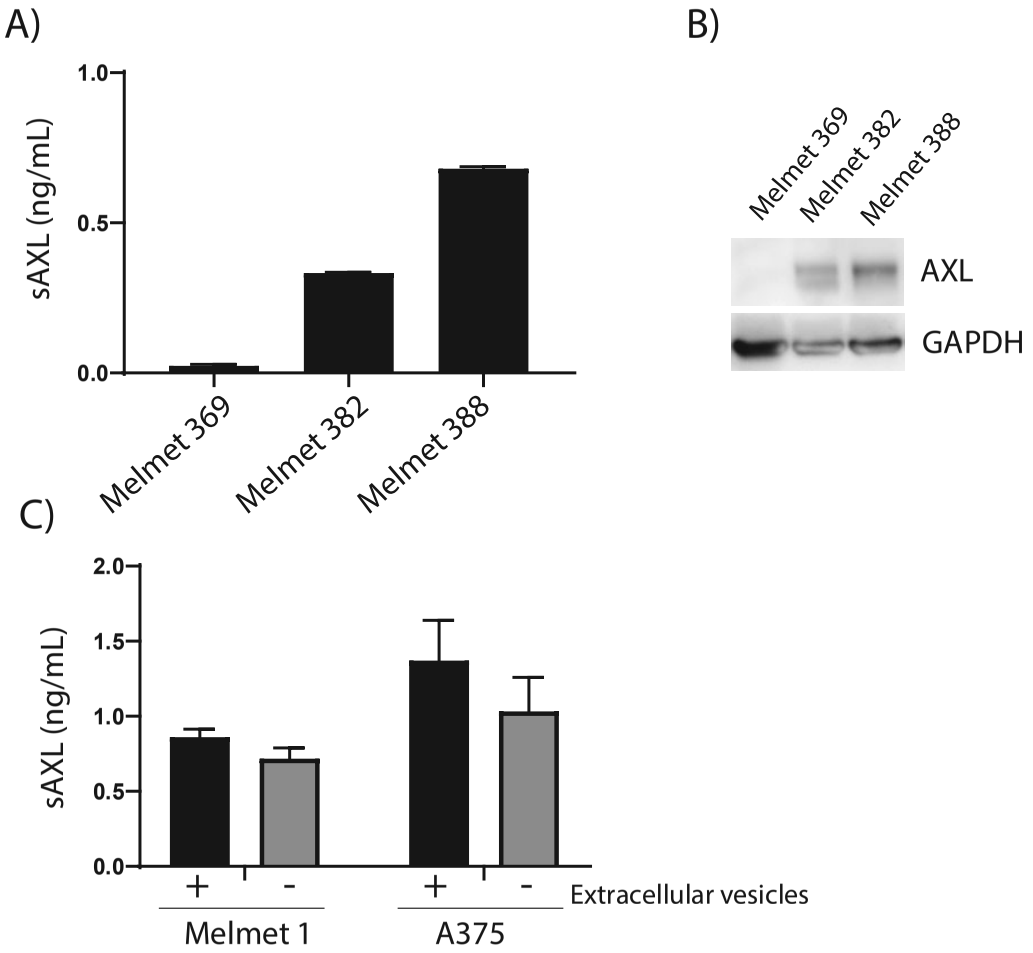
A)
1.0
0.5
0.0
sAXL (ng/mL)
Melmet 369
Melmet 382
Melmet 388
B)
Melmet 369
Melmet 382
Melmet 388
AXL
GAPDH
C)
2.0
1.5
1.0
0.5
0.0
sAXL (ng/mL)
+
-
+
-
Extracellular vesicles
Melmet 1
A375

S2 Fig

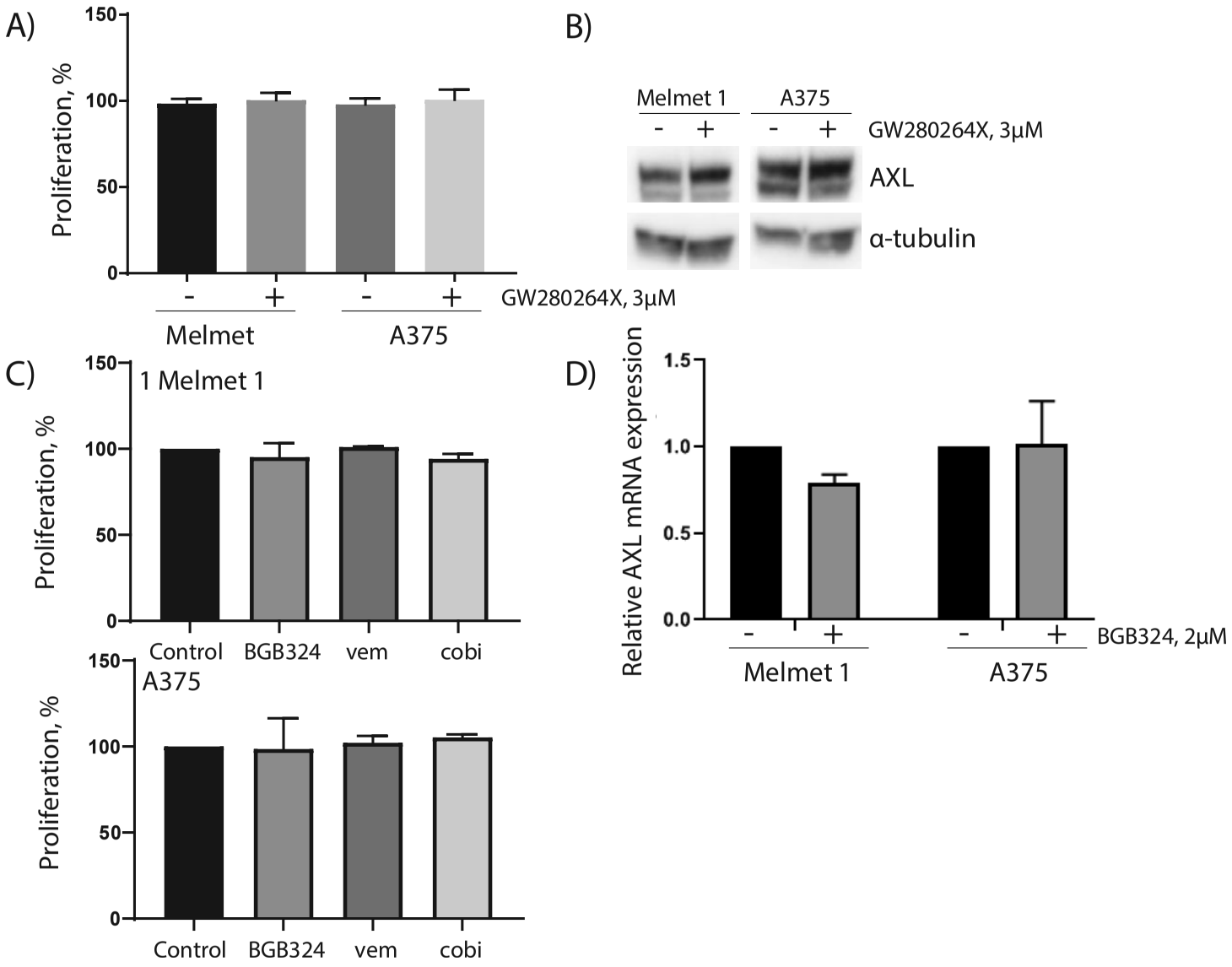
A)
Proliferation, %
150
100
50
0
- + - +
GW280264X, 3μM
Melmet
A375
B)
Melmet 1
A375
- + - +
GW280264X, 3μM
AXL
α-tubulin
C)
1 Melmet 1
Proliferation, %
Control
BGB324
vem
cobi
A375
D)
Relative AXL mRNA expression
1.5
1.0
0.5
0.0
BGB324, 2μM
Melmet 1
A375

S3 Fig

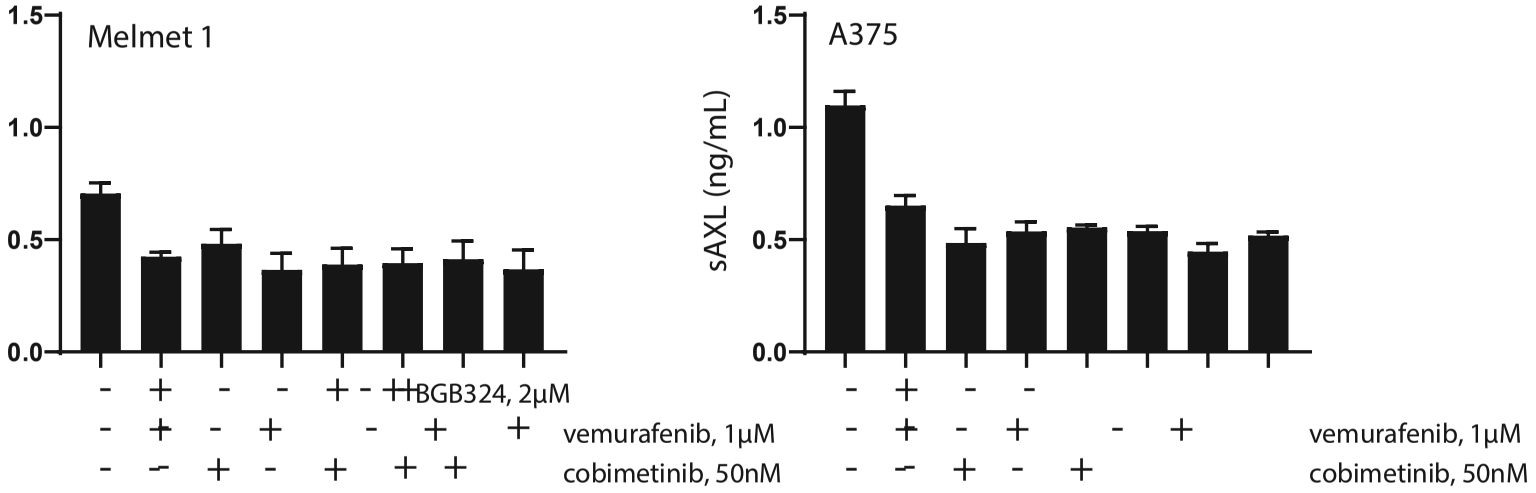
Melmet 1
A375
sAXL (ng/mL)
1.5
1.0
0.5
0.0
BGB324, 2μM
vemurafenib, 1μM
cobimetinib, 50nM

S4 Fig

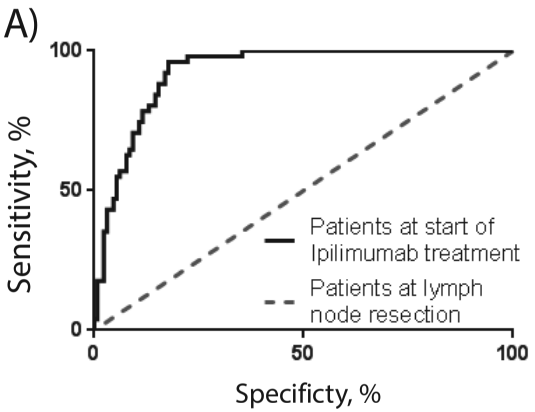

AUC = 0.9256
p < 0.0001

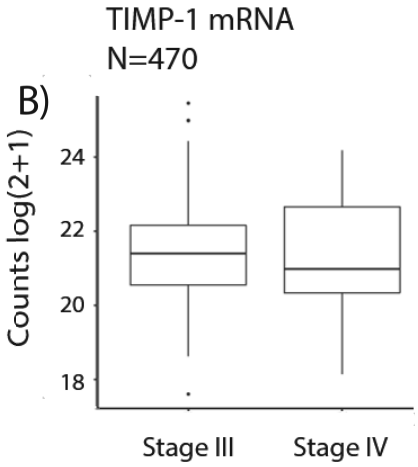

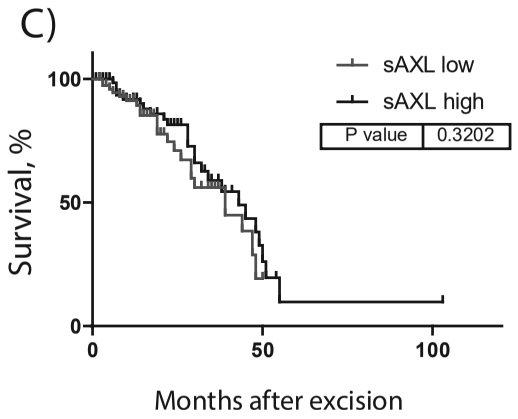

S5 Fig AXL

expressio

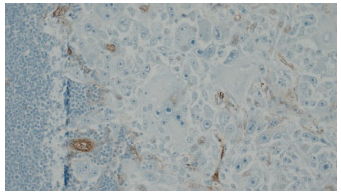

<10%

10-50%

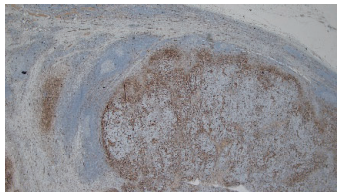

>50%

S6 Fig

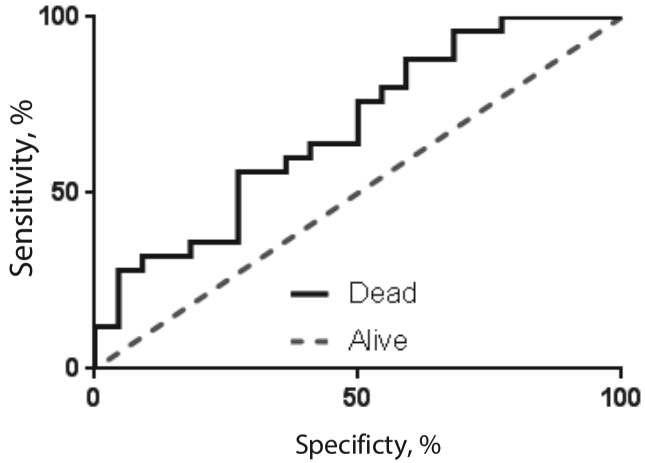

AUC = 0.6818
p = 0.0330

S1 Table

S1 Table. Patient parameters grouped by median sAXL value

		AXL low (n=80)	AXL high (n=80)	p value
Ulceration, count				0.993
	Yes	21	20	
	No	21	21	
	Uknown	38	39	
Gender, count				0.655
	Male	51	53	
	Female	29	27	
Age, median (range)		65 (31-94)	65 (25-93)	0.813
Breslow, mm (range)		2.85 (0.4-9)	4.3 (0.4-25)	0.09

IV

SCIENTIFIC REPORTS

OPEN

p38 MAPK activation through B7-H3-mediated DUSP10 repression promotes chemoresistance

Received: 3 January 2019
Accepted: 28 March 2019
Published online: 09 April 2019

Karine Flem-Karlsen[1,2], Christina Tekle[1], Tove Øyjord[1], Vivi A. Flørenes[3], Gunhild M. Mælandsmo[1,4], Øystein Fodstad[1,2] & Caroline E. Nunes-Xavier[1]

Immunoregulatory protein B7-H3 is involved in the oncogenic and metastatic potential of cancer cells, as well as in drug resistance. Resistance to conventional chemotherapy is an important aspect of melanoma treatment, and a better understanding of how B7-H3 enhances drug resistance may lead to the development of more effective therapies. We investigated the *in vitro* and *in vivo* sensitivity of chemotherapeutic agents dacarbazine (DTIC) and cisplatin in sensitive and drug resistant melanoma cells with knockdown expression of B7-H3. We found that knockdown of B7-H3 increased *in vitro* and *in vivo* sensitivity of melanoma cells to the chemotherapeutic agents dacarbazine (DTIC) and cisplatin, in parallel with a decrease in p38 MAPK phosphorylation. Importantly, in B7-H3 knockdown cells we observed an increase in the expression of dual-specific MAP kinase phosphatase (MKP) DUSP10, a MKP known to dephosphorylate and inactivate p38 MAPK. DUSP10 knockdown by siRNA resulted in a reversion of the increased DTIC-sensitivity seen in B7-H3 knockdown cells. Our findings highlight the potential therapeutic benefit of combining chemotherapy with B7-H3 inhibition, and indicate that B7-H3 mediated chemoresistance in melanoma cells is driven through a mechanism involving DUSP10-mediated inactivation of p38 MAPK.

B7-H3, a member of the B7 family of immune checkpoint proteins, is upregulated in many different cancer types[1], and B7-H3 targeted therapy is currently being tested in several clinical trials[2]. B7-H3 has been found to favor tumor growth, cell proliferation, migration, invasion, and drug resistance[3–5], although many aspects regarding its oncogenic potential are still unknown. For instance, B7-H3 has been involved in various signal transduction pathways, including the JAK/STAT, PI3K/Akt, and the mitogen activated protein kinase (MAPK) Raf/MEK/ERK pathways[2], but their relation with chemoresistance is not fully understood.

The MAPK pathways regulate various cellular processes, such as proliferation, differentiation, apoptosis and stress responses, and include four major pathways, as defined by their MAPK effector: ERK1/2, ERK5, JNKs and p38s MAPK[6]. The p38 MAPK pathway is mainly activated by stress signals such as UV light, osmotic shock and cytokines[7]. When activated, the p38 MAPK pathway can phosphorylate a wide range of proteins. This include activating phosphorylation of various transcription factors that may, amongst many physiological processes, lead to the maintenance of a tumor aggressive phenotype and/or resistance to chemotherapy[8].

The MAPKs are activated by phosphorylation by upstream kinases and inactivated by dephosphorylation of a group of dual specificity phosphatases called MAP kinase phosphatases (MKPs). MKPs include 10 active enzymes that show different specificity towards subgroups of MAPKs and have different localization patterns which permits a tight regulation, spatially and temporally, of the MAPK signaling. The MKPs can be divided into three groups: 1) the nuclear MKPs DUSP1, DUSP4, DUSP2, and DUSP5; 2) the cytoplasmic, ERK1/2-specific MKPs DUSP6, DUSP9, and DUSP7; and 3) the stress-activated, p38/JNK-specific MKPs: DUSP8, DUSP10, and DUSP16[9].

Melanomas have classically been treated with chemotherapy, including DNA alkylating, platinum-based, and microtubule-interacting agents[10]. However, low response rates, high toxicity and resistance are commonly found[11]. In the past years, therapies with small-molecule inhibitors or antibodies targeting immune checkpoint

[1]Department of Tumor Biology, Institute for Cancer Research, Oslo University Hospital Radiumhospitalet, Oslo, Norway. [2]Institute for Clinical Medicine, Faculty of Medicine, University of Oslo, Oslo, Norway. [3]Department of Pathology, Oslo University Hospital Radiumhospitalet, Oslo, Norway. [4]Department of Medical Biology, Faculty of Health Sciences, UiT/The Arctic University of Norway, Tromsø, Norway. Correspondence and requests for materials should be addressed to C.E.N-X. (email: carnun@rr-research.no)

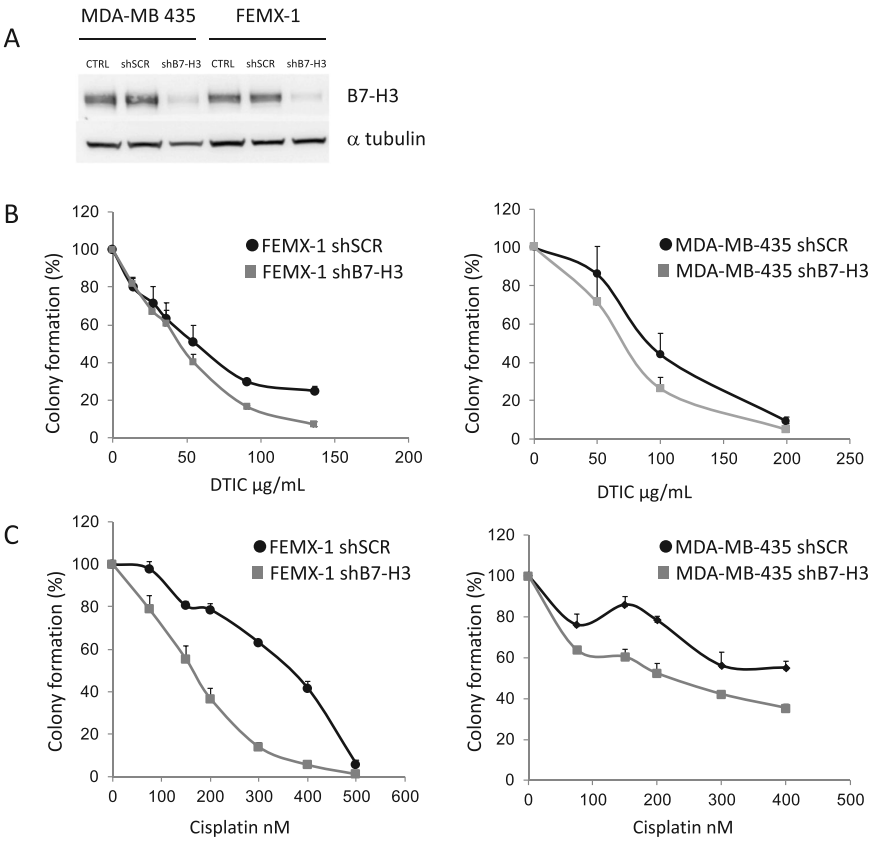

Figure 1. Melanoma cells with decreased B7-H3 expression have increased sensitivity to dacarbazine (DTIC) and cisplatin chemotherapy. (**A**) Immunoblot verifying the lentiviral knockdown of B7-H3 in MDA-MB-435 and FEMX-I cells. In cells were B7-H3 expression was decreased (short hairpin B7-H3, shB7-H3), the ability to form colonies in response to (**B**) DTIC and (**C**) Cisplatin chemotherapy treatment was reduced compared to control short hairpin scramble (shSCR) cells. Results show the average of three independent experiments ± SEM.

proteins or BRAF have become more prominent[12], but treatment resistance is frequent[13]. Despite the recent advances in melanoma treatment, dacarbazine (DTIC) chemotherapy is still being widely used even though its response rate as a single agent is only 10–20%[14,15]. Thus, improvement in melanoma therapy is highly needed. DTIC treatment combined with targeted therapy may improve the overall response, and is a promising way forward for treatment of metastatic melanoma[16].

Inhibiting expression of B7-H3 has been found to increase cell and tumor sensitivity to various chemotherapeutic agents[4,17–21]. In this study, we investigated the mechanism behind B7-H3 mediated resistance to DTIC and cisplatin, using melanoma as a model. We identified modulation of p38 MAPK activation by DUSP10 as a novel mechanism of B7-H3-mediated chemoresistance.

Results

Reduced B7-H3 expression increases *in vitro* and *in vivo* sensitivity of melanoma cells to chemotherapy. We have previously observed in *in vitro* proliferation assays that cells with decreased expression of B7-H3 display increased sensitivity to DTIC and small anti-cancer drugs, including molecular inhibitors[4]. However, the mechanism by which B7-H3 induces resistance to therapy is still unknown. To determine if the B7-H3 associated drug resistance might involve effects asserted by stress signaling, we treated melanoma cells with two chemotherapeutic agents, DTIC and cisplatin. The melanoma cell lines FEMX-I and MDA-MB-435 had stably reduced B7-H3 expression by short hairpin RNA (shRNA), as previously described (Fig. 1A; and in reference[5]). Diminished B7-H3 protein expression reduced the colony-formation ability of the cells upon treatment with both DTIC and cisplatin (Fig. 1B,C). This effect was also observed *in vivo* utilizing nude mice. Subcutaneous injection of cells with knocked down B7-H3 expression led to decreased relative tumor volume compared to control cells (Fig. 2A,B), and was further decreased when the mice were subjected to DTIC treatment (Fig. 2A). Of the DTIC treated mice 6/10 animals had regrowth at 100 days, while tumors in mice injected with B7-H3 knockdown cells showed regrowth in only 1/11 animals (Fig. 2A). Thus, melanoma cells with low expression of B7-H3 are more sensitive to DTIC and cisplatin chemotherapy.

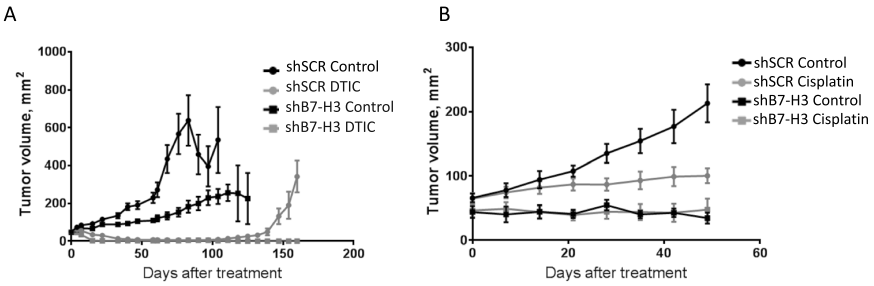

Figure 2. Tumor volume is reduced *in vivo* in shB7-H3 cells upon chemotherapy treatment. Mice were injected subcutaneously with 5×10^6 MDA-MB-435 melanoma control cells (shSCR) and cells having diminished B7-H3 expression (shB7-H3). Upon B7-H3 knockdown, the relative tumor volume was reduced compared to control cells in response to (**A**) Dacarbazine (DTIC) (n = 20–22 in each group) and (**B**) Cisplatin (n = 5–6 in each group) chemotherapy treatment. Results show the relative tumor volume of the tumors ± SEM.

Chemotherapy resistance is abrogated in cells with reduced expression of B7-H3. Interestingly, we observed 1.228-fold (SD ± 0.136265, p-value 0.004) higher B7-H3 expression in FEMX-V DTIC resistant (DR) cell line as compared to the sensitive parental cell line (Fig. 3A). Next, we investigated if reducing B7-H3 expression could increase sensitivity to chemotherapy in cells with induced drug resistance. To this end, we used the FEMX-V DTIC resistant (DR) cell line stably transduced with shRNA to reduce the B7-H3 expression as previously described (Fig. 3A). Upon DTIC treatment, the ability of FEMX-V shB7-H3 DR cells to form colonies was reduced to the level of FEMX-V sensitive control shSCR cells (Fig. 3B). Similarly, in xenograft experiments (Fig. 3C) the tumor growth curves were similar for mice injected with FEMX-V shB7-H3 DR cells to that of mice injected with FEMX-V sensitive cells. These data reinforce the notion that reducing B7-H3 expression independently abrogates the DTIC resistance of melanoma cells.

DUSP10 expression is increased in shB7-H3 cells, and correlates with lower p-p38 MAPK levels. In attempts to reveal the molecular basis of the involvement of B7-H3 in the drug resistance of FEMX-V DR cells, we performed a comparative DNA microarray gene expression analysis on FEMX-V DR control (shSCR) and shB7-H3 cells. Top differentially expressed genes with log2 value ±1 and p-value less than 0.05 are listed in Supplementary Table 1. Interestingly, one of the up-regulated genes was the dual-specific phosphatase DUSP10 (log2 Ratio = 1.052, p-value = 0.000124284). DUSP10 is a MAP kinase phosphatase known to dephosphorylate and negatively regulate p38 MAPK[9]. Up-regulation of DUSP10 mRNA expression was validated by qPCR (Fig. 4A). Additionally, we observed up-regulation of DUSP10 in FEMX-I shB7-H3 cells, and to a less extent in MDA-MB-435, shB7-H3 cells (Fig. 4A). To test the involvement of DUSP10 in regulating p38 MAPK activation, we analyzed p38 MAPK activation status in shSCR and shB7-H3 FEMX-I cells treated with DTIC or cisplatin. Both drugs induced p38 MAPK activation. Notably, this activation was lower in shB7-H3 knockdown cells compared to control cells treated with DTIC or cisplatin (Fig. 4B,C), suggesting that B7-H3 protein expression is involved in p38 MAPK activation.

Increased drug sensitivity in shB7-H3 cells is reversed upon siRNA-induced down-regulation of DUSP10. To analyze if DUSP10 levels affected the sensitivity to chemotherapy, we knocked down DUSP10 by siRNAs in shSCR and shB7-H3 FEMX-I cells. We observed a lower DTIC-induced activation of p38 MAPK in FEMX-I shB7-H3 cells compared to the shSCR cells, in consistence with higher DUSP10 expression (Figs 4A and 5A). Upon DUSP10 silencing, p38 MAPK activation was increased in both shSCR and shB7-H3 cells treated with DTIC. Moreover, the increased DTIC and cisplatin drug sensitivity achieved by B7-H3 knockdown was abrogated upon DUSP10 silencing (Fig. 5A,B and Supplementary Fig. 2). These results suggest that the increased chemosensitivity displayed by shB7-H3 cells is mediated through increased expression of DUSP10.

Discussion

B7-H3 expression is associated with tumor progression and epigenetic regulatory activity in cutaneous melanoma[22]. B7-H3 expression in melanoma cells is also associated with sensitivity to various anti-cancer agents[4], here including cisplatin. The mechanisms by which B7-H3 promotes drug resistance are largely unknown, although various pathways, such as JAK/Stat and PI3K/mTOR have been proposed to be involved[20,21]. In this study, we have identified the p38 MAPK pathway as a major effector of B7-H3-mediated resistance to chemotherapy and unveiled a novel B7-H3-associated regulation of p38 MAPK activation in melanoma cells. This regulation is mediated, at least in part, through the downregulation of the MAP kinase phosphatase DUSP10. Whether this B7-H3-DUSP10-p38 regulatory axis could be operative in other tumor types requires further studies. In this regard, p38 MAPK inactivation has been also observed in breast cancer cells upon knockdown of the B7-protein B7-H1/PD-L1[23].

Our results suggest that B7-H3 suppresses the expression of DUSP10 at the mRNA level, which in turn leads to higher p38 MAPK activation and increases tumor cell resistance to chemotherapy (Fig. 6). Thus, in our model, pharmacological inhibition of p38 MAPK would be beneficial and increase chemosensitivity of melanoma cells. It would be of interest to identify candidate DUSP10 transcription factors potentially repressed by B7-H3. DUSP10

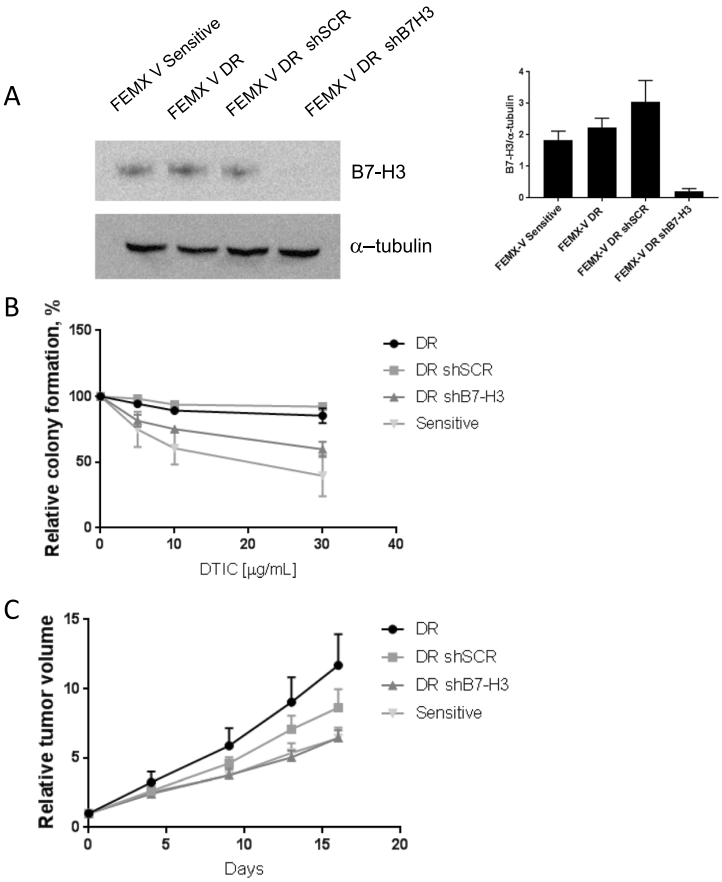

Figure 3. Reduced B7-H3 levels abolish dacarbazine (DTIC) resistance in DTIC resistant cells. FEMX-V cells with sensitivity (FEMX-V sensitive) or induced resistance to DTIC (FEMX-V DR), where knocked down for B7-H3. (**A**) Representative immunoblot of B7-H3 and α-tubulin expression in the four FEMX-V cell variants. (**B**) When these cells were subjected to DTIC treatment, little effect of DTIC was seen in the ability of drug resistant DR and DR shSCR cells to form colonies. FEMX-V DR shB7-H3 cells, however, displayed a reduced capacity to form colonies. Results show the average of two independent experiments ± SEM. (**C**) This effect was also seen *in vivo*, where FEMX-V shB7-H3 cells and FEMX-V sensitive cells displayed reduced relative tumor growth ± SEM compared to FEMX-V DR and FEMX-V DR shSCR cells (n = 7–8 in each group).

is a stress-activated, JNK/p38-specific MKP widely expressed, reported to be involved in cancer progression and in the regulation of immune response[9]. Overexpression of DUSP10 in human colorectal cancer (CRC) cells resulted in reduced tumor formation in immune deficient mice, and high DUSP10 expression was associated with better survival in CRC patients[24]. Our *in vitro* and *in vivo* results also suggest an anti-oncogenic role for DUSP10 in melanoma. In addition, our findings support the existence of a B7-H3-DUSP10-p38 axis important for cell proliferation which is independent of the immune system.

Interestingly, up-regulation of DUSP10 in prostate cancer cells correlated with inactivation of p38 MAPK and decreased production of the inflammatory cytokine IL-6[25], and DUSP10 was found to down-regulate the release of cytokines (IL-6 and TNF) by regulating p38 MAPK pathway in macrophages[26]. We have previously found B7-H3 expression to correlate with IL-8 secretion in melanoma cells[5]. Whether this phenomenon is mediated through DUSP10 needs further investigation.

In melanoma, activation of p38 MAPK has been associated with various cellular functions, including suppression of anti-tumor immune responses[27], and resistance to chemotherapy[28], and p38 MAPK inhibition has been found to suppress inflammation-induced metastasis[29]. Here, we observed activation of p38 MAPK in melanoma cells treated with either DTIC or cisplatin, indicating that these drugs affect cell proliferation through similar pathways. Inhibition of p38 MAPK is getting increased attention as a promising therapeutic approach in cancer[30]. Relevant to this, there are currently many clinical trials with various p38 MAPK inhibitors either alone or in combination with other chemotherapeutic agents in different types of cancers[31,32]. p38 MAPK inhibition increased the sensitivity to cisplatin in colorectal cancer[33], and to taxanes in breast cancer cells[34]. It would be interesting to test whether these mechanisms could be dependent on B7-H3 expression.

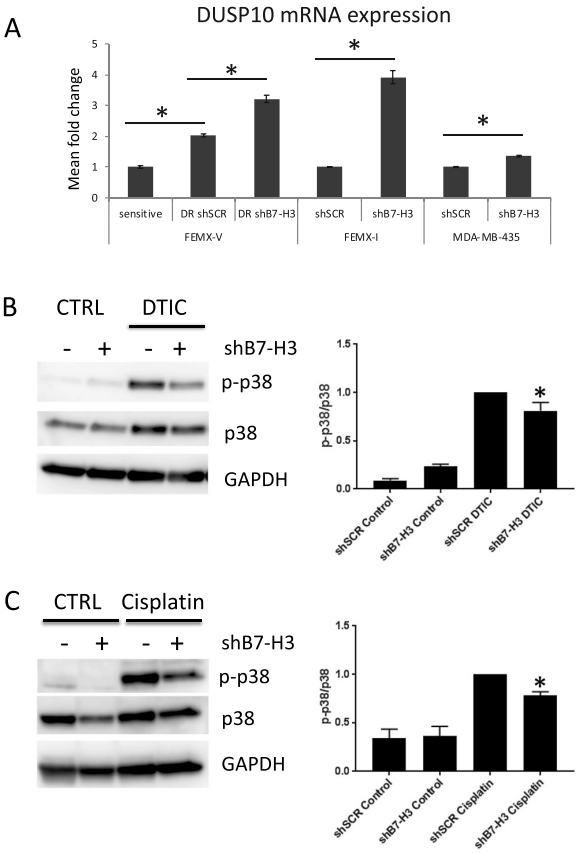

Figure 4. DUSP10 is induced in shB7-H3 cells and correlates with lower activation of p38 MAPK signaling by dacarbazine (DTIC) and cisplatin. (**A**) Mean fold change in gene expression of DUSP10 by qPCR of FEMX-V sensitive and DTIC resistant (DR), FEMX-I and MDA-MB-435 control (shSCR) and shB7-H3 cells. Representative immunoblot of phospho-p38 (p-p38), p38, and GAPDH levels in FEMX-I shSCR and shB7-H3 melanoma cells treated with: (**B**) 5 μg/mL DTIC or (**C**) 10 μg/mL cisplatin treatment. Right panels in B and C, average of three independent immunoblot values of p-p38 levels divided by p38 levels ± SEM.

Our findings support the idea that inhibiting B7-H3 may be a promising therapeutic concept in combination with chemotherapy. However, our *in vitro* and mouse xenograft models have limitations, and only reflect the B7-H3 tumor-intrinsic role. As B7-H3 is an immune checkpoint protein that prevents T cell activation, its inhibition could also affect immune function in the melanoma tumor microenvironment. Additional studies in immune competent mouse models would be necessary to assess the role of B7-H3 as an immune checkpoint protein and the potential of B7-H3 inhibition to promote both the anti-tumor immune response and sensitivity to chemotherapy in melanoma. Moreover, p38 MAPK signaling has been shown to induce the proliferation of regulatory T cells, thus dampening the immune response[35]. As B7-H3 expression correlates with the number of regulatory T cells[36] and is known to exhibit a co-inhibitory signal on the immune system[37], it would be interesting to investigate the activation of p38 MAPK by B7-H3 expression in immune competent models.

Materials and Methods

Cell cultures and silencing. FEMX-I and FEMX-V cell lines were established from a metastatic lymph node harvested from a melanoma patient operated at The Norwegian Radium Hospital[38]. FEMX-1 cells corresponds to the first generation of brain metastasis, and FEMX-V cells corresponds to the fifth generation, established by disaggregation, single cell formation and intraveneous re-injection in nude mice of the harvested cells as previously described[39]. MDA-MB-435 was acquired from ATCC. FEMX-V DTIC drug resistant (FEMX-V DR) cell lines were described previously[40]. B7-H3 knockdown in FEMX-V DR cells were made as reported for FEMX-I and MDA-MD-435 cells[5], using HuSH 29mer shRNA constructs against B7-H3 (shB7-H3; sequence shRNA-2, 5′-TCGTGTGCTGGAGAAAGATCAAACAGAGC-3′) and control plasmid pRS nontarget TR30003 (shSCR; sequence 5′-GCACTACCAGAGCTAACTCAGATAGTACT-3′) (both from Origene Technologies). All cells were grown in RPMI-1640 (Sigma Aldrich) with addition of 10% fetal bovine serum and 2 mM L-glutamine. DUSP10 knockdown was performed by transfection of specific siRNAs using Lipofectamine 3000 (Thermo Fisher) following manufacturer's protocol. DUSP10 siRNAs (siDUSP10 #1, SI03119998; siDUSP10 #2, SI03118178) were

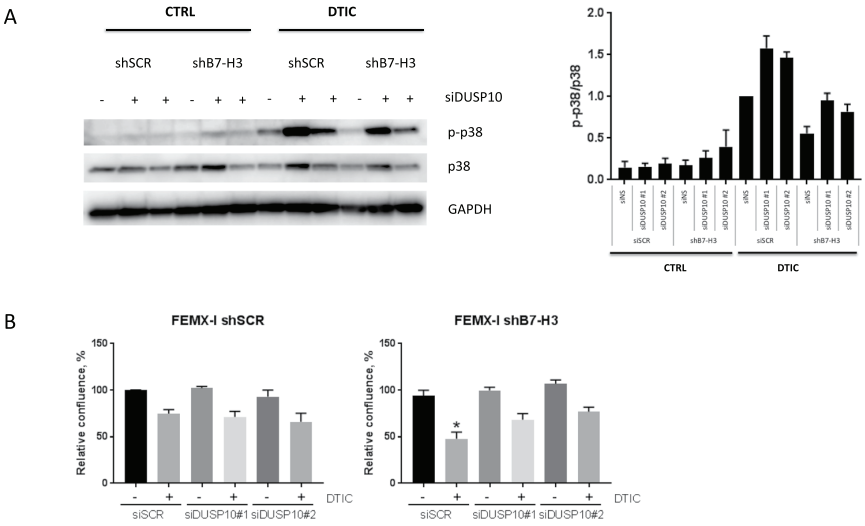

Figure 5. Reduced DUSP10 expression decreases chemosensitivity in shB7-H3 cells. (**A**) Left panel; Immunoblot analysis of phospho-p38 (p-p38), p38, and GAPDH expression upon DTIC treatment and right panel; average of three independent immunoblot values of p-p38 levels divided by p38 levels ± SEM in FEMX-I shSCR and shB7-H3 cells upon DUSP10 knockdown by siRNA. (**B**) Average proliferation of three independent experiments ± SEM of FEMX-I shSCR and shB7-H3 cells with DUSP10 knockdown and DTIC treatment as measured by the Incucyte FLR imaging system 72 h after treatment.

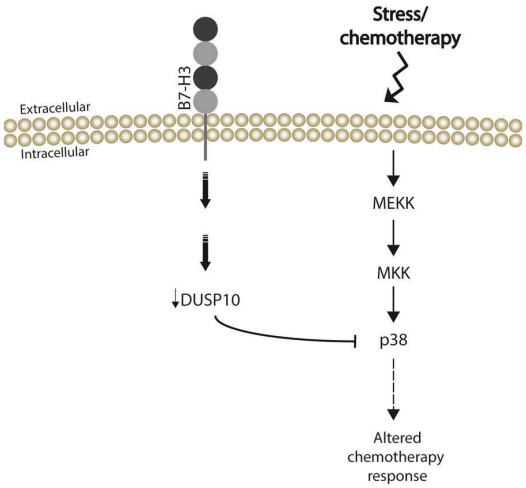

Figure 6. Schematic figure of how B7-H3 affects p38 MAPK signaling through modulation of DUSP10. In response to DTIC treatment, cells expressing B7-H3 have a lower level of DUSP10, which results in higher activation of p38 MAPK and resistance to chemotherapy. In cells with reduced B7-H3 levels, DUSP10 levels are higher and thus, p38 MAPK activation is lower, which leads to chemotherapy sensitivity. Upon reduction of DUSP10 levels, this sensitivity is eliminated.

from Qiagen (Thermo Scientific), and siNS (non-specific) siRNA (J-003104-13) was from Dharmacon. The final concentration of Lipofectamin3000 and siRNAs were 2 μl/mL and 50 nM, respectively. DUSP10 knockdown was verified 72 h post-transfection at mRNA level by RT-qPCR, as described below.

RNA isolation, DNA microarray and qPCR. The RNA was prepared for microarray analysis using the Illumina™ TotalPrep™ RNA amplification kit (Thermo Scientific) according to manufacturer's protocol. The concentration of the samples was measured using NanoDrop spectrophotometer (Thermo Scientific) and the quality of the finished cRNA was assessed using the Bioanalyzer (Agilent Genomics). 1.5 μg biotin labeled cRNA was hybridized onto Illumina Human-6 Expression BeadChips (Illumina) using the Whole-Genome Gene Expression Direct Hybridization Assay (Illumina) according to manufacturer's protocol. After scanning, the results were

quality checked in Ilumina BeadStudio, and raw data were quantile normalized in log2 scale. The DNA microarray analyses were performed at the Genomics core facility, Oslo University Hospital (OUH), Norway. Total RNA was isolated for RT followed by qPCR using QuantiTect Primers (Qiagen) for DUSP10 and HPRT as a housekeeping gene as described previously in reference[41].

Reagents, immunoblot and antibodies. Decarbazine (DTIC) (Lipomed GmbH) and cisplatin (Accord Healthcare) were used at indicated concentrations, during the indicated times. Dimethyl sulfoxide (DMSO) was used as a control. Whole cell protein extracts were prepared by total cell lysis and immunoblot was performed as described previously in reference[4]. Antibodies used for Western blotting were: B7-H3 (1:1000, AF1027, R&D), phosoho-p38 (#9211), p38 (#8690), GAPDH (#5174) (1:1000, Cell Signaling) and α-tubulin (1:50000, CP06, Millipore). Protein concentrations from total cell lysates were measured using Pierce® BCA Protein Assay Kit (Thermo Scientific). Immunoblot expression levels were quantified using ImageJ. Uncropped blots are provided in the Supplementary Information.

Cell proliferation and colony formation. To assess cell proliferation, 5000 cells/well were seeded on 96-well plates and the cell confluence was measured every three hours by the IncuCyte FLR or IncuCyte Zoom imaging microscopes (Essen Biosciences). The cells were treated with indicated drugs at indicated concentrations 21 h post-plating and were scanned for 72 h after adding the drugs. DMSO was added to control cells. For colony formation assays, 500 or 1000 cells/well were seeded on 6-well plates in media containing DMSO or indicated drugs. The cells were treated with drugs for 48 h, and plates were processed after 7 days. Colonies were counted after they were fixed with methanol and stained with 0.05% crystal violet.

***In vivo* studies.** The *in vivo* studies were performed using female nude athymic (fox1nu) mice bred at the Department of Comparative Medicine, Institute for Cancer Research, OUH Radiumhospitalet. When the animals were 6–8 weeks of age, 5×10^6 cells were injected subcutaneously into both flanks of the nude mice. The treatment was initiated when the tumors were between 5–6 mm in diameter and consisted of a single treatment of 250 mg/kg DTIC or 10 mg/kg Cisplatin administered intravenously. Solvent was administered for control mice. Tumors were measured twice a week and the tumor volume was calculated by the formula $0.5 \times \text{length} \times \text{width}^2$. The data is presented as the average ± standard error of the mean (SEM) of three independent experiments. All animals were kept according to regulations of the Norwegian Animal Welfare Act and the experiments were approved by the Norwegian Animal Research Authority and conducted according to the FELASA guidelines (FOTS application number 1748 and 2499).

Statistical analysis. Data shows average values ± SEM for the average of three representative experiments and *in vivo* experiments. All experiments were performed in technical and biological triplicates, if not otherwise specified. Data was analyzed by Graphpad Prism 7.0 (Graphpad Software), where significance was calculated using two-tailed students t-test. P values of less than 0.05 were considered significant and were marked with an asterisk.

Conclusions

By using melanoma cells resistant to DTIC, we found that knocking down B7-H3 in these cells abolished the acquired resistance. These findings support the idea that inhibiting B7-H3 may be a promising therapeutic concept in combination with chemotherapy. Furthermore, we observed a parallel upregulation of the mRNA levels of the dual-specific MAPK phosphatase DUSP10 in the B7-H3 knockdown cells. Consistently, lower p38 MAPK activation upon chemotherapy was observed in cells with reduced B7-H3 expression in parallel with increased sensitivity. Moreover, the increased sensitivity of B7-H3 knockdown cells was abolished by DUSP10 knockdown by siRNA. Taken together, we have discovered a novel mechanism that contributes to B7-H3-mediated drug resistance through attenuating DUSP10 expression thereby activating p38 MAPK in melanoma cells.

References

1. Ni, L. & Dong, C. New B7 Family Checkpoints in Human Cancers. *Mol Cancer Ther* **16**, 1203–1211, https://doi.org/10.1158/1535-7163.MCT-16-0761 (2017).
2. Flem-Karlsen, K., Fodstad, O., Tan, M. & Nunes-Xavier, C. E. B7-H3 in Cancer - Beyond Immune Regulation. *Trends Cancer* **4**, 401–404, https://doi.org/10.1016/j.trecan.2018.03.010 (2018).
3. Chen, Y. W., Tekle, C. & Fodstad, O. The immunoregulatory protein human B7H3 is a tumor-associated antigen that regulates tumor cell migration and invasion. *Curr Cancer Drug Targets* **8**, 404–413 (2008).
4. Flem-Karlsen, K. *et al*. Immunoregulatory protein B7-H3 promotes growth and decreases sensitivity to therapy in metastatic melanoma cells. *Pigment cell melanoma res* **30**, 467–476, https://doi.org/10.1111/pcmr.12599 (2017).
5. Tekle, C. *et al*. B7-H3 contributes to the metastatic capacity of melanoma cells by modulation of known metastasis-associated genes. *Int J Cancer* **130**, 2282–2290, https://doi.org/10.1002/ijc.26238 (2012).
6. Qi, M. & Elion, E. A. MAP kinase pathways. *J Cell Sci* **118**, 3569–3572, https://doi.org/10.1242/jcs.02470 (2005).
7. Zarubin, T. & Han, J. Activation and signaling of the p38 MAP kinase pathway. *Cell Res* **15**, 11–18, https://doi.org/10.1038/sj.cr.7290257 (2005).
8. Cuenda, A. & Rousseau, S. p38 MAP-kinases pathway regulation, function and role in human diseases. *Biochim Biophys Acta* **1773**, 1358–1375, https://doi.org/10.1016/j.bbamcr.2007.03.010 (2007).
9. Nunes-Xavier, C. *et al*. Dual-specificity MAP kinase phosphatases as targets of cancer treatment. *Anticancer Agents Med Chem* **11**, 109–132, BSP/ACAMC/E-Pub/0013 (2011).
10. Hsan, K. M., Chen, C. C. & Shyur, L. F. Current research and development of chemotherapeutic agents for melanoma. *Cancers (Basel)* **2**, 397–419, https://doi.org/10.3390/cancers2020397 (2010).
11. Soengas, M. S. & Lowe, S. W. Apoptosis and melanoma chemoresistance. *Oncogene* **22**, 3138–3151, https://doi.org/10.1038/sj.onc.1206454 (2003).
12. Wong, D. J. & Ribas, A. Targeted Therapy for Melanoma. *Cancer Treat Res* **167**, 251–262, https://doi.org/10.1007/978-3-319-22539-5_10 (2016).

13. Lito, P., Rosen, N. & Solit, D. B. Tumor adaptation and resistance to RAF inhibitors. *Nat Med* **19**, 1401–1409, https://doi.org/10.1038/nm.3392 (2013).
14. Megahed, A. I. & Koon, H. B. What is the role of chemotherapy in the treatment of melanoma? *Curr Treat Options Oncol* **15**, 321–335, https://doi.org/10.1007/s11864-014-0277-5 (2014).
15. Ugurel, S., Paschen, A. & Becker, J. C. Dacarbazine in melanoma: from a chemotherapeutic drug to an immunomodulating agent. *J Invest Dermatol* **133**, 289–292, https://doi.org/10.1038/jid.2012.341 (2013).
16. Davey, R. J., van der Westhuizen, A. & Bowden, N. A. Metastatic melanoma treatment: Combining old and new therapies. *Crit Rev Oncol Hematol* **98**, 242–253, https://doi.org/10.1016/j.critrevonc.2015.11.011 (2016).
17. Fauci, J. M. *et al*. Monoclonal antibody-based immunotherapy of ovarian cancer: targeting ovarian cancer cells with the B7-H3-specific mAb 376.96. *Gynecol Oncol* **132**, 203–210, https://doi.org/10.1016/j.ygyno.2013.10.038 (2014).
18. Jiang, B., Liu, F., Liu, Z., Zhang, T. & Hua, D. B7-H3 increases thymidylate synthase expression via the PI3k-Akt pathway. *Tumour Biol* **37**, 9465–9472, https://doi.org/10.1007/s13277-015-4740-0 (2016).
19. Kasten, B. B. *et al*. B7-H3-targeted 212Pb radioimmunotherapy of ovarian cancer in preclinical models. *Nucl med biol* **47**, 23–30, https://doi.org/10.1016/j.nucmedbio.2017.01.003 (2017).
20. Liu, H. *et al*. B7-H3 silencing increases paclitaxel sensitivity by abrogating Jak2/Stat3 phosphorylation. *Mol Cancer Ther* **10**, 960–971, https://doi.org/10.1158/1535-7163.MCT-11-0072 (2011).
21. Nunes-Xavier, C. E. *et al*. Decreased expression of B7-H3 reduces the glycolytic capacity and sensitizes breast cancer cells to AKT/mTOR inhibitors. *Oncotarget* **7**, 6891–6901, https://doi.org/10.18632/oncotarget.6902 (2016).
22. Wang, J. *et al*. B7-H3 associated with tumor progression and epigenetic regulatory activity in cutaneous melanoma. *J Invest Dermatol* **133**, 2050–2058, https://doi.org/10.1038/jid.2013.114 (2013).
23. Wu, X. *et al*. Targeting B7-H1 (PD-L1) sensitizes cancer cells to chemotherapy. *Heliyon* **4**, e01039, https://doi.org/10.1016/j.heliyon.2018.e01039 (2018).
24. Png, C. W. *et al*. DUSP10 regulates intestinal epithelial cell growth and colorectal tumorigenesis. *Oncogene* **35**, 206–217, https://doi.org/10.1038/onc.2015.74 (2016).
25. Nonn, L., Peng, L., Feldman, D. & Peehl, D. M. Inhibition of p38 by vitamin D reduces interleukin-6 production in normal prostate cells via mitogen-activated protein kinase phosphatase 5: implications for prostate cancer prevention by vitamin D. *Cancer Res* **66**, 4516–4524, https://doi.org/10.1158/0008-5472.CAN-05-3796 (2006).
26. Hommo, T., Pesu, M., Moilanen, E. & Korhonen, R. Regulation of Inflammatory Cytokine Production by MKP-5 in Macrophages. *Basic Clin Pharmacol Toxicol* **117**, 96–104, https://doi.org/10.1111/bcpt.12380 (2015).
27. Zhao, F. *et al*. Activation of p38 mitogen-activated protein kinase drives dendritic cells to become tolerogenic in ret transgenic mice spontaneously developing melanoma. *Clin Cancer Res* **15**, 4382–4390, https://doi.org/10.1158/1078-0432.CCR-09-0399 (2009).
28. Lopez-Bergami, P. The role of mitogen- and stress-activated protein kinase pathways in melanoma. *Pigment cell melanoma res* **24**, 902–921, https://doi.org/10.1111/j.1755-148X.2011.00908.x (2011).
29. Tang, Y. M. *et al*. Inhibition of p38 and ERK1/2 pathways by Sparstolonin B suppresses inflammation-induced melanoma metastasis. *Biomed Pharmacother* **98**, 382–389, https://doi.org/10.1016/j.biopha.2017.12.047 (2017).
30. Igea, A. & Nebreda, A. R. The Stress Kinase p38alpha as a Target for Cancer Therapy. *Cancer Res* **75**, 3997–4002, https://doi.org/10.1158/0008-5472.CAN-15-0173 (2015).
31. Zou, X. & Blank, M. Targeting p38 MAP kinase signaling in cancer through post-translational modifications. *Cancer Lett* **384**, 19–26, https://doi.org/10.1016/j.canlet.2016.10.008 (2017).
32. Garcia-Cano, J. *et al*. p38MAPK and Chemotherapy: We Always Need to Hear Both Sides of the Story. *Front Cell Dev Biol* **4**, 69, https://doi.org/10.3389/fcell.2016.00069 (2016).
33. Pereira, L., Igea, A., Canovas, B., Dolado, I. & Nebreda, A. R. Inhibition of p38 MAPK sensitizes tumour cells to cisplatin-induced apoptosis mediated by reactive oxygen species and JNK. *EMBO Mol Med* **5**, 1759–1774, https://doi.org/10.1002/emmm.201302732 (2013).
34. Cánovas, B. *et al*. Targeting p38a; Increases DNA Damage, Chromosome Instability, and the Anti-tumoral Response to Taxanes in Breast Cancer Cells. *Cancer Cell* **33**, 1094–1110, https://doi.org/10.1016/j.ccell.2018.04.010.
35. He, T. *et al*. The p38 MAPK Inhibitor SB203580 Abrogates Tumor Necrosis Factor-Induced Proliferative Expansion of Mouse CD4+ Foxp3+ Regulatory T Cells. *Frontiers in Immunology* **9**, 1556, https://doi.org/10.3389/fimmu.2018.01556 (2018).
36. Jin, Y. *et al*. B7-H3 in combination with regulatory T cell is associated with tumor progression in primary human non-small cell lung cancer. *Int J Clin Exp Pathol* **8**, 13987–13995 (2015).
37. Castellanos, J. R. *et al*. B7-H3 role in the immune landscape of cancer. *Am J Clin Exp Immunol* **6**, 66–75 (2017).
38. Fodstad, O. *et al*. Extrapulmonary, tissue-specific metastasis formation in nude mice injected with FEMX-I human melanoma cells. *Cancer Res* **48**, 4382–4388 (1988).
39. Fodstad, O. & Kjonniksen, I. Microenvironment revisited: time for reappraisal of some prevailing concepts of cancer metastasis. *J Cell Biochem* **56**, 23–28, https://doi.org/10.1002/jcb.240560106 (1994).
40. Risberg, K., Fodstad, O. & Andersson, Y. Anti-melanoma activity of the 9.2.27PE immunotoxin in dacarbazine resistant cells. *J Immunother* **33**, 272–278, https://doi.org/10.1097/CJI.0b013e3181c54991 (2010).
41. Nunes-Xavier, C. E. & Pulido, R. Global RT-PCR and RT-qPCR Analysis of the mRNA Expression of the Human PTPome. *Methods Mol Biol* **1447**, 25–37, https://doi.org/10.1007/978-1-4939-3746-2_2 (2016).

Acknowledgements

We thank Ms. I. Dybsjord and Alexandr Kristian for excellent technical assistance, and Dr. S. Tveito for sharing of reagents. We also thank Arne E. Ingels' legacy for financial support. Funding: This work was funded by The Research Council of Norway (grant number 239813) to CENX.

Author Contributions

Ø.F. and C.E.N-X. designed the study. K.F-K., C.T., T.Ø. and C.E.N-X. performed acquisition and analysis of data, K.F-K., C.T., T.Ø., V.A.F., G.M.M., Ø.F. and C.E.N-X. interpreted the data; and K.F-K., Ø.F. and C.E.N-X. wrote and revised the manuscript.

Additional Information

Supplementary information accompanies this paper at https://doi.org/10.1038/s41598-019-42303-w.

Competing Interests: The authors declare no competing interests.

Publisher's note: Springer Nature remains neutral with regard to jurisdictional claims in published maps and institutional affiliations.

Supplementary figure legends

Figure S1) qPCR analysis of DUSP10 expressionin FEMX-I cells.

qPCR verifying DUSP10 knocked down in FEMX-I shSCR and shB7-H3 cells using two different siRNAs (siDUSP10 #1 and siDUSP #2).

Figure S2)Reduced DUSP10 expression decreases cisplatin chemosensitivity in shB7-H3 cells.

Average proliferation of three independent experiment ±SEM of FEMX-IshSCR and shB7-H3 cells with DUSP10 knockdown and indicated concentrations of cisplatintreatment as measured by the Incucyte FLR imaging system 72 h after treatment.

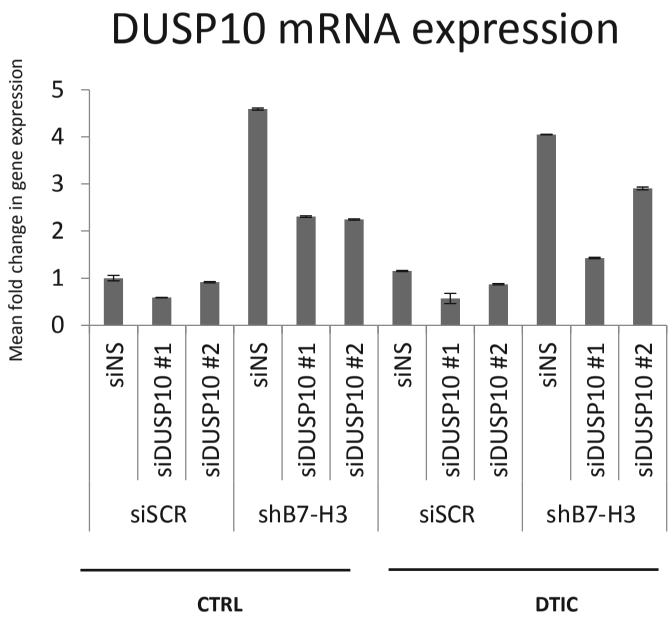

Supplementary Figure 1

Supplementary Figure 2

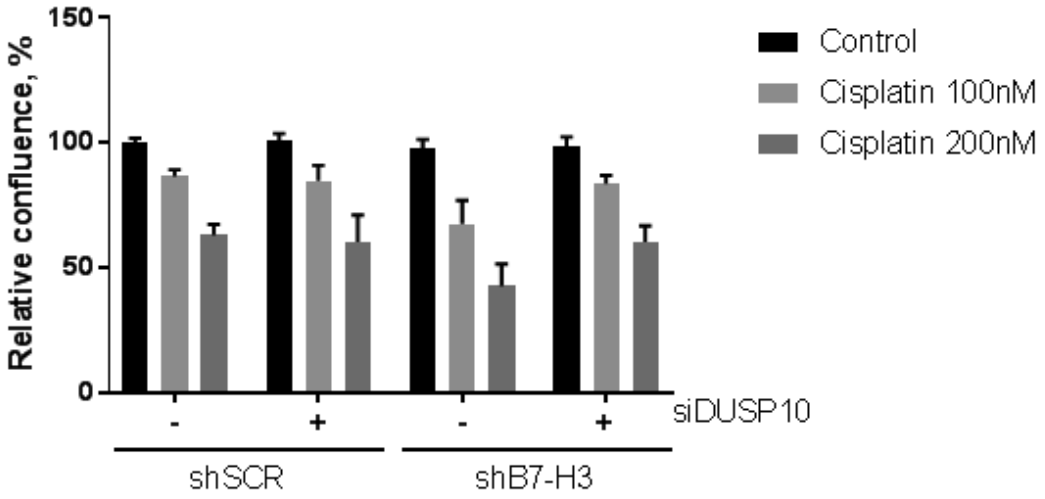

Supplementary Table 1

Contrast nr 1 - Adjustment method: BH, P-value: 0.05

Entrez ID	Probe	Symbol	Acc	Description	log2 Ratio (logFC)	Average log2-expression	Moderated t-statistic (t)	Raw p-value	Adjusted p-value
9503	5220753	XAGE1D	9503	X antigen family, member 1D	4,308	7,693	25,108	5,44E-09	8,86E-05
9503	4490743	XAGE1D	9503	X antigen family, member 1D	4,038	7,528	23,121	1,05E-08	0,00012872
653219	4390386	XAGE1	653219	X antigen family, member 1	2,686	7,153	25,503	4,80E-09	8,86E-05
4109	2490541	MAGEA10	4109	melanoma antigen family A, 10	2,533	7,035	30,048	1,28E-09	6,26E-05
8842	7400452	PROM1	8842	prominin 1	2,337	8,993	8,087	3,69E-05	0,01278534
63827	2100446	BCAN	63827	brevican	2,15	7,162	14,228	4,99E-07	0,00105815
283463	5390196	MUC19	283463	mucin 19, oligomeric	2,124	7,279	19,342	4,39E-08	0,00023819
63827	1090246	BCAN	63827	brevican	1,935	8,344	9,241	1,38E-05	0,00784719
1573	1570661	CYP2J2	1573	cytochrome P450, family 2, subfamily J, polypeptide 2	1,873	6,855	16,875	1,30E-07	0,00048457
10763	670278	NES	10763	nestin	1,62	6,574	14,63	4,01E-07	0,00090407
1824	2710400	DSC2	1824	desmocollin 2	1,605	7,118	20,972	2,30E-08	0,00016059
80381	5900575	CD276	80381	CD276 molecule	1,588	8,575	10,438	5,48E-06	0,00490451
10319	6280541	LAMC3	10319	laminin, gamma 3	1,56	7,083	8,501	2,56E-05	0,01089917
22871	1660037	NLGN1	22871	neuroligin 1	1,536	7,367	7,998	4,01E-05	0,01349089
871	7650017	SERPINH1	871	serpin peptidase inhibitor, clade H (heat shock protein 47), member 1, (collagen binding protein 1)	1,532	6,28	16,732	1,39E-07	0,00048457
26018	5090408	LRIG1	26018	leucine-rich repeats and immunoglobulin-like domains 1	1,522	6,914	9,918	8,08E-06	0,00571576
3800	2570402	KIF5C	3800	kinesin family member 5C	1,488	6,829	18,571	6,07E-08	0,00029055
6527	6620603	SLC5A4	6527	solute carrier family 5 (low affinity glucose cotransporter), member 4	1,39	6,199	8,22	3,28E-05	0,01231398
7368	1580196	UGT8	7368	UDP glycosyltransferase 8 (UDP-galactose ceramide galactosyltransferase)	1,293	6,401	7,959	4,15E-05	0,01378951
130574	6840220	LYPD6	130574	LY6/PLAUR domain containing 6	1,276	7,724	17,586	9,37E-08	0,00038095
4600	5490470	MX2	4600	myxovirus (influenza virus) resistance 2 (mouse)	1,274	8,6	12,502	1,37E-06	0,00230231
79961	6020327	DENND2D	79961	DENN/MADD domain containing 2D	1,272	9,648	15,138	3,06E-07	0,00078713
114818	510703	KLHL29	114818	kelch-like 29 (Drosophila)	1,257	6,914	15,852	2,13E-07	0,00064975
29851	2070037	ICOS	29851	inducible T-cell co-stimulator	1,249	6,475	7,944	4,21E-05	0,01378951
375295	6940059	LOC375295	375295	hypothetical gene supported by BC013438	1,247	9,05	11,794	2,15E-06	0,00283514
6819	1470689	SULT1C2	6819	sulfotransferase family, cytosolic, 1C, member 2	1,245	6,895	7,094	9,51E-05	0,02178187
23635	6480349	SSBP2	23635	single-stranded DNA binding protein 2	1,228	6,98	7,826	4,69E-05	0,01497571
91179	5390703	SCARF2	91179	scavenger receptor class F, member 2	1,203	7,753	6,561	0,000165	0,02988749
3588	5670719	IL10RB	3588	interleukin 10 receptor, beta	1,187	9,891	12,115	1,75E-06	0,0025066
4037	730458	LRP3	4037	low density lipoprotein receptor-related protein 3	1,187	6,533	7,998	4,01E-05	0,01349089
117854	6040653	TRIM6	117854	tripartite motif-containing 6	1,15	6,703	13,309	8,41E-07	0,0015782
440145	1660181	RP11-11C5.2	440145	similar to RIKEN cDNA 2410129H14	1,146	8,118	11,672	2,33E-06	0,0028414
2739	6770619	GLO1	2739	glyoxalase I	1,141	12,087	14,898	3,47E-07	0,00084779

79339	630400	OR51B4	79339	olfactory receptor, family 51, subfamily B, member 4	1,118	6,574	6,608	0,000157	0,0289656
56666	4070300	PANX2	56666	pannexin 2	1,11	7,486	8,963	1,73E-05	0,00883743
1949	2680070	EFNB3	1949	ephrin-B3	1,108	7,653	6,551	0,000166	0,02995907
25853	3290091	WDR40A	25853	WD repeat domain 40A	1,078	8,217	11,501	2,61E-06	0,00303132
57631	4730731	LRCH2	57631	leucine-rich repeats and calponin homology (CH) domain containing 2	1,047	6,216	15,233	2,92E-07	0,00078713
8745	110731	ADAM23	8745	ADAM metallopeptidase domain 23	1,04	7,023	11,971	1,92E-06	0,00259757
80728	4850300	KIAA1688	80728	KIAA1688 protein	1,03	10,378	14,599	4,08E-07	0,00090407
4678	4260682	NASP	4678	nuclear autoantigenic sperm protein (histone-binding)	1,021	8,877	7,945	4,21E-05	0,01378951
9124	1410010	PDLIM1	9124	PDZ and LIM domain 1 (elfin)	1,016	6,184	11,593	2,45E-06	0,00292069
23576	3170292	DDAH1	23576	dimethylarginine dimethylaminohydrolase 1	1,013	5,965	11,97	1,92E-06	0,00259757
3588	5050368	IL10RB	3588	interleukin 10 receptor, beta	1,011	8,154	7,731	5,13E-05	0,01577546
146330	6840390	FBXL16	146330	F-box and leucine-rich repeat protein 16	1,006	6,501	10,009	7,54E-06	0,00556866
7001	5960674	PRDX2	7001	peroxiredoxin 2	-1,011	10,079	-7,41	6,96E-05	0,01864077
8309	1010114	ACOX2	8309	acyl-Coenzyme A oxidase 2, branched chain	-1,016	6,339	-9,032	1,63E-05	0,00847779
390	4210524	RND3	390	Rho family GTPase 3	-1,016	8,587	-6,619	0,000155	0,0289656
834	450491	CASP1	834	caspase 1, apoptosis-related cysteine peptidase (interleukin 1, beta, convertase)	-1,041	10,891	-12,363	1,49E-06	0,00239869
11221	4830315	DUSP10	11221	dual specificity phosphatase 10	-1,046	9,41	-10,557	5,03E-06	0,00471316
199777	630767	ZNF626	199777	zinc finger protein 626	-1,051	6,105	-10,175	6,66E-06	0,00541643
5803	130754	PTPRZ1	5803	protein tyrosine phosphatase, receptor-type, Z polypeptide 1	-1,051	7,427	-9,461	1,15E-05	0,00686489
11221	10259	DUSP10	11221	dual specificity phosphatase 10	-1,052	8,748	-12,152	1,71E-06	0,0025066
284119	4850301	PTRF	284119	polymerase I and transcript release factor	-1,052	8,119	-7,281	7,90E-05	0,02008496
834	7050382	CASP1	834	caspase 1, apoptosis-related cysteine peptidase (interleukin 1, beta, convertase)	-1,054	10,802	-10,569	4,99E-06	0,00471316
125893	780471	ZNF816A	125893	zinc finger protein 816A	-1,061	6,962	-10,076	7,17E-06	0,00556866
493	6900630	ATP2B4	493	ATPase, Ca++ transporting, plasma membrane 4	-1,191	9,975	-9,788	8,93E-06	0,00605535
23462	6220201	HEY1	23462	hairy/enhancer-of-split related with YRPW motif 1	-1,195	8,433	-5,885	0,000347	0,04350344
90226	4220437	UCN2	90226	urocortin 2	-1,214	10,619	-7,902	4,37E-05	0,01423179
7033	7570484	TFF3	7033	trefoil factor 3 (intestinal)	-1,243	6,78	-11,175	3,25E-06	0,00352951
25907	3130220	TMEM158	25907	transmembrane protein 158	-1,247	11,058	-8,252	3,19E-05	0,01223156
493	6100482	ATP2B4	493	ATPase, Ca++ transporting, plasma membrane 4	-1,275	9,975	-9,121	1,52E-05	0,00813938
389816	2140541	LRRC26	389816	leucine rich repeat containing 26	-1,29	6,73	-9,804	8,82E-06	0,00605535
4145	5670605	MATK	4145	megakaryocyte-associated tyrosine kinase	-1,313	6,965	-8,846	1,91E-05	0,00921346
5468	830019	PPARG	5468	peroxisome proliferator-activated receptor gamma	-1,327	6,532	-11,332	2,92E-06	0,00331141
3347	5550598	HTN3	3347	histatin 3	-1,395	6,6	-12,794	1,14E-06	0,00205927
3914	730040	LAMB3	3914	laminin, beta 3	-1,413	7,682	-16,45	1,59E-07	0,00051737
140689	4640315	CBLN4	140689	cerebellin 4 precursor	-1,435	7,076	-15,602	2,42E-07	0,00069346
3347	6770674	HTN3	3347	histatin 3	-1,464	6,811	-10,051	7,31E-06	0,00556866

222553	1850138	SLC35F1	222553	solute carrier family 35, member F1	-1,488	7,923	-11,301	2,99E-06	0,00331141
9912	110575	RICH2	9912	Rho-type GTPase-activating protein RICH2	-1,496	6,434	-12,257	1,59E-06	0,00243245
139221	270176	MUM1L1	139221	melanoma associated antigen (mutated) 1-like 1	-1,538	6,289	-21,069	2,22E-08	0,00016059
10886	4260128	NPFFR2	10886	neuropeptide FF receptor 2	-1,745	6,91	-7,136	9,12E-05	0,0215973
8608	4200041	RDH16	8608	retinol dehydrogenase 16 (all-trans)	-2,224	6,524	-18,396	6,55E-08	0,00029055
19	4060358	ABCA1	19	ATP-binding cassette, sub-family A (ABC1), member 1	-3,211	8,31	-21,558	1,85E-08	0,00016059